CONTROLLED RADICAL POLYMERIZATION IN THE DISPERSED PHASE

by

MARY E. THOMSON

A thesis submitted to the
Department of Chemical Engineering
in conformity with the requirements for
the degree of Doctor of Philosophy

Queen's University
Kingston, Ontario, Canada
December, 2010

Abstract

Controlled radical polymerization (CRP) has emerged as a powerful method of creating polymers with tailored molecular architectures under mild reaction conditions. However, production of these polymers efficiently at an industrial scale will likely require them to be synthesized in the dispersed phase. Three types of CRP are explored, Atom Transfer Radical Polymerization (ATRP), Nitroxide Mediated Polymerization (NMP) and Catalytic Chain Transfer (CCT) to elucidate the intricacies of creating these novel polymer colloids.

Compartmentalization in an ATRP dispersed phase system is explored theoretically to understand the effects of particle size and catalyst concentration on the polymerization. The results suggest that there is an optimal range of particle sizes where the rate of polymerization is greater than that in an equivalent bulk system while maintaining both a lower PDI (polydispersity index) and higher livingness. All three factors are desirable in ATRP but generally cannot be achieved simultaneously in bulk. Compartmentalization manifests itself differently in CCT dispersed phase systems, where the segregation of the CCT agents into different polymer particles leads to multimodal molecular weight distributions.

Control over the particle size is notoriously difficult for nitroxide mediated polymerization, as it is challenging to decouple an increase in the particle size with an increase in target molecular weight using a two stage emulsion polymerization approach. This often leads to colloidally unstable latexes for low molecular weight, high solids conditions which are the result of superswelling. We offer several strategies to minimize this problem and create colloidally stable, high solids, n-butyl acrylate latexes by NMP with moderate to high molecular weight targets (>70 kg·mol^{-1}). Using this synergy between target molecular weight and particle size, high solids (>40 wt.%), high molecular weight (<200 kg·mol^{-1}) microemulsions (∼20 nm) of methyl methacrylate-co-styrene were prepared.

Finally, the monomer type and nucleation mechanisms also play a role in determining the particle size distribution in NMP emulsion systems. Using n-butyl methacrylate in emulsion with surfactant concentrations above the critical micelle concentration yields latexes with bimodal particle size distributions. However a surfactant-free approach allows monomodal latexes to be created.

Statement of Co-Authorship

All of the material presented in Chapters 3, 4 and 7 have been accepted and published in *Macromolecules*, a refereed journal. The material presented in Chapter 6 has been submitted to *Macromolecules*. The bulk of the research was carried out independently by myself, under the supervision of Dr. Michael Cunningham. The work in Chapter 4 was done in close collaboration with Dr. Niels Smeets, and the simulations demonstrated there were undertaken based on Dr. Smeets' previously published experimental work. He assisted in defining the scope of the project and played a large role in the revision of the manuscript. Dr. Jason Ness, of Arkema, Inc., provided technical guidance for the work presented in Chapter 5. Anna Manley, and undergraduate student, performed some of the preliminary experiments, under my supervision, for the work presented in Chapter 7. The preparation and editing of the aforementioned manuscripts and of this thesis was conducted under the supervision of Dr. Michael Cunningham.

Acknowledgments

I would like to thank Dr. Michael Cunningham for his guidance, encouragement, support and enthusiasm in working towards my PhD here at Queen's. I have had wonderful opportunities for learning, development, travel and great experiences over the past four plus years.

I would also like to thank my great friends Nicky, Niels, Jordan, Ula and Mikey for lots of fun and memories both in the lab and out. Thanks to the rest of the polymer group and the other graduate students in Chem. Eng. for discussions and great times too! Thanks also to all my friends, family and loved ones for their support throughout all of this.

Over the years I have had the opportunity to work in collaboration with others, including Dr. Niels Smeets from Queen's and Eindhoven, Dr. Ale Butté from ETH in Zurich (who taught me Fortran!), Dr. Jason Ness at Arkema and Anna Manley. Thank you to everyone!

Table of Contents

List of Tables

List of Figures

Nomenclature

Acronyms

AGET	Activators Generated by Electron Transfer
ARGET	Activators ReGenerated by Electron Transfer
ATRP	Atom Transfer Polymerization
BA	Butyl Acrylate
BB	BlocBuilder MA®
BMA	Butyl Methacrylate
BPMODA	bis(2-pyridylmethyl)octadecylamine
CCT	Catalytic Chain Transfer
CCTA	Catalytic Chain Transfer Agent
CLD	Chain Length Distribution
CMC	Critical Micelle Concentration
COBF	bis[(difluoroboryl)dimethylglyoximato]cobalt(II)
CRP	Controlled Radical Polymerization
DiBB	Di-BlocBuilder
DP	Degree of Polymerization
DP_n	Number Average Degree of Polymerization
DP_n^{inst}	Instantaneous Number Average Degree of Polymerization
dNbpy	4,4-di(5-nonyl)-2,2-bipyridine
EHA_6TREN	tris[2-di(2-ethylhexyl acrylate)aminoethyl]amine
ICAR	Initiators for Continuous Activator Regeneration
KR	Kumar and Ramkrishna
LRP	Living Radical Polymerization
MA	Methyl Acrylate
MMA	Methyl Methacrylate
MWD	Molecular Weight Distribution
NMP	Nitroxide Medicated Polymerization
PDI	Polydispersity Index
PRE	Persistent Radical Effect
PSD	Particle Size Distribution
RAFT	Radical Addition Fragmentation
RITP	Reverse Iodine Transfer Polymerization
SFRP	Stable Free Radical Polymerization
SFS	Sodium Formeldahyse Sulfoxylate
SG1	1-diethylphosphono-2,2-dimethylpropyl
St	Styrene
TEMPO	2,2,6,6-tetramethylpiperidiny-1-oxy
QSS	Quasi-Steady State

Parameters

C	concentration of CCTA in the polymer phase [mol·L^{-1}]
C_w	concentration of CCTA in the aqueous phase [mol·L^{-1}]
$\mathrm{D}_{i,j,k}$	Double Distinguished particle, fraction of particles with i radicals, chains of length j and k
$D_{s,i,c,j,k}$	fraction of particle with s short radicals, i propagating radicals, one of which with a chain length of j, another with a chain length of k and c CCTA molecules
d_p	particle diameter [nm]
f_{cin}	frequency of CCTA entry into a particle [s^{-1}]
f_{cout}	frequency of CCTA exit from a particle [s^{-1}]
f_{des}	frequency of desorption radicals from the particle [s^{-1}]
f_{fm}	frequency of uncatalyzed transfer to monomer [s^{-1}]
f_p	frequency of propagation [s^{-1}]
f_t	overall frequency of termination [s^{-1}]
f_{trans}	frequency of catalytic chain transfer [s^{-1}]
k_{act}	rate constant for activation [s^{-1} or L·mol^{-1}·s^{-1}]
k_{deact}	rate constant for deactivation [L·mol^{-1}·s^{-1}]
k_{dm}	rate constant for radical desorption [s^{-1}]
K_{eq}	equilibrium constant of k_{act}/k_{deact}
k_{fm}	rate constant of uncatalyzed transfer to monomer [L·mol^{-1}·s^{-1}]
k_p	rate constant of propagation [L·mol^{-1}·s^{-1}]
k_t	rate constant of termination by disproportionation [L·mol^{-1}·s^{-1}]
k_{trans}^{app}	apparent rate constant of catalytic transfer to monomer [L·mol^{-1}·s^{-1}]
M	concentration of monomer inside the particles [mol·L^{-1}]
M_0	initial concentration of monomer inside the particles [mol·L^{-1}]
$\bar{n}$	average number of radicals per particle
$\bar{n}_{\mathrm{chain}}$	average number radicals per chain per particle
$\bar{n}_{\mathrm{CCTA}}$	average number of CCTA (in this case COBF) molecules per particle
$\bar{n}_{\mathrm{Cu(I)}}$	average number of Cu(I) molecules per particle
$\bar{n}_{\mathrm{Cu(II)}}$	average number of Cu(II) molecules per particle
$\bar{n}_{\mathrm{Cu(II)chain}}$	average number of Cu(II) molecules per particle
n_{CCTA}	number of CCTA molecules in a distinct particle
N_A	Avogadro's number [mol^{-1}]
N_p	Number of particles [L^{-1}]
R_p	Rate of polymerization [mol·L^{-1}·s^{-1}]
N_i	Fraction of particles that contain i radicals
$N_{s,i,c}$	fraction of particle with s short radicals, i propagating radicals and c CCTA molecules
R_{deact}	Rate of deactivation [L·mol^{-1}·s^{-1}]
$R_j^{\bullet}$	concentration of radicals of chain length j [mol·L^{-1}]
$R_{short}^{\bullet}$	concentration of short (monomeric) radicals [mol·L^{-1}]
$R_w^{\bullet}$	concentration of radicals in the aqueous phase [mol·L^{-1}]
R_{trans}	rate of catalytic transfer to monomer [L·mol^{-1}·s^{-1}]
$\mathrm{S}_{i,j}$	Singly Distinguished particle, fraction of particles with i radicals and a chain length of j
$\mathrm{S}_{i,j,m}$	Singly Distinguished particle, fraction of particles with i radicals j Cu(II) molecules and a distinguished chain length of m
$S_{s,i,j,c}$	fraction of particle with s short radicals, i propagating radicals, one of which with a chain length of j, and c CCTA molecules
p	conversion

$P_n^\bullet$	concentration of propagating polymer chains of length n [mol·L^{-1}]
P_j	total concentration of dead polymer with a degree of polymerization of j [mol·L^{-1}]
$P_k^=$	concentration of dead polymer chains of length k with an unsaturation [mol·L^{-1}]
P_j	total concentration of dead polymer with a degree of polymerization of m [mol·L^{-1}]
P_{short}	concentration of dead polymer chains formed from short radical termination [mol·L^{-1}]
V_p	volume of a particle [L]
w(DP)	differential weight chain length distribution
w(log DP)	differential logarithmic chain length distribution
X	Mediating species can be a halogen or nitroxide molecule
x	conversion
ρ	frequency of (short) radical entry into a particle [s^{-1}]
$\lambda_{i,j}^k$	kth moment of the growing chains present in each type of particle state with i radicals and j Cu(II) molecules
$\mu^{(k)}$	kth order moment of the distribution of dormant chains [mol·L^{-1}]
$\zeta^{(k)}$	kth moment of dormant chains [mol·L^{-1}]
$\lambda_{Co,0}$	Characteristic time of a particle remaining devoid of a CCTA, with n_{COBF}= 0 [s]
$\lambda_{rad,c}$	Characteristic time of a radical existing inside a particle, with n_{COBF}= c [s]
$\lambda_{trans,c}$	Characteristic time of a CCT reaction on an active radical in a particle with $n_{\text{COBF}} = c$ [s]
δ	Kronecker index

subscripts

c	number of CCTA molecules inside the particle
C_{max}	maximum number of CCTA molecules per particle
i	total number radicals in the particle (short and propagating)
I_{max}	maximum number of radicals present in a particle
j	chain length of one distinguished propagating radical in the particle or the number of free Cu(II) molecules in the particle
k	chain length of one distinguished propagating radical in the particle or indicates the order of moments
m	chain length of one distinguished propagating radical in the particle
s	number of short radicals in the particle

List of Publications

Thomson, M. E., Cunningham, M. F. "Compartmentalization Effects on the Rate of Polymerization and the Degree of Control in ATRP Aqueous Dispersed Phase Polymerization", *Macromolecules*, **2010**, *43* (6) 2772–2779.

Thomson, M. E., Smeets, N. M. B., Heuts, J. P. A., Meuldijk, J., Cunningham, M. F. "Catalytic Chain Transfer Mediated Emulsion Polymerization: Compartmentalization and Its Effects on the Molecular Weight Distribution", *Macromolecules*, **2010**, *43* (13) 5647–5658.

Thomson, M. E., Manley, A., Ness, J., Schmidt, S., Cunningham, M. F. "Nitroxide Mediated Surfactant-Free Emulsion Polymerization of n-Butyl Methacrylate with a Small Amount of Styrene", *Macromolecules*, **2010**, *43* (19), 7958–7963.

Thomson, M. E., Ness, J., Schmidt, S., Cunningham, M. F. "High Solids Nitroxide Mediated Microemulsion Polymerization of MMA with a Small Amount of Styrene and the Synthesis of (MMA-co-St)-block-(BMA-co-St) Polymers", *submitted to Macromolecules.*

Thomson, M. E., Ness, J., Schmidt, S., McKenna, T. F. L., Cunningham, M. F. "Nucleation and Colloidal Characteristics of High Solids Nitroxide Mediated Emulsion Polymerization of n-Butyl Acrylate with Di-BlocBuilder MA", *in preparation.*

Chapter 1

Introduction

Controlled radical polymerization (CRP) has emerged as an elegant and versatile method of creating polymers with tailored molecular architectures which cannot be synthesized by conventional free radical chemistries. These types of polymers are useful in a variety of advanced materials including thermoplastic elastomers, blend compatiblizers, high performance adhesives and coatings. In CRP, all of the reaction mechanisms of free radical polymerization still apply; however, a mediating species is employed to control the polymerization and can aid in the creation of block copolymers, very short oligomers and polymers with narrow molecular weight distributions. CRP has been successfully implemented in bulk or solution polymerization, but to truly produce these specialty polymers at an industrially viable scale and to reduce the use of volatile organic compounds, successful transfer of these polymerization reactions into aqueous dispersed phase systems, such as emulsion, miniemulsion or microemulsion is necessary. Further, novel polymer colloids, which could only be created by dispersed phase polymerization, can also be discovered.

1.1 Overview

In this work, a variety of controlled radical chemistries are investigated in the dispersed phase, include Atom Transfer Radical Polymerization (ATRP), Nitroxide Mediated Polymerization (NMP) and Catalytic Chain Transfer (CCT). The objective is to highlight and provide new understanding of the challenges of implementing these chemistries into dispersed phase systems, especially because knowledge gained in one type of controlled chemistry can also be applied in others. The challenges addressed include radical and mediating

species compartmentalization into the polymer particles, particle nucleation and the creation of new materials. An in-depth exploration will be made into all of these challenges both through mathematical simulation and experimental evidence.

In this thesis, mathematical studies concerning compartmentalization of both the radicals and the mediating species in dispersed phase ATRP and CCT are conducted to shed light on previous experimental findings, but also to illustrate appropriate reaction conditions to prepare the desired products. Chapter 3 focuses on the study of compartmentalization effects in ATRP. Through mathematical simulations, an optimal range of particle sizes, at which rates of reaction faster than bulk polymerization can be obtained but with narrower molecular weight distributions, was predicted. Compartmentalization effects are also the focus of Chapter 4, but the effects manifest themselves very differently in dispersed phase CCT. Compartmentalization of the catalytic chain transfer agents can produce multimodal molecular weight distributions when a seeded emulsion system is used. Each of the modes on the MWD (molecular weight distribution) can be attributed to a discrete number of chain transfer agents per particle, regardless of the overall concentration of catalyst.

Another great challenge of CRP lies in the nucleation of particles and the creation of high solids latexes by *ab-initio* and two stage emulsion polymerization, which is the focus of Chapters 5–7, where experimental investigations of the more difficult monomer systems for polymerization by nitroxide mediated polymerization (n-butyl acrylate (BA), methyl methacrylate (MMA) and n-butyl methacrylate (BMA)) were undertaken. In Chapter 5, we investigate the relationship between particle size and target molecular weight for NMP of BA; this relationship is in direct opposition of that generally observed in conventional emulsion polymerization. Using strategies to minimize the particle size, colloidally stable latexes can now be produced at 45 wt.% solids. In Chapter 6, again using these strategies, we create latexes with very small particles sizes ($\sim$20 nm) of MMA up to 40 wt.% solids, including block copolymers with BMA by microemulsion polymerization. In this work it was found that *ab-initio* NMP emulsion polymerization of BMA results in bimodal particle size distributions. The cause of this is explored in Chapter 7 and found to be the result of multiple nucleation methods. However, performing these polymerizations under surfactant-free conditions yields monomodal latexes.

With this work, significant steps have been taken in increasing the understanding of

performing CRP in the dispersed phase, with a focus on industrially important issues like particle size distributions and solids content. Not only were multiple facets of dispersed phase polymerization investigated; multiple types of CRP chemistries were also included. Because all of these controlled chemistries include the use of a mediating species, conclusions drawn in one type of system may shed light on similar phenomena in others.

1.2 Research Objectives

- To study a variety of controlled chemistries in the dispersed phase to allow concepts studied in one system to be applied to others.
- To consider industrially important issues such as reaction rate, control of the polymerization, particle size and solids content of the latexes.
- To perform mathematical simulations of compartmentalization effects, particularly in the prediction of full molecular weight distributions.
- To understand the connection between initiator concentration and particle size in SG1 mediated emulsion polymerization.
- To create novel polymer colloids and high solids content latexes for a variety of monomer types by NMP.
- To understand the cause of bimodal particle size distributions in SG1 mediated BMA emulsion polymerization.

1.3 Summary of Original Contributions

- Identification of an optimal range of particle sizes where ATRP dispersed phase polymerization proceeds with both a faster rate of polymerization and a lower polydispersity and higher chain livingness than an equivalent bulk system.
- Discussions on the impact of performing ATRP in the dispersed phase with very low catalyst concentrations; unlike in bulk, the rate of polymerization is dependent directly on the catalyst concentration and termination is not an important consideration.

- The first mathematical simulation to predict the full molecular weight distribution of any controlled radical polymerization which includes both the compartmentalization of the radical species and the mediating agent was created for dispersed phase catalytic chain transfer system.

- The multimodal molecular weight distributions observed experimentally for a seeded CCT system were simulated. The main parameter governing compartmentalization in these systems is the entry and exit of the catalyst, which is related to the viscosity of the particles.

- Several strategies were introduced to minimize the impact of initiator concentration on the final particle size of SG1 mediated, two stage emulsion polymerization systems. By applying these strategies, well controlled, colloidally stable n-BA latexes can be created at 45 wt.% polymer content for moderate to high target molecular weights.

- Well controlled SG1 mediated MMA-co-St microemulsion latexes were prepared with small, monomodal particle size distributions, very low surfactant to monomer ratios, polymer contents up to 40 wt.% and high molecular weights. These microemulsions can be easily chain extended to create MMA-co-St-block-BMA-co-St block copolymers.

- Monomodal particle size distributions and well controlled BMA latexes can be created in a surfactant-free, two stage emulsion polymerization procedure. The cause of the bimodal latexes created in NMP BMA emulsion systems with surfactant concentrations above the critical micelle concentration is the result of multiple nucleation pathways.

Chapter 2

Background and Literature Review

2.1 Aqueous Dispersed Phase Polymerization

Emulsion polymerization is a common laboratory and industrial method of synthesizing polymers via free radical polymerization. Its benefits over bulk polymerization include improved heat transfer (as polymerization is strongly exothermic), decreased viscosity and minimizing the cost of specialized equipment for processing and monomer removal. It also reduces the amount of volatile organic compounds used compared to solution polymerization. A traditional emulsion polymerization formulation consists of monomer, water, surfactant, usually added above the critical micelle concentration (CMC), and a water soluble initiator. When the monomer, water and surfactant are mixed, an emulsion is formed of monomer droplets (1–10 μm) suspended in water with $\sim 10^{19}$–10^{21} micelles$\cdot$L^{-1} present in the aqueous phase. Initiation begins when radicals are formed by the thermal decomposition of the water soluble initiator. Propagation occurs initially in the aqueous phase until the oligomeric radical becomes sufficiently hydrophobic to enter a particle. This occurs when the chain reaches the z-meric length, ~2-5 monomer units, which depends on the temperature, monomer solubility and initiator end-group.[1] This oligomeric radical can nucleate a particle in one of three ways: micellar, droplet and aggregative nucleation. In emulsion polymerization, where the surfactant concentration is above the CMC, the entry of the z-meric oligomer into a micelle is favoured over entry into a droplet, as the micelles have a very high surface area for radical capture at ~5200 m$^2\cdot$L^{-1} compared to the surface area of the droplets of ~250 m$^2\cdot$L^{-1}.[2] However, entry of the oligomeric radicals into the droplets

does occur, and is referred to as droplet nucleation. Aggregative nucleation involves the precipitation of the oligomeric radicals (at a chain length greater than the z-meric length, referred to as the j_{crit} length[1]) out of the aqueous phase to form a very small precursor particle. Several precursor particles aggregate to form larger particles that are stabilized by surfactant and ionic initiator end groups. Aggregative nucleation is more common for moderately water soluble monomers,[2] which can preferentially add more monomer units in the aqueous phase and exceed the z-meric length to reach the j_{crit} length, which is necessary for the radical to precipitate. It is also the dominant nucleation method in surfactant-free emulsion polymerizations.

This period where new polymer particles are being nucleated and micelles are present is referred to as Interval I. This period ends when there are no micelles remaining and micellar particle nucleation ends. In Interval II, monomer continuously diffuses through the water phase from the large monomer droplets to replenish the monomer consumed by propagation in the particles, maintaining a relatively constant monomer concentration inside the particles, $[M]_p$. This leads to a relatively constant reaction rate if the number of particles remains unchanged. The same reaction mechanisms that occur in bulk (propagation, chain transfer and termination) occur inside the polymer particles. However, termination is often diffusion limited in bulk, while in small particles termination is limited by the rate of entry of radicals into the particle; this will be more fully explained below. Finally, Interval III is marked by a decrease in monomer concentration in the particles, as all the monomer droplets have disappeared.[1]

Miniemulsion polymerization differs from emulsion polymerization as droplet nucleation is the main particle formation process and there are no large monomer droplets to act as reservoirs for the particles. Thus the concentration of monomer inside the particles will decrease continuously over the course of the reaction. A miniemulsion is created by passing water, monomer, costabilizer, and surfactant through a high shear device to create droplets between 50–500 nm. These droplets will be stabilized by the surfactant, with few or no micelles present in the aqueous phase. In an ideal miniemulsion, the final polymer particles will be copies of the starting droplets, as every droplet is nucleated and the final number of particles is equal to the number of starting droplets, $\sim 10^{16}$–10^{18} L^{-1}. Monomer transfer is also minimal, so the particle size distribution ideally remains nearly the same as the initial

miniemulsion. Miniemulsion polymerization requires the use of a very hydrophobic, low molecular weight molecule as a costabilizer. This minimizes Ostwald ripening, the diffusion of monomer from the smaller droplets to the larger ones due to a higher chemical potential in the former.[2]

Another motivation to perform polymerization reactions in emulsion and miniemulsion is the ability to achieve high molecular weights without compromising reaction rate. In order to increase the molecular weight of the polymer in bulk, the reaction rate must be slowed by reducing the concentration of radicals, which can be accomplished by lowering the initiator concentration. However, in emulsion polymerization, the segregation of the propagating radicals in the particles leads to an effect called radical compartmentalization. Radical compartmentalization is very well understood for traditional emulsion polymerization, where higher molecular weight and overall reaction rates can be achieved because radicals in different particles cannot terminate with each other, leading to an overall larger concentration of radicals in the system than bulk and longer radical lifetimes.[3] This effect of compartmentalization is enhanced with diminishing particle sizes.

As early pioneers in the mechanistic study of emulsion polymerization Harkins,[4] and Smith and Ewart[5] reported that the rate of reaction increased with an increase in the number of particles with similar formulations. Smith and Ewart are credited with the first proposal of radical compartmentalization by developing a kinetic scheme to describe the average number of radicals per particle, $\bar{n}$ (Equation 2.1[6]), and in turn, the overall reaction rate in emulsion polymerization (Equation 2.2[7]).

$$\bar{n} = \sum_{i=0}^{\infty} i N_i \tag{2.1}$$

$$R_p = k_p \frac{N_p \bar{n}}{N_A} [M]_p \tag{2.2}$$

Using Smith-Ewart kinetics, the rate of change of N_i (the fraction of particles with i radicals) can be written incorporating the main reactions in an emulsion system, including entry of a radical into the particle, ρ, radical desorption, f_{des}, and termination, f_t (Equation 2.3[1]).

$$\frac{dN_i}{dt} = \rho\{N_{i-1} - N_i\} + f_{des}\{(i+1)N_{i+1} - (i)N_i\} + f_t\{(i+2)(i+1)N_{i+2} - (i)(i-1)N_i\} \quad (2.3)$$

The Smith-Ewart equations are limited by their inability to add chain-length distinctions to any of the rate coefficients, but still provide a good basis of understanding compartmentalization in emulsion polymerization.[1]

2.1.1 Modeling of Emulsion and Miniemulsion Systems

Most population balance emulsion polymerization models begin with the Smith-Ewart equations (explored in Section 2.1) and are expanded to track the chain length distributions (CLD), the particle size distributions and to include the chain length dependence upon the rate of termination and propagation. One of the first examples of this was produced by Chamberlain, Napper, Gilbert and Litchi in 1982.[8, 9]

The approach to modeling reaction rate and conversion, in its most simplified form without chain length dependent rate coefficients, depends on the number of radicals inside the particles and the particle size. Zero-one kinetics applies for situations where entry of aqueous oligoradicals into the particles is rate determining, rather than bimolecular termination. A particle can contain only zero or one propagating radicals, and the entry of a new radical into a particle containing one radical will result in instantaneous termination between the entering oligoradical and the propagating macroradical chain inside the particle. $\bar{n}$ is found by the Smith-Ewart equations of N_0 and N_1 only (Equation 2.3). When termination between two propagating macroradicals inside the particle is rate determining, each particle can be considered a mini-bulk reactor and considerations of compartmentalization are not applicable. Instead the number of radicals in a "typical" particle is used to calculate $\bar{n}$. The $\bar{n}$ of a pseudo-bulk system gives a lower limit of the compartmentalized case, and the Smith-Ewart equations (Equation 2.3) reduce to pseudo-bulk as $f_t \rightarrow 0$. For conditions of $\bar{n} > 0.7$, the system can be approximated by the pseudo-bulk model.[1]

Modeling the chain length distribution in emulsion and miniemulsion polymerization is often done by examining exclusively the kinetic reactions that occur in Interval II and III

of the polymerization while neglecting the particle size distribution, coagulation, and the method of nucleation. The CLD can be modeled by direct methods, which evaluates the chain length distribution as it evolves with time,[10] by indirect methods, such as the method of moments,[11] or through Monte Carlo simulations.[12]

Lichti et al.[13] introduced the concept of singly and doubly distinguished particles in their work expanding the Smith-Ewart equations to evaluate the CLD through the probability of finding radicals with different chain lengths in the same particle. The distribution of singly distinguished particles is a probability density function where $S_{i,t,t'}$ is the probability of finding a radical chain that started growing at time t, and is continuing to grow at time t' in a particle of i radicals. Similarly, through the distribution of doubly distinguished particles, $D_{i,t,t',t''}$ is the probability of finding a particle with i radicals and two propagating chains, one that is still growing at time t+t'+t" and the other still growing at time t'+t". The length of time the chains grow gives a direct measure of their chain length.[13]

The concept of singly and doubly distinguished particles was expanded on by Butté et al.,[10] but instead of expressing the length of the chains by the time of propagation, it was done by the degree of polymerization. The distribution of singly distinguished particles is a probability density function where $S_{i,j}$ is the probability of finding a particle with i radicals and one of those chains has a degree of polymerization j. Similarly, through the distribution of doubly distinguished particles, $D_{i,j,k}$ is the probability of finding a particle with i radicals and two distinguished chains of length j and k. The method of evaluation by degree of polymerization overcomes the limitation of the method by Lichti et al.,[13] where propagation is the fastest of all reactions and can easily introduce other reactions, including reversible termination (Section 2.2).

In addition to the Smith-Ewart equations (2.1), the singly (2.4) and doubly (2.5) distinguished particle balances for propagation, radical entry and termination are:[10]

$$\begin{aligned}\frac{dS_{i,j}}{dt} = & -[\rho + k_p[M] + f_t i(i-1)]S_{i,j} + k_p[M]S_{i,j-1} + \rho S_{i-1,j} \\ & + f_t i(i+1)S_{i+2,j} + \sigma_{j=1}\rho N_{i-1}\end{aligned} \tag{2.4}$$

$$\frac{dD_{i,j,k}}{dt} = -[\rho + 2k_p[M] + f_t i(i-1)]D_{i,j,k} + k_p[M](D_{i,j-1,k} + D_{i,j,k-1}) + \rho D_{i-1,j,k} + f_t i(i-1)D_{i+2,j,k} + \sigma_{j=1}\rho S_{i-1,k} \quad (2.5)$$

Modeling Intervals II and III in emulsion polymerization, Butté et al.[14] demonstrated that the majority of termination events (by combination or disproportionation) inside the particles occurred between short and long chains. Modeling of the full CLD is particularly important in instances where the primary mode of termination is by disproportionation, as a bimodal peak is expected especially when termination occurs between short and long chains, but can be overlooked in modeling techniques which only estimate molecular weights by the method of moments. Finally, Butté also showed that this numerical technique could be applied to systems with kinetic events faster than propagation, such as degenerative chain transfer in living/controlled polymerization.

2.2 Controlled Radical Polymerization

Controlled radical polymerization (CRP) reactions are a subset of traditional radical polymerization that use a mediating species to create specially designed molecular architectures including block copolymers, very short oligomers and polymers with narrow molecular weight distributions. The reaction mechanisms of radical polymerization still apply, including initiation, propagation, chain transfer and termination by combination and disproportionation. However, in CRP, the dominant radical ending event involves a bimolecular reaction between the radical and mediating species.

Polymers with special architectures can be produced by ionic polymerization, which has been in use for decades; however, this method is very sensitive to impurities and transfer of the ionic polymerization to a water-based system is nearly impossible because of the sensitivity of the reagents to water. In comparison, CRP is an exceptionally simple and robust system for producing novel polymer products.

2.2.1 Nitroxide Mediated Polymerization

Nitroxide mediated polymerization (NMP) uses a stable nitroxide radical to reversibly terminate a propagating polymer chain, yielding a dormant alkoxyamine. In 1993, Georges et al. demonstrated that low polydispersity polystyrene could be prepared with TEMPO (2,2,6,6-tetramethylpiperidiny-1-oxy) as the mediating species.[15] In a reversible termination mechanism such as this, the equilibrium of the activation/deactivation reactions between the dormant and active chains is shifted strongly towards the dormant species. As a result, the concentration of propagating radicals tends to be lower than in conventional free radical polymerization, although this is not a requirement. The reaction mechanism for NMP is shown in Figure 2.1.

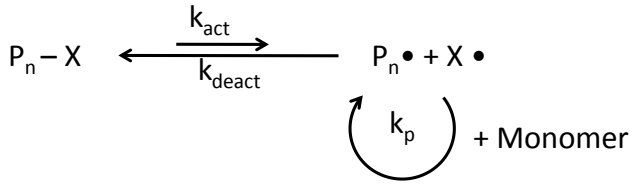

Figure 2.1: The activation/deactivation equilibrium in nitroxide mediated polymerization (NMP). X represents the nitroxide molecule.

In all radical polymerization systems, the rate of polymerization at steady state, R_p, is governed by the concentration of the radical species [P•]. In reversible termination systems, this is a function of chains generated by initiation, R_i, and activation, R_{act}, and radical loss, through termination, R_t, and deactivation, R_{deact}.[16]

$$\begin{aligned} R_p &= k_p[P\bullet][M] \\ \frac{d[P\bullet]}{dt} &= R_i + R_{act} - R_t - R_{deact} \end{aligned} \tag{2.6}$$

For a living system with limited termination, the main radical creation event is activation and main radical loss event is deactivation. Thus, at steady state, the rate of polymerization is determined by the equilibrium between the dormant and active chains:

$$\begin{aligned} R_p &= k_p[P\bullet][M] \\ &= k_p \frac{k_{act}}{k_{deact}} \frac{[P-X]}{[X]}[M] \end{aligned} \tag{2.7}$$

The polydispersity (PDI) of chain lengths obtained by NMP is dependent on several factors. The breadth of the CLD can be narrowed by initiating all the chains at the same time (very fast initiator decomposition or using a nitroxide-capped macroinitiator[17]), minimizing the number of active chains at any time and, finally, increasing the number of activation/deactivation cycles. It is desirable for a chain to undergo many short periods of propagation rather than few long ones. Statistically this will lead to a narrower breadth of the CLD at any time, and also decrease the likelihood of termination. The length of each cycle is controlled by the rate of chain deactivation by the nitroxide, thus narrower PDIs can be obtained in systems with greater rate coefficients of deactivation, k_{deact}, and/or larger concentrations of free nitroxide, [X]. The PDI decreases with increasing conversion (denoted as p, as shown in Equation 2.8) for the ideal case with no bimolecular termination.[18]

$$PDI = \frac{M_w}{M_n} = 1 + \frac{1}{DP_n} + \frac{k_p[P-X]_0}{k_{deact}[X]} \left(\frac{2}{p} - 1 \right)$$

at full conversion:

$$PDI = 1 + \frac{1}{DP_n} + \frac{k_p[P-X]_0}{k_{deact}[X]} \tag{2.8}$$

Polymerization reactions with reversible termination are subject to the Persistent Radical Effect (PRE),[19, 20, 21] which elucidates the cross reactions that occur between a "persistent" radical (the nitroxide) and a "transient"(propagating) radical. PRE predicts that even when irreversible bimolecular termination of the transient radicals is suppressed, there will be a slow buildup of the persistent radical during polymerization. This further shifts the equilibrium towards the dormant species and results in a slow down and possible end to the polymerization.

While Georges et al.[15] first demonstrated NMP with TEMPO, this system has many limitations. These include the high temperatures required to have appreciable homolysis of

the C-O bond and the thermal initiation of styrene can lead to broader molecular weight distributions as new chains are formed over time. However, it appears that to have appreciable reaction rates in NMP, a mechanism must be present to minimize the effect of nitroxide buildup over time due to radical termination. There has been little evidence to suggest that TEMPO can be applied with monomers other than styrenics due to the negligible thermal initiation of other monomers coupled with the stability of TEMPO. However, it has been demonstrated that acrylates can be polymerized with TEMPO derivatives above 140^{O}C only when a reducing agent is added to scavenge the excess TEMPO built up over time.[22]

More recently, the nitroxide SG1 (N-*tert*-butyl-N-(1-diethylphosphono-2,2-dimethylpropyl)) has received considerable attention. SG1 has been shown to polymerize a wide variety of monomers, including styrenics, acrylates, and methacrylates with more limited success in copolymer systems[23] at temperatures considerably lower than those required for TEMPO, between 45–125^{O}C, depending on the monomer.

Homopolymerization of methyl methacrylate mediated with SG1 has not yet been demonstrated. Although disproportionation between SG1 and MMA radical is minimal without a large excess of nitroxide,[24, 25] the k_{act} remains too large at temperatures where there can be an appreciable k_p. However, it has been shown that MMA can be controlled with the addition of only small amounts of St monomer (∼4–8 mol%) and the large majority of reversibly terminated chains posses a styrene (St) terminal unit.[26, 27, 28]

2.2.2 Atom Transfer Radical Polymerization

Atom Transfer Radical Polymerization (ATRP) is another type of reversible termination mechanism, but uses a transition metal catalyst as the mediating species. Although ATRP was first demonstrated using an iron catalyst,[29] the use of a copper catalyst for ATRP was pioneered by Matyjaszewski's group in 1995.[30] The catalyst changes oxidation states as it reversibly transfers a halogen atom (often a Cl or Br, denoted as X) to deactivate a growing radical chain. Regular ATRP polymerization requires an alkyl halide initiator and the transition metal catalyst present in the Cu(I)/Ligand form, considered the "activating" species. The polymerization begins as the halogen is transferred from the alkyl halide to produce Cu(II)/Ligand ("deactivating" species) and a free radical. The transfer of the

halogen between the transition metal catalyst and the end of the growing chain mediates the polymerization, and the degree of polymerization increases with time. The reaction mechanism is shown in Figure 2.2. The transition metal is bound to a ligand which increases solubility in the monomer phase and plays a primary role in dictating the activity ($K_{eq} = k_{act}/k_{deact}$) of the system.

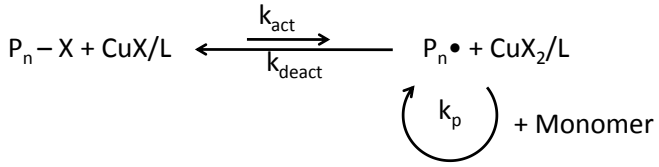

Figure 2.2: The activation/deactivation equilibrium in atom transfer radical polymerization (ATRP). X represents the transferable halogen atom.

Many of the phenomena present in NMP are also observed in ATRP, including the continual increase of molecular weight with time and the dependence of the PDI upon the concentration of deactivating species, Cu(II)/Ligand (similar to Equation 2.8).

The reaction kinetics differ from NMP, as ATRP involves a bimolecular reaction for both the activation and deactivation of the chain. While the reaction rate for NMP was described by Equation 2.7, the reaction rate for ATRP in solution and bulk is dependent upon the ratio of [Cu(I)/Ligand] to [Cu(II)/Ligand] as shown below.[31]

$$\begin{aligned} R_p &= k_p[M][P^\bullet] \\ &= k_p[M]\frac{k_{act}}{k_{deact}}[\text{P-X}]\frac{[\text{CuX/ Ligand}]}{[\text{CuX}_2\text{ /Ligand}]} \end{aligned} \tag{2.9}$$

For ATRP, this indicates that catalysts with high values of k_{deact} can be used in lower concentrations. However, this is not possible for NMP, which requires a stoichiometric amount of deactivating species per propagating chain.[31]

Reverse ATRP A major limitation of regular ATRP is the oxygen sensitivity of the Cu(I). During reagent preparation, any residual oxidants can cause the oxidation of the Cu(I) into Cu(II). This ultimately shifts the equilibrium towards the dormant alkyl halide

and can inhibit the reaction. Reverse ATRP uses a conventional radical initiator and the copper complex in its higher transition state, Cu(II).[30]

Although reverse ATRP is far less sensitive to oxygen than regular ATRP, it also has several drawbacks. With conventional radical initiators, complex and highly specialized molecular architectures cannot be formed (for example, star polymers) and it is impossible to independently reduce the catalyst concentration without also reducing the number of chains created by the radical initiator. It is suggested by equations 2.8 and 2.9, and also demonstrated experimentally,[32, 33] that less than a stoichiometric amount of catalyst to polymer chains can be used to mediate ATRP reactions, but this reduction is impossible for reverse ATRP, as the added catalyst provides the only source of transferable halogen atoms.

Activators Generated by Electron Transfer (AGET) ATRP Activators Generated by Electron Transfer (AGET) ATRP is a method of initiation that combines the benefits of reverse ATRP, the ability to use the less air sensitive Cu(II) complexes, while also allowing the flexibility of architectures and lower catalyst:initiator ratios of regular ATRP.[34, 35] A reducing agent (tin(II) ethyl hexanoate in bulk/solution systems or ascorbic acid in aqueous dispersed systems) is used to convert the Cu(II) to Cu(I) in-situ and begin the polymerization. The concentration of reducing agent is crucial to the success of the process. If all of the Cu(II) is reduced, uncontrolled polymerization will result. Alternatively, if insufficient Cu(II) is reduced, the system will be inhibited. In a trial and error type fashion, AGET ATRP can also be performed in the presence of air, with additional reducing agent added to scavenge the oxygen.[34]

Activators ReGenerated by Electron Transfer (ARGET) ATRP Activators ReGenerated by Electron Transfer (ARGET) ATRP allows the concentration of copper catalyst to be reduced significantly, down to 50 ppm (Cu to monomer) for acrylate polymerization,[36] and down to 10 ppm for styrene polymerizations[37] in solution. This can be done with an active copper/ligand system which can mediate several hundred polymer chains at once. However, even with an active catalyst, irreversible radical terminations will still lead to a buildup of deactivator species. To rectify this, a reducing agent is added in excess to continuously regenerate the activator species via a redox process. This gives an appreciable

rate of polymerization at low catalyst levels by maintaining an appropriate Cu(I):Cu(II) ratio (Equation 2.9).

Initiators for Continuous Activator Regeneration (ICAR) ATRP Initiators for Continuous Activator Regeneration (ICAR) ATRP[38] also employs a catalyst regeneration mechanism similar to ARGET. Instead of using a reducing agent, a conventional radical initiator slowly decomposes to furnish additional chains which reduces excess Cu(II) in a similar fashion as reverse ATRP. This is very similar to the consumption of the persistent species through the thermal autoinitiation of styrene, but in a much more controlled fashion.

Experimentally, ICAR ATRP has been observed to allow a far larger range of ligand complexes to be used than ARGET because the main catalyst regeneration mechanism relies upon the thermal decomposition of the initiator and not the reductive reaction between Cu(II)/Ligand and the reducing agent. However ICAR limits the creation of block copolymers as new chains are generated throughout the polymerization.[31]

2.2.3 Catalytic Chain Transfer

Catalytic chain transfer (CCT) is a type of controlled radical polymerization, but does not use the reversible termination mechanism to mediate the polymerization; instead CCT uses a highly active Co(II) catalyst to produce low molecular weight polymers. Only low concentrations of catalyst are required ($\sim 10^{-6}$ mol·L^{-1}) to control the molecular weight, making it a very efficient process.[39] The presence of Co(II) during the polymerization catalyzes chain transfer to monomer; this reaction has a very large chain transfer coefficient ($C_{Co(II)} = 3x10^4$ for bulk polymerization of MMA at 60^{o}C with COBF[39, 40]). The main reactions for CCT involve the abstraction of a β-H from the growing chain by the Co(II) complex resulting in a dead polymer chain with a terminal saturation and the catalyst in the Co(III)-H form. The H-abstraction reaction is rate determining. The Co(III)-H complex is very reactive and reacts quickly with a monomer unit by hydrogen transfer. This results in formation of a monomeric radical and the regeneration of the original Co(II) catalyst.[39] The CCT mechanism is shown in Figure 2.3

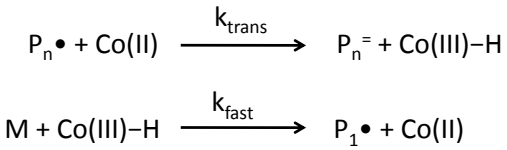

Figure 2.3: CCT Mechanism

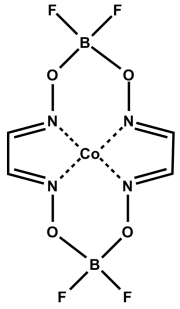

Figure 2.4: COBF ((bis[(difluoroboryl) dimethylglyoximato]cobalt(II)) catalyst for CCT.

2.3 Controlled Radical Polymerization in the Dispersed Phase

2.3.1 Dispersed Phase Nitroxide Mediated Polymerization

Early attempts to conduct TEMPO mediated emulsion polymerization demonstrated evidence of livingness but suffered massive colloidal instability.[41, 42] This is often attributed to the nucleation of the large monomer droplets, especially when thermal autoinitiation of styrene (St) is prominent at the given operating temperatures.[17, 41, 42, 43] Instead, successful styrene NMP with TEMPO has been conducted in miniemulsion via both a bimolecular initiation system (TEMPO with both oil and water soluble initiators)[44, 45] and a unimolecular system (beginning with an alkoxyamine inside the droplets).[46] The use of the water soluble reducing agent ascorbic acid also led to significant increases in the polymerization rate by scavenging excess TEMPO and also led to controlled butyl acrylate (BA) systems with TEMPO in miniemulsion.[47, 48]

Investigations of aqueous dispersed polymerization with SG1 began with miniemulsion polymerization, predominantly using the alkoxyamine BlocBuilder MA® from Arkema (Figure 2.5) to polymerize both styrene and butyl acrylate. For BA, it was necessary to begin with an excess of nitroxide of ∼2.5 mol% to maintain control at the very beginning of the reaction because of its very high propagation rate.[49]

Although colloidal stability has been achieved with NMP miniemulsions, they are almost always subjected to broad particle size distributions. The superswelling theory[50] has been put forward to explain this phenomenon. The large concentration of oligomers (the predominant initial product in living systems) present in the particles early in the polymerization lowers the chemical potential of the nucleated particles with respect to droplets or monomer-swollen micelles. This promotes the swelling of the newly nucleated droplets, and can lead to very broad particle size distributions, or in the worst case, colloidal instability. It has been suggested that superswelling could be minimized through the use of higher levels of costabilizers, the addition of a high polymer fraction or the addition of a nonionic polymeric surfactant.[2, 50]

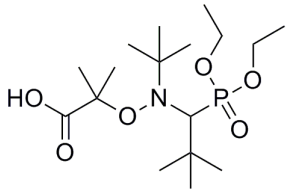

Figure 2.5: The alkoxyamine initiator BlocBuilder MA® is water soluble in its ionized form (not shown).

Emulsion polymerization for water soluble monofunctional and difunctional alkoxyamine initiators has been demonstrated by Charleux's group using a multi-step procedure.[51, 52, 53, 54, 55] BlocBuilder MA® is a water soluble alkoxyamine initiator when it is present in its ionized form. First, a living seed latex is created by micellar nucleation at low monomer concentrations and then the rest of the monomer is added batchwise or fed in slowly (Figure 2.6). The alkoxyamine begins as a water soluble molecule, and undergoes polymerization in the aqueous phase. Once sufficient monomer units are added, the chain becomes hydrophobic and enters a monomer swollen micelle, droplet or particles. High initiator efficiencies were seen for butyl acrylate, but not for styrene. This is the result of the low rate of aqueous phase polymerization of styrene, which delays the entry of the chains into the particles as they are reversibly terminated before becoming surface active.[56] The carboxylated chain endgroups also help to impart stability to the particles by remaining close to the surface.

Although nitroxide mediated emulsion polymerization has been successfully demonstrated, broad particle size distributions and other strange colloidal behaviours have been

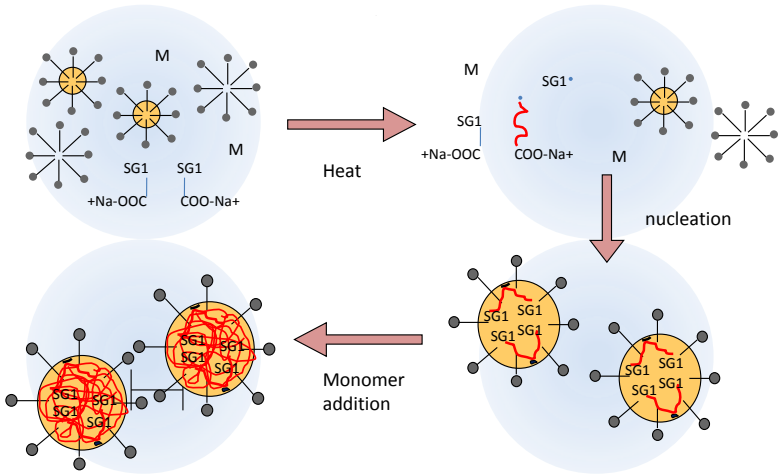

Figure 2.6: Two stage emulsion NMP scheme.[51]

observed. In conventional emulsion polymerization, when the concentration of water soluble initiator is increased, all other factors remaining constant, the particle size tends to decrease, because of the additional stabilizing effect the charged initiator end groups can provide, which increases the colloidal stability of the particles. However, in NMP emulsion, the opposite trend is observed, where an increase in the concentration of BlocBuilder MA® or Di-BlocBuilder leads to an increase in the particle size, regardless of the addition of further charged groups to stabilize the particles. It has been noted that the particle size distribution (PSD) is narrower and smaller for Di-BlocBuilder, with respect to BlocBuilder MA®, initiated emulsion polymerization under similar conditions.[51] Similar trends of increasing particle size with increasing initiator or RAFT agent concentrations are also observed in other controlled chemistries, specifically reversible addition-fragmentation chain transfer (RAFT)[57] and reverse iodine transfer polymerization (RITP).[58] A surfactant-free RAFT emulsion polymerization found no correlation between particle size and RAFT agent/initiator addition, but did report that the final particle size was largest when the highest concentration of RAFT agent was used.[59] Such phenomenon has been referred to in passing in the NMP literature as a possible side effect of the "superswelling" theory like that observed in miniemulsion[53] and described thermodynamically for nucleation in a RAFT emulsion system.[57] Other theories have included differences in ionic strength effects and shell thickness when acrylic acid is also present in the seed stage.[58]

To overcome this difficulty, many groups have begun pre-fabricating amphiphilic macroini-

tiators which act both as the stabilizing moiety and the initiator to perform emulsion polymerization in the absence of additional surfactant. Although in these polymerizations, increasing the concentration of initiator decreases the particle size,[60, 61, 62] all other conditions being equal, it still does not eliminate the difficulty of having a strong correlation between the initiator concentration and the particle size. However, changing the amphiphilic block sizes on macro-RAFT agents has been shown to modify the particle size independently,[59] but requires individualized pre-synthesis for each experiment of a different solids content or molecular weight target.

Many instances of creating BA/St and BA/MMA block copolymers have been reported by NMP, including "onion-like" microphases inside the latex particles[54] where the two polymers undergo phase separation inside the particles to create novel latex films. The range of monomers and morphologies of the polymer colloids created by NMP has also expanded to include self assembly of amphiphilic block copolymers into vesicles with 4-vinylpyridine,[63] and thermosensitive nanogels created with N,N-diethyl acrylamide.[64]

2.3.2 Dispersed Phase Atom Transfer Radical Polymerization

Regular ATRP has often shown poor results in miniemulsion; the result of the air sensitivity of Cu(I) and its exposure to air during the miniemulsification process. Miniemulsions were first conducted in reverse ATRP, using the non-ionic surfactant Brij 98.[65] However, at high temperatures, this led to colloidal instability, but it was shown by Simms et al. that the cationic surfactant CTAB could stabilize the system even at 90^{o}C.[66]

Reverse ATRP with BMA has stood out as the benchmark for ATRP miniemulsion, but often produces somewhat higher polydispersities than a bulk equivalent.[67] For water-based ATRP miniemulsion, care still needs to be taken in choosing the proper initiator (fast decomposition) and the appropriate Cu(II):initiator ratio to strike a delicate balance between induction time and control.[43]

ARGET ATRP has emerged as the simplest method of conducting ATRP in the dispersed phase,[35, 34, 68, 69, 70, 71, 72] but it appears to be very ligand specific with the reaction of the reducing agent to reduce the Cu(II) to Cu(I) in situ. AGET ATRP has been successfully employed in miniemulsion with a butyl acrylate/BPMODA (bis(2-pyridylmethyl)octadecylamine) system stabilized by Brij 98.[34, 35] This method employed the very strong, water soluble re-

ducing agent ascorbic acid (AA) in a ratio of 0.1-0.5 AA:copper. It proved to be a very robust process with respect to the amount of reducing agent added, and it was also demonstrated that AGET miniemulsion can also be conducted in the presence of air, but larger amount of AA was required to scavenge oxygen.[34]

Hydrophobic ligands are used for miniemulsion polymerizations because they have appreciable monomer solubility and are less likely to partition into the water phase to ensure the mediating agents will be present at the site of polymerization.[73, 17] Work has been done primarily with EHA_6TREN (tris[2-di(2-ethylhexyl acrylate)aminoethyl]amine)[66, 74, 75] and BPMODA[34, 35, 76, 74] in aqueous dispersed systems.

An ARGET miniemulsion polymerization system has been claimed,[70] beginning with an amphiphilic ATRP initiator, which acts as both the surfactant and the alkyl halide initiator for polymerization. The ligand BPMODA was added in 10 times excess to the $CuBr_2$, and ascorbic acid was used as the reducing agent to reduce the Cu(II) to Cu(I). The reduction of chains:$CuBr_2$ was not significant in this system, where controlled polymerization was demonstrated with only 10 chains:$CuBr_2$, when true ARGET conditions in solution polymerization are often in the 100–1000 $CuBr_2$ per chain range and can be conducted without excess ligand, which is the most costly of the raw materials.[77]

Recently, Simms et al.[75] demonstrated that extremely high molecular weights ($\sim 10^6$ g·mol^{-1}) can be achieved in reverse ATRP miniemulsion employing a redox initiation system of hydrogen peroxide/ascorbic acid. This result is extremely novel as there was no noticeable diminishment of rate due to a buildup of the persistent radical. It has been suggested that a possible catalyst regeneration mechanism is at work (similar to ARGET). However, unlike typical ARGET polymerizations, this system employed extremely high concentrations of catalyst per chain (7 $CuBr_2$:chain).

2.3.3 Dispersed Phase Catalytic Chain Transfer

CCT has successfully been demonstrated in the aqueous disperse systems of emulsion and miniemulsion polymerization.[78, 79, 40, 80, 81] When the catalyst COBF (bis[(difluoroboryl) dimethylglyoximato]cobalt(II), Figure 2.4) is employed, it undergoes partitioning into both the monomer and water phases.[79, 80, 81] Nucleation can be suppressed in systems with a high amount of COBF in the aqueous phase, as monomeric radicals are caught in a continuous

loop of chain transfer and never reach the z-meric length necessary for particle entry.[79] Because of the high activity of the Co(II) catalyst, many monomeric radicals are produced within the particles, which can lead to a high rate of radical exit from the particles.

CCT-mediated emulsion polymerizations typically proceed in a regime where the polymer particles outnumber the catalytic chain transfer agent (CCTA) molecules; consequently CCTA mass transport has to be sufficiently fast to ensure that multiple polymer particles can be mediated by a single CCTA molecule.[79, 82, 78, 83, 84, 80] However, evidence of compartmentalization was observed experimentally in seeded emulsion polymerization of methyl methacrylate (MMA).[85] Polymerization of the second stage monomer in the presence of COBF in PMMA seed particles, swollen below the maximum saturation concentration, exhibited multimodal MWDs. The multimodal MWDs were observed independently of the size of the swollen PMMA particles and the average number of CCTA molecules per particle ($\bar{n}_{\mathrm{CCTA}}$). The observed multimodal MWDs were attributed to compartmentalization of the catalytic chain transfer agent (CCTA) as a consequence of the reduced mobility at the high instantaneous conversion of the polymer particles.[85]

2.3.4 Compartmentalization in Controlled Dispersed Phase Polymerizations

Understanding of compartmentalization effects in controlled aqueous dispersed systems has remained elusive. When a rate enhancement was not observed in early studies of St/TEMPO miniemulsion compared to bulk, it was assumed that no compartmentalization effects could occur because $\bar{n}$ was so low. This was attributed not to enhanced radical exit but instead to dominating chain deactivation.[86] However, Pan et al.[87] found that the length of induction period for a miniemulsion with TEMPO initiated solely by styrene autopolymerization was much longer than in bulk. This suggested a confined space effect, where generated radical pairs were unable to diffuse away fast enough, and preferentially underwent termination rather than generating new chains.

The discussion of compartmentalization in living systems began when Butté et al.[88] and Charleux[89] independently published simulations of NMP miniemulsions with different conclusions. Butté et al. included instances of thermal polymerization and the compartmentalization of the nitroxide in different particles. Using an alkoxyamine initiator, the

total amount of free TEMPO inside a particle was assumed to be dependent upon the number of radicals and dead chains in the system if TEMPO was unable to exit the particle. In these conditions, it was found that the rate slowed, but control of the PDI was enhanced with diminishing particle sizes. It was rationalized that compartmentalization decreases termination between growing chains, but maximized the germinate termination of the radicals produced by thermal initiation. Charleux, on the other hand, discussed a situation absent of thermal polymerization and one where SG1 was assumed to be uncompartmentalized and able to freely diffuse through the aqueous phase to maintain a constant concentration of free SG1 in each particle. Using this situation, she commented on the buildup of free nitroxide and rederived the PRE for miniemulsions. She found that diminishing particle size led to an enhancement in the rate, as a consequence of slow termination reactions and thus a slower buildup of SG1.

Zetterlund et al.[90, 91, 92, 93, 94] built on the framework of Butté et al.[88] and discussed the different and opposing compartmentalization effects that could occur in a dispersed living system:

Confined Space Effect This leads to an increase in the rate of deactivation and termination inside a particle because the two molecules involved in the reaction are physically closer to one another than in a bulk polymerization. During deactivation, the radicals will recombine faster, adding fewer monomer units and shifting the equilibrium towards the dormant chains. This would increase the degree of "livingnes" by suppressing termination. When compartmentalization of the deactivation species is considered, the confined space effect is incorporated into the population balances by:

$$R_{deact} = \frac{k_{deact}}{N_A V_p}(i_{radicals})(j_{nitroxide}) \tag{2.10}$$

where the rate of deactivation becomes inversely proportional to the particle volume, which is not the case when nitroxide compartmentalization is neglected.

Termination also experiences a confined space effect, but this is only evident in systems where thermal polymerization is prevalent, as it is rare to have more than one radical active at a time. This increase in radical termination was suggested by Butté et al.[88] and Pan et al.[87] but was not fully understood as the confined space effect. This effect is accounted for

through the compartmentalization of the radicals.

Radical Segregation This is the dominant compartmentalization effect in conventional emulsions where the rate of reaction is increased as radicals propagating in different particles cannot terminate with each other. This effect is accounted for through compartmentalization of the radicals, and the overall reaction rate is calculated as a function of N_p (Equation 2.2).

Through simulations of both NMP[90] and ATRP[91] miniemulsions up to only 10% conversion, Zetterlund proposed that at smaller particle sizes the confined space effect dominated and the rate of polymerization was diminished while control was increased. At moderate particle sizes and in the absence of thermal initiation, it was possible to exceed the predicted rate of reaction in bulk whereby the effect of radical segregation dominated. At large particle sizes, the rate of polymerization tended to that of bulk. The particle sizes at which these effects change depend upon the reaction conditions and the total concentration of chains in the system. Compartmentalization effects will become more pronounced at larger particle sizes with a lower concentration of chains in the system.[93] Looking specifically at the first 1% conversion of an ATRP polymerization, the extent of compartmentalization increased if Br, rather than Cl, is used as the halogen to mediate polymerization; the result of the increased deactivation rate with Br.[95]

While Butté included the compartmentalization of nitroxide, and thus accounted for the confined space effect, both he and Zetterlund did not include the possibility of partitioning of the deactivating species into the water phase. There is experimental evidence of this for TEMPO[96] and for Cu(II) species.[97] Charleux did include aqueous-phase effects, but simplified the system. Thus, the simulations performed by each of these groups can be successfully applied to some experimental systems, but cannot serve as a definitive conclusion on compartmentalization effects for different living chemistries.

Experimentally, compartmentalization has been found for TEMPO/St system[92], where smaller particle sizes showed lower rates of polymerization and a higher degree of livingness, while bulk polymerization was found to be fastest of all, but a degree of control equivalent to the medium sized particles (90 nm). With the nitroxide SG1, compartmentalization effects have been found to only reduce the rate of polymerization to a small extent in

microemulsion[94] and not at all in emulsion polymerization.[98] This is the result of SG1's slower deactivation rate and higher rate of exit from the particles into the aqueous phase.

Compartmentalization has also been seen experimentally in a reverse ATRP system which employed a redox initiator of hydrogen peroxide and ascorbic acid.[99] Here, very low concentrations of chains per particle allowed extremely high molecular weight ($\sim 10^6$ g·mol^{-1}) in short reaction times ($\sim$8 hours). A reduction in particle size tended to reduce the average number of radicals per particle per chain, and diminishing particle size led to increased control, but lower rates of reaction.

In catalytic chain transfer, the manifestation of compartmentalization of both the radicals and the CCTA (catalytic chain transfer agent) are quite different. Experimentally this has been observed to create multimodal molecular weight distributions (MWDs) in seeded emulsion systems with COBF as the CCTA.[85] This is attributed to the statistical distribution of the CCTA over all of the polymer particles, and suggests that there are two limiting cases in CCT-mediated emulsion: the early stage of the polymerization where the global concentration of the CCTA governs the MWD and a later stage where the compartmentalization of CCTA in the particles governs the MWD.

2.3.5 Modeling of Compartmentalization in Controlled Systems

Approaches to modeling controlled systems depend upon the type of effects that are being investigated. PREDICI has been favoured when the emulsified system is considered to be operating in pseudo-bulk conditions, and both radical and nitroxide segregation can be discounted. It is in this realm where issues concerning partitioning of the catalyst between the water and monomer phases[100] and interfacial effects have been considered.[101, 102]

Butté,[88] Charleux[26] and Zetterlund[90] have derived, and solved numerically, the population balance equations to account for compartmentalization effects and demonstrate the effect of particle size on the rate of polymerization and the polydispersity. Butté and Charleux both used the method of moments to calculate the polydispersity of the dormant chains, a method that allows the effect of bimolecular termination to be included. Zetterlund et al. tended to focus on commenting on the individual rates of propagation, activation and deactivation and their influence by particle size for the early stages of polymerization. Insights into the theoretical polydispersity these types of conditions would produce are

made based solely on the number of activation/deactivation steps (Equation 2.8) and do not include termination or the loss of chains over the course of the reaction. No population balance approach, which also takes into account compartmentalization effects, has ever demonstrated a predicted chain length distribution over the course of the polymerization for a controlled chemistry.

Compartmentalization effects have been modeled using the Monte Carlo approach,[103, 104, 105] where the possible reaction schemes for 10^5 different particles needed to be determined in order to estimate the chain length distribution. The conclusions they drew were identical to those of Zetterlund et al.[90] in that there are opposing effects on the reaction rate and degree of livingness from both the confined space effect and radical segregation.

Finally, no modeling compartmentalized studies of ATRP or NMP have included the possibility of mediating species partitioning, although Peklak and Butté[106] have discussed RAFT seeded emulsion from a population balance approach which included both radical segregation and entry/exit coefficients for radicals and the RAFT agent. This study was also unique as it provided experimental data to complement the compartmentalization studies, something that has not yet been done for NMP or ATRP.

References

[1] Gilbert, R. G. *Emulsion Polymerization - a Mechanistic Approach.* Academic Press, San Diego, CA, (1995).

[2] Schork, F. J., Luo, Y., Smulders, W., Russum, J. P., Butte, A., and Fontenot, K. *Advances in Polymer Science* **175**(Polymer Particles), 129–255 (2005).

[3] de la Cal, J. C., Leiza, J. R., Asua, J. M., Butte, A., Storti, G., and Morbidelli, M. *Handbook of Polymer Reaction Engineering* **1**, 249–322 (2005).

[4] Harkins, W. D. *Journal of the American Chemical Society* **69**(6), 1428–1444 (1947).

[5] Smith, W. V. and Ewart, R. H. *Journal of Chemical Physics* **16**, 592–599 (1948).

[6] Roberts, G. E., Barner-Kowollik, C., Davis, T. P., and Heuts, J. P. A. *Macromolecules* **36**(4), 1054–1062 (2003).

[7] Odian, G. *Principles of Polymerization.* John Wiley & Sons, Inc, (2004).

[8] Chamberlain, B. J., Napper, D. H., and Gilbert, R. G. *Journal of the Chemical Society, Faraday Transactions 1: Physical Chemistry in Condensed Phases* **78**(2), 591–606 (1982).

[9] Lichti, G., Gilbert, R. G., and Napper, D. H. *Theoretical predictions of the particle size and molecular weight distributions in emulsion polymerizations.*, 93–144. Emulsion Polymerization. Academic Press, New York (1982).

[10] Butte, A., Storti, G., and Morbidelli, M. *Macromolecular Theory and Simulations* **11**(1), 37–52 (2002).

[11] Ghielmi, A., Storti, G., Morbidelli, M., and Ray, W. H. *Macromolecules* **31**(21), 7172–7186 (1998).

[12] Tobita, H. *Acta Polym.* **46**(3), 185–203 (1995).

[13] Lichti, G., Gilbert, R. G., and Napper, D. H. *Journal of Polymer Science: Polymer Chemistry Edition* **18**(4), 1297–1323 (1980).

[14] Butte, A., Storti, G., and Morbidelli, M. *Macromolecular Theory and Simulations* **11**(1), 22–36 (2002).

[15] Georges, M. K., Veregin, R. P. N., Kazmaier, P. M., and Hamer, G. K. *Macromolecules* **26**(11), 2987–2988 (1993).

[16] Moad, G. and Solomon, D. H. *The Chemistry of Radical Polymerization - Second fully revised edition.* Elsevier Ltd., Oxford UK, (2006).

[17] Cunningham, M. F. *Progress in Polymer Science* **27**(6), 1039–1067 (2002).

[18] Braunecker, W. A. and Matyjaszewski, K. *Journal of Molecular Catalysis. A, Chemical* **254**(1-2), 155–164 (2006).

[19] Fischer, H. *Macromolecules* **30**(19), 5666–5672 (1997).

[20] Fischer, H. *Chemical Reviews* **101**(12), 3581–3610 (2001).

[21] Tang, W., Fukuda, T., and Matyjaszewski, K. *Macromolecules* **39**(13), 4332–4337 (2006).

[22] Keoshkerian, B., Georges, M., Quinlan, M., Veregin, R., and Goodbrand, B. *Macromolecules* **31**(21), 7559–7561 (1998).

[23] Benoit, D., Harth, E., Fox, P., Waymouth, R. M., and Hawker, C. J. *Macromolecules* **33**(2), 363–370 (2000).

[24] Mchale, R., Aldabbagh, F., and Zetterlund, P. B. *Journal of Polymer Science Part A: Polymer Chemistry* **45**(11), 2194–2203 (2007).

[25] Dire, C., Belleney, J., Nicolas, J., Bertin, D., Magnet, S., and Charleux, B. *Journal of Polymer Science Part A: Polymer Chemistry* **46**(18), 6333–6345 (2008).

[26] Charleux, B., Nicolas, J., and Guerret, O. *Macromolecules* **38**(13), 5485–5492 (2005).

[27] Nicolas, J., Dire, C., Mueller, L., Belleney, J., Charleux, B., Marque, S. R. A., Bertin, D., Magnet, S., and Couvreur, L. *Macromolecules* **39**(24), 8274–8282 (2006).

[28] Nicolas, J., Mueller, L., Dire, C., Matyjaszewski, K., and Charleux, B. *Macromolecules* **42**(13), 4470–4478 (2009).

[29] Kato, M., Kamigaito, M., Sawamoto, M., and Higashimura, T. *Macromolecules* **28**(5), 1721–1723 (1995).

[30] Matyjaszewski, K. *Macromolecules* **31**(15), 4710–4717 (1998).

[31] Braunecker, W. A. and Matyjaszewski, K. *Progress in Polymer Science* **32**(1), 93–146 (2007).

[32] Faucher, S., Okrutny, P., and Zhu, S. *Industrial and Engineering Chemistry Research* **46**(9), 2726–2734 (2007).

[33] Fu, Y., Mirzaei, A., Cunningham, M. F., and Hutchinson, R. A. *Macromolecular Reaction Engineering* **1**(4), 425–439 (2007).

[34] Min, K., Jakubowski, W., and Matyjaszewski, K. *Macromolecular Rapid Communications* **27**(12), 982–982 (2006).

[35] Min, K., Gao, H., and Matyjaszewski, K. *Journal of the American Chemical Society* **127**(11), 3825–3830 (2005).

[36] Jakubowski, W. and Matyjaszewski, K. *Angewandte Chemie International Edition* **45**(27), 4482–4486 (2006).

[37] Jakubowski, W., Min, K., and Matyjaszewski, K. *Macromolecules* **39**(1), 39–45 (2006).

[38] Matyjaszewski, K., Jakubowski, W., Min, K., Tang, W., Huang, J., Braunecker, W. A., and Tsarevsky, N. V. *Proceedings of the National Academy of Sciences U.S.A.* **103**(42), 15309–15314 (2006).

[39] Heuts, J. P. A., Roberts, G. E., and Biasutti, J. D. *Australian Journal of Chemistry* **55**(6,7), 381–398 (2002).

[40] Smeets, N. M. B., Meda, U. S., Heuts, J. P. A., Keurentjes, J. T. F., van Herk, A. M., and Meuldijk, J. *Macromolecular Symposia* **259**(1), 406–415 (2007).

[41] Bon, S. A. F., Bosveld, M., Klumperman, B., and German, A. L. *Macromolecules* **30**(2), 324–326 (1997).

[42] Marestin, C., Noel, C., Guyot, A., and Claverie, J. *Macromolecules* **31**(12), 4041–4044 (1998).

[43] Cunningham, M. F. *Progress in Polymer Science* **33**(4), 365–398 (2008).

[44] MacLeod, P. J., Barber, R., Odell, P. G., Keoshkerian, B., and Georges, M. K. *Macromolecular Symposia* **155**(Emulsion Polymers), 31–38 (2000).

[45] Prodpran, T., Dimonie, V. L., Sudol, E. D., and El-Aasser, M. S. *Macromol.Symp.* **155**(Emulsion Polymers), 1–14 (2000).

[46] Pan, G., Sudol, E. D., Dimonie, V. L., and El-Aasser, M. S. *Macromolecules* **34**(3), 481–488 (2001).

[47] Keoshkerian, B., Szkurhan, A. R., and Georges, M. K. *Macromolecules* **34**(19), 6531–6532 (2001).

[48] Georges, M. K., Lukkarila, J. L., and Szkurhan, A. R. *Macromolecules* **37**(4), 1297–1303 (2004).

[49] Farcet, C., Charleux, B., and Pirri, R. *Macromolecular Symposia* **182**(1), 249–260 (2002).

[50] Luo, Y., Tsavalas, J., and Schork, F. J. *Macromolecules* **34**(16), 5501–5507 (2001).

[51] Nicolas, J., Charleux, B., and Magnet, S. *Journal of Polymer Science Part A: Polymer Chemistry* **44**(13), 4142–4153 (2006).

[52] Nicolas, J., Charleux, B., Guerret, O., and Magnet, S. *Macromolecules* **38**(24), 9963–9973 (2005).

[53] Nicolas, J., Charleux, B., Guerret, O., and Magnet, S. *Angewandte Chemie International Edition* **43**(45), 6186–6189 (2004).

[54] Nicolas, J., Ruzette, A.-V., Farcet, C., Gerard, P., Magnet, S., and Charleux, B. *Polymer* **48**(24), 7029–7040 (2007).

[55] Charleux, B. and Nicolas, J. *Polymer* **48**(20), 5813–5833 (2007).

[56] Simms, R. W., Hoidas, M. D., and Cunningham, M. F. *Macromolecules* **41**(4), 1076–1079 (2008).

[57] Luo, Y. and Cui, X. *Journal of Polymer Science Part A: Polymer Chemistry* **44**(9), 2837–2847 (2006).

[58] Tonnar, J. and Lacroix-Desmazes, P. *Soft Matter* **4**(6), 1255–1260 (2008).

[59] Rieger, J., Osterwinter, G., Bui, C., Stoffelbach, F., and Charleux, B. *Macromolecules* **42**(15), 5518–5525 (2009).

[60] Dire, C., Magnet, S., Couvreur, L., and Charleux, B. *Macromolecules* **42**(1), 95–103 (2009).

[61] Wi, Y., Lee, K., Lee, B. H., and Choe, S. *Polymer* **49**(26), 5626–5635 (2008).

[62] Rieger, J., Stoffelbach, F., Bui, C., Alaimo, D., Jerome, C., and Charleux, B. *Macromolecules* **41**(12), 4065–4068 (2008).

[63] Delaittre, G., Dire, C., Rieger, J., Putaux, J.-L., and Charleux, B. *Chemical Communications* (20), 2887–2889 (2009).

[64] Delaittre, G., Save, M., and Charleux, B. *Macromolecular Rapid Communications* **28**(15), 1528–1533 (2007).

[65] Li, M. and Matyjaszewski, K. *Macromolecules* **36**(16), 6028–6035 (2003).

[66] Simms, R. W. and Cunningham, M. F. *Journal of Polymer Science Part A: Polymer Chemistry* **44**(5), 1628–1634 (2006).

[67] Li, M. and Matyjaszewski, K. *Journal of Polymer Science Part A: Polymer Chemistry* **41**(22), 3606–3614 (2003).

[68] Stoffelbach, F., Belardi, B., Santos, J. M. R. C. A., Tessier, L., Matyjaszewski, K., and Charleux, B. *Macromolecules* **40**(25), 8813–8816 (2007).

[69] Min, K., Yu, S., il Lee, H., Mueller, L., Sheiko, S. S., and Matyjaszewski, K. *Macromolecules* **40**(18), 6557–6563 (2007).

[70] Stoffelbach, F., Griffete, N., Bui, C., and Charleux, B. *Chemical Communications* (39), 4807–4809 (2008).

[71] Dong, H., Mantha, V., and Matyjaszewski, K. *Chemistry of Materials* **21**(17), 3965–3972 (2009).

[72] Li, W., Matyjaszewski, K., Albrecht, K., and Moller, M. *Macromolecules* **42**(21), 8228–8233 (2009).

[73] Qiu, J., Charleux, B., and Matyjaszewski, K. *Progress in Polymer Science* **26**(10), 2083–2134 (2001).

[74] Li, M., Min, K., and Matyjaszewski, K. *Macromolecules* **37**(6), 2106–2112 (2004).

[75] Simms, R. W. and Cunningham, M. F. *Macromolecules* **40**(4), 860–866 (2007).

[76] Min, K., Gao, H., and Matyjaszewski, K. *Journal of the American Chemical Society* **128**(32), 10521–10526 (2006).

[77] Chan, N., Cunningham, M. F., and Hutchinson, R. A. *Macromolecular Chemistry and Physics* **209**(17), 1797–1805 (2008).

[78] Suddaby, K. G., Haddleton, D. M., Hastings, J. J., Richards, S. N., and O'Donnell, J. P. *Macromolecules* **29**(25), 8083–8091 (1996).

[79] Kukulj, D., Davis, T. P., and Gilbert, R. G. *Macromolecules* **30**(25), 7661–7666 (1997).

[80] Smeets, N. M. B., Heuts, J. P. A., Meuldijk, J., and van Herk, A. M. *Journal of Polymer Science Part A: Polymer Chemistry* **46**(17), 5839–5849 (2008).

[81] Smeets, N. M. B., Heuts, J. P. A., Meuldijk, J., Cunningham, M. F., and van Herk, A. M. *Macromolecules* **42**(17), 6422–6428 (2009).

[82] Bon, S. A. F., Morsley, D. R., Waterson, J., Haddleton, D. M., Lees, M. R., and Horne, T. *Macromolecular Symposia* **165**(1), 29–42 (2001).

[83] Kukulj, D., Davis, T. P., Suddaby, K. G., Haddleton, D. M., and Gilbert, R. G. *Journal of Polymer Science Part A: Polymer Chemistry* **35**(5), 859–878 (1997).

[84] Haddleton, D. M., Morsley, D. R., O'Donnell, J. P., and Richards, S. N. *Journal of Polymer Science Part A: Polymer Chemistry* **37**(18), 3549–3557 (1999).

[85] Smeets, N. M. B., Heuts, J. P. A., Meuldijk, J., Cunningham, M. F., and van Herk, A. M. *Macromolecules* **42**(19), 7332–7341 (2009).

[86] Pan, G., Sudol, E. D., Dimonie, V. L., and El-Aasser, M. S. *Macromolecules* **35**(18), 6915–6919 (2002).

[87] Pan, G., Sudol, E. D., Dimonie, V. L., and El-Aasser, M. S. *Journal of Polymer Science Part A: Polymer Chemistry* **42**(19), 4921–4932 (2004).

[88] Butte, A., Storti, G., and Morbidelli, M. *DECHEMA Monogr.* **134**(6th International Workshop on Polymer Reaction Engineering), 497–507 (1998).

[89] Charleux, B. *Macromolecules* **33**(15), 5358–5365 (2000).

[90] Zetterlund, P. B. and Okubo, M. *Macromolecules* **39**(26), 8959–8967 (2006).

[91] Kagawa, Y., Zetterlund, P. B., Minami, H., and Okubo, M. *Macromolecular Theory and Simulations* **15**(8), 608–613 (2006).

[92] Maehata, H., Buragina, C., Cunningham, M., and Keoshkerian, B. *Macromolecules* **40**(20), 7126–7131 (2007).

[93] Zetterlund, P. B. and Okubo, M. *Macromolecular Theory and Simulations* **16**(3), 221–226 (2007).

[94] Zetterlund, P. B., Wakamatsu, J., and Okubo, M. *Macromolecules* **42**, 6944–6952 (2009).

[95] Zetterlund, P. B., Kagawa, Y., and Okubo, M. *Macromolecules* **42**(7), 2488–2496 (2009).

[96] Ma, J. W., Cunningham, M. F., McAuley, K. B., Keoshkerian, B., and Georges, M. K. *Macromol.Theory Simul.* **11**(9), 953–960 (2002).

[97] Qiu, J., Pintauer, T., Gaynor, S. G., Matyjaszewski, K., Charleux, B., and Vairon, J. P. *Macromolecules* **33**(20), 7310–7320 (2000).

[98] Delaittre, G. and Charleux, B. *Macromolecules* **41**(7), 2361–2367 (2008).

[99] Simms, R. W. and Cunningham, M. F. *Macromolecules* **41**, 5148–5155 (2008).

[100] Kagawa, Y., Zetterlund, P. B., Minami, H., and Okubo, M. *Macromolecules* **40**(9), 3062–3069 (2007).

[101] Zetterlund, P. B., Nakamura, T., and Okubo, M. *Macromolecules* **40**(24), 8663–8672 (2007).

[102] Nakamura, T., Zetterlund, P. B., and Okubo, M. *Macromol.Rapid Commun.* **27**(23), 2014–2018 (2006).

[103] Tobita, H. and Yanase, F. *Macromolecular Theory and Simulations* **16**(4), 476–488 (2007).

[104] Tobita, H. *Macromolecular Theory and Simulations* **16**(9), 810–823 (2007).

[105] Tobita, H. *Macromolecular Symposia* **261**(1), 36–45 (2008).

[106] Peklak, A. D. and Butte, A. *Journal of Polymer Science Part A: Polymer Chemistry* **44**(20), 6114–6135 (2006).

Chapter 3

Compartmentalization Effects on the Rate of Polymerization and the Degree of Control in ATRP Aqueous Dispersed Phase Polymerization

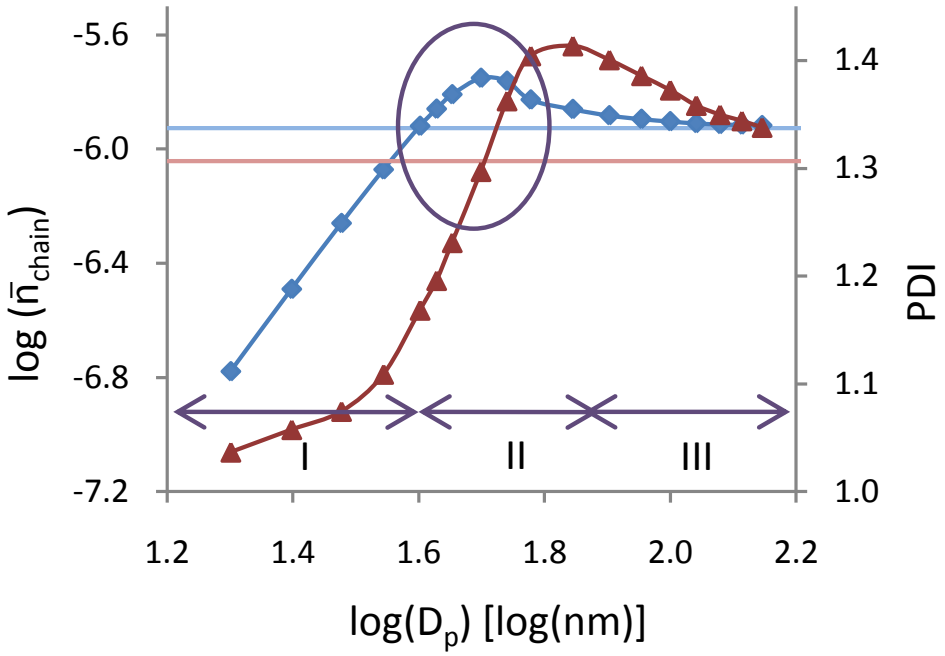

Preface

When I began working on my PhD at Queen's, the first experimental evidence of compartmentalization in both ATRP and NMP had just been reported by the Cunningham lab. Also, there was a great deal of activity in the creation of models to describe the phenomenon; however, it was more predominant in the NMP chemistry. ATRP simulations had been published, but none took into account the higher activity ligands now in use in most ATRP dispersed phase systems nor made any direct comment about the polydispersity or livingness of the polymer chains. While the conclusions made in this work about the rate of polymerization correspond both to the experimental evidence and previously published simulations, the conclusions about PDI and chain livingness, and especially the discussion concerning lowering of catalyst concentration, are relevant for future investigation into the feasibility of performing dispersed phase ATRP in an economically viable manner.

Abstract

Compartmentalization in atom transfer radical polymerization (ATRP) in an aqueous dispersed phase system has been investigated theoretically to understand the effects of particle size on the rate of polymerization and the degree of control on the livingness and polydispersity index (PDI) for the system n-butyl methacrylate/CuBr/EHA_6TREN. The simulations indicate that there exists a defined range of particle sizes where the rate of polymerization is higher than that of a bulk system, and where PDI and frequency of termination remain below that of bulk polymerization. For this highly active catalyst system, the livingness of the chains is a function only of the particle size and is independent of the rate of reaction. Furthermore, simulations conducted with very low catalyst concentrations suggest that the rate of polymerization is dependent on the absolute amount of catalyst in the system rather than the steady-state Cu(I)/Cu(II) ratio that applies for bulk polymerization. At low catalyst concentrations, the rate of polymerization decreases, and the PDI increases with diminishing catalyst concentration, whereas the chain livingness is improved.

3.1 Introduction

Controlled/living polymerization has emerged as a powerful method for creating polymers with tailored molecular architectures under mild reaction conditions. However, this technology has not yet found widespread adoption for industrial production. One of the limitations is the difficulty associated with performing these polymerizations in aqueous dispersed systems such as emulsion or miniemulsion. While dispersed phase polymerization is possible, the complexities of performing heterogeneous living polymerization are not yet fully understood.[1, 2]

Recent experimental advances in ATRP miniemulsion polymerization have begun to make this polymerization technique more amenable to large-scale polymerization, especially AGET (activators generated by electron transfer) ATRP[3, 4, 5, 6, 7, 8, 9] in which a reducing agent converts the less air-sensitive Cu(II) into Cu(I) in situ to begin the reaction. AGET ATRP also lends itself to lower catalyst concentrations. Simms and Cunningham have shown that reverse ATRP with the ligand EHA_6TREN can be performed in miniemulsion using a cationic surfactant,[10] which increases the stability of the emulsion system and allows higher temperature polymerization, and have also achieved very high molecular weight polymers with a fast reaction rate in a similar system.[11]

In bulk or solution ATRP, the steady state rate of polymerization is controlled by the concentration of alkyl halide, $[P-X]$, and the ratio of Cu(I)/Cu(II) in the system, when termination reactions are considered negligible (Equation 3.1). In this work, we discuss the first implications of low catalyst concentrations in aqueous dispersed phase polymerization. In bulk or solution polymerization, the basis for low catalyst ATRP is that the Cu(I)/Cu(II) ratio, rather than the absolute concentrations of either species, is rate determining. Thus low catalyst concentration ATRP systems, like ARGET (Activators ReGenerated by Electron Transfer) and ICAR (Initiators for Continuous Activator Regeneration), maintain a constant, high Cu(I)/Cu(II) ratio by regenerating Cu(I) from Cu(II) created through termination reactions either through the addition of a reducing agent or new radical generation respectively.[12]

$$R_p = k_p[M]\frac{k_{act}}{k_{deact}}[P-X]\frac{[Cu(I)]}{[Cu(II)]} \tag{3.1}$$

Conventional free radical emulsion polymerization exhibits a phenomenon called radical compartmentalization, whereby the propagating radicals present in different particles are unable to terminate mutually, thereby causing an increasing overall rate of reaction with diminishing particle size. In living/controlled polymerization, compartmentalization affects both the rate of termination and the rate of deactivation by the physical isolation of radicals and deactivating species inside separate particles; this was first observed through simulations for living polymerization controlled by reversible termination, namely, nitroxide mediated polymerization (NMP)[13, 14] and later for ATRP.[15] Compartmentalization has since been demonstrated experimentally in miniemulsion for both chemistries[16, 17] with the observed rate of polymerization decreasing with decreasing particle size. In NMP, these compartmentalization effects appear to be dependent on the nitroxide type; whereas rate decreases were observed in miniemulsion using TEMPO,[16] with the higher activity and more hydrophilic nitroxide, SG1, compartmentalization effects have been found to reduce the rate of polymerization only to a small extent in microemulsion[18] and not at all in emulsion polymerization.[19] This was attributed to the SG1's slower deactivation rate and higher rate of exit from the particles into the aqueous phase. Mathematically, Charleux[20] has described NMP compartmentalization without the segregation of the nitroxide SG1. The lack of compartmentalization effects observed experimentally in these systems can be explained if the nitroxide is able to diffuse easily through the aqueous phase so fluctuations of the nitroxide concentration in each particle are negligible.

The compartmentalization effects of enhanced deactivation and radical segregation were first discussed by Zetterlund and Okubo[14] in simulations of TEMPO-mediated styrene polymerization. The confined space effect leads to an increase in the rates of deactivation and termination inside the particle (compared to bulk polymerization) because the two molecules involved in the reactions are physically confined to a small reaction volume. Because of the confined space effect in ATRP, the rate of deactivation can mathematically be shown to be dependent on the volume of the particle as[15]

$$R_{deact} = \frac{k_{deact}}{(N_A V_p)^2} \sum_i \sum_j (i)(j) N_{i,j} \tag{3.2}$$

where $N_{i,j}$ is the fraction of particles containing i propagating radicals and j Cu(II) deactivator molecules, k_{deact} is the rate constant for deactivation, N_A is Avogadro's number,

and V_p is the volume of the particle. Using a population balance approach, these studies by Zetterlund and Okubo[14] for NMP and by Kagawa et al.[15] for ATRP show that in the absence of new chain generation, the rate of polymerization first increases (due to radical segregation) and then diminishes (due to enhanced deactivation) with decreasing particle sizes.

Tobita[21, 22, 23] conducted Monte Carlo simulations to investigate compartmentalization effects in NMP. Whereas his results are consistent with the conclusions of Butte et al.[13] and Zetterlund and Okubo,[14], he also suggests that fluctuations in the number of deactivator molecules in the particles can lead to instances of higher radical concentrations and result in an increase in rate.[22] Zetterlund and Okubo attributed the same rate acceleration to radical segregation.[14]

Simulations of ATRP in dispersed systems have only been conducted for the ligand dNbpy,[15, 24, 25] which is a lower activity ligand and requires high catalyst concentrations and higher polymerization temperatures. Whereas dNbpy is soluble in monomer, the catalyst in the Cu(II) form does have a small but finite water solubility, which is known to be detrimental to maintaining control in ATRP miniemulsion polymerizations. Simulations examining the effect of Cu partitioning between the monomer and aqueous phases in a dNbpy ATRP system have been undertaken by Kagawa et al.[24] in the absence of compartmentalization effects. They concluded that the loss of deactivator, Cu(II), to the aqueous phase increased both the rate of polymerization and the polydispersity index (PDI). No previous published research has involved simulations using an active and highly hydrophobic ligand to study ATRP compartmentalization effects. We have simulated an ATRP system with the catalyst CuBr/EHA_6TREN.[10, 11, 17, 26, 27] This catalyst/ligand is a more suitable choice for examining compartmentalization, especially considering that compartmentalization effects have been observed experimentally with this catalyst system.[17] Compared with the low activity ligand dNbpy, EHA_6TREN has negligible water solubility and a significantly higher K_{eq}, allowing polymerizations to be conducted at lower temperatures and with reduced catalyst concentrations. Whereas previous simulations[25] with dNbpy were limited to 1% conversion, we were able to run simulations with the high activity CuBr/EHA_6TREN catalyst up to 10% conversion.

Presented here is the first theoretical investigation of ATRP compartmentalization with

a highly active catalyst/ligand (CuBr/EHA_6TREN) system and with low catalyst concentrations. We focus, in particular, on the PDI and livingness of the growing chains. There is a defined range of particle sizes where the rate of polymerization can be enhanced above that of bulk polymerization while maintaining excellent control, with an expected PDI and degree of termination below that of bulk polymerization. The implications of our findings to the possibility of using very low catalyst concentrations in ATRP-dispersed systems are discussed. These simulations differ significantly from previous ATRP simulations[15, 25] in the selection of a high-activity catalyst/ligand system and in-depth examination of the effect of particle size on the PDI and the livingness of the system.

3.2 Model Development

3.2.1 Compartmentalized Model

The modified Smith-Ewart equations developed by Kagawa et al.[15] for ATRP were adapted and expanded to also track the moments of dormant and dead chains in the system, similar to the approach of Butte et al.[13] for NMP.

Both the propagating radicals and the deactivator, Cu(II), were considered to be compartmentalized species, as the contribution of individual molecules on the rates of reactions were accounted for, and these rates scale with the volume of the particle. The activating species, Cu(I), was considered to be uncompartmentalized because it is present in sufficient concentration in all particles that the fluctuations on a molecular basis inside individual particles will not be enough to significantly alter the rate.

The modified Smith-Ewart equations, including the compartmentalization of both radicals and Cu(II) are

$$\begin{aligned}\frac{dN_{i,j}}{dt} &= N_A V_p k_{act} \mu^{(0)} [Cu(I)] \left(N_{i-1,j-1} - N_{i,j}\right) \\ &+ \frac{k_t}{N_A V_p} \left((i+2)(i+1)N_{i+2,j} - (i)(i-1)N_{i,j}\right) \\ &+ \frac{k_{deact}}{N_A V_p} \left((i+1)(j+1)N_{i+1,j+1} - (i)(j)N_{i,j}\right)\end{aligned} \tag{3.3}$$

$N_{i,j}$ is the fraction of particles with i radicals and j free $CuBr_2$/EHA_6TREN molecules,

N_A is Avogadro's number, V_p is the volume of a particle and $\mu^{(0)}$is the zeroth order moment of the distribution of dormant chains (see below). The average number of radicals, Cu(II) and Cu(I) molecules per particle can be calculated by

$$\bar{n} = \sum_i \sum_j (i) N_{i,j} \tag{3.4}$$

$$\bar{n}_{Cu(II)} = \sum_i \sum_j (j) N_{i,j} \tag{3.5}$$

$$\bar{n}_{Cu(I)} = N_A V_p [Cu(I)] \tag{3.6}$$

Using the above averages directly makes it difficult to compare the rates of polymerization and concentrations of activating/deactivating species in particles of different sizes and systems with different concentrations of catalyst and initiator. Instead, the approach developed by Simms and Cunningham[17] is used where $\bar{n}_{chain}$ is defined as the average number of radicals per polymer chain in the system and $\bar{n}_{Cu(II)chain}$, similarly, is the average number of deactivating species per polymer chain. This method gives an absolute variation of polymerization rate on a chain-by-chain basis in the absence of other effects including that of catalyst and initiator concentration and also the number of particles in the system.

$$\bar{n}_{chain} = \frac{\bar{n}}{N_A V_p \mu_0^{(0)}} \tag{3.7}$$

$$\bar{n}_{Cu(II)chain} = \frac{\bar{n}_{Cu(II)}}{N_A V_p \mu_0^{(0)}} \tag{3.8}$$

To estimate the degree of polymerization (DP_n), the distribution of singly distinguished particles, $S_{i,j,m}$ is introduced, where $S_{i,j,m}$ is the fraction of particles containing i radicals, j Cu(II) molecules, and with a chain of length m.

$$\begin{aligned}\frac{dS_{i,j,m}}{dt} = {} & N_A V_p k_{act}[Cu(I)] \left(\mu^{(0)} S_{i-1,j-1,m} + [P_m - X] N_{i-1,j-1} - \mu^{(0)} S_{i,j,m}\right) \\ & + \frac{k_{deact}}{N_A V_p} \left((i)(j+1) S_{i+1,j+1,m} - (i)(j) S_{i,j,m}\right) + k_p[M] \left(S_{i,j,m-1} - S_{i,j,m}\right) \\ & + \frac{k_t}{N_A V_p} \left((i)(i+1) S_{i+2,j,m} - (i)(i-1) S_{i,j,m}\right)\end{aligned} \tag{3.9}$$

The PDI was estimated for the dormant chains only, as active chains were present in only extremely small concentrations. Likewise, dead chains will account for only a small fraction of total chains if the system is assumed to be highly living. The infinite set of equations (Equation 3.9) is transformed into a finite set of equations by the method of moments, such that $\lambda_{i,j}^{(k)}$ is the kth moment of growing chains present in each type of particle state, with i radicals and j Cu(II) molecules (Equation 3.10). Therefore, the zeroth order moment, $\lambda_{i,j}^{(0)}$, is simply the overall number of active chains inside the particles of state *i,j* (Equation 3.11).

$$\lambda_{i,j}^{(k)} = \sum_m m^k S_{i,j,m} \tag{3.10}$$

$$\lambda_{i,j}^{(0)} = (i) N_{i,j} \tag{3.11}$$

The mass balances for the uncompartmentalized species, such as monomer (Equation 3.12), the zeroth through second moments of the dormant chains (Equation 3.13), the concentration of activator, [Cu(I)] (Equation 3.14), and the zeroth moment of the dead chains (Equation 3.15) were also calculated.

$$\frac{d[M]}{dt} = -\frac{k_p[M]}{N_A V_p} \bar{n} \tag{3.12}$$

$$\frac{d\mu^{(k)}}{dt} = -k_{act}[Cu(I)]\mu^{(k)} + \frac{k_{deact}}{(N_A V_p)^2} \sum_i \sum_j (j) \lambda_{i,j}^{(k)} \tag{3.13}$$

$$\frac{d[Cu(I)]}{dt} = \frac{k_{deact}}{(N_A V_p)^2} \sum_i \sum_j (j) \lambda_{i,j}^{(0)} - k_{act}[Cu(I)]\mu^{(0)} \tag{3.14}$$

$$\frac{d\zeta^{(0)}}{dt} = \frac{2k_t}{(N_A V_p)^2} \sum_{i=2} \sum_{j} (i-1)\lambda_{i,j}^{(0)} \tag{3.15}$$

This system of differential equations was solved in Fortran by numerical integration with the solver DLSODI (backwards Euler method) with a step size of 1 s. The differential equations were closed with a maximum of 6 radicals (i) and 75 Cu(II) molecules (j) per particle, well in excess of the ranges where compartmentalization effects are expected. Throughout all simulations, these boundary conditions were checked to ensure these boundaries were not approached. Simulations investigating the livingness of the chains at 90% conversion were run with a maximum of 6 radicals and 200 Cu(II) molecules.

3.2.2 Bulk Polymerization Model

A bulk polymerization model was developed to estimate an $\bar{n}_{chain}$ equivalent, $\bar{n}^b_{chain}$, and PDI to compare directly with the dispersed phase polymerization system by applying the method of moments to the active chains of length m and the dormant chains of length m in a bulk polymerization system (Equations 3.16-3.19).

$$\frac{d[P_m\bullet]}{dt} = k_{act}[P_m - X][Cu(I)] - k_{deact}[P_m\bullet][Cu(II)] - k_t[P_n\bullet]\sum_m [P_m\bullet] + k_p[M][P_{m-1}\bullet] - k_p[M][P_m\bullet] \tag{3.16}$$

$$\frac{d[Cu(I)]}{dt} = k_{deact}\sum_m [P_m\bullet][Cu(II)] - k_{act}[Cu(I)]\mu^{(0)} \tag{3.17}$$

$$\frac{d[P_m - X]}{dt} = -k_{act}[P_m - X][Cu(I)] + k_{deact}[P_m\bullet][Cu(II)] \tag{3.18}$$

$$\bar{n}^b_{chain} = \frac{\sum_m [P_m\bullet]}{\sum_m [P_m - X]} \tag{3.19}$$

3.2.3 Choice of Polymerization System

Compartmentalization in ATRP miniemulsion has been shown in a reverse ATRP system with n-butyl methacrylate (BMA) and using $CuBr_2$/EHA_6TREN.[17] Because compartmentalization effects on the rate of polymerization and the degree of control are similar regardless of the initiation system (forward ATRP, reverse ATRP or AGET ATRP), a system of forward ATRP with BMA was chosen for these simulations for ease of calculation. (Also note that the use of a forward ATRP system is a simplification on an ARGET system, where all the $CuBr_2$ is reduced to CuBr in situ at the beginning of the polymerization, independent of the generation of dormant chains.) The ligand EHA_6TREN complexed to Cu(I) or Cu(II) demonstrates excellent monomer solubility and extreme hydrophobicity, and thus it is unlikely to partition to any appreciable degree into the aqueous phase, and phase transfer events can be neglected from the model with confidence. Other ligand systems used in miniemulsion, including BPMODA and dNbpy, possess some water solubility, especially for the $CuBr_2$/ligand species.

The rate coefficients of activation/deactivation for CuBr/EHA_6TREN have not been estimated in the literature, but approximate calculations from the apparent K_{ATRP} along with the published estimates for the structurally similar CuBr/BA_6TREN with EBiBr initiator (a 3^o alkyl halide radical initiator with a structure similar to a BMA radical) were used in these simulations.[28] These calculated values are appropriate, best available estimates for the rate constants of CuBr/EHA_6TREN with BMA.

Table 3.1: Values of the Parameters Used in the Simulation of ATRP of BMA with the Ligand EHA_6TREN.

parameter	**value**
$[M]_0$	6.29 mol·L^{-1}
k_{act}	2.05 L·mol^{-1}·s^{-1} [28]
k_{deact}	3.9x10^7 L·mol^{-1}·s^{-1} [28]
k_p	1.24x10^3 L·mol^{-1}·s^{-1} [29]
k_t	1.03x10^7 L·mol^{-1}·s^{-1} [30]

The simulations were conducted up to 10% conversion to minimize any conversion dependence on the rate coefficients. Chain length dependencies of these constants were not

taken into consideration. These simulations were conducted for varying particle sizes with targeted degree of polymerization (at 100% conversion) between 100 and 5000 monomer units and with chain-to-catalyst ratios of 10:1, 2:1, and 1:1. The values of the parameters used are listed in Table 3.1.

3.3 Results and Discussion

3.3.1 Rate of Polymerization and the Degree of Control

Figure 3.1 shows the average number of radicals per chain (which is directly proportional to the rate of polymerization) and the PDI at 10% conversion over a range of particle sizes for the BMA/CuBr/EHA_6TREN system simulated at 70^{O}C for a targeted degree of polymerization (DP_n) of 500 and an initiator/Cu(I) ratio of 10:1 (one Cu molecule mediates ten chains). The rate of polymerization increases with increasing particle size to a maximum and levels out to the rate in an equivalent bulk system. This type of correlation is expected based on previous ATRP simulations[15, 25] but the relationship of PDI with particle size has not yet been discussed because previous models were unable to estimate this. The PDI also increases, goes through a maximum, and subsequently levels out to the same PDI as an equivalent bulk system with increasing particle size, but the maximum occurs at an offset with respect to the maximum of the rate of polymerization. In the system presented here (Figure 3.1) the time required to reach 10% conversion at 45 nm is 15 times faster than that for the particle size of 20 nm. Similarly, in a system with a target DP_n of 5000 and a chain/catalyst ratio of 10:1, the time to reach 10% conversion in a 120 nm particle is four times as fast as a particle of 60 nm (in the enhanced deactivation region) while also being 1.3 times faster than a 240 nm particle (in the approach to bulk region).

In an effort to aid the comparison of these living/controlled dispersed phase polymerization systems to the better known conventional systems, $\bar{n}$, not just $\bar{n}_{chain}$, was also evaluated. Whereas in conventional systems (for the simplified case of termination as the main chain stopping event), $\bar{n}$ remains $\sim$0.5 regardless of the particle size. The situation is much more complicated in controlled polymerization because $\bar{n}$ is dependent not only on the size of the particles but also the total concentration of chains in the system. This difference arises because deactivation, not termination, becomes the dominant chain stopping effect.

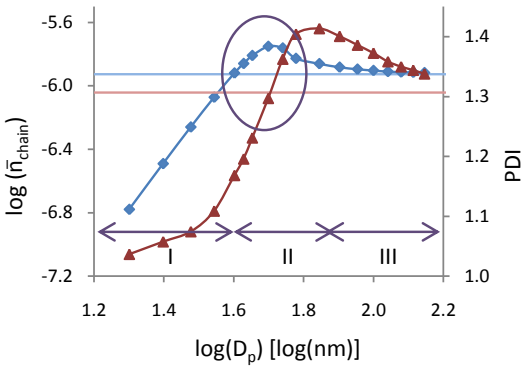

Figure 3.1: Effect of particle size on the reaction rate, as represented by $\bar{n}_{chain}$, (♦) and PDI (▲) at 10% conversion for the system with a targeted degree of polymerization of 500 and a 10:1 ratio of chains to Cu(I) at the start of the reaction. The solid lines represent the bulk equivalent $\bar{n}^b_{chain}$ and PDI.

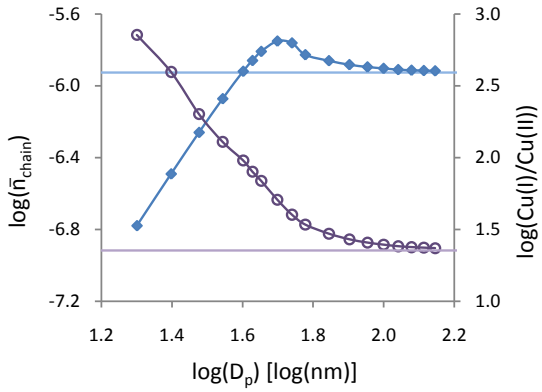

Figure 3.2: Effect of particle size on the reaction rate, as represented by $\bar{n}_{chain}$ (♦), and Cu(I)/Cu(II) (○) at 10% conversion for the system with a targeted degree of polymerization of 500 and a 10:1 ratio of chains to Cu(I) at the start of the reaction. The solid lines represent the bulk equivalent $\bar{n}^b_{chain}$ and Cu(I)/Cu(II).

Over a range of particle sizes (keeping a constant targeted degree of polymerization), $\bar{n}$ increases with increasing particle size (or with a decrease in the total number of particles). For the simulations discussed in Figures 3.1–3.2, the absolute $\bar{n}$ is much lower than in conventional systems and varies between 10^{-7}–10^{-6} over the range of particle sizes discussed. As a result, the rate of ATRP is always much slower than the rate of polymerization of regular free radical systems.

The rate of polymerization (as indicated by $\bar{n}_{chain}$) and PDI change dramatically with particle size and can be considered to span three different regions, as explained below.

Region I: Enhanced Deactivation At very small particle sizes, the rate of reaction and the PDI are significantly lower than bulk and decrease with diminishing particle size. This can be attributed to the effect of enhanced deactivation described by Kagawa et al.[15] In this regime, the concentration of radicals in the system is proportional to the volume of the particle (or [P] is proportional to d^3) and termination is negligible. The slope of the log-log plot (Figures 3.1 and 3.2) of $\bar{n}_{chain}$ versus particle size is linear with a slope of 3. In qualitative terms, this means that following a single activation, the concentration of deactivator in the system is greater (based on $\bar{n}_{Cu(II)}/N_A V_p$) in smaller particles, causing the chain to deactivate more quickly. In terms of reaction rate, this leads to a slower polymerization, assuming that activation occurs at a consistent rate regardless of the particle size. This is always the case, regardless of the particle size region, for nitroxide mediated polymerization, where activation is controlled by a thermal process; it is also the case in region I for ATRP when the activator Cu(I) is considered uncompartmentalized and termination is negligible, and thus the Cu(I) local concentration is not affected by the change of a single molecule from Cu(I) to Cu(II). In this region, the PDI of the living chains is also lower because fewer units are added per activation cycle with diminishing particle size, and more cycles are required to reach the same conversion. This will be discussed later in further detail.

Region II: Acceleration Window The increase in the rate of reaction above that predicted in an equivalent bulk system was described by Kagawa et al.[15] in terms of radical segregation (because radicals in different particles are unable to mutually terminate) and in NMP by Tobita[22] as the fluctuation effect, where the local concentration of deactivator in the particles changes with every activation/deactivation reaction. Our results indicate that the acceleration window observed in an ATRP system can be attributed to the nonestablishment of a Cu(I)/Cu(II) steady state ratio, as is observed in bulk polymerization (Equation 3.1), owing to fewer instances of termination early in the polymerization, which is the result of both enhanced deactivation and radical segregation. Kagawa et al.[15] reported that with moderate particle sizes, lower numbers of deactivator molecules in the particles reduced the degree of control by increasing the number of units added per activation. However, in our simulations, the effect of a lower number of deactivating molecules can also be seen as an increase in the frequency of activation events by the presence of a larger concentration of

activator and an overall faster rate of polymerization.

Figures 3.2 shows the Cu(I)/Cu(II) ratio and the variation in the average number of radicals per chain with particle size for the same system with a target DP_n of 500 and an initiator/Cu(I) ratio of 10:1. The steady-state Cu(I)/Cu(II) equilibrium ratio, which is a characteristic of bulk and solution ATRP, is not achieved in the acceleration window because very little termination occurs in the particles (due to the enhanced deactivation allowing fewer active radicals as well as radical compartmentalization preventing the mutual termination of radicals present in different particles). Therefore, at small particle sizes, the system will always possess a concentration of activator, Cu(I), which is larger than in bulk systems. This leads to more frequent activation cycles than in bulk polymerization, increasing the $\bar{n}_{chain}$. Whereas Cu(II) compartmentalization serves as the major compartmentalization effect in these systems, lowering $\bar{n}_{chain}$ with diminishing particle sizes, the secondary and contrary effect of more frequent activation cycles, owing to lower termination and leading to an increase in $\bar{n}_{chain}$ with diminishing particle sizes (described above), is also at play. Without the secondary enhanced activation effect, the $\bar{n}_{chain}$ and PDI trends with particle size would overlap; it is this secondary effect arising from the minimization of termination and the increase in the absolute concentration of Cu(I) inside the particles that allows a region of particle sizes where the rate of reaction can be above that in an equivalent bulk system while still maintaining a PDI below that in bulk.

Region III: Approach to a Bulk System At larger particle sizes, the anticipated $\bar{n}_{chain}$ approaches that of a bulk polymerization (Figure 3.1) because more radicals are present at any time, with consequently less influence of enhanced deactivation and increased termination. The Cu(I)/Cu(II) ratio approaches that of the bulk system (Figure 3.2).

Regions for the PDI According to the method developed by Goto and Fukuda[31] for bulk systems, the PDI of the living chains is influenced by both the number of units added per activation as well as the number of activation cycles to reach a given conversion.

$$
\begin{aligned}
no.units &= \frac{propagation}{deactivation} \\
&= \frac{k_p[M][P\bullet]}{k_{deact}[Cu(II)][P\bullet]} \\
&= \frac{k_p[M]\dfrac{\sum_i (i)N_{i,j}}{N_A V_p}}{k_{deact}\dfrac{\sum_i \sum_j (i)(j)N_{i,j}}{(N_A V_p)^2}} \\
&= \frac{k_p[M]N_A V_p \bar{n}}{k_{deact}\sum_i \sum_j (i)(j)N_{i,j}} \propto d^3
\end{aligned}
\tag{3.20}
$$

The multiple influences of compartmentalization on the PDI in the dispersed phase can be broken down into several different effects. As previously discussed, the number of units added per activation is influenced by enhanced deactivation in smaller particle sizes. The number of units added is a function of the ratio of the rate of propagation with respect to the rate of deactivation and can be transformed to a proportionality (Equation 3.20) with respect to the particle diameter cubed, d^3, through the application of the Equations 3.2 and 3.4 along with the understanding that $[P\bullet]$ can be obtained by $\bar{n}/N_A V_p$. However the frequency of the activation cycles is similarly influenced by the concentration of Cu(I), which is higher in smaller particles (because there are fewer termination reactions and little buildup of Cu(II)). Finally, the number of activations required to reach a given conversion is different for each particle size. Therefore, the contrasting effects of enhanced deactivation and the concentration of Cu(I) in the calculation of the PDI are influenced in a different manner than the rate of polymerization. This leads to a general trend of increasing PDI with particle size in region I of enhanced deactivation (because of to the number of units added per activation increasing with particle size). At moderate particle sizes, the PDI passes through a range of particle sizes where the simulated PDIs of the living chains are greater than that in bulk (attributed to the lower instances of termination in the dispersed phase, which lead to a lower rate of deactivation and the addition of more units per cycle than in

the bulk system). Finally the PDI decreases with increasing particle size in region III owing to irreversible termination and the buildup of Cu(II) in the system, pushing the equilibrium to favour the dormant chains (Figure 3.1). The window where the PDI is greater in the emulsion system than in bulk occurs at larger particle sizes than the acceleration window for the rate of polymerization. Therefore, there exists a range of particle sizes where the rate of polymerization is higher than that of bulk polymerization but where we can preserve a high degree of control over the PDI and livingness, which is greater than an equivalent bulk system.

3.3.2 Effect of the Targeted Degree of Polymerization

In ATRP systems, modifying the targeted degree of polymerization is simply a matter of modifying the alkyl halide initiator concentration. Because the polymerization kinetics are often thought in terms of the number of chains each Cu(I) molecule can mediate, the overall concentration of Cu(I) is similarly modified with the target DP_n. This section presents the results of simulations for the system of BMA/CuBr/EHA_6TREN with a alkyl halide initiator/catalyst ratio of 2:1 and targeted degrees of polymerization ranging from 100 to 5000, or targeted molecular weights (M_n) of 14,200 g/mol to 710,000 g/mol.

As expected, the degree of livingness of the polymer chains increases with diminishing particle size (Figure 3.3c), and is attributed to the suppression of termination due to the compartmentalization of the radicals. It should be noted that the degree of termination never exceeds that expected in the bulk system, indicating that although there is a particle size range where the rate of polymerization exceeds that in bulk (Figure 3.4a), the livingness of the system will not be adversely affected by operating in that range.

At a given particle size, log(Cu(I)/Cu(II)) increases when the targeted DP_n is increased (or the concentration of initiator is decreased) (Figure 3.4b). This trend is contrary to that predicted by the persistent radical effect[32] in bulk polymerization. The persistent radical effect predicts that when the concentration of initiator is increased, the concentration of deactivator (Cu(II)) will increase to maintain an equilibrium through the mutual termination of chains. However, in the dispersed phase, where termination is suppressed through compartmentalization, the persistent radical effect is similarly suppressed. Because the concentration of Cu(II) does not rise considerably in systems with lower concentrations of

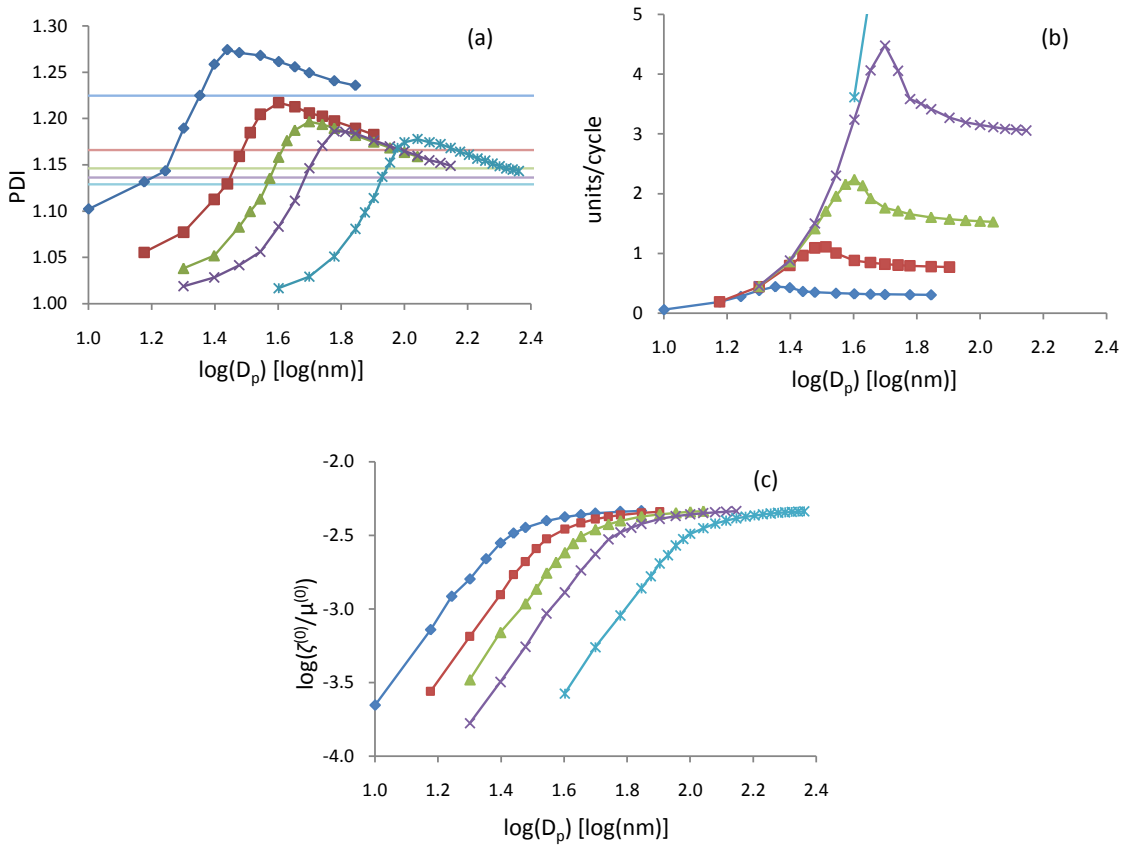

Figure 3.3: Simulations conducted up to 10% conversion with an initiator:Cu(I) ratio of 2:1 to investigate the effect of (a) the PDI, (b) the number of units added per activation cycle and (c) the ratio of dead/dormant chains at 10% conversion with respect to particle size for systems with target degrees of polymerization (at 100% conversion) of 100 (♦), 250 (■), 500 (▲), 1000 (×), 5000 (∗).

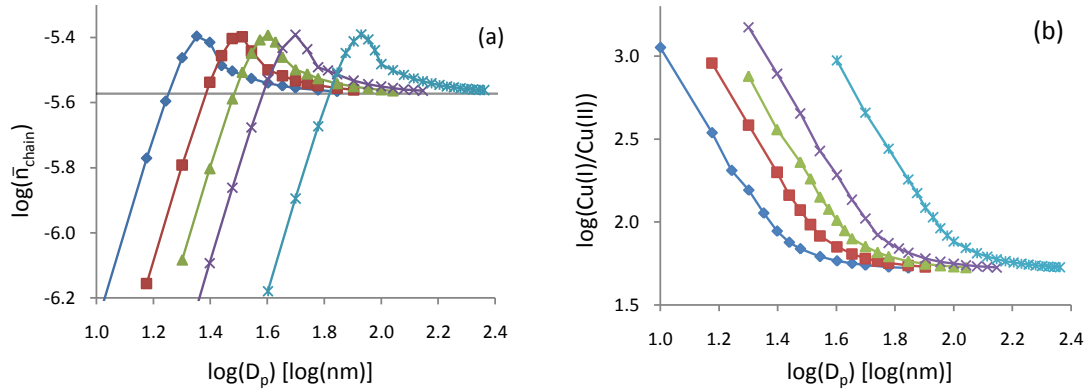

Figure 3.4: Simulations conducted up to 10% conversion with an initiator/Cu(I) ratio of 2:1 to investigate the effect of (a) the rate of polymerization as represented by the average number of radicals per chain, $\bar{n}_{chain}$, and the bulk system, $\bar{n}^{b}_{chain}$(solid line) and (b) the ratio of Cu(I)/Cu(II) with respect to particle size for systems with target degrees of polymerization (at 100% conversion) of 100 (♦), 250 (■), 500 (▲), 1000 (×), 5000 (∗).

initiator, and termination is further suppressed in these particles (Figure 3.3c), the ratio of Cu(I)/Cu(II) will be greater in systems with higher targeted DP_n values.

There is a similar argument concerning the higher PDIs obtained in systems with lower initiator concentrations (or higher target DP_n values) specifically in the approach to bulk region (Figure 3.3a). This is contrary to what is expected in a bulk polymerization. Because the PDI is dependent on a ratio of the concentration of chains with respect to the concentration of Cu(II) in the system,[31] the persistent radical effect predicts that the PDI would be uniformly higher for the systems with higher initiator concentrations. However, the lower instances of termination in systems with higher target DP_ns lead to a lower-than-predicted concentration of Cu(II) present in the particles, yielding higher PDIs at higher target DP_n values. The PDI trends in the other regions (enhanced deactivation and the acceleration window) are discussed below.

In simulations up to 10% conversion in compartmentalized systems, the livingness of the chains remains above 98% for all of the conditions simulated, including different targeted DP_n values and with different concentrations of catalyst. This is a common phenomenon in previous ATRP[25] and NMP[14] population balance simulations. However, this livingness is likely dependent on the activity of the nitroxide or ATRP catalyst. When the simulations here are run to a higher conversion, for example, in the system of 100 nm particles with a targeted DP_n of 1000 and a 1:1 chain/catalyst ratio, the livingness of the system at 90% conversion is calculated to be 94%. Simulations to high conversion are quite computationally intensive because the number of free Cu(II) molecules accounted (j) must be increased from 75 to 200 to maintain a closed system of equations.

While removing the effect of the total concentration of chains in the system, through the use of $\bar{n}_{chain}$ rather than $\bar{n}$ or $[P\bullet]$ directly, the rate of monomer addition per chain in the system levels out to the same rate for larger particle sizes and for the bulk system (Figure 3.4a), however the PDI of these chains does not (Figure 3.3a). The PDI is affected by the total number of activations required to reach 10% conversion and also the number of units added in each of these activations. In general, the PDI diminishes with increasing particle size because of a balance between the number of activations (DP_n 5000 experiences the most, generally lowering the PDI) and the number of units added (at 10% conversion, DP_n 5000 adds far more units per activation, which in general tends to increase the PDI).

Under the conditions simulated here (Figures 3.3a, 3.3b), the number of activations plays a far more important role in determining the overall PDI of the dormant chains than does the number of units added per activation.

3.3.3 Effect of the Catalyst Concentration

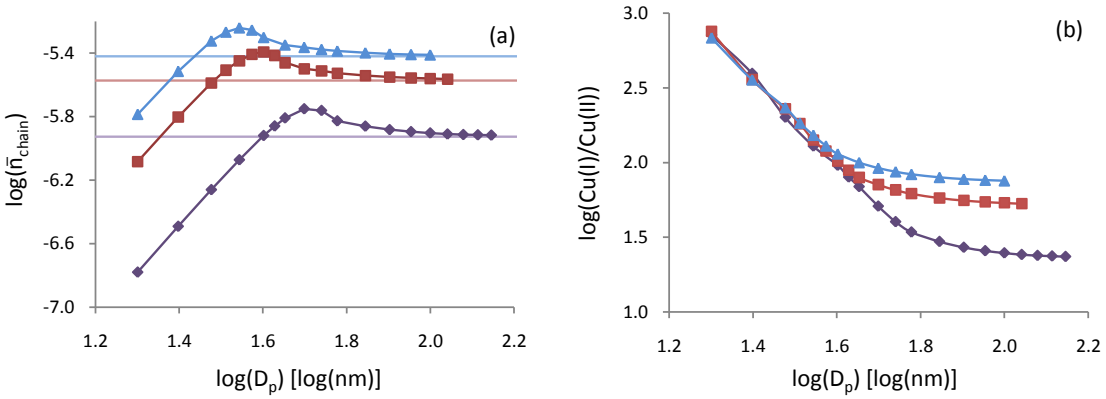

Figure 3.5: Simulations conducted up to 10% conversion with a targeted degree of polymerization of 500 (at 100% conversion) to investigate the effect of (a) the rate of polymerization as represented by the average number of radicals per chain, $\bar{n}_{chain}$, and the bulk system, $\bar{n}^{b}_{chain}$(solid lines) and (b) the ratio of Cu(I)/Cu(II) with respect to particle size for systems with initiator:Cu(I) ratios of 10:1 (♦), 2:1 (■) and 1:1 (▲).

With considerable interest in achieving lower catalyst concentrations in solution and bulk ATRP, preliminary investigations into the reduction of catalyst concentration in aqueous dispersed phase polymerization were undertaken. Unlike ARGET and ICAR chemistries, no Cu(I) regeneration mechanisms are included in the simulations, but it will become apparent that the nonestablishment of a steady state Cu(I)/Cu(II) ratio and diminishing instances of termination (Figures 3.5b and 3.6c) allows the total catalyst concentration to be reduced and polymerization to continue without a large buildup of Cu(II) occurring and suppressing the polymerization rate.

Simulations were conducted for the system with a targeted degree of polymerization of 500 and varying initiator/catalyst ratios of 10:1, 2:1, and 1:1 (Figures 3.5 and 3.6). These are the first simulation results that detail the effects of diminishing catalyst concentration in dispersed phase ATRP polymerization, and some unique features are revealed. First, in the

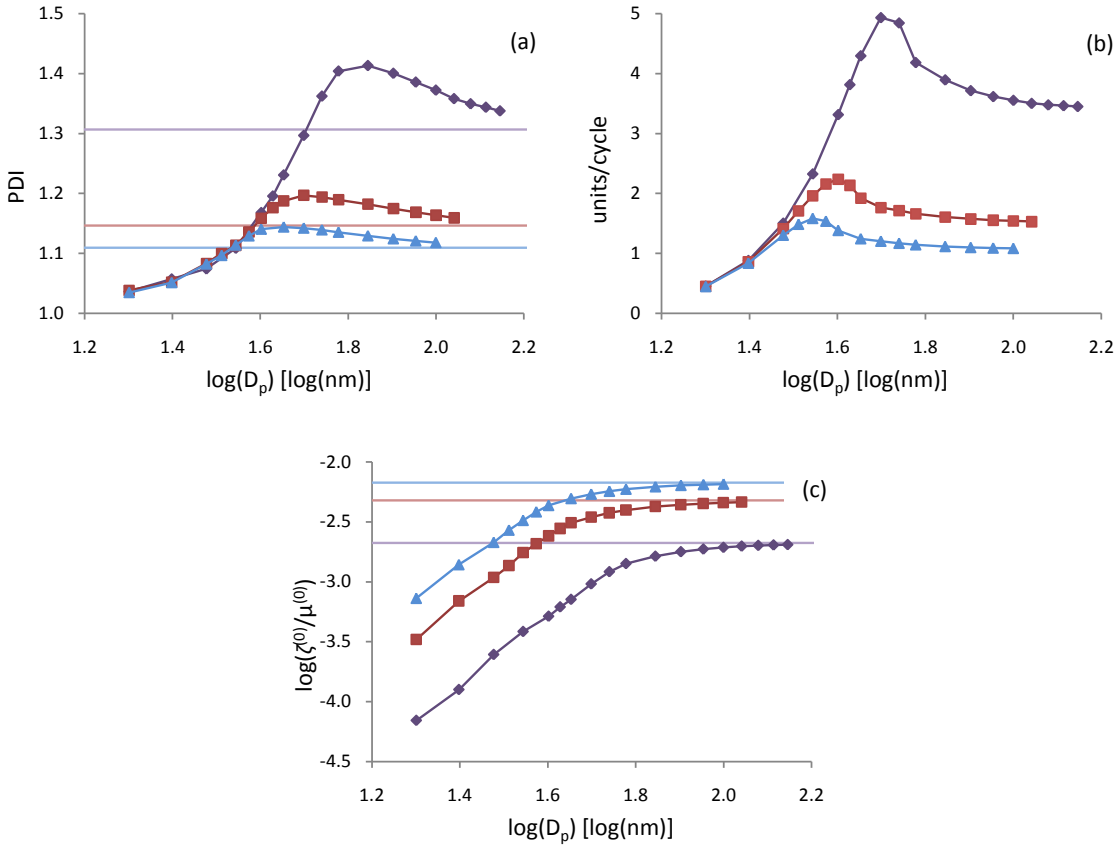

Figure 3.6: Simulations conducted up to 10% conversion with a targeted degree of polymerization of 500 (at 100% conversion) to investigate the effect of (a) the PDI, (b) the number of units added per activation cycle, and (c) the ratio of dead/dormant chains at 10% conversion with respect to particle size for systems with initiator/Cu(I) ratios of 10:1 (♦), 2:1 (■) and 1:1 (▲).

region I (enhanced deactivation) of Figure 3.5, the Cu(I)/Cu(II) ratio remains the same for all three catalyst concentrations, however the rate of polymerization ($\bar{n}_{chain}$), which takes into account the effect of the initiator concentration, diminishes with diminishing catalyst concentration. This result is contrary to the commonly accepted rate expression for solution ATRP (Equation 3.1), in that the rate in the dispersed phase is dependent on the absolute concentration of catalyst. However, in bulk, only the ratio of Cu(I)/Cu(II), which remains unchanged in these simulations, should affect the rate. Therefore, in aqueous dispersed phase polymerizations, the rate of polymerization is dependent on the total concentration of activator, Cu(I), present in the system when termination is suppressed, and a steady-state Cu(I)/Cu(II) ratio is not achieved in the early stages of the polymerization, as is the case for bulk and solution polymerization. In regions II and III, it becomes clear that the

steady-state Cu(I)/Cu(II) ratio achieves different values and $\bar{n}_{chain}$ also reaches different steady state (and bulk) rates with diminishing catalyst concentration.

The PDI is greatly influenced by the total concentration of deactivating species in the system, Cu(II), because larger concentrations of deactivator lead to the addition of fewer units per activation, and thus more activations are required to reach a given conversion. In these simulations, which all possess the same concentration of initiator but varying concentrations of catalyst, the system with the lowest catalyst concentration (10:1 initiator/catalyst ratio) shows the lowest Cu(I)/Cu(II) ratio (Figure 3.5b) but possesses the lowest overall concentration of Cu(II). Therefore, the PDI (Figure 3.6a) and the number of units added per activation event (Figure 3.6b) are significantly larger than those for the other systems. Therefore, targeting a lower catalyst concentration not only leads to diminished rates of polymerization but also results in a significantly higher PDI. It should be noted, however, that the livingness of the system is higher in systems possessing a lower concentration of catalyst because the ratio of dead chains/dormant chains is lower for all particle sizes (Figure 3.6c).

On the basis of these simulations, a discussion of the application to low catalyst systems, such as ARGET and ICAR, is warranted. In the ARGET system, regeneration of the Cu(I) from Cu(II) may lead to increasing the Cu(I)/Cu(II) ratio for larger particle sizes (especially in region III) but will have no effect in region I, where termination is negligible and Cu(I) regeneration is not necessary. In this region, the PDI will increase, and the rate will diminish as the concentration of Cu is lowered, but the chains will retain a greater livingness. In regions I and II, ICAR chemistry and the addition of a secondary radical source may cause further irreversible terminations. In small particles, when a second radical enters into a particle that is already containing an active radical, termination is instantaneous (a zero-one system), decreasing the livingness of the system and termination reactions lead to the buildup of Cu(II) which slows the polymerization. In region III, ICAR may be of use to generate new chains because termination is not instantaneous between radicals and there is a larger buildup of Cu(II) at any given conversion. However, in this region, ARGET is less likely to diminishing the livingness of the system.

3.4 Conclusions

Compartmentalization effects can influence the rate of polymerization, the degree of control of the PDI and the livingness of the polymer formed in aqueous dispersed phase ATRP polymerizations. For the highly active catalyst CuBr/EHA_6TREN, it was found that for small particle sizes, both the rate of polymerization and the number of units added per activation decreased proportionally to the volume of the particles, attributed to the confined space effect influencing the rate of deactivation of the chains. It was also found that there exists a window of particle sizes where the rate of polymerization is higher than that of a bulk system but where the PDI and the degree of termination remain below that of bulk, indicating an optimal region of particle sizes. Whereas the rate of polymerization is directly controlled by an equilibrium ratio of Cu(I)/Cu(II) for bulk ATRP systems, this is not true for the compartmentalized system, where the rate is instead controlled by enhanced deactivation and also the relative concentration of Cu(I) and Cu(II), which are dependent on the size of the particles.

When changing the concentration of initiator in the system to target different DP_n values, the range of particle sizes where the rate of polymerization exceeds that of bulk is shifted to lower particle sizes with increased initiator concentration, but as the effect of enhanced deactivation is minimized (at larger particle sizes), the rate at which monomer units are added to a single polymer chain in the system does not change with initiator concentration, provided that the initiator/catalyst concentration remains constant. However, the number of activations required to reach a given conversion has a greater effect on the final PDI than does the number of units added per activation because systems with the lowest initiator concentration achieve the lowest PDI for all particle sizes, even while adding the most monomer units per activation.

In this ATRP system, several important points concerning ATRP with low catalyst concentrations in the aqueous dispersed phase are highlighted. First, lower catalyst concentrations lead to slower polymerization rates because the frequency of activation events is lower, whereas the PDI and the number of units added per chain are higher. However, polymerizations conducted under these conditions do possess a greater livingness. The application of ARGET or ICAR chemistries will not improve the rate of polymerization in the smallest particles, and the generation of new radicals in the ICAR chemistry may have

a detrimental effect on the livingness of the system.

Acknowledgments

We thank Dr. A. Butté from ETH (Zurich) for many helpful discussions on compartmentalization and the Natural Sciences and Engineering Research Council of Canada (NSERC) for financial support.

References

[1] Cunningham, M. F. *Progress in Polymer Science* **33**(4), 365–398 (2008).

[2] Zetterlund, P. B., Kagawa, Y., and Okubo, M. *Chemical Reviews* **108**(9), 3747–3794 (2008).

[3] Min, K., Gao, H., and Matyjaszewski, K. *Journal of the American Chemical Society* **127**(11), 3825–3830 (2005).

[4] Min, K., Jakubowski, W., and Matyjaszewski, K. *Macromolecular Rapid Communications* **27**(12), 982–982 (2006).

[5] Stoffelbach, F., Belardi, B., Santos, J. M. R. C. A., Tessier, L., Matyjaszewski, K., and Charleux, B. *Macromolecules* **40**(25), 8813–8816 (2007).

[6] Min, K., Yu, S., il Lee, H., Mueller, L., Sheiko, S. S., and Matyjaszewski, K. *Macromolecules* **40**(18), 6557–6563 (2007).

[7] Stoffelbach, F., Griffete, N., Bui, C., and Charleux, B. *Chemical Communications* (39), 4807–4809 (2008).

[8] Dong, H., Mantha, V., and Matyjaszewski, K. *Chemistry of Materials* **21**(17), 3965–3972 (2009).

[9] Li, W., Matyjaszewski, K., Albrecht, K., and Moller, M. *Macromolecules* **42**(21), 8228–8233 (2009).

[10] Simms, R. W. and Cunningham, M. F. *Journal of Polymer Science Part A: Polymer Chemistry* **44**(5), 1628–1634 (2006).

[11] Simms, R. W. and Cunningham, M. F. *Macromolecules* **40**(4), 860–866 (2007).

[12] Braunecker, W. A. and Matyjaszewski, K. *Progress in Polymer Science* **32**(1), 93–146 (2007).

[13] Butte, A., Storti, G., and Morbidelli, M. *DECHEMA Monogr.* **134**(6th International Workshop on Polymer Reaction Engineering), 497–507 (1998).

[14] Zetterlund, P. B. and Okubo, M. *Macromolecules* **39**(26), 8959–8967 (2006).

[15] Kagawa, Y., Zetterlund, P. B., Minami, H., and Okubo, M. *Macromolecular Theory and Simulations* **15**(8), 608–613 (2006).

[16] Maehata, H., Buragina, C., Cunningham, M., and Keoshkerian, B. *Macromolecules* **40**(20), 7126–7131 (2007).

[17] Simms, R. W. and Cunningham, M. F. *Macromolecules* **41**, 5148–5155 (2008).

[18] Zetterlund, P. B., Wakamatsu, J., and Okubo, M. *Macromolecules* **42**, 6944–6952 (2009).

[19] Delaittre, G. and Charleux, B. *Macromolecules* **41**(7), 2361–2367 (2008).

[20] Charleux, B. *Macromolecules* **33**(15), 5358–5365 (2000).

[21] Tobita, H. and Yanase, F. *Macromolecular Theory and Simulations* **16**(4), 476–488 (2007).

[22] Tobita, H. *Macromolecular Theory and Simulations* **16**(9), 810–823 (2007).

[23] Tobita, H. *Macromolecular Symposia* **261**(1), 36–45 (2008).

[24] Kagawa, Y., Zetterlund, P. B., Minami, H., and Okubo, M. *Macromolecules* **40**(9), 3062–3069 (2007).

[25] Zetterlund, P. B., Kagawa, Y., and Okubo, M. *Macromolecules* **42**(7), 2488–2496 (2009).

[26] Li, M. and Matyjaszewski, K. *Macromolecules* **36**(16), 6028–6035 (2003).

[27] Li, M., Min, K., and Matyjaszewski, K. *Macromolecules* **37**(6), 2106–2112 (2004).

[28] Tang, W., Kwak, Y., Braunecker, W., Tsarevsky, N. V., Coote, M. L., and Matyjaszewski, K. *Journal of the American Chemical Society* **130**(32), 10702–10713 (2008).

[29] Beuermann, S., Buback, M., Davis, T. P., Gilbert, R. G., Hutchinson, R. A., Kajiwara, A., Klumperman, B., and Russell, G. T. *Macromolecular Chemistry and Physics* **201**(12), 1355–1364 (2000).

[30] Buback, M. and Junkers, T. *Macromolecular Chemistry and Physics* **207**(18), 1640–1650 (2006).

[31] Goto, A. and Fukuda, T. *Progress in Polymer Science* **29**(4), 329–385 (2004).

[32] Fischer, H. *Chemical Reviews* **101**(12), 3581–3610 (2001).

Chapter 4

Catalytic Chain Transfer Mediated Emulsion Polymerization: Compartmentalization and Its Effects on the Molecular Weight Distribution

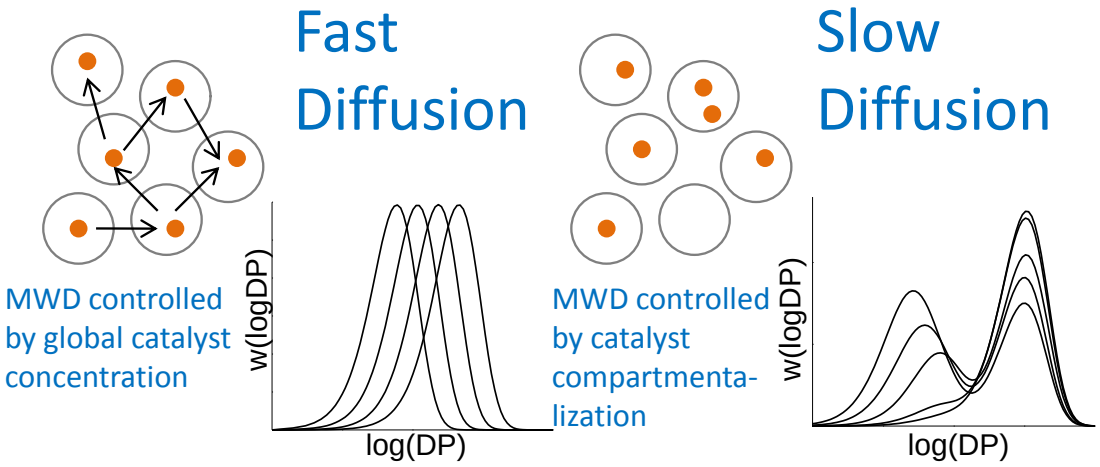

Preface

In fall 2007, I was very fortunate to spend three months at the Swiss Federal Institute of Technology (ETH) in Zurich working with Dr. Alessando Butté and the Morbidelli group and learning their techniques for the modeling of the full molecular weight distribution, while also accounting for radical segregation, in conventional emulsion polymerization. At the same time, Dr. Niels Smeets was at Queen's University, on exchange from Eindhoven Technical University in the Netherlands, working on Catalytic Chain Transfer (CCT) in the dispersed phase. This model was built using the techniques learned in ETH, in collaboration with Dr. Smeets, to describe mathematically what had been observed experimentally: seeded CCT emulsion systems produce multimodal molecular weight distributions and is the result of compartmentalization of the chain transfer agent inside the particles. Not only does this work represent the first instance of modeling in dispersed phase CCT-mediated systems, it is also the first model to simulate the full molecular weight distribution for any dispersed phase, CRP system which includes the compartmentalization of both the propagating radicals and the mediating species.

Abstract

We present the first population balance calculations which encompass the complete molecular weight distribution (MWD) to discuss the implications of both radical and catalytic chain transfer agent (CCTA) compartmentalization in a catalytic chain transfer (CCT) mediated emulsion polymerization system. Compartmentalization effects are attributed to reduced frequencies of entry and exit of the CCTA (bis[(difluoroboryl)dimethyl-glyoximato]cobalt(II) or COBF). Two limiting scenarios were identified. In instances of fast CCTA entry and exit, monomodal MWDs are obtained governed by a global CCTA concentration. In instances of slow entry and exit, bimodal MWDs are obtained; one peak can be attributed to the generation of a bimolecular termination product produced in polymer particles devoid of CCTA, while a transfer-derived peak can be attributed to polymer particles containing one or more CCTA molecules. We present theoretical evidence that experimentally observed multimodal MWDs (*Macromolecules* **2009**, 42, 7332-7341) originate from a reduced mobility of the CCTA and that when viscosity is high in the polymer particles, compartmentalization of the CCTA becomes important.

4.1 Introduction

In comparison to bulk polymerization, high rates of polymerization and high molecular weights in emulsion polymerization originate from compartmentalization effects, which include radical segregation and the confined space effect. Bimolecular termination between two radicals located in two separate particles cannot occur (radical segregation). Additionally, rates of reaction, including termination between two radicals, increase with decreasing particle size (confined space effect). However, compartmentalization in emulsion polymerization is not restricted to radicals only. In controlled/living radical polymerization (CLRP), such as nitroxide mediated polymerization (NMP) and atom transfer radical polymerization (ATRP), mediating agents are added to achieve control over the molecular weight distribution (MWD).[1, 2] Compartmentalization of these controlling agents[3, 4, 5, 6] affects the rate, livingness, and control of the polymerization. Recently, experimental evidence of compartmentalization was also reported for catalytic chain transfer (CCT) in emulsion.[7]

CCT is a controlled, but not living, free radical technique that allows control over the average molecular weight of the polymer formed. In CCT-mediated free radical polymerizations a low-spin Co(II) complex is added which transfers the radical activity of a propagating chain to a monomer molecule, resulting in the formation of an unsaturated dead polymer chain and a monomeric radical capable of propagation.[8, 9]

Evidence of compartmentalization was observed experimentally in seeded emulsion polymerization of methyl methacrylate (MMA).[7] Polymerization of the second stage monomer in the presence of bis[(difluoroboryl)dimethylglyoximato]cobalt(II) (COBF) in PMMA seed particles, swollen below the maximum saturation concentration, exhibited multimodal MWDs (Figure 4.1). The multimodal MWDs were observed independently of the size of the swollen PMMA particles and the average number of CCTA molecules per particle ($\bar{n}_{\mathrm{CCTA}}$). The observed multimodal MWDs were attributed to compartmentalization of the catalytic chain transfer agent (CCTA) as a consequence of the reduced mobility at the high instantaneous conversion of the polymer particles.[7]

CCT-mediated emulsion polymerizations typically proceed in a regime where the polymer particles outnumber the catalytic chain transfer agent (CCTA) molecules; consequently CCTA mass transport has to be sufficiently fast to ensure that multiple polymer particles can be mediated by a single CCTA molecule.[10, 11, 12, 13, 14, 15] In other words, proper con-

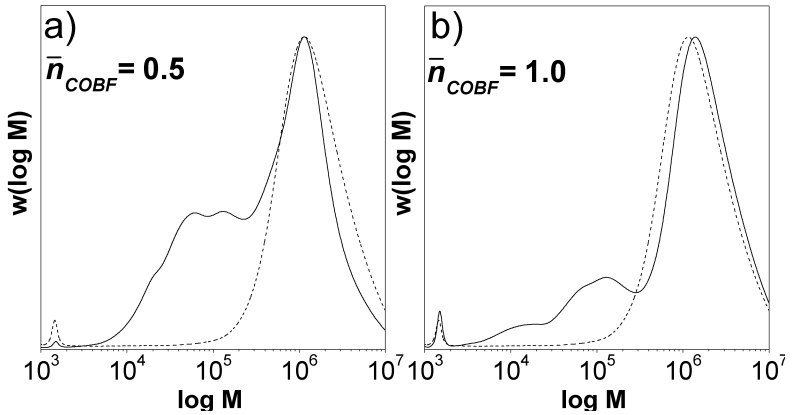

Figure 4.1: Example of the multimodal MWDs obtained in the seeded emulsion polymerization of methyl methacrylate in the presence of COBF.[7] The solid lines represent the MWD at the end of the polymerization, the dotted lines represent the MWD of the seed polymer. Experimental conditions: $T = 70\ ^{o}$C, solid content = 20%, 48 nm seed particles, swollen with MMA to a radius of 65 nm. The average number of CCTA molecules per polymer particle ($\bar{n}_{\mathrm{CCTA}}$): (a) $\bar{n}_{\mathrm{CCTA}} = 0.5$; (b) $\bar{n}_{\mathrm{CCTA}} = 1.0$.

trol of the MWD can only be achieved if the resistances toward CCTA mass transport (i.e., entry, exit, and transport through the aqueous phase) are negligible. In such systems, the MWD is governed by a global CCTA concentration where every particle polymerizes in the presence of an average number of CCTA molecules ($\bar{n}_{\mathrm{CCTA}}$).[7] This results in similar polymerization conditions in all the polymer particles, excellent control and a monomodal MWD. Conversely, when the resistance against CCTA mass transport is high, for instance when the increased viscosity of the polymer particles reduces the frequencies of entry and exit of the CCTA molecules, the polymerization proceeds inside the polymer particles containing discrete numbers of CCTA molecules ($n_{\mathrm{CCTA}} = 0$, 1, 2, etc.).[7] Consequently, during the polymerization, several different reaction environments simultaneously exist, corresponding to polymer particles with $n_{\mathrm{CCTA}} = 0$, 1, 2 etc. Under these specific conditions, a broad or even multimodal MWD is obtained with contributions from CCT in the presence of varying numbers of CCTA molecules and from bimolecular termination in the absence of a CCTA molecule (Figure 4.1).

We report on a theoretical investigation of the effects of compartmentalization of the CCTA on the MWD in CCT-mediated seeded emulsion polymerization. To the best of our knowledge, this is the first model describing CCT-mediated polymerization in a dispersed phase using a population balance approach, considering both the segregation of radicals and CCTA molecules inside the polymer particles. Using the concept of distinguished particle

distributions,[16, 17] the effects of the particle size, the overall concentration of CCTA, the rate of chain transfer, and the rate of entry and exit of the CCTA molecules on the chain length distribution (CLD) are investigated. While also interesting, discussions concerning the kinetics of these CCT-emulsion systems is beyond of the scope of this work, where a focus on the compartmentalization events and their effects on the CLD can be viewed in isolation and related to previous experimental studies.[7, 10, 15]

4.2 Theoretical Background

4.2.1 Model Assumptions

The effects of compartmentalization on the molecular weight distribution (MWD) in catalytic chain transfer CCT-mediated seeded MMA emulsion polymerization are described mathematically. The model equations were formulated with the following assumptions:

- The simulations were conducted up to low conversion, i.e., 30% based on the amount of second stage monomer added.
- The frequencies for radical entry and exit are set to a predetermined value and considered to be constant over the course the polymerization.
- The volumes of the swollen seed polymer particles remain constant over the course of the reaction and only the concentration of monomer decreases.
- The aqueous phase kinetics are neglected in the model, with the exception of entry and exit of "short" radicals (R_{short}).
- A "short" radical can undergo entry and exit from a polymer particle and ceases to be "short" following a single propagation step inside the particle.
- All rate coefficients used in the simulations are chain length independent.
- Decomposition of the CCTAs in the aqueous phase is neglected. The simulations are conducted for a short duration of time to low conversions (30%), over which catalyst deactivation is not significant.[8, 18]
- Cobalt-carbon bonding has been neglected.[19]

- The presence of a H-Co(III) complex is neglected in this system, as it assumed that the transfer to monomer from the Co(III) complex is very fast (and therefore not rate determining).[8, 9]

- Dead polymer chains with terminal double bonds, originating from catalytic chain transfer and termination by disproportionation, do not participate in further polymerization.

In the model, aqueous phase kinetics are neglected with the exception of entry and desorption of the radical species R_{short}. We will elaborate on this assumption. The kinetic events in the aqueous phase of an emulsion polymerization (i.e. initiation, propagation, termination and chain transfer) have been captured in a simplified model as presented by Maxwell et al.[20] In this model, a hydrophilic primary radical, derived from initiator decomposition, has to propagate to a certain length (referred to as the z-meric length) in order to achieve sufficient surface activity to enter a polymer particle. However, prior to entry, chain stoppage may occur by termination or chain transfer in the aqueous phase. In the presence of a CCTA, particle initiation proceeds predominantly by monomeric radicals originating from the CCT process[9] and desorption of monomeric radicals from the polymer particles. Because there is a lack of mechanistic understanding of the aqueous phase kinetics in the presence of a CCTA, the aqueous phase kinetics are neglected in the model and the entry frequency was set to a predetermined and constant value.

Because all kinetic events in the aqueous phase are neglected, entry and exit are set to proceed through an average radical species, referred to as R_{short}. In the model, radicals generated by initiator decomposition in the aqueous phase are converted to R_{short} radicals upon entry. An R_{short} radical ceases to be "short" following one propagation step in the particle phase. Following a catalytic transfer event, the produced monomeric radical is also considered in the model as R_{short}. These radicals can desorb from the polymer particle to the aqueous phase. This results in a situation where an R_{short} radical has an effective chain length of 1. The use of an R_{short} species is expected to have only minor influence on the CLD, as the propagating oligomers in the aqueous phase only reach a maximum chain length of 5 (in the case of MMA),[21] which is significantly less than the chain lengths obtained in the polymer particles.

4.2.2 Kinetic Scheme

The kinetic scheme used for the modeling of the CCT-mediated emulsion polymerization systems is based on classical free radical polymerization (FRP) kinetics. Fundamental steps occurring within the polymer particles include propagation, bimolecular termination by disproportionation, which is the dominant termination mechanism for MMA polymerization,[22] and chain transfer to monomer. These reactions are summarized, along with their corresponding reaction frequencies, in the Supporting Information.

For emulsion polymerization, the FRP kinetic scheme has to be extended to include radical entry from the water phase and radical desorption from the polymer particles (Equations 4.1 and 4.2).[23] As mentioned previously, both entry and desorption proceed via the average radical species R_{short}.

Radical entry:

$$R_w^{\bullet} \xrightarrow{\rho} R_{short}^{\bullet} \qquad \rho \tag{4.1}$$

Radical desorption:

$$R_{short}^{\bullet} \xrightarrow{k_{dM}} R_w^{\bullet} \qquad f_{des} = k_{dM} \tag{4.2}$$

In CCT-mediated polymerizations, the radical activity of a propagating chain is transferred to a monomer molecule resulting in the formation of a dead polymer chain with an unsaturated chain-end (Equation 4.3). In the first step, the active Co(II) complex abstracts a hydrogen atom from the propagating polymer chain, resulting in a dead polymer chain and a Co(III)-H (Equation 4.3a). Subsequently, the hydrogen atom is transferred from the Co(III)-H to a monomer molecule, regenerating the active Co(II) complex and a yielding a monomeric radical (R_{short} in the model) capable of propagation (Equation 4.3b). The hydrogen abstraction by the Co(II) catalyst (Equation 4.3a) is assumed to be the rate-determining step,[24] hence the chain transfer frequency (f_{trans}) is given by rate of the hydrogen abstraction step. In CCT-mediated polymerizations, chain transfer is the

dominant chain stoppage event and the MWD is governed by the chain transfer to monomer reaction. In many emulsion polymerization conditions, the CCTA has to be able to mediate multiple polymer particles, therefore entry and exit of the cobalt catalyst are included in the kinetic scheme (Equations 4.4 and 4.5). A balance of the Co(III)-H species is not included because it is a transient product and is assumed not to undergo entry and exit from the particles, as it is quickly reformed into Co(II) (Equation 4.3).[8, 9]

Catalytic chain transfer:

$$\begin{aligned} &R_j^{\bullet} + Co(II) \xrightarrow{k_{trans}} P_j^{=} + HCo(III) \\ &HCo(III) + M \xrightarrow{fast} R_{short}^{\bullet} + Co(II) \end{aligned} \qquad f_{trans} = k_{trans}/N_A V_p \tag{4.3}$$

Co(II) entry:

$$C_w \xrightarrow{f_{cin}} C \qquad f_{cin} \tag{4.4}$$

Co(II) desorption:

$$C \xrightarrow{f_{cout}} C_w \qquad f_{cout} \tag{4.5}$$

The values of the kinetic parameters used in this modeling study are collected in Table 4.1. The simulations were in part designed to encompass the experimental observations of Smeets et al.,[7] where the CCTA used was COBF (bis((difluoroboryl)/dimethylglyoximato)/-cobalt(II)) with methyl methacrylate polymerized at 70$^{\mathrm{O}}$C. The initial concentration of monomer inside the particles was calculated from the experimental data following the swelling of the 45 nm seed particles to a diameter of 65 nm. Note that the simulated MWDs shown in the remainder of this paper do not include the contribution of the seed polymer.

The characteristic time (λ) for a given reaction or mass transport event is the average time it takes for that reaction or event to occur. The characteristic lifetime of a radical present inside a particle devoid of a CCTA (no transfer reactions) ($\lambda_{rad,0}$) will be the time

Table 4.1: Values of the Kinetic Parameters Used in the Simulations of MMA CCT-Mediated Seeded Emulsion Polymerization.

constant	**description**	**unit**	**value**	**reference**
k_p	propagation	$L{\cdot}mol^{-1}{\cdot}s^{-1}$	$1.0x10^3$	[25]
k_t	termination	$L{\cdot}mol^{-1}{\cdot}s^{-1}$	$2.0x10^7$– $2.0x10^{12}$	[26]
k_{fm}	transfer to monomer	$L{\cdot}mol^{-1}{\cdot}s^{-1}$	10^{-2}	[27]
k_{trans}	catalyzed chain transfer	$L{\cdot}mol^{-1}{\cdot}s^{-1}$	$1.5x10^7$	[15, 28, 29]
f_{des}	radical desorption	s^{-1}	$1.4x10^4$, $8.5x10^3$, $5.3x10^3$	See Appendix B
ρ	radical entry	s^{-1}	1, 0.1	
M_0	initial monomer conc.	$L{\cdot}mol^{-1}$	5.86	
d_p	particle diameter	nm	65, 82, 103	
$\bar{n}_{\mathrm{CCTA}}$	average CCTA/particle	-	0.05 – 5.0	
f_{cin}	entry of CCTA	s^{-1}	10^{-4} – 10^3	
f_{cout}	exit of CCTA	s^{-1}	10^{-4} – 10^3	

between two successive radical entries (from the aqueous phase) into the particle plus the time required for the mutual termination of these radicals (Equation 4.6). However, transfer reactions are frequent when a CCTA is present inside the particle; although this does not consume the radical through termination, it creates a short radical which is susceptible to desorption. The characteristic lifetime of a radical existing in particles containing n_{CCTA} (denoted c as a subscript) CCTA molecules ($\lambda_{rad,c}$) is expressed by Equation 4.7.

$$\lambda_{rad,0} = \frac{1}{\rho} + \frac{1}{k_t/N_A V_p} \tag{4.6}$$

$$\lambda_{rad,c} = \frac{1}{f_{trans}(n_{\mathrm{CCTA}})}\left(\frac{f_{des} + k_p[M]}{f_{des}}\right) \tag{4.7}$$

The characteristic time for a catalytic chain transfer reaction to occur and create a dead chain inside a particle containing one or more CCTA molecule is

$$\lambda_{trans,c} = \frac{1}{f_{trans}(n_{\mathrm{CCTA}})} \tag{4.8}$$

The characteristic time that a CCTA molecule resides inside a polymer particle is important for the evolution of the molecular weight distribution. In the absence of a CCTA, bimolecular termination by disproportionation is dominant, whereas in the presence of a CCTA, chain transfer is the dominant chain stopping event. The characteristic time in which the particle is devoid of a CCTA ($\lambda_{Co,0}$), and bimolecular termination reactions dominate, is given by the reciprocal entry frequency for a CCTA molecule (Equation 4.9). Assuming a constant frequency of CCTA exit (f_{cout}), the frequency of CCTA entry will be greater for systems possessing more CCTAs/particle, resulting in a shorter characteristic time for CCTA entry.

$$\lambda_{Co,0} = \frac{1}{f_{cin}} \tag{4.9}$$

These characteristic times will be used in the following sections to illustrate the modeling results.

4.2.3 Development of Population Balances

Modeling the effect of radical segregation on the chain length distribution (CLD) based on the concept of distinguished particle distributions has been investigated by Butte et al.[16, 17] Equations were solved using the discretization method proposed by Kumar and Ramkrishna.[30, 31, 32] The concept of distinguished particle distributions was first introduced by Lichti et al.,[33] where the distribution of singly distinguished particles, $S_{i,t,t'}$, gives the probability of finding a radical chain which began growing at a given time t, and is still growing at time t' in a particle possessing i radicals. Butte et al. reported a simplified approach to determine the probability of having a radical chain of length j inside a particle possessing i radicals, which allows for reactions other than termination to be the chain-stopping event.[17] The singly distinguished particle distribution, $S_{s,i,j}$, can be extended to account for the number of radicals that are "short" (subscript s) inside a particle: radicals created by entry or transfer reactions and that are also able to undergo radical desorption. Similarly, the doubly distinguished particle distribution, $D_{s,i,j,k}$, gives the probability of having a particle possessing i radical chains, s of which are short, and with at least two radical chains of lengths j and k respectively.

The generalized population balance equations used to simulate the CCT-mediated seeded

emulsion polymerization of MMA are listed below (Equations 4.10–4.14).

Modified Smith-Ewart equation:

$$\begin{aligned}\frac{dN_{s,i,c}}{dt} =& -[\rho + (s)f_{des} + f_{cin} + (c)f_{cout} + (s)f_p + (i-s)f_{fm} \\ &+ (c)(i-s)f_{trans} + (i-s)(i-s-1)f_t + 2(i-s)(s)f_t + (s)(s-1)f_t]N_{s,i,c} \\ &+ \rho N_{s-1,i-1,c} + [(i-s+1)f_{fm} + (c)(i-s+1)f_{trans}]N_{s-1,i,c} \\ &+ f_{cin}N_{s,i,c-1} + (c+1)f_{cout}N_{s,i,c+1} + (s+1)f_{des}N_{s+1,i+1,c} \\ &+ (i-s+2)(i-s+1)f_tN_{s,i+2,c} + 2(i-s+1)(s+1)f_tN_{s+1,i+2,c} \\ &+ (s+2)(s+1)f_tN_{s+2,i+2,c} + f_p(s+1)N_{s+1,i,c} \end{aligned} \tag{4.10}$$

Singly distinguished particles:

$$\begin{aligned}\frac{dS_{s,i,j,c}}{dt} =& -[\rho + (s)f_{des} + f_p + f_{cin} + (c)f_{cout} + (s)f_p + (i-s)f_{fm} \\ &+ (c)(i-s)f_{trans} + (i-s)(i-s-1)f_t + 2(i-s)(s)f_t + (s)(s-1)f_t]S_{s,i,j,c} \\ &+ \rho S_{s-1,i-1,j,c} + [(i-s)f_{fm} + (c)(i-s)f_{trans}]S_{s-1,i,j,c} \\ &+ f_pS_{s,i,j-1,c} + f_{cin}S_{s,i,j,c-1} + (c+1)f_{cout}S_{s,i,j,c+1} \\ &+ (s+1)f_{des}S_{s+1,i+1,j,c} + 2(i-s+1)(i-s)f_tS_{s,i+2,j,c} \\ &+ (i-s)(s+1)f_tS_{s+1,i+2,j,c} + (s+2)(s+1)f_tS_{s+2,i+2,j,c} \\ &+ (s+1)f_pS_{s+1,i,j,c} + \underset{j=1}{\sigma}(s+1)f_pN_{s+1,i,c} \end{aligned} \tag{4.11}$$

Dead chains:

$$\frac{dP_j}{dt} = \frac{1}{N_A V_p}\left[\begin{array}{l} \sum_{i=1}^{I_{\max}} \sum_{s=0}^{I_{\max}-1} \sum_{c=0}^{c_{\max}} (f_{fm} + (c) f_{trans}) S_{s,i,j,c} \\ +\rho \frac{1}{I_{\max}} \sum_{s=0}^{I_{\max}-1} \sum_{c=0}^{c_{\max}} S_{s,I,j,c} \\ +2 f_t \sum_{i=2}^{I_{\max}} \sum_{s=1}^{I_{\max}-1} \sum_{c=0}^{c_{\max}} (s) S_{s,i,j,c} \\ +2 f_t \sum_{i=2}^{I_{\max}} \sum_{s=0}^{I_{\max}-2} \sum_{c=0}^{c_{\max}} (i-s-1) S_{s,i,j,c} \end{array}\right] \tag{4.12}$$

Average number of radicals per particle:

$$\bar{n} = \sum_{i=0}^{I_{\max}} \sum_{s=0}^{I_{\max}} \sum_{c=0}^{c_{\max}} (i) N_{s,i,c} \tag{4.13}$$

Average number of CCTA molecules per particle:

$$\bar{n}_{\mathrm{CCTA}} = \sum_{i=0}^{I_{\max}} \sum_{s=0}^{I_{\max}} \sum_{c=0}^{c_{\max}} (c) N_{s,i,c} \tag{4.14}$$

In considering distinguished particle distributions, expressions for the doubly distinguished particles are often required to calculate the contribution of termination by combination to the chain length distribution.[17] Since it is assumed that the majority of chain-stoppage in this system occurs either by catalytic chain transfer (in the presence of a CCTA) or termination by disproportionation[22] (in the absence of a CCTA), the double distinguished distribution was not included to simplify the simulation.

4.2.4 Development of the Numerical Solution

The simulations were conducted for small polymer particles ($d_p < 100$ nm). Although the assumption of a zero-one system may have been appropriate (i.e., termination occurs instantaneously when a radical enters a particle already containing a propagating radical), a zero-one-two system was chosen to allow instances where more than one radical was present inside a particle. The generalized form of these equations for the zero-one-two system is available in Appendix **??**. The Kumar and Ramkrishna method of numerical discretization described by Butte et al.[16, 17] was also employed here to reduce the 10^6 points of integration down to 100. The grid independence of the solution was tested by running the simulations

with 500, 200 and 100 points of integration of the CLD, and no loss of resolution of the solution was observed. The maximum number of CCTA per particle (C_{max}) was set at 20 and the maximum number of radicals per particle (I_{max}) was set at 2; throughout the simulations the boundary conditions were observed to ensure the system did not approach these. This system of differential equations was solved in Fortran by numerical integration with the solver DLSODI (backward Euler method) with a step size of 1 s.

4.3 Results and Discussion

In this work, two limiting cases of compartmentalization effects in CCT-based emulsion are investigated: (i) when the global concentration of CCTA ($\bar{n}_{\mathrm{CCTA}}$) dictates the chain length distribution, as in low viscosity systems like early miniemulsion polymerizations and (ii) when the discrete numbers of CCTA molecules (n_{CCTA}) per particle influences the CLD, as is expected in a seeded emulsion based system.[7] The model will first be validated by simulating miniemulsion like conditions, in the absence of mass transfer limitations, then the remaining simulations will discuss a seeded emulsion system, when transport of the CCTA between particles is limited.

4.3.1 Validation of the Model

In CCT-mediated miniemulsion polymerization, good control over the MWD can be achieved[10, 15] by adding low quantities of CCTA to the polymerization. Typically, monomodal MWDs are obtained with a polydispersity index (PDI) of approximately 2. It has been shown that the instantaneous DP_n can be described with a modified Mayo Equation based on a global CCTA concentration (i.e., a noncompartmentalized situation). A rewritten form of the modified Mayo Equation is presented below based on the average number of CCTA per particle in the system (Equation 4.15).

$$\frac{1}{DP_{inst}} = \frac{1}{\frac{k_p M}{\rho} + \frac{k_p M}{k_t / N_A V_p}} + \frac{k_{fm}}{k_p} + \frac{k_{trans}^{app}(\bar{n}_{\mathrm{CCTA}})/N_A V_p}{k_p[M]} \tag{4.15}$$

The derived model was validated by simulating the CLD in a CCT-mediated miniemulsion polymerization system. This is a well-defined system as at low conversion, the miniemulsion particles (or droplets) pose little resistance to CCTA entry and exit due to the low

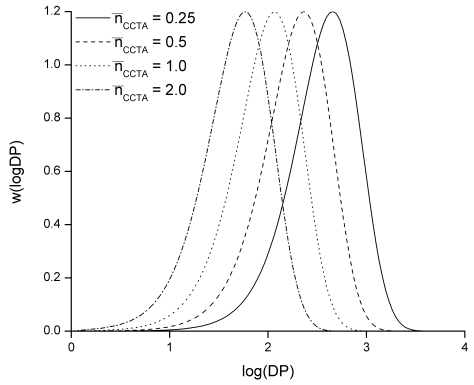

Figure 4.2: w(log DP) plot of instantaneous CLD of CCT-mediated miniemulsion-like systems with a low mass transfer barrier to CCTA entry and exit. Simulations conducted assuming 65 nm particles, $[M]_0 = 9.4$ mol·L^{-1}, $k_{trans} = 1.5\text{x}10^7$ L·mol^{-1}·s^{-1}, $k_t = 2.0\text{x}10^7$ L·mol^{-1}·s^{-1}, $\rho = 1$ s^{-1} and $f_{cout} = 10^{12}$ s^{-1} at different $\bar{n}_{\text{CCTA}}$.

Table 4.2: Simulated and Predicted Instantaneous DP$_n$ and PDI for a CCT-Mediated Miniemulsion-like System.

$\bar{n}_{\text{CCTA}}$	**DP$_n$ (Model)**	**PDI (Model)**	**DP$_n$ (Mayo)**
0.25	218	2.24	212
0.50	113	2.21	107
1.0	58	2.17	54
2.0	30	2.10	27

internal viscosity of the system. Mathematically this is simulated by maintaining an extremely high and constant frequency of CCTA exit from the particles, $f_{cout} = 10^{12}$ s^{-1}. The frequency of entry of CCTA is thus simultaneously high as it is determined by $f_{cin} = \bar{n}_{\text{CCTA}} f_{cout}$. Simulations were conducted with various amounts of CCTA, $\bar{n}_{\text{CCTA}} = 0.25$, 0.5, 1.0 and 2.0. The instantaneous DP$_n$ and PDI at the start of the polymerization were estimated from the resulting CLDs (Figure 4.2). In Table 4.2, it is shown that these DP$_n$s match well with the calculated DP$_n$s from the modified Mayo equation (Equation 4.15), and furthermore that the PDIs of the simulations are close to 2, as estimated from the Flory-Schulz most probable distribution in transfer dominated systems.[22] This type of system is considered "uncompartmentalized" with respect to the CCTA, and each particle experiences approximately the same average concentration or number ($\bar{n}_{\text{CCTA}}$) throughout the course of the polymerization.

From the results presented in Figure 4.2 and Table 4.2, it can be concluded that the derived model is capable of predicting the instantaneous DP_n and the PDI when there is low resistance to mass transport of the CCTA. Moreover, the results illustrate that the kinetic events in CCT-mediated emulsion polymerization are captured to an extent that a reliable output in terms of the CLD is obtained. This allows us to apply this model with confidence to simulate CLDs in a polymerization at high instantaneous conversion. The effect of apparent chain transfer activity, size of the polymer particles, the amount of CCTA, and the resistance toward mass transport on the CLD will be discussed in detail in the following sections.

4.3.2 Effect of the Apparent Rate Coefficient of Catalytic Chain Transfer

The compartmentalization effects on the CLD for 65 nm particles in a seeded, CCT-mediated polymerization system were investigated with different apparent chain transfer rate coefficients, k_{trans}^{app}. The rate coefficient of catalyzed chain transfer (k_{trans}) is an intrinsic property of a CCTA, governed by the type of monomer and solvent used in the polymerization. For CCTA, typically k_{trans} values on the order of 10^7 $L{\cdot}mol^{-1}{\cdot}s^{-1}$ are measured experimentally in MMA bulk polymerization.[9] However, in MMA emulsion polymerizations typically lower values are reported when compared to bulk polymerization as a consequence of the coordination of hydroxyl groups to the axial ligand positions of the complex.[15, 28, 29] Previously, it was shown that at high instantaneous conversion of the polymer particles (i.e., at high viscosity) the value of the chain transfer constant ($C_T = k_{trans}/k_p$) appeared to decrease with increasing viscosity.[34] Although there is no hard evidence that the chain transfer reaction is diffusion limited, there are very strong indications that this may be the case. Heuts and co-workers reported a relationship between the reaction rate and the microscopic viscosity (or monomeric friction coefficient).[35, 36] Although the bulk viscosity might increase several orders of magnitude with increasing polymer fractions, the diffusion coefficient of small molecules (such as the CCTA), remains approximately constant. However, for higher polymer fractions the diffusion coefficient will start to decrease strongly,[37, 38, 39, 40, 41] and, consequently, so will the value of the chain transfer constant. Compartmentalization in CCT-mediated emulsion polymerization was suggested to originate from a reduced mobility of the CCTA due to the high viscosity of the polymer particles. In the current simulations,

the instantaneous conversion is 0.80 and higher, therefore it is not unlikely that, besides compartmentalization, the observed value of the chain transfer coefficient for COBF is lower than the expected value of 1.5x10^7 L·mol^{-1}·s^{-1} [15, 28, 29] as determined in MMA miniemulsion polymerization. The effects of the compartmentalization of COBF and a lower apparent rate coefficient of chain transfer (k_{trans}^{app}) on the CLD are shown in Figure 4.3.

In the simulations, similar to the experiments (Figure 4.1),[7] the average number of CCTA molecules per polymer particle ($\bar{n}_{\mathrm{CCTA}}$) has been simulated at 0.5 and 1.0. Mathematically this is done by changing the initial fraction of particles containing a CCTA molecule and the frequency of CCTA entry, f_{cin} ($= \bar{n}_{\mathrm{CCTA}} f_{cout}$), while maintaining a constant f_{cout} of 10^{-3} s^{-1}. For clarity in interpreting the results, termination is considered to be nearly instantaneous upon the entry of a second radical into the particle. (This eliminates the creation of a disproportionation product that can obscure the chains created through chain transfer when they occur at a similar chain length.) Simulations at different k_ts are shown in the Appendix **??** to demonstrate that CLDs still display contributions from termination and CCT, however, depending on the value of k_t, the disproportionation product will partially obscure the CLD. This assumption is employed in all the following simulations.

It can be seen from Figure 4.3a–4.3c that the chain length of the polymer produced by catalytic chain transfer increases with diminishing k_{trans}^{app}. Because the transfer-derived product is relatively short and present in low concentrations, it is only visible on the w(DP) plot at $\bar{n}_{\mathrm{CCTA}} = 0.5$ (Figure 4.3a) and not at all on the w(log DP) plot (not shown), where there is a greater emphasis on the higher molecular weight chains. The w(DP) plot displays the weight fraction of polymer present at each chain length, such that $\int_0^\infty w(DP)dDP = 1$. The w(log DP)plot is the differential log MWD and is often used in comparison with GPC traces, in which the molecular weight of polymers eluting from the columns decreases approximately exponentially with the elution volume. This distribution can be obtained from the w(DP) distribution through $w(\log DP) = DP/(\log_{10} e)w(DP)$. The w(log DP) plot also maintains the normalized distribution such that $\int_0^\infty w(\log DP)d\log DP = 1$.[42] However, since the low molecular weight polymer population is present in larger concentrations for $\bar{n}_{\mathrm{CCTA}} = 1$, both the w(DP) and w(log DP) plots are presented for those simulations (Figures 4.3b, 4.3c).

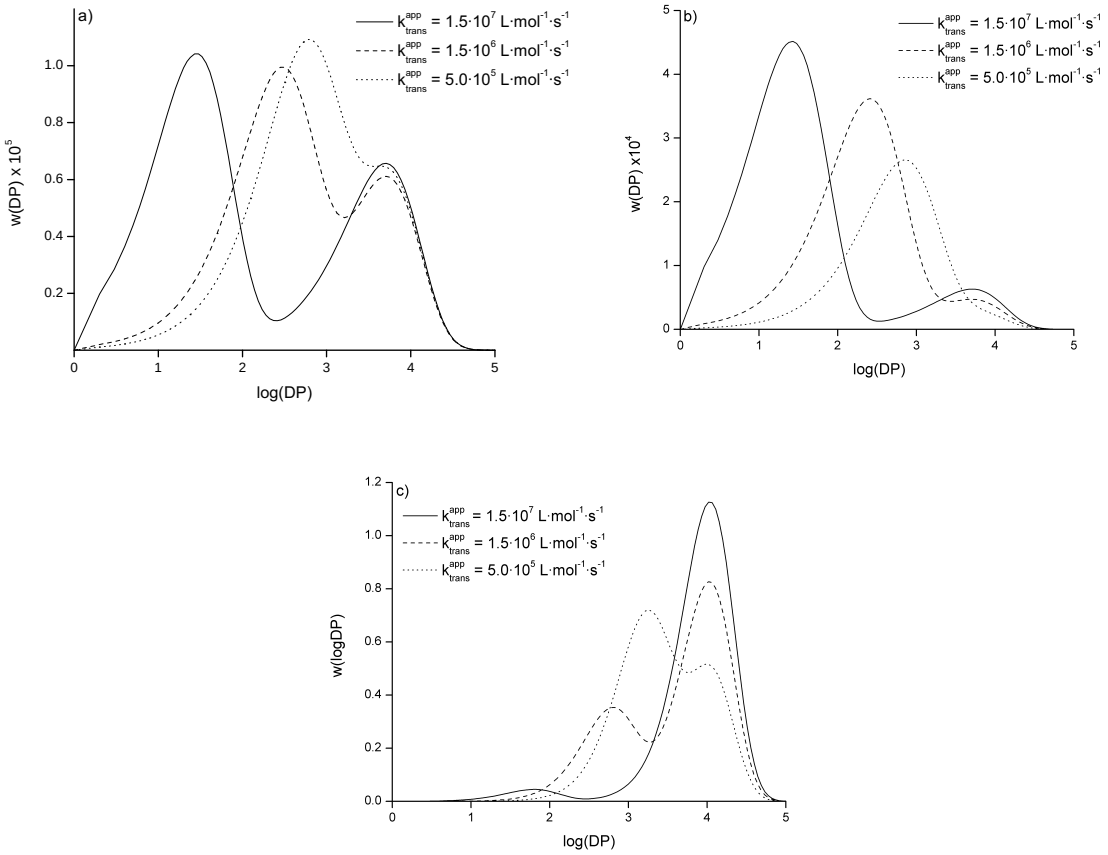

Figure 4.3: Simulated CLD for 65 nm particle with varying k_{trans}^{app} at 30% conversion, assuming $f_{cout} = 10^{-4}$ s^{-1} and $\rho = 1$ s^{-1}. (a) w(DP) plot, $\bar{n}_{\mathrm{CCTA}} = 0.5$; (b) w(DP) plot, $\bar{n}_{\mathrm{CCTA}} = 1$; (c) w(log DP) plot, $\bar{n}_{\mathrm{CCTA}} = 1$. The presence of seed polymer is not accounted for in the simulations.

Using the published value of k_{trans} in emulsion polymerization, $k_{trans} = 1.5\text{x}10^7$ L·mol^{-1}·s^{-1} (Table 4.1), the resulting CLD is bimodal for $\bar{n}_{\mathrm{CCTA}} = 0.5$ (Figure 4.3a). This indicates that one peak is originating from polymer created mainly through bimolecular termination in the absence of CCTA (although other chain stopping events may also contribute, including uncatalyzed chain transfer to monomer) with a DP = 5210. The DPs reported in this discussion correspond to the peak values of the w(DP) distribution. The DP of this polymer population corresponds with the expected DP based on a zero-one system (DP = kp[M]/ρ). The secondary peak at DP = 24 originates from polymer chains formed by catalytic chain transfer. The chain length of the transfer-dominated polymer is extremely short, indicating that chain transfer occurs quickly following the entry of a radical into a particle containing a CCTA, or after the entry of a CCTA into a particle containing a propagating radical

($\lambda_{trans,1}$ = 0.058 s). The characteristic life time of a radical inside a particle containing a single CCTA molecule is $\lambda_{rad,1}$ = 0.0075 s, which is significantly less than that of the characteristic residence time of a CCTA molecule residing there, $\lambda_{Co,1}$ = 1000 s. Therefore, numerous radical entries, and subsequent transfer reactions, will occur during the residence time of a single CCTA inside that particle, resulting in polymer with a relatively low DP (Figure 4.3a). A similar situation can be observed for the system containing $\bar{n}_{\mathrm{CCTA}}$ = 1.0, and a similar values for k_{trans}^{app} (Figures 4.3b, 4.3c); the bimolecular termination peak and the transfer-dominated peak are present at the same degrees of polymerization (DP = 5160 and 22 respectively) as was the case for the system with a $\bar{n}_{\mathrm{CCTA}}$ = 0.5. Because a larger fraction of polymer particles will contain 1 or more CCTA molecules at any given point in time in the $\bar{n}_{\mathrm{CCTA}}$ = 1 system, the amount of transfer-dominated polymer is greater when compared to the system with $\bar{n}_{\mathrm{CCTA}}$ = 0.5. This explains why the bimodal distribution is also visible on the w(log DP) plot. Polymer chains of this short length (DP = 23) would be rarely visible on a GPC trace because they are present in low concentrations compared to the longer chains and may also be obscured by the disproportionation product in systems not exhibiting zero-one behavior.

Lowering the rate coefficient of chain transfer by an order of magnitude (k_{trans}^{app} = 1.5x10^6 L·mol^{-1}·s^{-1}) also results in a bimodal CLD for $\bar{n}_{\mathrm{CCTA}}$ = 0.5. The bimolecular termination peak remains at approximately the same DP = 5030, but the transfer-dominated peak shifts to a higher DP of 258, which is clearly visible on the w(log DP) plot, and likely also on a GPC trace. Similarly, the bimolecular termination peak and the transfer-dominated peak occur at similar DP for both the system $\bar{n}_{\mathrm{CCTA}}$ = 1 and 0.5.

Simulations with an even lower rate coefficient of catalytic transfer (k_{trans}^{app} = 5.0x10^5 L·mol^{-1}·s^{-1}), result in an identical DP for the bimolecular termination peak, and shifts the DP of the transfer-derived population to a higher value (Figures 4.3a–4.3c). This example illustrates that the two polymer populations may start to overlap when the rate of catalytic chain transfer reaches a certain value. In this scenario, the characteristic times for transfer ($\lambda_{trans,1}$) and for bimolecular termination in a particle without of a CCTA molecule ($\lambda_{rad,0}$) are in the same order of magnitude (∼1 s).

The chain length of the transfer-derived product obtained in our simulations with k_{trans}^{app} = 1.5x10^6 L·mol^{-1}·s^{-1} is easily distinguishable on both the w(DP) and w(log DP) plots.

Therefore, this value for k_{trans}^{app} was used primarily throughout the remainder of the simulations. The conditions chosen for the simulations were based on the experimental system as reported by Smeets et al.[7] The DP range of the experimentally observed multimodal MWDs (Figure 4.1) correspond to the simulation with a k_{trans}^{app} value of 1.5x10^6 L·mol^{-1}·s^{-1}. This result supports the ideology that the chain transfer reaction is diffusion controlled and that the chain transfer activity is decreasing at higher polymer fractions in the polymer particles.

4.3.3 Particle Size and the Confined Space Effect

An important characteristic of compartmentalization in emulsion polymerization is the confined space effect. This refers to the increase in the reaction rate as the volume of the polymer particle decreases. The effect of the confined space effect on the CLD is shown in simulations of polymerizations with 65, 82 and 103 nm polymer particles (Figure 4.4). The global COBF concentrations were kept constant for all the polymerizations, which corresponds to the values $\bar{n}_{\mathrm{CCTA}} = 0.25$, 0.5 and 1.0 for the 65, 82 and 103 nm particles, respectively. The frequency of radical entry remained constant for all the simulations at $\rho = 1\ \mathrm{s}^{-1}$, which does not represent a constant global concentration of initiator. The frequency of radical exit, f_{des}, was adjusted for particle size (please see Appendix **??**). As with the simulations presented above, bimolecular termination is considered instantaneous upon the entry of a second radical into a particle.

In the simulations presented in Figure 4.4, the COBF concentration was kept constant with respect to the monomer concentration. From the Mayo equation (in the absence of compartmentalization effects) it is expected that the instantaneous DP$_n$ (DP$_n^{inst}$) of the chain transfer dominated CLD should be 92 (at 30% conversion, Equation 4.15 used in its classical form). In Figure 4.4 it can be concluded that there is a clear shift in DP as a function of the particle size. Moreover, the ratio of polymer originating from chain transfer and from bimolecular termination increases as the particle size increases. In these simulations, both the radicals and CCTA molecules are considered compartmentalized species. As such, the rates of reaction involving radicals and the CCTA molecules are subjected to changes based on the volume of the particle, i.e. the confined space effect. The effect of particle volume on the rate of chain transfer dictates that the rate of chain transfer is 4 times faster in a 65 nm particle when compared to an 82 nm particle and

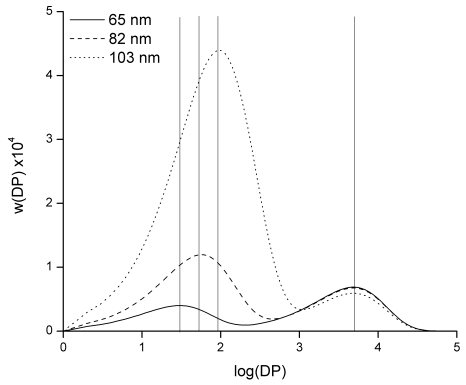

Figure 4.4: w(DP) plot for the simulated CLD at different particle sizes at 30% conversion, assuming k_{trans}^{app} = 1.5x10^7 L·mol^{-1}·s^{-1} and f_{cout} = 10^{-3} s^{-1}. The total concentration of CCTA in the system was kept constant, resulting in $\bar{n}_{\mathrm{CCTA}} = 0.25$ (65 nm particles), $\bar{n}_{\mathrm{CCTA}} = 0.5$ (82 nm particles), and $\bar{n}_{\mathrm{CCTA}} = 1.0$ (103 nm particles). The frequency of radical entry into the particles remained at $\rho = 1$ s^{-1} for all simulations. The vertical lines are added to guide the eye to the peak degrees of polymerization.

16 times faster when compared to a 103 nm particle (Equation 4.16). Therefore, it is expected that the chain length of the transfer-dominated product will reflect the effects of compartmentalization (Figure 4.4).

$$R_{trans} = \frac{k_{trans}^{app}(n_{\mathrm{CCTA}})}{(N_A V_p)^2} \quad \mathrm{mol \cdot L^{-1} \cdot s^{-1}} \tag{4.16}$$

The transfer-dominated peak in the 65 nm particle is extremely small (DP = 30), which corresponds to the very short characteristic time for chain transfer, $\lambda_{trans,1}$ = 0.00577 s. In the 82 nm particles, the rate of transfer is sufficiently fast to clearly observe separate bimolecular termination and transfer-dominated peaks. The transfer-dominated peak has a DP of 61, indicating that more propagation steps occurred prior to a chain transfer event, as the characteristic time of a transfer reaction is longer, i.e., $\lambda_{trans,1}$ = 0.0116 s. The 103 nm particles experienced a higher characteristic time for chain transfer ($\lambda_{trans,1}$ = 0.0230 s), and the transfer-derived peak is still distinguishable, although it begins to overlap with the lower end of the bimolecular termination peak.

The characteristic time for chain transfer decreases with decreasing particle size. Therefore the probability of chain transfer is higher in smaller polymer particles, which ultimately results in a somewhat lower DP for the 65 nm particles when compared to the 82 and 103 nm particles, respectively. The ratio of polymer originating from chain transfer and bimolecular

termination increases with increasing particle size as a consequence of the changes in $\bar{n}_{\mathrm{CCTA}}$ (which is particle size dependent). Even though the global concentration of CCTA remained constant with respect to monomer (which is particle size independent), the average number of CCTA molecules per particle increases with diminishing particle size. The probability that a polymer chain is terminated by CCT increases with the particle size, which results in an increase of the fraction of polymer terminated by CCT.

4.3.4 Changes in the Average Number of CCTA Molecules per Particle

Varying $\bar{n}_{\mathrm{CCTA}}$ illustrates a situation where the concentration of CCTA in the system is changing at a constant particle concentration. In bulk and solution polymerization this results in changes in the DP of the formed polymer, which is described by the Mayo equation.[43] In CCT-mediated emulsion polymerization, this relationship also holds.[10, 11, 12, 44] However, when the viscosity is high inside the particles, compartmentalization of the CCTA can occur which results in a discrete distribution of CCTA molecules over the population of polymer particles.[7] Consequently, independent of $\bar{n}_{\mathrm{CCTA}}$, multimodal MWDs were obtained experimentally where the individual contributions to the multimodal MWD are believed to correspond to polymer particles containing 0, 1, 2, etc. CCTA molecules. Moreover, polymer populations formed in the presence of 0, 1, 2, etc. CCTA molecules proved to have a DP independent of the total amount of CCTA in the system.[7] Conditions similar to this can be simulated by changing $\bar{n}_{\mathrm{CCTA}}$while maintaining a fixed f_{cout}, which is representative of a system with significant mass transfer barriers to CCTA entry and exit from the particles (Figure 4.5).

In these simulations, bimodal distributions are observed, independent of $\bar{n}_{\mathrm{CCTA}}$. Only the relative amounts of transfer-derived and bimolecular termination-derived products change (Figure 4.5). The latter result originates from the fact that the characteristic time of a CCTA molecule residing in a polymer particle ($\lambda_{Co,c}$) increases with increasing CCTA concentration. For the reported simulations, the characteristic time of a polymer particle without a CCTA molecule ($\lambda_{Co,0}$), which is dependent on the global CCTA concentration, is longer than the characteristic time of a radical existing inside those particles ($\lambda_{rad,0}$ = 1 s) even at $\bar{n}_{\mathrm{CCTA}} = 5$. This results in a situation where several bimolecular termination events occur prior to the entry of a CCTA molecule. Consequently a bimolecular

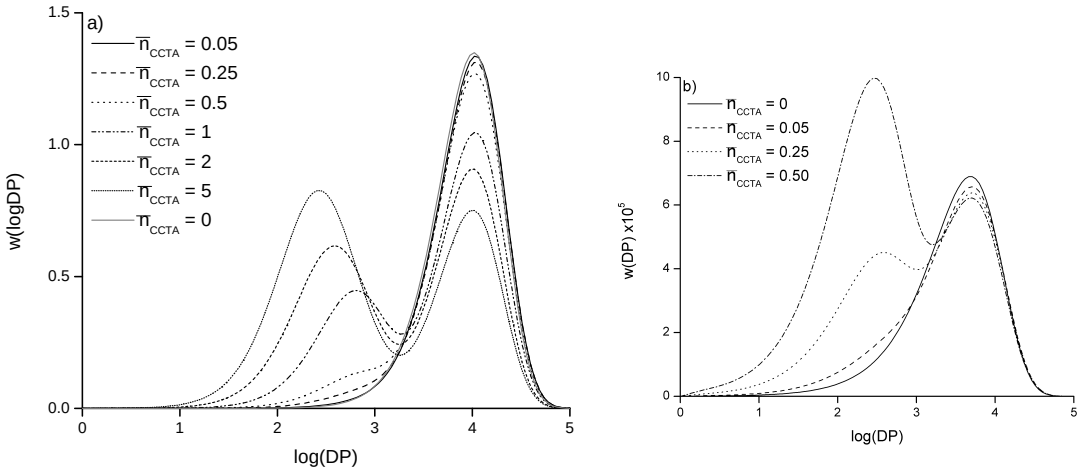

Figure 4.5: Simulated CLDs of 65 nm particles with varying $\bar{n}_{\mathrm{CCTA}}$ at 30% conversion, assuming k_{trans}^{app} = 1.5x10^6 L·mol^{-1}·s^{-1}, ρ = 1 s^{-1} and f_{cout} = 10^{-4} s^{-1}. (a) w(log DP) plot; (b) w(DP) plot with $\bar{n}_{\mathrm{CCTA}}$ = 0.50.

termination-derived peak is observed for each system at DP 5100, regardless of the amount of CCTA. The most extreme case presented here, with $\bar{n}_{\mathrm{CCTA}} = 5$, still shows a bimolecular termination peak, although its concentration is significantly lower than for the other simulations with lower $\bar{n}_{\mathrm{CCTA}}$ (Figure 4.5a). In this case, the characteristic time of a particle devoid of a CCTA molecule is $\lambda_{Co,0}$ = 200 s, which is still significantly longer than the residence time of a radical in a polymer particle, $\lambda_{rad,0}$ = 1 s. Whereas this explains why high MW polymer is formed in the $\bar{n}_{\mathrm{CCTA}} = 5$ system, it must be noted that instances of particles devoid of CCTA are extremely rare, owing to the very small concentration of such products. The concentration of dead polymer created by bimolecular termination is the highest in particles possessing $\bar{n}_{\mathrm{CCTA}} = 0.05$, as the characteristic time that such a particle remains devoid of a CCTA molecule is $\lambda_{Co,0}$ = 2x10^4 s, which allows for a significant number of bimolecular termination events prior to the entry of a CCTA molecule. Note that due to computational limitations it was not possible to investigate a pseudo-bulk case where $\bar{n}_{\mathrm{CCTA}}$was significantly higher than 5.

A striking observation is that the molecular weight peak for the transfer-dominated population in simulations with $\bar{n}_{\mathrm{CCTA}} = 0.25$ and 0.5, and to a lesser resolution for $\bar{n}_{\mathrm{CCTA}}$ 0.05, are all located at DP 310 (Figure 4.5b), further confirming that the evidence of compartmentalization observed experimentally by Smeets et al.[7] can be attributed to a discrete distribution of CCTA molecules over the polymer particles. The relative amounts of the polymer populations, however, do vary with $\bar{n}_{\mathrm{CCTA}}$. In these systems the particles

experience either 0 or 1 CCTA molecule per particle. Note that instances where a polymer particle possesses 2 or more CCTA molecules are rare, although they cannot be excluded. This result reinforces the hypothesis that the MWD of the polymer product is not dependent on the absolute concentration of CCTA in the system, but instead on the discrete number of CCTA molecules compartmentalized inside each particle over the course of the polymerization.

When the amount of CCTA is further increased, i.e. $\bar{n}_{\mathrm{CCTA}} > 1.0$, the peak of the transfer-dominated polymer population is shifted to lower chain lengths. At these conditions, the likelihood of polymer particles containing more than 1 CCTA molecule is greatly enlarged. This would result in a multimodal CLD, where the individual contributions originate from polymer particles containing 0, 1, 2, 3, etc. CCTA molecules. The simulation shows that the width of the CLD increases with increasing CCTA concentration (Figure 4.5a). Notice that the transfer-dominated peak for $\bar{n}_{\mathrm{CCTA}} = 5$ encompasses a large range of the low molecular weight end of the $w(\log \mathrm{DP})$ plot, extending towards a lower DP, when compared to the distributions obtained with $\bar{n}_{\mathrm{CCTA}} \leq 0.50$. The CLDs originating from polymer particles experiencing different number of CCTA molecules per particle are close in DP, especially on a logarithmic scale, and this explains why a broad CLD is observed in the simulations, rather than a distinct multimodal CLD.

4.3.5 Changing the Diffusional Resistance to CCTA Entry and Exit from the Particles

The rates of CCTA entry and desorption are governed by the resistance against mass transport of the catalyst. As the reaction proceeds and monomer is consumed, the viscosity of the polymer particle increases, reducing the rate of diffusion. In this model, the effects of diffusion limitations can be simulated by changing the frequencies of entry and exit of CCTA molecules from the polymer particles, f_{cin} and f_{cout} respectively (Figure 4.6).

There are two limiting cases. First, when the frequencies of CCTA entry and exit are both low, i.e., f_{cin} and $f_{cout} < 0.1\ \mathrm{s}^{-1}$, the simulations mimic a scenario where the viscosity of the polymer particles is high and consequently significant resistance against CCTA mass transport can be expected, as shown experimentally in seeded emulsion polymerization.[7] Second, when the frequencies of CCTA entry and exit are both high, i.e., f_{cin} and f_{cout}

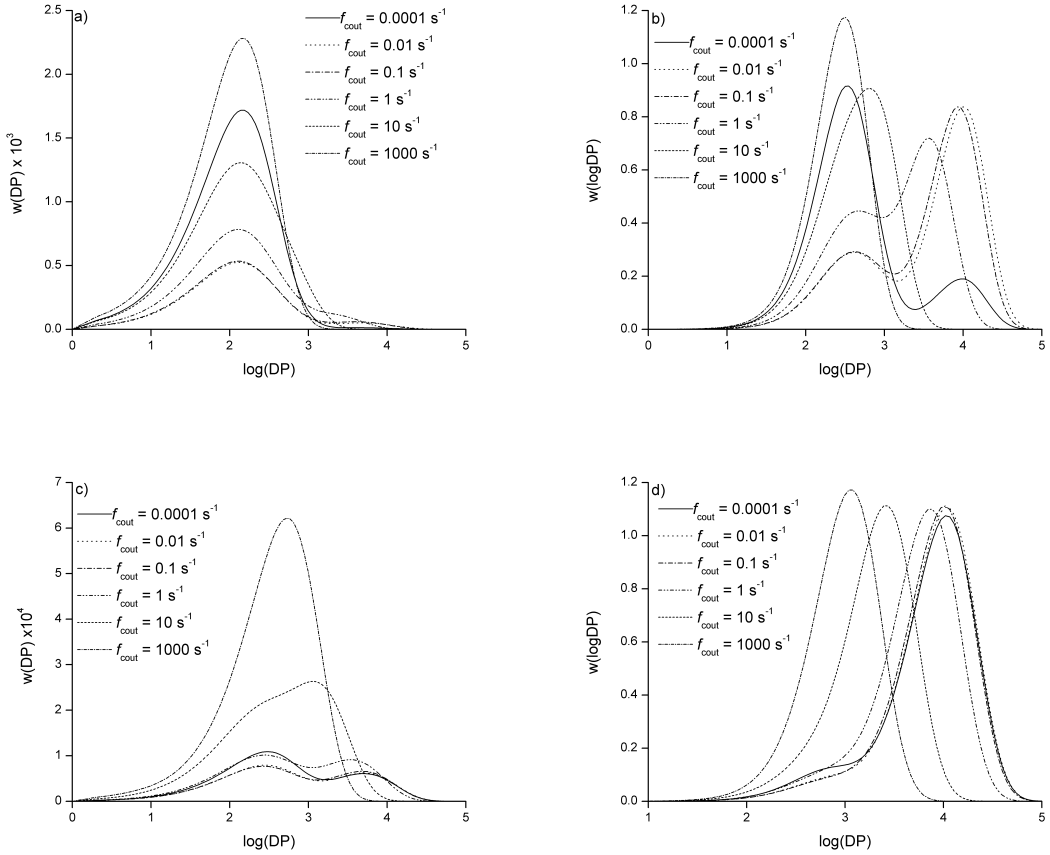

Figure 4.6: Simulated CLDs with different diffusion resistances (f_{cout} and f_{cin}) to CCTA entry and exit from the particles at 30% conversion, assuming 65 nm particles, $\rho = 1$ s^{-1} and $k_{trans}^{app} = 1.5\text{x}10^6$ L·mol^{-1}·s^{-1}. (a) w(DP) plot for $\bar{n}_{\text{CCTA}} = 2$; (b) w(log DP) plot with $\bar{n}_{\text{CCTA}} = 2$; (c) w(DP) plot with $\bar{n}_{\text{CCTA}} = 0.5$; d) w(log DP) plot with $\bar{n}_{\text{CCTA}} = 0.5$.

≥ 10 s^{-1}, this mimics a scenario where the viscosity of the polymer particles is low and consequently mass transport limitations are negligible, as is often seen at low conversion in *ab initio* emulsion and miniemulsion polymerization.[10, 14, 15] The changes in f_{cout} (and the respective f_{cin}) reflect viscosity effects on the CLD.

In the simulations for $\bar{n}_{\text{CCTA}} = 2$, both bimolecular termination-dominated (DP = 5000) and transfer-dominated (DP = 139) peaks are obtained at identical DP for f_{cout} between 10^{-4} and 0.01 s^{-1}. This indicates that the characteristic time of a particle devoid of CCTA molecules (50 s $\leq \lambda_{Co,0} \leq 5\text{x}10^3$ s) is greater than the characteristic time of a radical inside similar particles ($\lambda_{rad,0} = 1$ s), allowing many instances of bimolecular termination prior to the entry of a CCTA. In the same system, f_{cout} between 0.1 and 1 s^{-1} represents a transitional region where the characteristic time of a particle devoid of CCTA (0.5 s $\leq$

$\lambda_{Co,0} \leq 5$ s) is of the same order of magnitude of the characteristic radical lifetime inside such particles ($\lambda_{rad,0} = 1$ s). Consequently some polymer is created through bimolecular termination, but also a significant portion of the population in the bimolecular termination-dominated peak is formed by polymer chains which begin propagating in a polymer particle devoid of CCTA and are terminated upon the entry of a CCTA molecule. This explains why the transfer-dominated peak is present at the same DP as for systems with higher diffusional resistances, but the bimolecular termination-dominated distribution is shifted to a lower DP. This transitional zone behavior is also present in the $\bar{n}_{\mathrm{CCTA}} = 0.5$, where the characteristic times for particle devoid of CCTA are 2 and 0.2 s for $f_{cout} = 0.1$ and 1 s^{-1} respectively.

A monomodal peak is observed for $f_{cout} \geq 10\ \mathrm{s}^{-1}$ for the system with $\bar{n}_{\mathrm{CCTA}} = 2$ and with $f_{cout} \geq 10^3\ \mathrm{s}^{-1}$ for the system with $\bar{n}_{\mathrm{CCTA}} = 0.5$ (Figure 4.6a, 4.6c). At these conditions, the resistance toward CCTA diffusion is negligible and each particle experiences polymerization in the presence of at least 1 CCTA molecule during the lifetime of each radical inside the particle. Consequently all dead polymer chains are produced through chain transfer, and the expected DP_n can be calculated by the modified Mayo equation (Equation 4.15), as was illustrated in the model validation section.[18] Therefore, the simulated monomodal peak with a high f_{cout} and $\bar{n}_{\mathrm{CCTA}} = 2$ corresponds to the same DP as the transfer-dominated peaks with $n_{\mathrm{CCTA}} = 2$ in the simulations with significant diffusional resistances to CCTA transport between particles.

4.4 Comparison of Simulations with Experimental Results

Many of the simulated CLDs in this work reflect the effects of CCTA compartmentalization. It was shown that the frequencies of CCTA entry and exit are primarily responsible for governing the compartmentalization of the CCTA and hence the multimodality of the CLD. The presence of the bimodal CLD can be attributed to bimolecular termination and chain transfer in polymer particles in the absence or presence of a CCTA. Furthermore, it was illustrated that an increase of the overall CCTA concentration did not affect the DP of transfer-dominated molecular weight peak when $\bar{n}_{\mathrm{CCTA}} > 1$. These results are in agreement with the experimental observations made before[7] in seeded emulsion polymerization under comparable polymerization conditions.

Experimentally, the bimolecular termination-dominated peak corresponds to a DP of approximately 1050, which is much shorter than that described by the simulations. The chain length of the population created by bimolecular termination is influenced greatly by the choice of the frequency of radical entry in the particle (ρ). For the simulations, a much lower frequency of radical entry was chosen (1 and 0.1 s^{-1}) to allow a clearer separation between the bimolecular termination and the transfer-dominated peaks on the CLD. The transfer-dominated polymer population obtained by simulation is similar to that reported in the experimental studies.

To further confirm that the peaks on the simulated CLDs with different $\bar{n}_{CCTA}$ can be directly related to presence or absence of a CCTA, the expected DP of the produced polymer in polymer particles containing $n_{CCTA} = 1$, 2, etc. CCTA molecules can be calculated from a modified form of the Mayo equation (Equation 4.15) where $\bar{n}_{CCTA}$ is substituted for n_{CCTA}. The calculated instantaneous DP_n for the different amounts of CCTA ($n_{CCTA} = 0$, 1 and 2) at an instantaneous conversion of 30% and the peak DP from the w(DP) and n(DP) (number-average) distributions of a systems of $\bar{n}_{CCTA} = 0.25$ and 0.5 with $f_{cout} = 10^{-4}$ s^{-1} and $\rho = 0.1$ s^{-1} are compared in Table 4.3. It is clear that the peak DPs are dependent upon the number of CCTA in each particle rather than the average number of CCTA in the system.

Although the experimental results suggest that distinct peaks may be visible for transfer-dominated products with n_{CCTA} of 1, 2 or more, distinct peaks were not observed in the simulations. However, simulations with a higher average $\bar{n}_{CCTA}$ demonstrate much broader transfer-dominated peaks that center on lower DPs. We have to conclude that our current model is able to account for transfer products with widely varying peak molecular weights, but is unable to individually resolve individual distributions from one another.

As discussed in the model validation section, a miniemulsion system, where monomer droplets are transformed in situ into polymer particles over the course of the reaction, is an excellent system to evaluate the absence of significant mass transfer effects. Early in the reaction, when the instantaneous conversion, and thus the internal viscosity are quite low, CCTA is assumed to partition freely between the water and monomer phases. Experimentally, CCT-mediated miniemulsions at these conditions yield monomodal MWDs and the molecular weight of the formed product can be predicted by the modified Mayo equation

Table 4.3: Instantaneous DP_n Calculated with the Modified Mayo Equation (Equation 4.15) and Instantaneous Peak DP from Simulations at 30% Conversion in Particles of 65 nm Containing Different n_{CCTA}, Assuming k_{trans}^{app} = 1.5x10^6 L·mol^{-1}·s^{-1}, ρ = 0.1 s^{-1}, f_{cout} = 10^{-4} s^{-1} and $\bar{n}_{CCTA}$ = 0.25 and 0.5.

$\bar{n}_{CCTA}$	n_{CCTA}	**DP*n*** **(Mayo equation)**	**peak DP** ***n*(M) plot**	**peak DP** ***w*(M) plot**
0.25	0	29,088	30,500	30,500
	1	235	238	250
	0.25 ($\bar{n}_{CCTA}$)	917	-	-
0.5	0	29,088	30,400	30,400
	1	235	231	232
	0.5 ($\bar{n}_{CCTA}$)	466	-	-

(Equation 4.15). Our model predicts that monomodal CLDs with DP corresponding to the predicted values by the modified Mayo Equation can be obtained (Figure 4.2). Not only do the DP values match the Mayo Equation, but the PDIs are close to 2, which is predicted theoretically from the Schulz-Flory most probable distribution (Table 4.2).

Although this model may not be able to pick up every intricacy of CCT-mediated emulsion polymerization over a range of conversions and reaction conditions, it does suggest, along with experimental evidence, that the mass transfer limitations on the entry and exit of CCTA, which may be controlled by the instantaneous conversion and, as a consequence, the internal viscosity of the particles, can greatly affect the CLD. Multimodal CLDs are obtained when the contributions of discrete numbers of CCTA (n_{CCTA} = 1, 2, etc.) in each particle, along with slow transfer of these CCTAs between the particles, are accounted for. The contribution of each of these peaks can be attributed to a discrete distribution of CCTA molecules over the polymer particles. However, even when CCTA compartmentalization is accounted for, but the transfer of CCTAs between the particles is sufficiently fast, monomodal CLDs are obtained, with a DP_n that can be predicted by the Mayo equation (Equation 4.15).

4.5 Conclusions

We have presented the first simulations which demonstrate the effect of segregation of both the propagating radical and a mediating species on the chain length distribution in emulsion polymerization, specifically for catalytic chain transfer. The multimodal MWD observed

experimentally in seeded emulsion polymerization can be represented by our simulations and confirm that the diffusional resistance against CCTA transfer between particles limits the ability of the CCTA to effectively mediate numerous polymer particles, which results in multimodal CLDs. In instances of fast CCTA diffusion, the expected degree of polymerization can be predicted by the Mayo equation using the average concentration of CCTA per particle in the system, which is confirmed by the model. However, when the diffusional resistances are significant, the individual contributions to the CLD can be attributed to the compartmentalization of CCTA in the particles, whereby the peaks at different DPs are due to polymerization in the presence of zero or more CCTA molecules inside each particle over the course of the polymerization. The main parameter governing the compartmentalization effects is the entry and exit of the CCTA, which is related to the viscosity of the polymer particles.

Acknowledgments

The authors thank Dr. A. Butté from ETH (Zurich) for many helpful discussions on compartmentalization, and the Natural Sciences and Engineering Research Council of Canada (NSERC) and the Foundation Emulsion Polymerization (SEP) for financial support.

References

[1] Cunningham, M. F. *Progress in Polymer Science* **33**(4), 365–398 (2008).

[2] Zetterlund, P. B., Kagawa, Y., and Okubo, M. *Chemical Reviews* **108**(9), 3747–3794 (2008).

[3] Zetterlund, P. B. and Okubo, M. *Macromolecules* **39**(26), 8959–8967 (2006).

[4] Kagawa, Y., Zetterlund, P. B., Minami, H., and Okubo, M. *Macromolecular Theory and Simulations* **15**(8), 608–613 (2006).

[5] Maehata, H., Buragina, C., Cunningham, M., and Keoshkerian, B. *Macromolecules* **40**(20), 7126–7131 (2007).

[6] Simms, R. W. and Cunningham, M. F. *Macromolecules* **41**, 5148–5155 (2008).

[7] Smeets, N. M. B., Heuts, J. P. A., Meuldijk, J., Cunningham, M. F., and van Herk, A. M. *Macromolecules* **42**(19), 7332–7341 (2009).

[8] Gridnev, A. A. and Ittel, S. D. *Chemical Reviews* **101**(12), 3611–3660 (2001).

[9] Roberts, G. E., Barner-Kowollik, C., Davis, T. P., and Heuts, J. P. A. *Macromolecules* **36**(4), 1054–1062 (2003).

[10] Kukulj, D., Davis, T. P., and Gilbert, R. G. *Macromolecules* **30**(25), 7661–7666 (1997).

[11] Bon, S. A. F., Morsley, D. R., Waterson, J., Haddleton, D. M., Lees, M. R., and Horne, T. *Macromolecular Symposia* **165**(1), 29–42 (2001).

[12] Suddaby, K. G., Haddleton, D. M., Hastings, J. J., Richards, S. N., and O'Donnell, J. P. *Macromolecules* **29**(25), 8083–8091 (1996).

[13] Kukulj, D., Davis, T. P., Suddaby, K. G., Haddleton, D. M., and Gilbert, R. G. *Journal of Polymer Science Part A: Polymer Chemistry* **35**(5), 859–878 (1997).

[14] Haddleton, D. M., Morsley, D. R., O'Donnell, J. P., and Richards, S. N. *Journal of Polymer Science Part A: Polymer Chemistry* **37**(18), 3549–3557 (1999).

[15] Smeets, N. M. B., Heuts, J. P. A., Meuldijk, J., and van Herk, A. M. *Journal of Polymer Science Part A: Polymer Chemistry* **46**(17), 5839–5849 (2008).

[16] Butte, A., Storti, G., and Morbidelli, M. *Macromolecular Theory and Simulations* **11**(1), 22–36 (2002).

[17] Butte, A., Storti, G., and Morbidelli, M. *Macromolecular Theory and Simulations* **11**(1), 37–52 (2002).

[18] Smeets, N. M. B., Meda, U. S., Heuts, J. P. A., Keurentjes, J. T. F., van Herk, A. M., and Meuldijk, J. *Macromolecular Symposia* **259**(1), 406–415 (2007).

[19] Morrison, D. A., Davis, T. P., Heuts, J. P. A., Messerle, B., and Gridnev, A. A. *Journal of Polymer Science, Part A: Polymer Chemistry* **44**(21), 6171–6189 (2006).

[20] Maxwell, I. A., Morrison, B. R., Napper, D. H., and Gilbert, R. G. *Macromolecules* **24**(7), 1629–1640 (1991).

[21] van Berkel, K. Y., Russell, G. T., and Gilbert, R. G. *Macromolecules* **36**(11), 3921–3931 (2003).

[22] Odian, G. *Principles of Polymerization.* John Wiley & Sons, Inc, (2004).

[23] Gilbert, R. G. *Emulsion Polymerization - a Mechanistic Approach.* Academic Press, San Diego, CA, (1995).

[24] Gridnev, A. A., Ittel, S. D., Wayl, B. B., and Fryd, M. *Organometallics* **15**(24), 5116–5126 (1996).

[25] Buback, M., Garcia-Rubio, L. H., Gilbert, R. G., Napper, D. H., Guillot, J., Hamielec, A. E., Hill, D., O'Driscoll, K. F., Olaj, O. F., Shen, J., Solomon, D., Moad, G., Stickler, M., Tirrell, M., and Winnik, M. A. *J.Polym.Sci.C Polym.Lett.* **26**(7), 293–297 (1988).

[26] Kamachi, M. and Yamada, B. *Propagation and Termination Constants in Free Radical Polymerization*, II/84. Polymer Handbook. Wiley, New York, 4th edition (1999).

[27] Ueda, A. and Nagai, S. *Transfer Constants to Monomers, Polymers, Catalysts and Initiators, Solvents and Additives, and Sulfur Compounds in Free Radical Polymerization*, II/101. Polymer handbook. Wiley, 4th edition (1999).

[28] Haddleton, D. M., Maloney, D. R., Suddaby, K. G., Muir, A. V. G., and Richards, S. N. *Macromolecular Symposia* **111**, 37–46 (1996).

[29] Biasutti, J. D., Roberts, G. E., Lucien, F. P., and Heuts, J. P. A. *European Polymer Journal* **39**(3), 429–435 (2003).

[30] Kumar, S. and Ramkrishna, D. *Chemical Engineering Science* **52**(24), 4659–4679 (1997).

[31] Kumar, S. and Ramkrishna, D. *Chemical Engineering Science* **51**(8), 1333–1342 (1996).

[32] Kumar, S. and Ramkrishna, D. *Chemical Engineering Science* **51**(8), 1311–1332 (1996).

[33] Lichti, G., Gilbert, R. G., and Napper, D. H. *Journal of Polymer Science: Polymer Chemistry Edition* **18**(4), 1297–1323 (1980).

[34] Smeets, N. M. B., Heuts, J. P. A., Meuldijk, J., Cunningham, M. F., and van Herk, A. M. *Macromolecules* **42**(17), 6422–6428 (2009).

[35] Heuts, J. P. A., Forster, D. J., and Davis, T. P. *Macromolecules* **32**(12), 3907–3912 (1999).

[36] Roberts, G. E., Davis, T. P., Heuts, J. P. A., and Russell, G. T. *Journal of Polymer Science Part A: Polymer Chemistry* **40**(6), 782–792 (2002).

[37] Wisnudel, M. B. and Torkelson, J. M. *Macromolecules* **29**(19), 6193–6207 (1996).

[38] Lodge, T. P., Lee, J. A., and Frick, T. S. *Journal of Polymer Science Part B: Polymer Physics* **28**(13), 2607–2627.

[39] Gisser, D. J. and Ediger, M. D. *Journal of Physical Chemistry* **97**(41), 10818–10823 (1993).

[40] Meerwall, E. D. V., Amis, E. J., and Ferry, J. D. *Macromolecules* **18**(2), 260–266 (1985).

[41] Landry, M. R., Gu, Q., and Yu, H. *Macromolecules* **21**(4), 1158–1165 (1988).

[42] Shortt, D. W. *J.Liq.Chromatogr.; Journal of Liquid Chromatography* **16**(16), 3371–3391 (1993).

[43] Mayo, F. R. *Journal of the American Chemical Society* **65**, 2324–2329 (1943).

[44] Haddleton, D. M., Depaquis, E., Kelly, E. J., Kukulj, D., Morsley, S. R., Bon, S. A. F., Eason, M. D., and Steward, A. G. *Journal of Polymer Science Part A: Polymer Chemistry* **39**(14), 2378–2384 (2001).

Chapter 5

Nucleation and Colloidal Characteristics of High Solids Nitroxide Mediated Emulsion Polymerization of n-Butyl Acrylate with Di-BlocBuilder

Nucleation

⬇ Target M_n

⬆ Particle Size

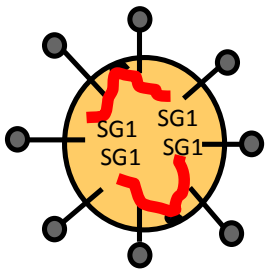

High Solids Latex (45 wt%)

Colloidally stable latexes

Moderate to high M_n

Controlled Polymerization

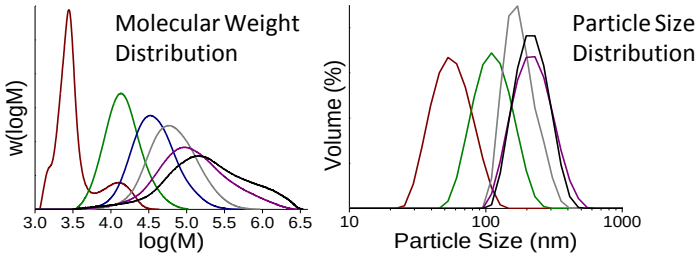

Preface

In the summer of 2008, a collaboration began with Arkema to investigate nitroxde mediated polymerization in emulsion with the alkoxyamine initiator BlocBuilder MA®. Early on, it became clear that a focus on the nucleation characteristics of these emulsion systems was an extremely interesting area of study, particularly in that initiator concentration appeared to greatly affect particle size in a manner opposite of regular emulsion systems. There is a dramatic increase in particle size with an increase in the concentration of initiator (or decrease in the target molecular weight). While this can sometimes be overlooked in these systems, it makes it impossible to create colloidally stable latexes of low molecular weight when targeting the high solids contents by emulsion polymerization. This is of the utmost importance however, if these polymers are to be produced at an industrial scale in an economically viable manner. In this work we explore the factors that affect the particle size and colloidal stability at high solids contents of latexes made with n-butyl acrylate and a Di-BlocBuilder initiator - the formulation which is involved in the first stage of creating tri-block copolymers with MMA (marketed commercially by Arkema, Inc. under the name nanostrength®), or other high glass transition polymer, to create thermoplastic elastomers.

Abstract

There is a strong correlation between the increases in initiator concentration with an increase in particle size for SG1 mediated, two stage emulsion polymerization. In a system of n-butyl acrylate and a di-functional alkoxyamine, based upon the commercially available BlocBuilder MA®, we studied the impact of various factors on the particle size in the 1st stage (nucleation) of the polymerization; these include the ionic strength, pH, buffer (type and concentration) and the concentration of surfactant. These results suggest that superswelling of the particles during nucleation has a great deal of influence on the behaviour of the system. In applying these strategies, we demonstrate that colloidally stable latexes can be created at 45 wt% solids with final molecular weight targets of >70 kg·mol^{-1}.

5.1 Introduction

Controlled/living polymerization has emerged as a versatile and elegant method of creating polymers with tailored molecular architectures, including block copolymers and polymers with narrow molecular weight distributions, under mild reaction conditions. Early attempts to perform nitroxide mediated *ab-initio* emulsion polymerization resulted in severe coagulation formation because of droplet polymerization,[1, 2] but a two stage emulsion polymerization procedure[3] introduced by Charleux's group, using the commercially available water soluble alkoxyamine initiator BlocBuilder MA® (BB) from Arkema (Figure 5.1a), based on the nitroxide SG1, has eliminated this problem. In this system, a small amount of monomer is added to the aqueous phase along with surfactant and the alkoxyamine initiator in its ionized form to create particles in the absence of monomer droplets. Following the formation of a 1st stage latex, the remainder of the monomer can be added in a batch or semi-batch manner.

Nitroxide mediated emulsion polymerization has also been demonstrated using a di-functional alkoxyamine, Di-BlocBuilder (DiBB),[4, 3, 5, 6] where two COOH groups and two SG1 groups are present on the initiator (Figure 5.1b). Using DiBB, tri-block copolymers can be created with ease. Tri-block copolymers can be very useful in applications including blend compatibilizers and in the formation of thermoplastic elastomers.

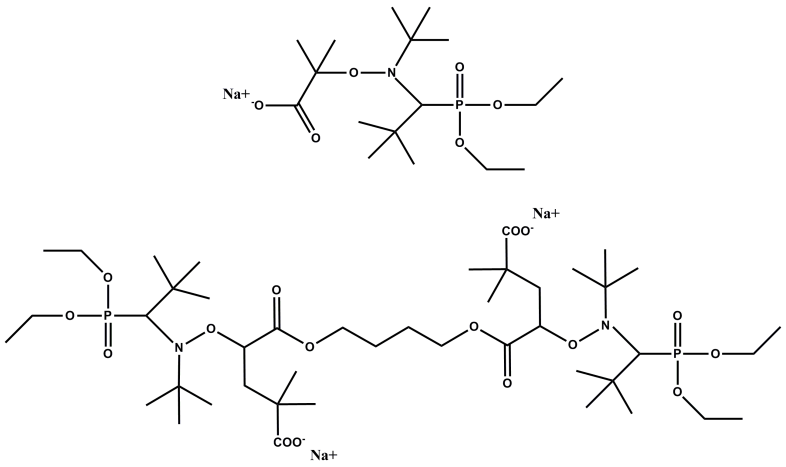

Figure 5.1: a) BlocBuilder MA® is a monofunctional alkoxyamine initiator. b) Di-BlocBuilder (DiBB) is a di-functional alkoxyamine initiator. Both of these are water soluble in their ionized forms (shown here).

Nitroxide mediated emulsion polymerization has been successfully demonstrated under laboratory conditions with low-to-moderate solids contents (<25 wt%), but broad particle size distributions and other unanticipated colloidal behaviours have been observed.[6, 5, 3, 4, 7, 8] In conventional emulsion polymerization, when the concentration of water soluble initiator is increased, all other factors remaining constant, the particle size tends to decrease because more micelles are nucleated and the charged initiator end groups provide additional stabilizing power.[9] However, in NMP emulsion, the opposite trend is observed, where an increase in the concentration of BB or DiBB leads to an increase in the particle size, regardless of the increase in the concentration of initiator to nucleate micelles or charged groups to stabilize the particles.[10, 11] It has been noted that the particle size distribution (PSD) is narrower and smaller for DiBB (compared to BB) initiated emulsions under similar conditions.[3] Similar trends of increasing particle size with increasing initiator concentration are also observed in other controlled radical polymerization chemistries performed in emulsion, specifically reversible addition-fragmentation chain transfer (RAFT)[8] and reverse iodine transfer polymerization (RITP).[12] A surfactant-free RAFT emulsion polymerization found no correlation between particle size and RAFT agent/initiator addition, but did report that the final particle size was largest when the highest concentration of RAFT agent was used.[13] Such phenomenon has been referred to in the NMP literature as a possible side effect of the "superswelling" theory[7] and has been described mathematically for nucleation in a RAFT system.[14] The superswelling theory was first discussed from a thermodynamic point of view by Luo et al.[15] in terms of NMP miniemulsion polymerization. The large concentration of oligomers (the predominant initial product in living systems) present in the particles early in the polymerization lowers the chemical potential of the nucleated particles with respect to droplets or monomer-swollen micelles. This promotes the swelling of the newly nucleated particles, and can lead to very broad particle size distributions, or in the worst case, colloidal instability. Other theories have included differences in ionic strength effects and shell thickness when acrylic acid is also present in the 1st stage.[12]

To overcome this difficulty, many groups have begun pre-fabricating amphiphilic macroinitiators which act both as the stabilizing moiety and the initiator to perform emulsion polymerization in the absence of additional surfactant. Although increasing the concentration of initiator decreases the particle size in these polymerizations,[16, 17, 18, 13] all other condi-

tions being equal, it still does not eliminate the difficulty of having a strong correlation between the target molecular weight and the particle size. Changing the amphiphilic block sizes on macro RAFT agents has been shown to modify the particle size independently,[13] but requires individualized pre-synthesis for each experiment of a different solids content or target molecular weight.

Although colloidally stable NMP latexes can be made with low-moderate solids contents (20 wt% or less) and moderate molecular weights, high solids latexes (up to 50 wt%) whose molecular weights can be controlled independent of particle size are necessary to produce these latexes at an industrial scale. The colloidal instability of high solids latexes is thought to be caused by one or a combination of factors, including insufficient monomer present in the 1st stage, such that water soluble oligomers are still present when the second feed of monomer is started, leading to droplet polymerization and similar difficulties to those experienced in early emulsion studies.[1, 2, 19] Another contributing factor is the size of the particles created during the 1st stage, where an increase in the concentration of initiator leads to the creation of larger particles. Upon the addition of the remaining monomer, these particles are expected to grow by 5300 vol% (with a target polymer content of 45 wt%). Larger particles created with higher initiator concentrations in the 1st stage are more likely to suffer from colloidal instability that latexes with smaller 1st stage particles.

In this work we attempt to isolate the influences of various factors on the particle size distributions obtained during the 1st stage of the polymerization; these include the ionic strength, pH, buffer (type and concentration) and the concentration of surfactant. These results suggest that superswelling of the particles during nucleation has a great deal of influence on the behaviour of the system. Although it is not possible to decouple the effect of initiator concentration and particle size completely, we offer many alternatives, without the required pre-fabrication of an amphiphilic alkoxyamine initiator, which can yield a colloidally stable, high solids latexes with moderate molecular weights of >70 kg·mol^{-1} at 45 wt% solids. We will highlight both the achievements and the difficulties associated with performing NMP emulsion polymerization of BA under high solids conditions.

5.2 Experiment Section

Materials The compounds n-butyl acrylate (BA, Aldrich, 99%), styrene (St, Aldrich, >99%), 2-((tert-butyl(1-(diethoxyphosphoryl)-2,2-dimethylpropyl)amino)oxy)-2-methylpropanoic acid (BlocBuilder MA® or BB, supplied by Arkema, 99%), N-tert-butyl-N-(1-diethylphosphono-2,2-dimethylpropyl) nitroxide (SG1, supplied by Arkema, 89%), methyl acrylate (MA, Aldich, 99%), Dowfax^{TM}8390 (Dow Chemicals, 35 wt% solution in water), sodium hydroxide (NaOH, 97+%), sodium bicarbonate ($NaHCO_3$, Aldrich 99.7–100.3%) and sodium carbonate (Na_2CO_3, Aldrich, >99%) were used as received. Di-BlocBuilder (DiBB) was synthesized as described elsewhere[4] from BlocBuilder MA® and 1,4 butanediol diacrylate (Sartomer).

1st Stage Latex Preparation Di-BlocBuilder (2.38 g, 2.48 mmol), Na_2CO_3 (0.47 g, 4.43 mmol) and DIW (4 g) were mixed overnight to form the ionized di-alkoxyamine initiator in solution. The 1st stage latex was prepared with Dowfax^{TM}8390 solution (10 g, 5.5 mmol), butyl acrylate (4.39 g, 34.30 mmol), DIW (278 g) and the ionized DiBB solution in a 1L Mettler Toledo glass reactor. Following a 30 minute N_2 purge, the reactor was heated slowly to 120^{O}C over 55 minutes and maintained at a pressure of 45 psi. The reactor was agitated by an anchor impeller at a rotation speed of 200 RPM. Samples were withdrawn periodically.

High Solids Latex The preparation and synthesis of the 1st stage remained identical to that describe above. The 1st stage latex remained at the reaction temperature, 120^{O}C, for 30 minutes prior to the monomer feed. The BA monomer (237 g) was purged with N_2 for 30 minutes prior to being pumped into the reactor over 3 hours. The polymerization continued for a further 4 hours with samples withdrawn periodically.

Characterization Monomer conversion was determined gravimetrically. Gel Permeation Chromatography (GPC) was used to measure the molecular weight and polydispersity of the polymer samples. The MWD was characterized by a Viscotek GPC (containing two PolyAnalytik SupeRes Series PAS-10^{6}M mixed bed columns) with a differential refractive index detector calibrated with PS standards ranging from 6,900 - 860,000 g·mol^{-1}. THF was used as the eluent with a flow rate of 1.0 mL·min. The system was calibrated with PS

standards ranging from 6,900–860,000 g·mol^{-1}. A universal calibration was used to correct the molecular weights from PS to PBA. The Mark Houwink parameters for PS are k = 1.14·10^{-3} L·g^{-1}, a = 0.716, and for PBA are k = 6.47·10^{-4} L·g^{-1}, a = 0.765.[20] Particle size measurements were done by dynamic light scattering on a Zetasizer Nano ZS from Malvern Instruments at 25^{O}C and an angle of 173^{O}. Samples were diluted lightly with DIW prior to measurement. The pH of the latex samples was measured at room temperature with a pH probe calibrated with aqueous standards (pH 4, 7 and 10).

5.3 Results and Discussion

Two stage emulsion NMP has generally yielded colloidally stable latexes at solids contents below 25 wt%.[3, 4, 6, 5, 7, 8] However, in this work we are seeking to created high solids latexes about 45 wt% solids. It should be noted that the deleterious consequences of increased initiator concentration during the 1st stage can be alleviated by dilution of the 1st stage (therefore lowering the initiation concentration, however this leads to a higher target molecular weight at the same final polymer content) and/or lowering the amount of monomer added during the 2nd stage (therefore targeting a solids content lower than 45 wt%). Two hypotheses for the colloidal instability of low molecular weight, high solids NMP latexes have been proposed and both relate directly to the 1st stage of the polymerization. The first hypothesis is that there is insufficient monomer present during the 1st stage (in an attempt to minimize the presence of monomer droplets) to allow all of the water soluble alkoxyamines to propagate to a sufficient length for nucleation and entry into a particle or micelle. The continued presence of water soluble oligomers once the remaining monomer is added can lead to droplet nucleation and polymerization, which has been the cause of colloidal instability in NMP emulsions in the past.[1, 2] A second hypothesis is that the high initiator concentrations in the 1st stage create very large 1st stage latex particles (on the order of 300 nm+ at 1.5 wt% solids) and the volume increase of 5300% (when 45 wt% polymer content is targeted), upon the addition of the rest of the monomer in the 2nd stage, is too large to maintain colloidally stable particles. In this study we concentrate on the second hypothesis, with the majority of the work on particle size effects in the 1st stage conducted under conditions where there is sufficient monomer present in the 1st stage to ensure complete nucleation of all the water soluble initiators (please see Section 5.3.2 for

these calculations). After a discussion of the factors influencing nucleation, we investigate the creation of high solids latexes (45 wt%) with colloidally stable particles at a range of target molecular weights.

5.3.1 1st Stage Conditions

The 1st stage was studied by maintaining the 1st stage latex at the polymerization temperature for 3.5 hours or more and tracking how the particle size, onset of nucleation and pH changed with systematic changes in the initial formulation of the 1st stage latex. The findings highlighted in this work are listed in Table 5.1. The chosen initiator concentration would target a 95 kg·mol^{-1} latex at 45 wt% solids. However, the 1st stage itself is conducted with all of the surfactant, initiator and buffer initially present but only 1.6% of the final monomer content (or 1.5 wt% solids). We consider the onset of nucleation as the point where there is visible formation of particles in the reactor and a clear particle size distribution obtained on the Malvern Nanosizer; nucleation time was measured as a time difference between the onset of nucleation and when the reactor reached the reaction temperature of 120^{O}C. Depending on the pH and other conditions, this time was sometimes negative, indicating the onset of nucleation occurred prior to the reaction reaching 120^{O}C. The pH decreased over time in each of the 1st stage latex experiments, and this decrease was always coupled with an increase in the particle size. Because the DiBB initiator possesses two COO^- groups in its ionized form, it is believed that the drop in pH with an increase in particle size can be used as a qualitative measure of the burying of DiBB initiator head groups inside the particles.

Ionic Strength

The 1st stage latex particle size increased significantly with increasing ionic strength with the addition of excess NaCl (exps. A1, A3 and A4, Figure 5.2a). Increases in ionic strength are known to decrease the thickness of the electrical double layer of the particles, leading to poorer stabilization. However, the changes in the ionic strength did not influence the pH of the system or the nucleation time. In all experiments, the pH dropped over time as the particle size increased (Figures 5.2b, 5.2c), and may be evidence of the burying of DiBB end groups inside the particles. Nucleation consistently occured around pH 7.3–8,

Table 5.1: 1st Stage Latex Nucleation Experiments for DiBB Emulsion Polymerization.

Exp.	$\mathbf{M_n^{th}}$ [a] ($kg \cdot mol^{-1}$)	**DiBB:NaOH: $NaHCO_3$: Na_2CO_3:NaCl** [b]	**Monomer Content** (wt%)	**pH** (start)	**nuc. time** (min)	**particle size** 30 min. from nucleation [c]	**particle size** 210 min. from nucleation [c]	**ionic strength** [d] ($mmol \cdot L^{-1}$)
A1	95	1:1:0.75:0:0	1.55	9.60	2	193.1	265.8	72.2
A2	95	1:1:0:0:0	1.51	8.38	-5	391.8	589.8	54.8
A3	95	1:1:0.75:0:1	1.46	9.30	5	223.4	366.1	85.2
A4	95	1:1:0.75:0:3	1.45	8.74	5	324.2	597.0	118.8
A5	95	1:1:0.76:0:3	1.38	8.34	3	254.8	444.8	115.3
A6	95	1:4:0.76:0:0	1.49	12.59	77	221.5	382.5	125.4
A7	95	1:1:1.75:0:0	1.46	8.59	13	240.9	330.0	85.5
A8	95	1:1:0:0.75:0	1.47	10.59	2	204.6	300.6	68.7
A9	95	1:1:0:1.75:0	1.45	11.05	18	223.4	304.2	84.4
A10	95	1:0:0:1.75:0	1.49	8.94	1	95.16	152.8	69.2
A11	95	1:0:0:1:0	1.47	8.86	-4	274.3	465.3	55.4
A12	95	1:0:0:1.75:1	1.48	9.29	3	221.0	378.2	86.1
B1	190	0.5:1:0.75:0:0	1.46	9.96	0	51.07	72.59	67.4
B2	190	0.5:0.5:0.0.38:0:0.88	1.47	-	1	45.88	68.06	68.3
B3	190	0.5:1:0.38:0:0.0.38	1.46	10.22	8	45.86	71.22	68.7
C1	63	1.5:0:0:2.63	9.43	1.49	9	266.3	448.3	84.8

The standard recipe, which is modified systematically, is based on a target molecular weight of 95 $kg \cdot mol^{-1}$ at 45% solids, but further monomer is not fed to the 1st stage latexes.
All experiments listed here contain the same concentration of Dowfax^{TM}8390 and BA; all the components were added in a batch-wise manner prior to heating.
[a] Theoretical M_n at 45 wt% solids.
[b] Ratios are based on the charge equivalents. DiBB and Na_2CO_3 both have 2 charges per molecule.
[c] Particle size listed is the volume average particle size from the Malvern Nanosizer.
[d] Ionic strength also includes the contribution from the anionic surfactant Dowfax^{TM}8390. Ionic strength = 2[DiBB]+[NaOH]+[$NaHCO_3$]+2[Na_2CO_3]+[NaCl]+2[Dowfax^{TM}8390]

and, after several hours, the pH was often as low as 6–6.5. The influence of ionic strength is important, because when the target molecular weight is decreased, the ionic strength in the system increases through the addition of more DiBB and base required for its ionization.

pH

Increasing the amount of NaOH at a constant ionic strength, maintained through the addition of NaCl, resulted in higher initial pHs. These pH changes had a great influence on the nucleation time, with a higher initial pH resulting in the longest inhibition time prior to nucleation. For example A6 (4 molar equivalents of NaOH to DiBB) began at a pH of 12.59 and experienced a 77 minute inhibition period prior to nucleation, while A5 (1 molar

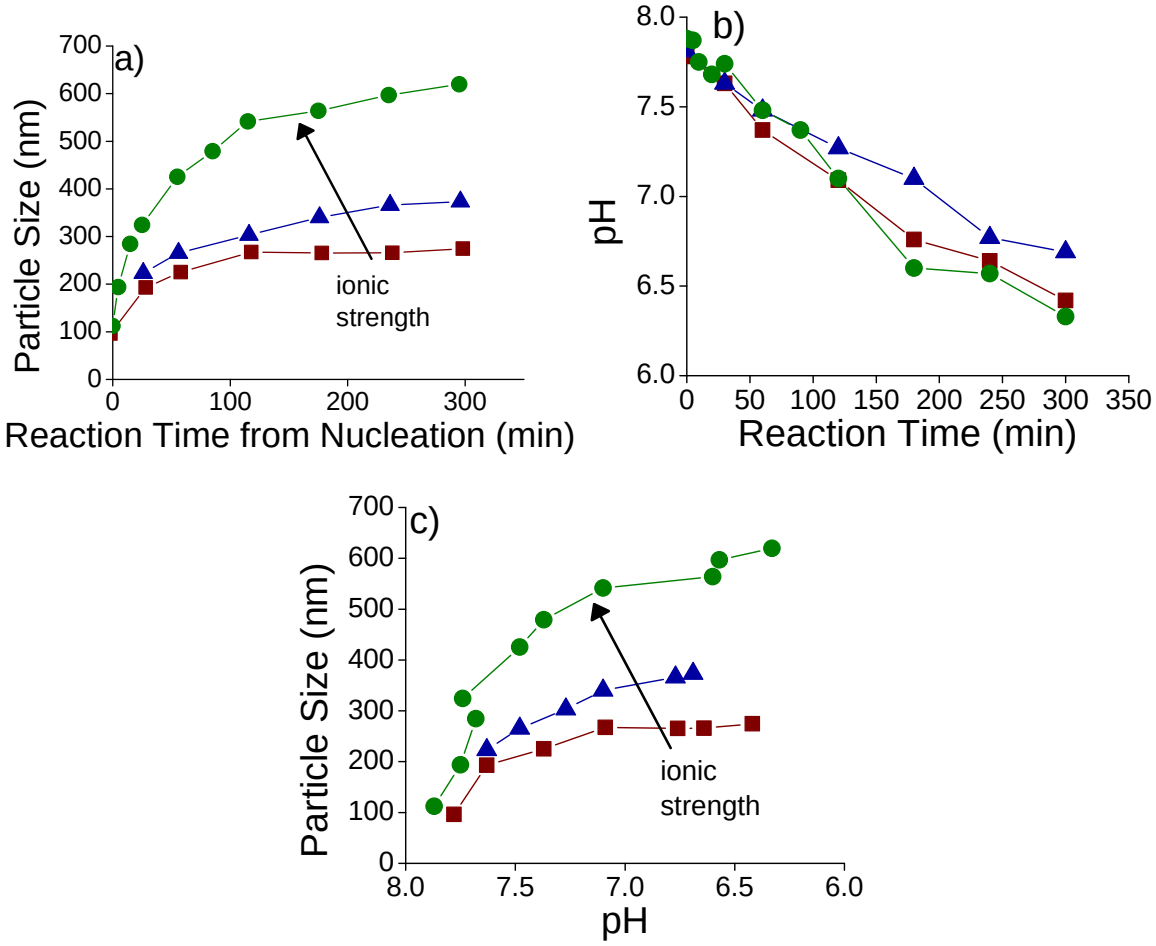

Figure 5.2: Experiments (A1 (■, 0 equivalents of NaCl to the DiBB end groups), A3 (▲, 1 equivalent of NaCl) and A4 (●, 3 equivalents of NaCl)) with varying ionic strength by the addition of NaCl are illustrated by a) the change in particle size with reaction time, b) the change in pH with reaction time and c) the change in particle size with system pH.

equivalent of NaOH to DiBB with additional NaCl) began at a pH of 8.34 and nucleated within 3 minutes of reaching 120^{O}C. However, the most surprising result is that both of these systems nucleated at a pH ~7.3. Following nucleation, the pH change with time and the particle size evolution were fairly similar for the two experiments, although A6 did finish with a lower overall particle size. These results are shown in Figure 5.3a.

This presents interesting insight that nucleation occurs at a pH 7.3–8 over a wide range of conditions; a phenomenon observed in all of the 1st stage latex experiments. The pKa of DiBB is approximately 6.66 (please see Appendix C[21, 4]) therefore, it is possible that pH ~7.3–8 is the point at which the water soluble oligomers become surface active. It should be noted that the pKa of the oligomers may vary slightly from the pKa of Di-BlocBuilder, but can be considered an appropriate order of magnitude estimate. Perhaps in the aqueous

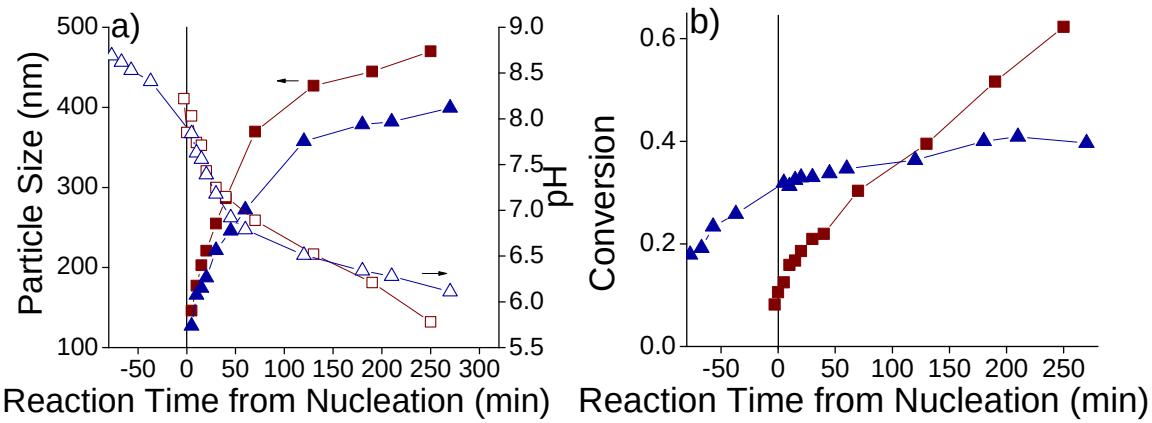

Figure 5.3: Experiments A5 (■, 1 equivalent of NaOH to DiBB) and A6 (▲, 4 equivalents of NaOH) where the concentration of NaOH used to ionize the DiBB was modified, while maintaining an overall consistent ionic strength by the addition of NaCl, are illustrated by (a) the change in pH (hollow markers) and particle size (solid markers) and (b) the conversion with reaction time following nucleation. Reaction time from nucleation refers to the time elapse prior or following the onset of nucleation, as indicated by the visible formation of particles in the reactor and a clear particle size distribution obtained on the Malvern Nanosizer. All of the data was collected after the reactor reached 120^{O}C.

phase the number of BA units a DiBB can add **prior** to it becoming surface active is highly dependent upon the pH (i.e. the z-meric length increases with increasing pH) and nucleation occurs once a portion (or all) of the oligomers switch from being charged to uncharged with a change in pH. This finding is important both on a fundamental basis with respect to the mechanisms involved in nucleation, but also an important practical result, as reaction conditions can be tailored to "hit" this target pH.

Also interesting are the conversion–time profiles of these two experiments (Figure 5.3b). A5 (1 molar equivalent of NaOH to BB) increases in conversion gradually from the onset of nucleation until about 60% conversion (when the experiment was terminated). In A6(4 molar equivalent of NaOH to BB), on the other hand, the conversion is clearly increasing prior to nucleation, and the onset of nucleation occurs close to 35% conversion. Following the onset of nucleation, only a small amount of further polymerization is observed and the system never increases in conversion to match that of A5. These results show there is significantly more polymerization occurring in the aqueous phase (yielding water soluble oligomers) at a higher pH. It again suggests that the pH is very important in determining surface activity of the water soluble oligomers, and the z-meric length may increase with increasing pH.

In conventional emulsion polymerization, higher radical fluxes usually lead to smaller particle sizes (the result of nucleating more micelles and an increase in stabilization by the initiator end groups), but in the absence of changes in the total number of surface charges, higher temperatures (and faster initiator decomposition and the nucleation of more micelles) also tends to lead to smaller particle sizes – which is again opposite to the above hypothesis, because Di-BlocBuilder decomposes very rapidly at 120^{O}C. A possible mechanism leading to large particles with high concentrations of water soluble initiator might be that all (or most) of the oligomers remain water soluble until the pH of the system reaches a critical point, below which all of the oligomers compete for entry into the micelles at the same time. When more chains are entering together, this could lead to higher rates of coagulation of the primary particles, resulting in greater 1st stage latex particle sizes. Also, large concentrations of short oligomers yield less stable particles by superswelling.[14]

Buffer Effects

In experiments using 1 molar equivalent of NaOH to ionize the DiBB end groups, the quantity and type of buffer added to the system was varied. These results are shown in Figure 5.3. Exps. A1 and A8 both used 0.75 mol equivalent of buffer ($NaHCO_3$ and Na_2CO_3 respectively). With these variations, no significant change was found in the nucleation time (2 min) and the particle size evolution (Figure 3a). When the buffer was increased to 1.75 molar equivalents (exp. A7 and A9 for $NaHCO_3$ and Na_2CO_3 respectively) the induction time prior to the onset of nucleation was extended to 13–18 min; therefore, excess buffering lengthens the time to reach the critical pH for the onset of nucleation. However, following nucleation, the particle size evolution was similar to the previous experiments, although particle size was slightly larger (the result of increased ionic strength). Finally, A2 contained no buffer, and its particle size is significantly larger than the other experiments, regardless of its lower ionic strength. Again, the onset of nucleation occurred around pH 7.5, but occurred 5 minutes before the reaction reached 120^{O}C. Over the course of the polymerization, the pH dropped considerably, and the particle size increased significantly.

While buffering is clearly important, increasing the amount of buffer above 0.75 mol equivalents to the DiBB end groups, or changing the buffer from $NaHCO_3$ to Na_2CO_3, does not greatly change the particle size or the pH drop over the course of the reaction. Buffering

the system at a moderate pH is important in order to prevent nucleation from beginning too quickly, but beginning with a very high pH can produce long induction periods (exp. A6). In addition, buffering appears to slow the rate of coagulation of the particles over time by keeping the acid end groups in their ionized form. If the pH drops too significantly, the DiBB acid end groups are less able to aid in stabilizing the particles and the acid end groups may become buried. This has been noticed in other experiments where a drop in pH is accompanied by an increase in the particle size (Figures 5.4a, 5.4b).

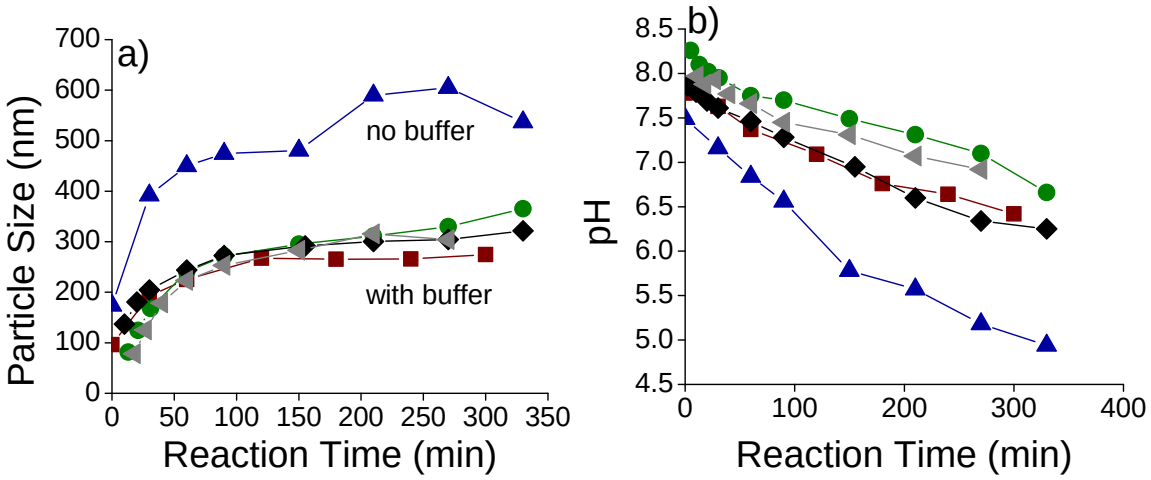

Figure 5.4: Experiments A1 (■, 0.75 equivalents of $NaHCO_3$ to the DiBB end groups), A2 (▲, no buffer), A7 (●, 1.75 equivalents of $NaHCO_3$), A8 (♦, 0.75 equivalents of $Na2_2CO_3$), and A9 (◄, 1.75 equivalents of Na_2CO_3) illustrating the effect of buffer concentration are shown through a) the change in particle size with reaction time, and b) the change in system pH in the reaction time following nucleation.

Type of Base Used to to Ionize the DiBB

The most notable conclusion of the 1st stage latex study was that using Na_2CO_3, rather than NaOH, to ionize the DiBB acid groups had a marked effect on the particle size. The 1st stage latex particles were significantly smaller using Na_2CO_3 (63 nm vs. 193 nm volume diameter after 30 minutes at 120°C for A10 and A1 respectively). It is interesting to note that A11, using a 1 molar equivalent of Na_2CO_3 to DiBB (just enough to ionize the DiBB acid groups, but not provide any buffering capacity), behaves in a very similar way to exp. A2 (with NaOH to ionize the DiBB acid groups and no buffer). In both of these

experiments (A11 and A2), the 1st stage latex particle size is significantly larger than all other experiments with buffer, the pH of the system drops more significantly over the course of the polymerization and the onset of nucleation is approximately 5 minutes prior to the reactor reaching 120^{O}C. This indicates that buffer is required in the system to maintain an alkaline pH during the nucleation period and maintain the ionized end groups to minimize coagulation. But it is the use of Na_2CO_3, rather than NaOH, to ionize the DiBB acid groups that gave the most marked effect on the particle size. NaOH is a strong base, while Na_2CO_3 is weak, so it is possible that, while they are added in the same molar concentration, the "apparent" ionic strength in the Na_2CO_3 system is lower, leading to more stabilization and smaller 1st stage particles. These results are shown in Figure 5.5.

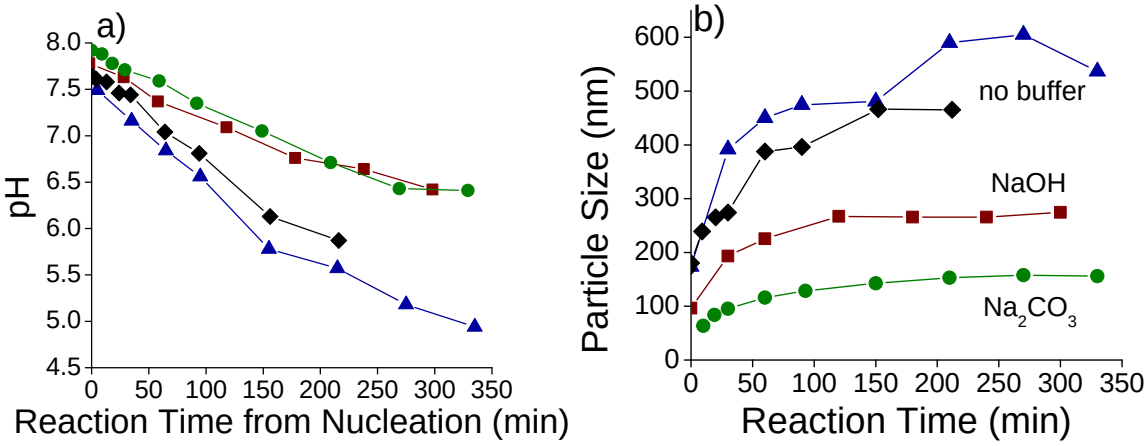

Figure 5.5: Experiments highlighting the use of NaOH and Na_2CO_3 to ionize the DiBB are shown in a) the change in the system pH with reaction time following nucleation, and b) the change in particle size with reaction time following nucleation. Experiments A1 (■, NaOH with buffer), A2 (▲, NaOH with no buffer), A10 (●, Na_2CO_3 with buffer), and A11 (♦, Na_2CO_3 with no buffer).

5.3.2 Changing Initiator Concentration to Target Different Molecular Weights

The effect of initiator concentration on the 1st stage latex particle size evolution was investigated by using Na_2CO_3 to both ionize the DiBB and act as a buffer in the system. Based on the high solids formulation listed in the experimental section, A12 is the 1st stage of a latex with a final target M_n of 95 kg·mol^{-1} at 45 wt% solids and C1 is the 1st stage of a

latex with a final target M_n of 63 kg·mol^{-1} at 45 wt% solids. Additional NaCl was added to A12 to ensure both C1 and A12 had the same ionic strength. In Figure 5.6, A10 is also included, which is the 1st stage of a latex with a final target M_n target of 95 kg·mol^{-1} at 45 wt% but the ionic strength is not matched to C1 with additional NaCl. Therefore, the difference in ionic strength alone is not able to account for the difference in size of the 1st stage latex particles with different concentrations of initiator.

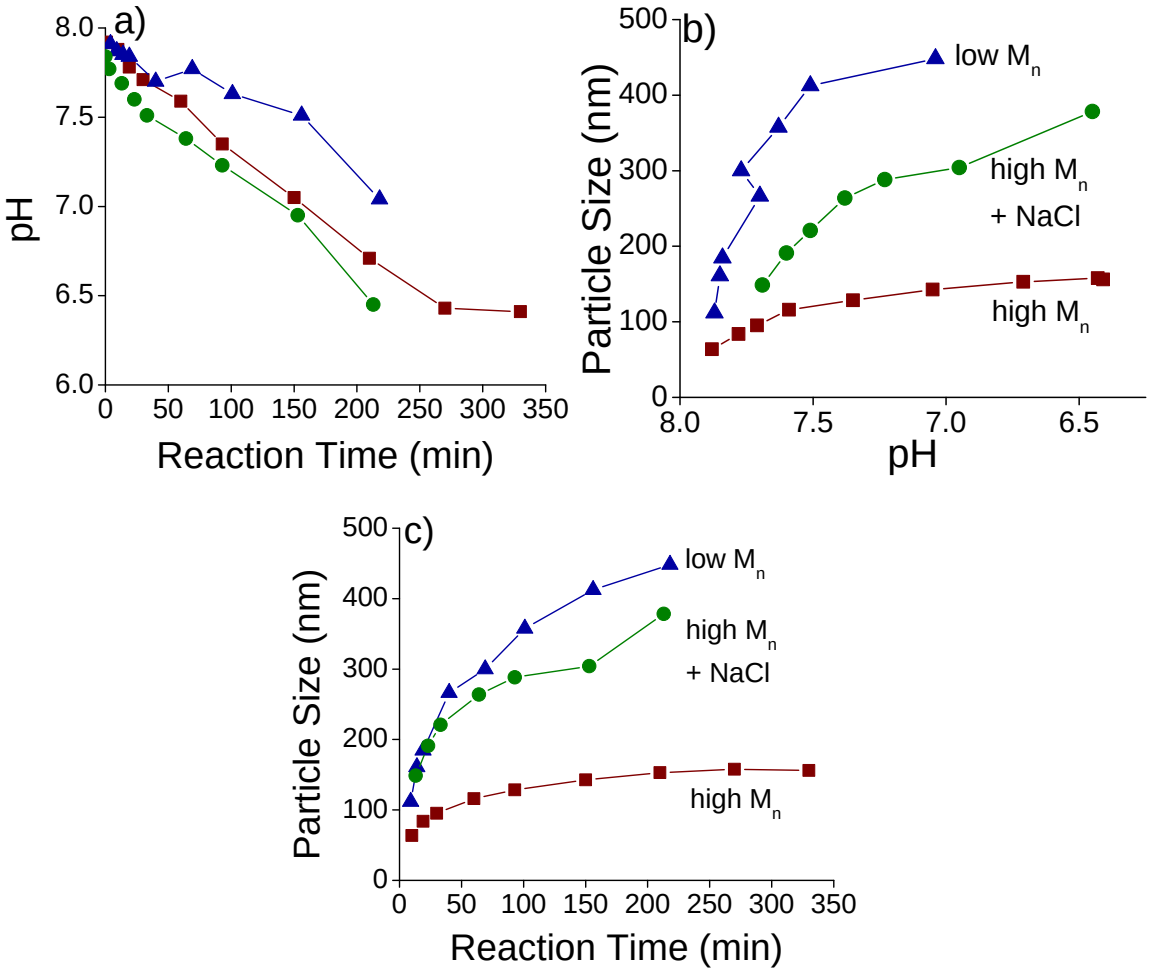

Figure 5.6: Experiments targeting different M_n, ionizing the DiBB with Na_2CO_3 and maintaining the same ionic strength by NaCl are illustrated by a) the evolution of system pH with reaction time, b) evolution of the particle size with system pH, and c) the particle size growth over the course of the reaction. Experiments A10 (■, high M_n target, no added NaCl), C1 (▲, low M_n target), A12 (●, low M_n target, NaCl added to match the ionic strength of C1).

The 1st stage latexes B1, B2, B3 have a M_n target of 190 kg·mol^{-1} at 45% solids, and

NaOH was used to ionized the DiBB but contained different reagent combinations to isolate the effects of pH, ionic strength, etc. (excess NaOH and $NaHCO_3$, excess NaCl and excess NaOH and NaCl respectively for exps. B1, B2 and B3) to match the ionic strength to experiments with a 95 kg·mol^{-1} M_n target at 45% solids (A1, ionized with NaOH, and A10, ionized with Na_2CO_3). As shown in Figure 5.6, the 1st stage latex particle size was significantly smaller when a higher M_n was targeted even when experiments were conducted at the same ionic strength. What reagent was used in excess to modify the ionic strength had little effect on the particle size, but did alter the pH in the system.

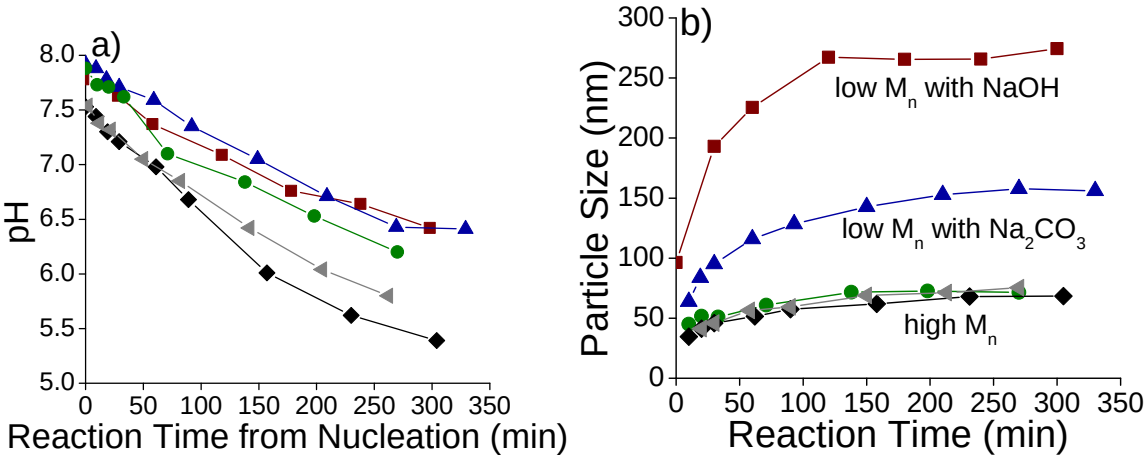

Figure 5.7: Experiments targeting different M_n, ionizing the DiBB with NaOH are illustrated by a) the evolution of the pH with reaction time, and b) the change in particle size over the course of the reaction. Experiments A1 (■, low M_n target, NaOH), A10 (▲, low M_n target, Na_2CO_3), B1 (●, high M_n target, excess NaOH and $NaHCO_3$) B2 (◆, high M_n target, excess NaCl) and B3 (◀, high M_n target, excess NaOH and NaCl).

Although in these experiments the concentration of initiator in the system was modified, the total monomer in the system was kept constant; therefore, the number of monomer units available to add to each alkoxyamine group varied. The 95 kg·mol^{-1} target (final) 1st stage recipe included 6.9 monomer units per chain end (13.8 per DiBB), while the 190 kg·mol^{-1} target (final) 1st stage had 27.6 monomer units per DiBB and the 63 kg·mol^{-1} target (final) 1st stage had only 9.1 units per DiBB.

The number of units each chain end *could* add (this is different from the monomer added in the formulation per chain end group) in the aqueous phase prior to being capped by an SG1 molecule, assuming that these chains do not enter into micelles and no SG1

partitions into the monomer phase, can be simply calculated in two steps. Assuming that, in the aqueous phase, chain activation and deactivation are the only major sources of chain generation and chain loss (and termination is minimal), the rate of change of radical concentration can be estimated as

$$\frac{d[R\bullet]}{dt} = k_{act}2[DiBB] - k_{deact}[R\bullet][SG1] \tag{5.1}$$

Applying the quasi steady state assumption ($d[R\bullet]/dt = 0$) and assuming that each end group of the DiBB decomposes independently, such that radicals, $[R\bullet]$, and free SG1, $[SG1]$, are created in pairs, the concentration of radicals and SG1 is

$$[SG1] = [R\bullet] = \sqrt{\frac{k_{act}}{k_{deact}}2[DiBB]} \tag{5.2}$$

The number of units a propagating chain will add prior to deactivation with a free SG1 is

$$\#units = \frac{k_p[M]}{k_{deact}[SG1]} \tag{5.3}$$

Assuming that each end group of the DiBB decomposes with the same k_{act} at 120^{O}C as BlocBuilder MA® (k_{act}= 0.3 s^{-1} [22]), the deactivation reaction occurs between a n-butyl acrylate radical and a free SG1 ($k_{deact} = 2.6{\cdot}10^7$ L·mol^{-1}·s^{-1} [23, 24]) and the rate coefficient of propagation k_p is 93,500 L·mol^{-1}·s^{-1} [25] and using the known concentration of monomer, $[M]$, and Di-BlocBuilder, [DiBB], added to the system, the number of monomer units which each end group can add during the 1st stage (for a final latex formulation with 95 kg·mol^{-1} target M_n at 45% solids), is 30. Therefore, if the oligomers do not become surface active, enter into a micelle or are deactivated by an SG1 at a length shorter than this, there will not be enough monomer present to allow entry of all DiBB species into the micelles in the 1st stage. This estimated chain length would increase if there is significant partitioning of the SG1 into the monomer phase. If there are still water soluble oligomers present when the next addition of monomer occurs, colloidal instability is likely if these oligomers nucleate droplets.

Therefore, it is paramount that sufficient monomer be present during the 1st stage of the polymerization to allow full nucleation of the particles through the entry of all of the DiBB molecules into the particles. As such, full mechanistic understanding of the nucleation is

Table 5.2: 1st Stage Latexes Synthesized with Different Concentrations of Dowfax^{TM}8390.

Exp.	**Conc. of surfactant** (mmol·L^{-1})	**Nucleation time** (min)	**Particle size** (nm)[b]	**PDI**	**Comments**
D1	19.3		157	0.093	Stable latex
D2	9.6	3	337	0.105	Stable latex
D3	3.9	-3 (at 115^{O}C)	425 (23%), 1517 (77%)	Very broad	Likely experienced droplet nucleation
D4	1.2 (above cmc)	-8 (at 106^{O}C)	1200	Very broad	Droplet nucleation
D5	0.6 (below cmc)		317 (3%), 1615 (97%)	Extremely broad	Droplet nucleation
D6	0	-20 (at 90^{O}C)	-	-	Unable to form a stable latex

The standard recipe is based on a target molecular weight of 95 kg·mol^{-1} at 45% solids, but further monomer is not fed to the 1st stage latexes.
[a]Surfactant is Dowfax^{TM}8390.
[b]Particle size listed is the volume average particle size from the Malvern Nanosizer. The sample is taken 30 minutes following nucleation.

not yet known, but it has been suggested that it is likely only one of the two alkoxyamine groups on the DiBB will activate at a time.[6] As suggested in experiment A6, the z-meric length, at which chains become surface active, can be greatly increased with increasing pH in the system.

5.3.3 Surfactant Concentration

Experiments were conducted while varying the amount of Dowfax^{TM}8390 in the system, and using 1 molar equivalent of NaOH to ionize the DiBB (Table 5.2). The findings are consistent with those found with a similar di-functional alkoxyamine (DIAMA) by Nicolas et al.[4, 3] in that the particle size increases with diminishing surfactant concentration. However, the results do illustrate that there is a minimum surfactant concentration required in the 1st stage to create a stable 1st stage latex. However, the increase in particle size is more significant with small increases in the ionic strength than with drastic decreases in the surfactant concentration.

The results in Table 5.2 suggests that when using the standard formulation but with half of the surfactant (D2) there is still enough surfactant present to avoid the presence of droplets in the system (as confirmed by the Malvern Nanosizer), but lower surfactant concentrations do lead to larger particle sizes because of the decrease of stabilization in the system. It is also very interesting that as the surfactant concentration decreases, nucleation

Table 5.3: High Solids NMP Emulsion Polymerization of n-Butyl Acrylate with Di-BlocBuilder at 45 wt% Polymer Content and Different Targeted Molecular Weights.

Exp.	**DiBB concentration in 1st stage latex** ($mmol \cdot L^{-1}$)	**Target M_n** ($g \cdot mol^{-1}$)	**Polymer content** (wt %)
E1	16.82	52,900	47.1
E2	12.25	69,600	46.0
E3	8.58	86,500	42.6
E4	6.46	130,700	45.8

occurs more quickly. It appears that the onset of homogenous nucleation (in the absence of micelles, exp. D6) occurs more quickly than micellar nucleation as particles were observed 20 minutes before the reactor reached 120^{O}C, at 90^{O}C. However, this system was unable to form a stable latex, and separation was observed immediately after the samples were taken.

As the calculations presented earlier suggest (Section 5.3.2), in the absence of entry into micelles, a chain propagating in the aqueous phase is able to add upwards of 30 units prior to deactivation. This may be enough units to create unstable primary particles which coagulate and undergo aggregative nucleation.

5.3.4 High Solids Content Experiments with Varying Molecular Weights

Using the strategies to minimize the particle size in the 1st stage (the presence of buffer, the lowest ionic strength possible and the use of Na_2CO_3 rather than NaOH to ionize the DiBB), we have explored the synthesis of 45 wt% solids latexes (Table 5.3). A monomer feed to the 1st stage latex was started 30 minutes after the reactor reached 120^{O}C (this is approximately 25–30 minutes after the onset of nucleation because all of these systems nucleated within 5 minutes of reaching 120^{O}C). Only a small amount of coagulum on the impeller shaft and on the reactor wall at the liquid-air interface was observed when the latex was removed at the end of the polymerization. Colloidally stable latexes (which suffered no visible separation within 24 hours of the polymerization) were created in formulations targeting >70 $kg \cdot mol^{-1}$ (Table 4). Experiment E1, targeting 57 $kg \cdot mol^{-1}$ failed to yield a final stable latex (other than the 1st stage latex); all other samples removed from the reactor separated instantly for this experiment. The evolutions of the particle size distributions are shown in Figure 5.8. All of the polymerizations were controlled and produced latexes with cleanly evolving molecular weight distributions over the course of the polymerization (Figure 5.9).

Table 5.4: Results of the High Solids NMP Emulsion Polymerization of n-Butyl Acrylate with Di-BlocBuilder at 45 wt% Polymer Content and Different Targeted Molecular Weights.

Exp.	E1						E2						E3						E4					
time (hr)	conv	PS[b]	N_px 10^{-14}	$M_n{}^{th}$	M_n	PDI	conv	PS[b]	N_px 10^{-14}	$M_n{}^{th}$	M_n	PDI	conv	PS[b]	N_px 10^{-14}	$M_n{}^{th}$	M_n	PDI	conv	PS[b]	N_px 10^{-14}	$M_n{}^{th}$	M_n	PDI
0.5[a]		317	2.37	1,418	2,395	1.13		224	6.71	1,079	2,431	1.28		188	11.4	1,682	2,829	1.45		106	62.9	1,785	2,943	1.59
1.5	0.17	-		9,915	8,453	1.34	0.09	615	6.12	7,112	4,939	1.10	0.08	453	13.6	8,180	9,241	1.26	0.13	214	126	18,600	12,620	1.36
2.5	0.39	-		21,520	18,110	1.49	0.23	895	3.88	17,250	12,320	1.24	0.30	597	11.5	26,880	18,960	1.31	0.34	287	118	45,770	29,890	1.58
3.5	0.61	-		33,450	28,190	1.54	0.40	1312	1.85	28,830	24,550	1.38	0.46	-	-	40,870	33,660	1.45	0.57	373	80.2	74,980	49,980	1.73
5.5	0.92	-		49,880	38,280	2.00	0.76	1473	1.31	54,000	37,760	1.58	0.83	918	4.77	72,870	46,010	1.88	0.93	398	66.3	122,000	67,870	3.12
7.5	1.03	-		55,380	43,280	2.98	0.94	1615	0.99	66,160	47,470	2.06	0.99	1110	2.70	86,370	52,580	2.87	1.02	399	65.9	134,000	81,850	4.46

[a] 1^{st} stage latex.

[b] Particle size listed is the volume average particle size from the Malvern Nanosizer (nm).

M_n measured on Viscotek GPC ($g{\cdot}mol^{-1}$)

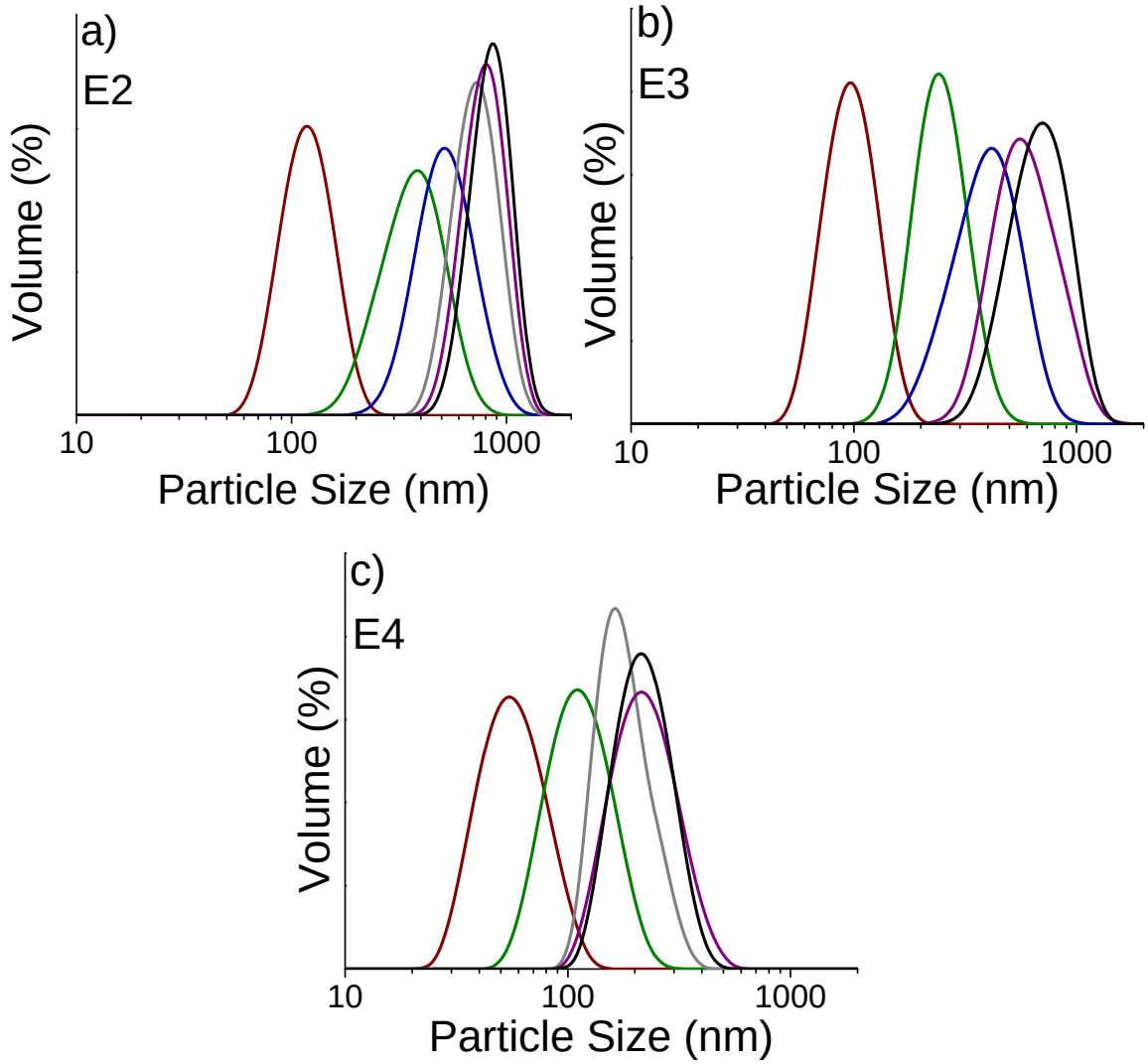

Figure 5.8: Particle size distributions (volume average) for (a) E2 (target M_n of 70 kg·mol^{-1}, samples shown at 30 min (1st stage), 90 min, 150 min, 220 min, 330 min, 450 min.), (b) E3 (target M_n of 87 kg·mol^{-1}, samples shown at 30 min (1st stage), 90 min, 150 min, 330 min, 450 min.)) and (c) E4 (target M_n of 131 kg·mol^{-1}, samples shown at 30 min (1st stage), 90 min, 220 min, 330 min, 450 min.)). Experiment E1 was unable to form a colloidally stable latex.

Although steps have been taken to minimize the particle size of the 1st stage latex, there is still a very clear trend of increasing particle size (in the 1st stage latex and following the monomer addition) with increasing initiator concentration. This difference in particle size is believed to be the result of superswelling during the nucleation stage. When the concentration of short oligomers is greater, the diffusion of monomer to the newly nucleated particles from other monomer swollen micelles or monomer droplets is enhanced. This leads to the creation of larger particles, which later will capture even more of these water

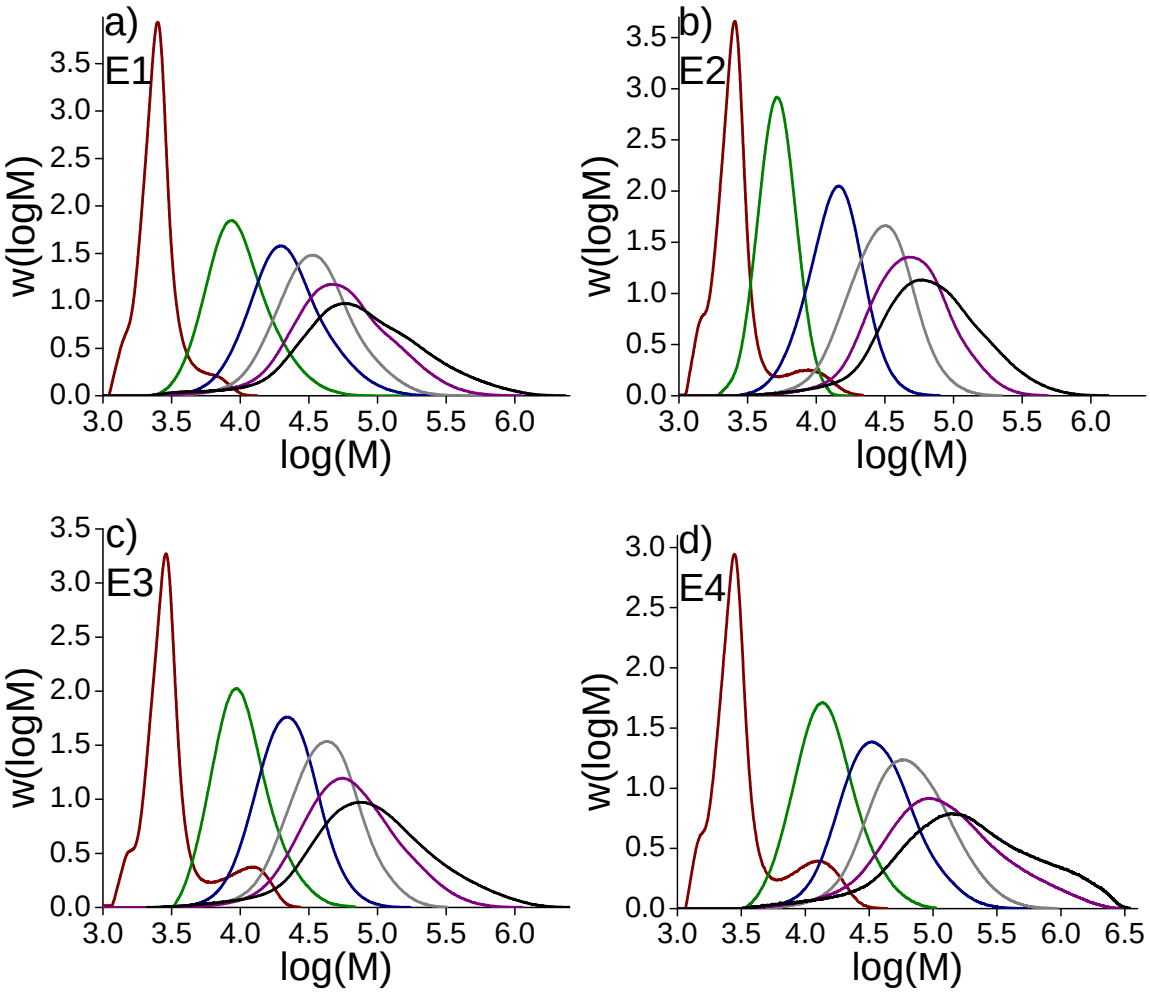

Figure 5.9: Molecular Weight Distributions for (a) E1 (target M_n of 53 kg·mol^{-1}), (b) E2 (target M_n of 70 kg·mol^{-1}), (c) E3 (target M_n of 87 kg·mol^{-1}), (d) E4 (target M_n of 131 kg·mol^{-1}). MWDs are shown for are shown for the 1st stage latex (red), and in intervals up to 7 hours past the start of the monomer feed.The MWDs are included for 30 min (1st stage), 90 min, 150 min, 220 min, 330 min and 450 min. The MWDs are normalized for area.

soluble oligomers and perpetuate the cycle. This same observation has been explained mathematically by Luo et al. for a RAFT ab-initio emulsion system.[14]

Larger 1st stage latex particles clearly lead to a larger final particle size upon the increase in monomer volume by 5300% after the 2nd stage monomer feed. When the 1st stage latex particles are too large the latexes can no longer remain colloidally stable (exp. E1) or have final particle sizes greater than 1 μm (exps. E2 and E3) following the monomer feed.

The control over the molecular weight distribution appears to follow the opposite trend of particle size, with lower final PDIs and narrower MWDs resulting in latexes with higher concentrations of initiator (Table 5.4). However, in each experiment there is a clear shifting

of most of the MWD to higher molecular weights even towards high conversion (Figure 5.9). The broader MWD with lower initiator concentrations is not the result of enhanced termination reactions, as there is no significant slowdown in the rate of polymerization, and termination reactions will be minimized by both having an overall lower concentration of chains in the system and a greater effect of radical segregation as there are fewer chains per particle (because the particle size is also smaller in these latexes). Rather, it could be the result of branching reactions, as BA is very susceptible to backbiting and transfer to polymer reactions, especially at higher conversion.[26] It should be mentioned that the creation of highly branched networks is low, as no gel was observed in any of the latexes. The particle sizes which all of these polymerizations are operating are well outside of the range in which compartmentalization effects on the rate of deactivation are significant,[27, 28]. As a result, backbiting and fragmentation reactions at the high reaction temperatures are the most likely cause of this MWD broadening.

In the MWD of the 1st stage latex for each experiment (Figure 5.9), a small, higher molecular weight shoulder can be observed, and this shoulder is more pronounced in experiments with a lower concentration of initiator. This is the result of multiple activation cycles occurring inside the 1st stage latex particles. When an oligomer enters into a monomer-swollen micelle containing an SG1 molecule, deactivation will be instantaneous, otherwise that oligomer will continue propagating inside the particle until an SG1 enters (See Chapter 7.[11] However, these oligomers can undergo another activation even during the 1st stage and will propagate if there is sufficient monomer present in the system, which will arrive to the particles either though superswelling or regular monomer diffusion to the particles. These activations can result from both the re-activation of the chain end which propagated previously, or more likely (due to the lower activation energy barrier) activation of the other side of the di-functional alkoxyamine. Because the concentration of monomer with respect to the number of chains is much greater in the systems with lower concentrations of initiator, this high molecular weight shoulder is more prominent and tends to be of higher molecular weight in these systems.

Butyl acrylate is a notoriously difficult monomer to polymerize and the process requires high temperatures to successfully mediate the system with SG1. In spite of these difficulties, we have demonstrated the successful synthesis of colloidally stable, high solids PBA

latexes of moderate to high molecular weight by NMP. These reactions are able to reach full conversion in approximately 7 hours and are highly living, as demonstrated by the clear shifting of the full MWD over the course of the reaction. These systems would be ideal to create tri-block copolymers with only two monomer addition stages.

The challenges of these polymerizations lie in ability to make lower molecular weight, high solids latexes. Strategies such as minimizing the monomer content during nucleation (to suppress superswelling), while still providing enough monomer to nucleate particles, may help in lower the possible M_n targets. Alternatively, although not always desirable, lower solids contents can be targeted which do not cause massive increases in the overall volume of the particles. Other strategies, such as beginning with a dead polymer 1^{st} stage latex (or seed) or adding the initiator slowly to the polymerization are also alternatives if the product requirements are not strict towards the presence of dead homopolymer or a low polydispersity of chain lengths.

5.4 Conclusions

In this work we studied how the characteristics of the 1^{st} stage latex will influence the colloidal stability of high solids latexes targeting a variety of molecular weights. Minimizing the size of the 1^{st} stage latex particles appears to be the best way to maintain colloidal stability at high solids, however these 1^{st} stage latex particles are very sensitive to changes in ionic strength, buffering, the type of base used to ionize the Di-BlocBuilder and the concentration of initiator. We have found that using Na_2CO_3 in excess, rather than that NaOH, to ionize the DiBB results in smaller 1^{st} stage latex particle sizes while also providing sufficient buffering capability to maintain the DiBB surface charges. The drastic changes in the 1^{st} stage latex particle size with changes in initiator concentration are the result of superswelling during nucleation, where large concentrations of short oligomers enhance the diffusion of monomer to the particles. We have demonstrated that colloidally stable latexes can be created at 45 wt% solids for n-BA mediated by Di-BlocBuilder with final molecular weight targets of >70 kg·mol^{-1}. There is a very clear trend of increasing particle size with increasing initiator concentration, making the creation of low target M_n difficult. All of the high solids polymerizations were controlled, but the breadth of the MWD increased with increasing conversion, especially when targeting high M_ns.

Acknowledgments

We wish to thank Arkema for providing financial support, materials and helpful discussions and the Natural Sciences and Engineering Research Council of Canada (NSERC) for financial support.

References

[1] Bon, S. A. F., Bosveld, M., Klumperman, B., and German, A. L. *Macromolecules* **30**(2), 324–326 (1997).

[2] Marestin, C., Noel, C., Guyot, A., and Claverie, J. *Macromolecules* **31**(12), 4041–4044 (1998).

[3] Nicolas, J., Charleux, B., and Magnet, S. *Journal of Polymer Science Part A: Polymer Chemistry* **44**(13), 4142–4153 (2006).

[4] Nicolas, J., Charleux, B., Guerret, O., and Magnet, S. *Macromolecules* **38**(24), 9963–9973 (2005).

[5] Nicolas, J., Ruzette, A.-V., Farcet, C., Gerard, P., Magnet, S., and Charleux, B. *Polymer* **48**(24), 7029–7040 (2007).

[6] Charleux, B. and Nicolas, J. *Polymer* **48**(20), 5813–5833 (2007).

[7] Nicolas, J., Charleux, B., Guerret, O., and Magnet, S. *Angewandte Chemie International Edition* **43**(45), 6186–6189 (2004).

[8] Thomson, M. E., Manley, A.-M., Ness, J., Schmidt, S., and Cunningham, M. F. *Macromolecules* **43**(19), 7958–7963 (2010).

[9] Gilbert, R. G. *Emulsion Polymerization - a Mechanistic Approach.* Academic Press, San Diego, CA, (1995).

[10] Ness, J. S. and Schmidt, S. C. (2008).

[11] Thomson, M. E., Ness, J. S., Schmidt, S. C., and Cunningham, M. F. in preparation (2010).

[12] Tonnar, J. and Lacroix-Desmazes, P. *Soft Matter* **4**(6), 1255–1260 (2008).

[13] Rieger, J., Osterwinter, G., Bui, C., Stoffelbach, F., and Charleux, B. *Macromolecules* **42**(15), 5518–5525 (2009).

[14] Luo, Y. and Cui, X. *Journal of Polymer Science Part A: Polymer Chemistry* **44**(9), 2837–2847 (2006).

[15] Luo, Y., Tsavalas, J., and Schork, F. J. *Macromolecules* **34**(16), 5501–5507 (2001).

[16] Dire, C., Magnet, S., Couvreur, L., and Charleux, B. *Macromolecules* **42**(1), 95–103 (2009).

[17] Wi, Y., Lee, K., Lee, B. H., and Choe, S. *Polymer* **49**(26), 5626–5635 (2008).

[18] Rieger, J., Stoffelbach, F., Bui, C., Alaimo, D., Jerome, C., and Charleux, B. *Macromolecules* **41**(12), 4065–4068 (2008).

[19] Maehata, H., Liu, X., Cunningham, M., and Keoshkerian, B. *Macromolecular Rapid Communications* **29**(6), 479–484 (2008).

[20] Gruendling, T., Junkers, T., Guilhaus, M., and Barner-Kowollik, C. *Macromolecular Chemistry and Physics* **211**(5), 520–528 (2010).

[21] Bates, R. G. *Medium effects and pH in nonaqueous solvents.* Determination of pH: Theory and Practice. John Wiley & Sons, New York, 2nd edition (1973).

[22] Chauvin, F., Dufils, P.-E., Gigmes, D., Guillaneuf, Y., Marque, S. R. A., Tordo, P., and Bertin, D. *Macromolecules* **39**(16), 5238–5250 (2006).

[23] Lacroix-Desmazes, P., Lutz, J.-F., Chauvin, F., Severac, R., and Boutevin, B. *Macromolecules* **34**(26), 8866–8871 (2001).

[24] Marque, S., Mercier, C. L., Tordo, P., and Fischer, H. *Macromolecules* **33**(12), 4403–4410 (2000).

[25] Asua, J. M., Beuermann, S., Buback, M., Castignolles, P., Charleux, B., Gilbert, R. G., Hutchinson, R. A., Leiza, J. R., Nikitin, A. N., Vairon, J.-P., and van Herk, A. M. *Macromolecular Chemistry and Physics* **205**(16), 2151–2160 (2004).

[26] Nikitin, A. N. and Hutchinson, R. A. *Macromolecules* **38**(5), 1581–1590 (2005).

[27] Zetterlund, P. B. and Okubo, M. *Macromolecules* **39**(26), 8959–8967 (2006).

[28] Zetterlund, P. B. and Okubo, M. *Macromolecular Theory and Simulations* **16**(3), 221–226 (2007).

Chapter 6

High Solids Nitroxide Mediated Microemulsion Polymerization of MMA with a Small Amount of Styrene and the Synthesis of (MMA-co-St)–block–(BMA-co-St) Polymers.

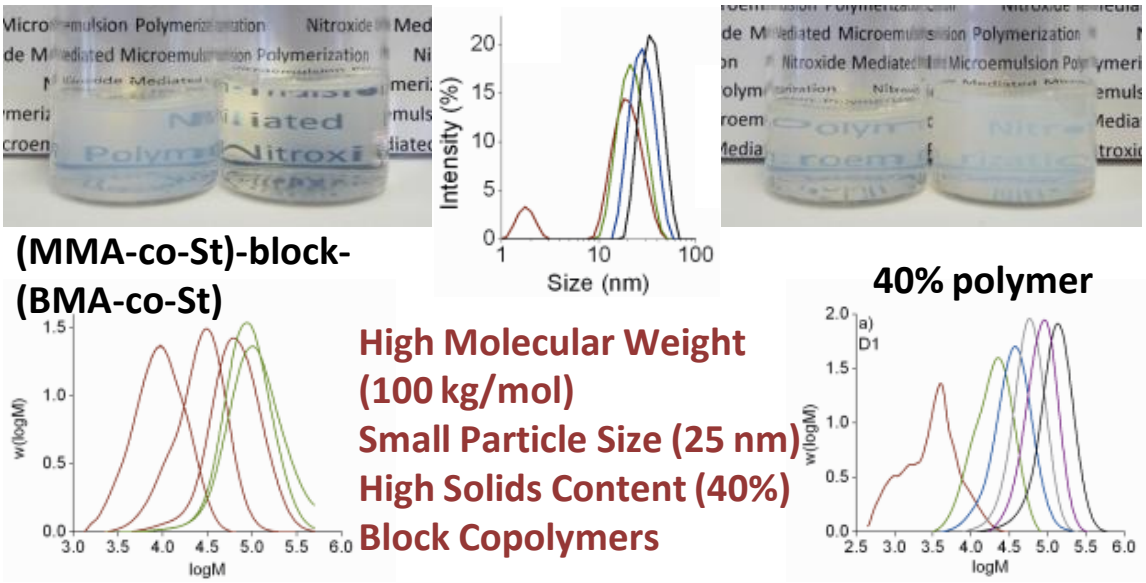

Preface

An attempt at nitroxide mediated microemulsion polymerization had been undertaken several years before by two undergraduate summer students in the Cunningham group, but had no success in synthesizing particles in the microemulsion domain (<50 nm). However, exploiting our earlier discovery of NMP emulsion systems producing smaller particles with higher molecular weight targets, as discussed in Chapter 5, we were able to make stable latexes with very small particle sizes (∼20 nm). Not only does targeting very high molecular weight allow small particles to be made, these are significantly more valuable as a product. Very interestingly, it is the compartmentalization of the chains into a great number of particles that allows such high molecular weights to be reached with very little termination. The low frequency of termination also allows high solids latexes (<40 wt.%) and block copolymers to be created with ease.

Abstract

We report the first nitroxide mediated microemulsion polymerization of methyl methacrylate-co-styrene as well as the synthesis of (MMA-co-St)-block-(n-BMA-co-St) polymers using a one-pot, two-stage differential monomer addition technique. These microemulsion polymerizations were conducted with commercially available materials and do not require a preliminary synthesis step. The latexes are optically translucent with monomodal particle size distributions, particle sizes ranging from 20–30 nm, polymer contents up to 40%, high initiator efficiencies, and low surfactant to monomer ratios (0.28–0.13 wt/wt). The polymerizations exhibited fast reaction rates resulting in well-controlled reactions yielding high molecular weight polymer (>100,000 $g \cdot mol^{-1}$). The styrene content and duration of the 1st stage were particularly important for obtaining narrow molecular weight distributions, with 30 mol% styrene in the 1st stage (∼8–10 mol% styrene overall in the polymer) resulting in the best controlled polymerizations. The overall styrene content in the latexes can be as low as 8 mol% while maintaining excellent control. These MMA-co-St microemulsion latexes can readily be chain extended with n-BMA-co-St while preserving monomodal particle size distributions

6.1 Introduction

Controlled/living polymerization has emerged as an elegant and simple method of synthesizing polymers with tailored molecular architectures under mild reaction conditions. Nitroxide mediated polymerization (NMP) was first reported using the nitroxide TEMPO (2,2,6,6-tetramethylpiperidine-1-oxyl) to reversibly terminate growing polymer chains, thereby minimizing the occurrence of irreversible termination and allowing the chains to grow over the course of the polymerization, giving narrow molecular weight distributions (MWDs), low polydispersities (PDIs) and the ability to extend the polymer chains.[1, 2] Unfortunately TEMPO proved capable of mediating only styrenic monomers with ease, but the introduction of other nitroxides, such as SG1(N-tert-butyl-N-(1-diethylphosphono-2,2-dimethylpropyl) nitroxide, has enabled the mediation of styrenics and acrylates at milder reaction conditions.

Early attempts to perform nitroxide-mediated emulsion polymerization resulted in latex coagulation,[3, 4] but the introduction of a two-step emulsion polymerization procedure using the commercially available water soluble alkoxyamine BlocBuilder MA® from Arkema, based on the nitroxide SG1 (*N*-*tert*-butyl-*N*-(1-diethylphosphono-2,2-dimethylpropyl) nitroxide), has resolved this problem.[5, 6, 7] A 1st stage latex was synthesized in the absence of monomer droplets and the initial reactor charge contained a small amount of monomer, surfactant and the alkoxyamine in its ionized form. The remainder of the monomer could be then be added to the 1st stage latex in either batch of semi-batch mode.

While NMP can effectively mediate the polymerization of styrenics and acrylates, successful polymerization of methacrylate monomers is limited by a very high activation/deactivation equilibrium constant (K_{eq}). This causes a large quantity of irreversible termination to occur early on in the polymerization, leading to an accumulation of nitroxide that suppresses further polymerization. However, methyl methacrylate (MMA) can be polymerized in a controlled manner, using SG1, through the addition of 4.4–8.8 mol% styrene (St) which acts to lower the equilibrium constant.[8] K_{eq} depends on both the terminal and penultimate units of the polymer chain, and the majority of the dormant chains possess the structure MMA-St-SG1 in these polymerizations.[9] Further modeling studies on the kinetics of these polymerizations suggest that the addition of too much styrene monomer can impede the polymerization through the formation of St-St-SG1 segments, which are extremely slow to re-activate.[10, 11] Another limitation of NMP with methacrylates is that in systems with

large excess of SG1 (> 40 mol%), β-hydrogen transfer from the methacrylate-derived radical to the nitroxide can also be a significant chain ending event.[12, 13]

A surfactant-free emulsion polymerization of MMA with a small amount of St has been achieved by first synthesizing an amphiphilic poly(methacrylic acid-co styrene)-SG1 macroinitiator in a 1,4-dioxane solution.[14] Following purification, the macroinitiator acts as both a surfactant-like species and the alkoxyamine initiator for the polymerization. This procedure resulted in well-controlled polymerization with high initiation efficiency, but sometimes produced bimodal particle distributions, attributed to the formation of aggregates. Particle size distributions were reported between 27–50 nm for the smaller domain and 150–300 nm for the larger domain. Molecular weights between 30,000 and 78,000 $g{\cdot}mol^{-1}$ were produced at conversions between 70–85% within 3–7 hours, depending upon the batch characteristics of the macroinitiator.[14] The solids contents were 15–20 wt%.

Microemulsions are defined as thermodynamically stable oil-in-water dispersions, and polymerization in such systems leads to extremely small (< 50 nm) polymeric nanoparticles suspended in water. These polymeric microemulsions have very high internal interfacial area and are both thermodynamically stable and optically transparent; characteristics which are desirable in specialized applications like adhesives, drug delivery or microencapsulation.[15] Often microemulsion polymerizations have very high amounts of surfactant with respect to monomer (>1:1 wt/wt), although it has been demonstrated in conventional microemulsion polymerization that high polymer to surfactant ratios can be achieved through the use of differential monomer feeding strategies over the course of the polymerization.[15, 16]

Nitroxide mediated microemulsion polymerization was first reported by Wakamatsu et al.[10] for styrene mediated by TEMPO or SG1 in a bi-component system (using the thermally decomposing initiator AIBN) at 120^{O}C. This system was of low solids content (2–5 wt%) and high surfactant to monomer ratios (between 2.5:1 and 6.7:1 wt/wt) such that rapid cooling of the system was not possible without the formation of a gel. Mean particle diameters were in the 40–129 nm region with TEMPO and 27–35 nm with SG1. In systems with SG1, the molecular weight increased monotonically with conversion, but the PDIs were over 2 upon reaching full conversion. Zetterlund et al.[17] have continued work with NMP microemulsion with the nitroxides SG1 and TIPNO to discuss compartmentalization effects in the dispersed phase. The system they studied was styrene polymerized at 100^{O}C

with 6% polymer content and a 2.50 surfactant to monomer ratio (wt/wt), and resulted in particles of $\sim$ 50 nm diameter at high conversion. They demonstrated that polymerization in microemulsion is slower than in bulk, but forms polymer with lower PDIs at conversions below 20%. However at high conversions, control over the MWD is superior in the bulk system. Experimentally, these microemulsion systems suffered from poor initiator efficiency as a result of the germinant recombination of AIBN radicals, but impact of the lower initiator efficiency is lessened by the exit of SG1 into the aqueous phase over the course of the polymerization.

Herein we report the first nitroxide mediated microemulsion polymerization of MMA-co-St along with the synthesis of MMA-co-St-block-BMA-co-St polymers. These microemulsion polymerizations were conducted with commercially available materials and do not require a preliminary synthesis step. These latexes are optically translucent with monomodal particle size distributions, particle sizes ranging from 20–30 nm, polymer contents up to 40 wt%, high initiator efficiencies, low monomer to surfactant ratios and yield well controlled polymerizations and high molecular weight (>100 kg·mol^{-1}) polymer.

6.2 Experimental

Materials Styrene (St, Aldrich, >99%), n-butyl methacrylate (BMA, Aldrich, 99%) and methyl methacrylate (MMA, Aldrich, 99%) were purified by passing through columns packed with inhibitor remover (Aldrich). The compounds 2-[N-tert-Butyl-N-(1-diethoxyphosphoryl-2,2-dimethylpropyl)aminoxy]-2-methylpropionic acid (BlocBuilder MA®, supplied by Arkema, 99%), Dowfax^{TM}8390 (Dow Chemicals, 35 wt.% solution in water) and sodium carbonate (Na_2CO_3, Aldrich, >99%) were used as received.

Microemulsion Polymerization BlocBuilder MA® (0.086 g, 0.225 mmol), Na_2CO_3 (0.060 g, 0.566 mmol) and DIW (4.0 g) were mixed and stored in the refrigerator overnight to form the ionized alkoxyamine in solution. The 1st stage latex was prepared with Dowfax^{TM}8390 solution (22.0 g, 11.98 mmol), methyl methacrylate (2.50 g, 25.0 mmol), styrene (0.225 g, 2.16 mmol, 8 mol%) and DIW (137 g). Following a 30 minute N_2 purge, the reaction mixture was immersed in a hot oil bath at 90^{O}C and the ionized BlocBuilder MA® solution, after also being purged under N_2 for 30 minutes, was injected. Following the 1st stage, the

monomer feed of methyl methacrylate (22.0 g, 220 mmol) and styrene (2.0 g, 19.23 mmol) was added over 3 hours via a syringe pump. The reaction mixture, remaining under N_2, was stirred at a speed of 300 RPM and continued to react for up to 24 hours with samples withdrawn periodically.

Block extension in microemulsion The preparation and synthesis of the 1st stage latex remained identical to that described for microemulsion polymerization. Following the 1st stage, a monomer feed of methyl methacrylate (11.0 g, 110 mmol) and styrene (1.0 g, 9.61 mmol) was added over 1.5 hours via a syringe pump. Following two hours of polymerization, after the end of the first feed, a second monomer feed of butyl methacrylate (11.28 g, 79.4 mmol) and styrene (0.72 g, 6.92 mmol) was added over 1.5 hours via a syringe pump. The reaction mixture remained under N_2 and continued to react for up to 24 hours with samples withdrawn periodically.

Characterization Monomer conversion was determined gravimetrically. Gel Permeation Chromatography (GPC) was used to measure the molecular weight and polydispersity of the polymer samples. The entire MWD was characterized by a GPC equipped with a Waters 2960 separation module containing four Styragel columns (HR 0.5, HR 1, HR 3, HR 4), coupled with a Waters 410 differential refractive index detector calibrated with standards ranging from 347 to 441,000 g·mol^{-1}. The final M_n, M_w and PDI were also determined by a Viscotek GPC (containing two PolyAnalytik SupeRes Series PAS-10^{6}M mixed bed columns) with a differential refractive index detector calibrated with PS standards ranging from 6,900 – 860,000 g·mol^{-1}. For both GPCs, THF was used as the eluent with a flow rate of 1.0 mL·min^{-1}. A universal calibration was used to correct the molecular weights obtained for the ratio of PS and n-PBMA or PMMA. The Mark Houwink parameters for PS are K = 1.14·10^{-3} L·g^{-1}, a = 0.716, for n-PBMA are K = 1.48·10^{-3} L·g^{-1}, a = 0.664 [18] and for PMMA are K = 7.56·10^{-4} L·g^{-1}, a = 0.731.[19] All of the MWD curves were measured on the Waters GPC. However, in many cases the final sample of each experiment was out slightly out of the calibration range of the Waters GPC and, as a result, the molecular weight data reported in the tables is from the Viscotek GPC. The M_n, M_w and PDI data measured on the Waters GPC are available in the Supporting Information and are in good agreement with those reported here. The separation efficiency of the Waters GPC is superior to the

Viscotek GPC at lower M_w ranges and was used as the primary source for evaluating the evolution of the MWDs. Particle size measurements were done by dynamic light scattering on a Zetasizer Nano ZS from Malvern Instruments at a temperature of 25^{O}C and an angle of 173^{O}. Samples, other than the 1st stage, were diluted with DIW prior to measurement.

6.3 Results and Discussion

In this work, SG1-mediated microemulsion polymerization was conducted with methyl methacrylate incorporating a low proportion of styrene. These microemulsion polymerizations were produced in a two-step, one-pot procedure, where a 1st stage latex was prepared by the addition of the alkoxyamine BlocBuilder MA in its ionized form to an aqueous solution of surfactant and a small amount of monomer. Following preparation of the 1st stage latex, which remained optically transparent, additional monomer was fed to continue the polymerization, and particles of approximately 20–25 nm were obtained at 17 wt% polymer content with high initiator efficiencies and a low surfactant to monomer ratio of 0.28:1 wt/wt. The effects of varying reaction conditions were investigated, including the proportion of styrene in both the 1st and 2nd (monomer feed) stages, the solids content in the 1st stage, the duration of the 1st stage, and the concentration of BlocBuilder MA used to target different molecular weights. Following these experiments, the synthesis of high solids MMA-co-St microemulsions, up to 40% polymer content, and the synthesis of (MMA-co-St)-block-(BMA-co-St) and (BMA-co-St)-block-(MMA-co-St) polymers were demonstrated.

The polymerizations described here were conducted in the absence of excess SG1 and styrene was used to lower the instances of bimolecular termination between the chains, which also minimized the accumulation of SG1. As a result, these polymerizations operated in a range where instances of β-hydrogen transfer from methacrylate-derived propagating radicals to the nitroxide were minimized.[12, 13]

6.3.1 Evolution of the 1st Stage Latex

An investigation of the 1st stage of the microemulsion polymerization (experiments A1 and A2, Table 6.1) examined the effects of styrene concentration during the 1st stage (8 mol% and 30 mol% respectively) on the MWD evolution and conversion. The observations

Table 6.1: Formulations for the 1st Stage Methyl Methacrylate (MMA) Microemulsion Latexes with Both 8 mol% and 30 mol% Styrene (St) Content.

Exp.	**1st stage formulation ratios (molar) MMA:St:BB**	**1st stage solids content** (wt.%)[a]	**Surfactant/ monomer** (g/g)
A1	110.9:9.7:1.0	1.8	2.8
A2	82.9:31.2:1.0	1.8	3.0

The alkoxyamine initiator BlocBuilder MA (BB) was added to the aqueous phase in its carboxylated form, neutralized with the weak base Na_2CO_3. The surfactant was Dowfax 8390. The polymerizations were conducted at 90°C and samples were withdrawn frequently for 300 minutes.
[a] Solids content refers to the loading of monomer in the system with respect to the other components.

are important for understanding the results presented later for the complete (two stage) experiments.

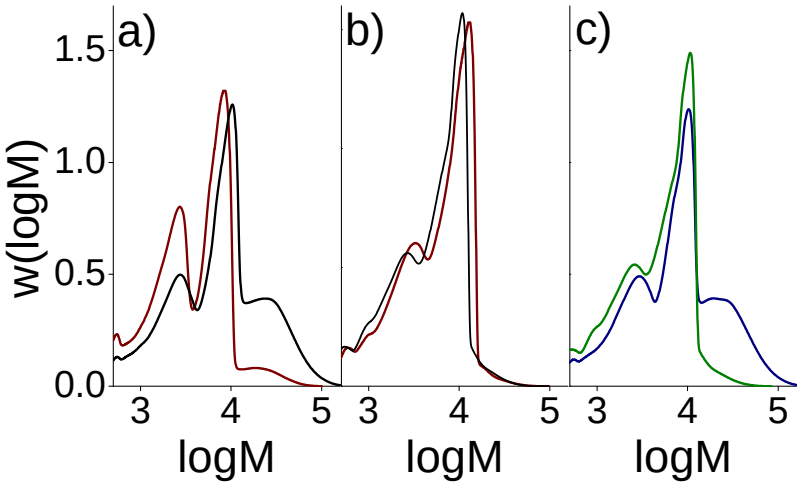

Figure 6.1: Molecular weight distributions for experiments A1 and A2 (Table 6.1), MMA-co-St 1st stage latexes sampled over 300 minutes (90°C, theoretical solids content = 1.5 wt% solids, DP_n^{th} = 120. Distributions are shown for samples collected at 15 minutes (-) and 300 minutes (-) for (a) 8 mol% styrene and (b) 30 mol% styrene. The final samples at 300 minutes are shown together (c) for both 8 mol% (-) and 30 mol% (-) styrene. The MWDs are normalized for area.

Early in the 1st stage, the conversion increased monotonically (Figure 6.2), but the entire MWD did not shift with conversion (Figure 6.1). This suggests that the BlocBuilder MA® activated over a period of time in the aqueous phase and each chain added a similar number of monomer units prior to deactivation. Both of these systems possess a $DP_n{}^{th}$ (theoretical degree of polymerization) of 120 at full conversion, but the DP of the main peak on the

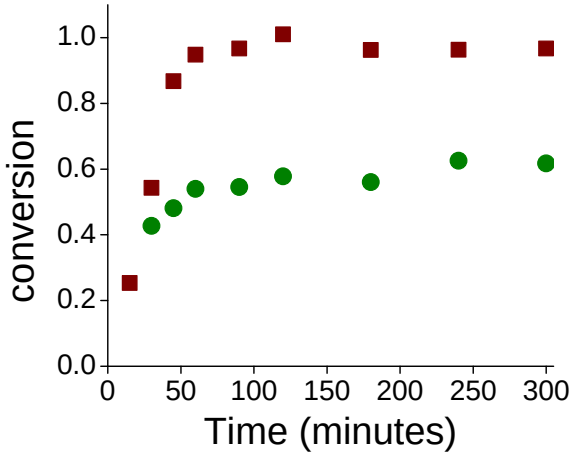

Figure 6.2: Conversion versus time profiles for experiments A1 and A2 (Table 6.1). The MMA-co-St 1st stage latexes (90°C, theoretical solids content = 1.5 wt%, DP_n^{th} 120) contain 92 mol% MMA, 8 mol% St (■) and 70 mol% MMA, 30 mol% styrene (●).

MWDs (Figure 6.1) is approximately 52 for both systems over the course of the entire 1st stage reaction.

However, based on the difference in concentration of styrene between the two systems, the system with more styrene (30 mol%) would statistically be expected to have a shorter DP_n than the system with less (8 mol%). The rate constant of deactivation depends only upon the terminal unit of the chain, which is higher for St (k_{deact} = $4.6 \cdot 10^6$ $L \cdot mol^{-1} \cdot s^{-1}$ [10]) than MMA (k_{deact} = $1.1 \cdot 10^6$ $L \cdot mol^{-1} \cdot s^{-1}$ [10]) and the rate coefficient of propagation is also lower for styrene (see Appendix D). Thus propagating chains in systems enriched in styrene will undergo a reversible deactivation reaction at a shorter DP than a styrene-poor system. In fact, the theoretical chain length of propagating radical prior to its first deactivation with an SG1 molecule can be calculated for a theoretical system in the absence of surfactant micelles, monomer partitioning, radical entry into particles and compartmentalization effects. These calculations (shown in the Appendix D) suggest that the first activation/deactivation cycle of a radical in these systems could reach DP_ns of 768 and 618 for the 92 mol% MMA, 8 mol% St and 70 mol% MMA, 30 mol% St systems respectively. The experimental results, however, do not reflect this difference in chain between the styrene-rich and styrene-poor systems nor such extremely high degrees of polymerization for the first activation/deactivation cycle .

The z-meric length, at which water-soluble MMA-co-St radicals become surface active and can enter into a monomer swollen micelle or existing particle, is ~ 4[20] (based on a chain

with a sulfate end group).[21] When an oligomer enters into a micelle or particle where an SG1 molecule is present, it will undergo nearly instantaneous deactivation (see Appendix D), which is a consequence of strong compartmentalization effects in very small particles.[22] The MMA monomer is added to this system at concentrations below its known water saturation,[21] while the St monomer is added at concentrations above the saturation limit. As a result, the more hydrophobic St will have a greater tendency to reside inside the monomer swollen micelles than the MMA. While the exact proportions are not known, it can be assumed that the micelles are enriched in styrene, with respect to the overall concentration, for both the experiments with 8 mol% and 30 mol% St, and this styrene enrichment is even greater for the 30 mol% St system.

Realizing that the DP these 1st stage latexes reach the first activation/deactivation cycle significantly exceeds the z-meric length (DP = 52) and that the DP for the systems with both 8 mol% and 30 mol% St is identical, it suggests that the limiting step in the deactivation reaction is the presence of a free SG1 molecule at the locus of deactivation (inside the micelles or particles). These microemulsion polymerization have a high target molecular weight for living polymerizations (M_n^{th} = 120,000 g·mol^{-1}), and, as such, possess a very low concentration of BlocBuilder MA® (1.60 mmol·L^{-1}) and an even lower concentration of free SG1, partitioned between the monomer and aqueous phase. At the beginning of the polymerization, there are approximately 10^{21} micelles·L^{-1} [23, 24, 25] (Appendix D) present as the locus of nucleation, but there are only $2{\cdot}10^{18}$ free SG1 molecules·L^{-1} [10] (Appendix D) capable of reversibly terminating the propagating oligomers (of which there are $2{\cdot}10^{18}$ propagating chains·L^{-1}). Therefore, most oligomers are able to polymerize in the aqueous phase without undergoing a deactivation reaction, and continue polymerization upon entry into a micelle, until a free SG1 molecule also enters that particular micelle from the aqueous phase. Because deactivation is nearly instantaneous upon the entry of an SG1 molecule into a particle containing a propagating radical, the difference in styrene concentration inside the micelles/particles for the two systems plays little role in determining the DP of the first activation/deactivation cycle.

Within one hour, all of the water-soluble alkoxyamine initiators had activated, added monomer units and undergone nucleation (entry into an existing particle or micelle) for the 1st stage latex with 30 mol% styrene (A2), but the conversion did not exceed 62% for

the remainder of the experiment (Figure 6.2). However, A1, with 8 mol% St, reached full conversion within the first hour of the experiment.

With 30 mol% St in the 1st stage latex, reactivation of the chains following nucleation appeared minimal (no secondary, higher M_w peaks are observed in Figure 6.1c for A2). Because enrichment of the hydrophobic styrene in the monomer swollen micelles/particles, instances of chains possessing terminal ends of St-St-SG1 are more prevalent in the 30 mol% St system than the 8 mol% St system. Observations about the penultimate and terminal units and the effect of styrene concentration support this claim.[10, 11]

The slow reactivation of the St-St-SG1 type chains in formulations with high proportions of styrene has been discussed in depth by Nicolas et al.[10] and Wang and Broadbelt.[11] In the 8 mol% St 1st stage latex, it is assumed that the majority of the chain ends are present in the MMA-St-SG1 form,[9] and further reactivation of these chains are observed, with the 1st stage reaching nearly full conversion within one hour and the evolution of a secondary, higher molecular weight peak on the MWD (Figures 6.1a and 6.1c).

Although a low concentration of styrene in an MMA polymerization may be recommended for most NMP systems to maintain control while stimulating growth through the suppression of St-St-SG1 terminated chains ends,[10] in the 1st stage, a higher concentration of styrene is advantageous. When subsequent activation and propagation cycles are suppressed in the 1st stage, with 30 mol% rather than 8 mol% St, the chains are all of similar length when the remainder of the monomer is added. This leads to lower PDIs throughout the rest of the polymerization (discussed below), but there is little difference in the polymer livingness of the two systems.

6.3.2 Duration of the 1st Stage Polymerization

The role of the duration of the 1st stage was investigated for systems with 8 mol% and 30 mol% St in the 1st stage, and 8 mol% St in the 2nd (feed) stage for lengths of 20, 90 and 300 minutes (Experiments B1-6 respectively, Table 6.1). In the experiments with 8 mol% St in the 1st stage, broader MWDs were observed for longer 1st durations (Figure 6.3). As discussed earlier, the conversion of the 1st stage leveled out within one hour, and continuing the 1st stage past this resulted in increased irreversible termination, a decrease in fraction of living chains in the system and an accumulation of free SG1. This slowed

Table 6.2: Microemulsion Formulations for the MMA-co-St Optimization Experiments, Including the Roles of: the Styrene Content in the 1st and 2nd Stages, the Duration of the 1st Stage, the Total Monomer Content of the 1st Stage and the Target Molecular Weight in the System.

Exp.	**1st stage** MMA:St:BB ratio	**1st stage reaction time** (min)	**1st stage solids**[a] (wt%)	**2nd stage feed** MMA:St:BB ratio	**surf/ mon** (g/g)	**total solids content**[a] (wt%)
B1	115:10:1	20	1.8	1026:88:1	0.28	17.6
B2	111:10:1	90	1.7	997:86:1	0.28	17.2
B3	111:10:1	300	1.7	990:85:1	0.28	17.1
B4	80:32:1	20	1.6	976:86:1	0.29	17.0
B5	79:32:1	90	1.6	991:85:1	0.28	17.3
B6	80:32:1	300	1.6	1000:86:1	0.28	17.2
B7	83:31:1	90	1.7	1016:64:1	0.30	17.6
B8	80:32:1	90	1.6	1014:64:1	0.28	17.4
B9	80:32:1	300	1.6	1023:64:1	0.28	17.2
C1	43:16:1	20	0.8	1094:82:1	0.28	17.4
C2	83:31:1	20	1.7	1018:64:1	0.28	17.4
C3	179:66:1	20	3.2	986:35:1	0.28	17.5
C4	77:5:1	20	1.2	1050:90:1	0.28	17.9
C5	110:10:1	20	1.8	969:85:1	0.29	17.6
C6	222:19:1	20	3.5	865:76:1	0.29	17.1
D1	28:3:0.5	30	1.8	248:22:0.5	0.28	17.5
D2	56:5:0.5	30	3.4	221:19:0.5	0.28	17.2

The alkoxyamine initiator BlocBuilder MA® (BB) was added to the aqueous phase in its carboxylated form, neutralized with the weak base Na_2CO_3. The surfactant was Dowfax 8390. The polymerizations were conducted at 90°C the end of the 1st stage of polymerization occurred when the monomer feed for the second stage began at a rate of 8 mL·min^{-1}.

[a] Solids content refers to the loading of monomer in the system with respect to the other components.

the rate of polymerization (Figure 6.4) and caused a broadening of the MWD (Figure 6.3). Particularly worth noting is the extensive tailing in the last MWD for B3 with a 1st stage (92 mol% MMA, 8 mol% St) duration of 300 minutes (Figure 6.3c); a low molecular weight tail resulted from significant termination during the 1st stage and early in the 2nd stage and remains evident in the GPC trace at 77% conversion.

With a 20 minute 1st stage, the final MWD is narrower for the system with 30 mol% St in the 1st stage (B4) with respect to the system with only 8 mol% St (B1). However, the difference in the breadth of the MWD is not the result of more instances of termination in the system with 8 mol% St with respect to the 30 mol% system, because both of the

Table 6.3: Microemulsion Polymerization Results for the MMA-co-St Optimization Experiments, Including the Roles of: the Styrene Content in the 1st and 2nd Stages, the Duration of the 1st Stage, the Total Monomer Content of the 1st Stage and the Target Molecular Weight in the System.

Exp.	**Reaction time** (hr)	**conversion** (%)	$\mathbf{M}_n^{th}$ (g·mol^{-1})	$\mathbf{M}_n^a$ (g·mol^{-1})	$\mathbf{M}_w^a$ (g·mol^{-1})	**PDI**^{a} (MWD)	**Particle size** $\mathbf{z}_{avg}$ (nm)	**Particle size dist.** PDI
B1	5.3	93.7	116,800	89,040	136,200	1.53	23.63	0.031
B2	8.0	59.8	72,620	54,950	85,870	1.56	23.82	0.057
B3	20.4	77.1	92,820	65,280	99,100	1.52	26.30	0.062
B4	5.3	95.8	113,200	141,300	197,200	1.40	21.93	0.078
B5	8.5	94.4	113,000	146,700	216,500	1.48	21.96	0.061
B6	21.5	71.0	85,840	96,100	160,300	1.67	21.28	0.082
B7	5.0	93.9	112,800	69,290	106,800	1.54	20.62	0.069
B8	8.5	91.0	108,900	131,300	205,600	1.57	22.51	0.098
B9	21.5	81.0	97,880	128,200	184,800	1.44	23.26	0.055
C1	6.3	92.5	115,000	122,700	174,800	1.43	19.87	0.066
C2	4.3	89.4	109,600	99,300	152,200	1.53	20.23	0.071
C3	6.3	56.3	71,890	111,300	167,000	1.50	19.39 + droplets	0.150
C4	7.3	91.6	112,700	101,400	161,900	1.60	34.05	0.029
C5	7.3	89.8	106,200	138,400	206,300	1.49	26.79	0.044
C6	12.9	86.6	103,000	144,300	230,900	1.60	23.43	0.069
D1	7.5	93.2	56,400	84,520	115,600	1.37	36.82	0.025
D2	9.5	80.5	48,860	72,760	116,300	1.60	24.21	0.068

[a] Measured on the Viscotek GPC. The results are in good agreement with those measured on the Waters GPC (Appendix D).

systems had similar rates of polymerization (Figure 6.4). Irreversible termination reactions leads to the accumulation of free SG1 in the system, which inhibits the polymerization reaction. Instead, the broadness of the MWD for the entire polymerization in system with 8 mol% St in the 1st stage (B1) is the result of the more varied distribution of chain lengths created during the 1st stage with respect to the system with 30 mol% St in the 1st stage (B4). As discussed earlier, there were secondary activations observed for the 1st stage with 8 mol% St which was not the case for the system with 30 mol% St. This led to larger PDIs throughout the remainder of the polymerization, but not a loss of livingness in the system.

6.3.3 Solids Content in the 1st Stage

We also conducted a series of experiments targeting 8 mol% St overall in the system while varying the solids content (i.e. total monomer concentration) in the 1st stage. Experiments

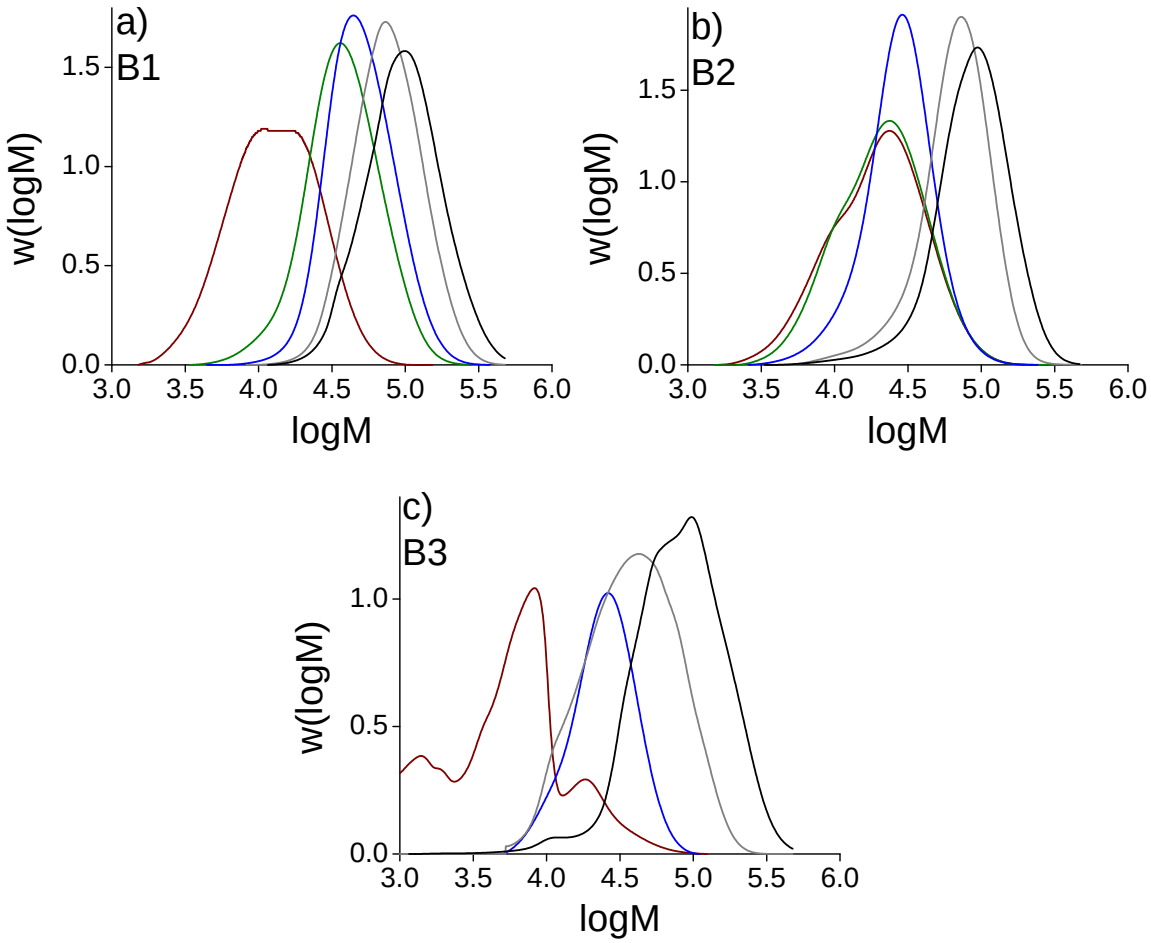

Figure 6.3: Molecular weight distributions for experiments B1-3. The 1st stage latex had a solids content 1.5 wt% (92 mol% MMA, 8 mol% St). The 1st stage latex remained for (a) 20 minutes (B1, MWD shown at 20 min (1st stage), 80 min, 140 min, 200 min, 320 min), (b) 90 minutes (B2, MWD shown at 90 min (1st stage), 150 min, 210 min, 330 min, 480 min) and (c) 300 minutes (B3, MWD shown at 300 min (1st stage), 420 min, 645 min, 1225 min) prior to the to the monomer feed (92 mol% MMA, 8 mol% St); M_n^{th} = 120,000 g·mol^{-1}, theoretical solids content = 17 wt%. The MWDs are normalized for area.

were done with 30 mol% St in the 1st stage. Experiments C1-3 had 1st stage solids contents of 0.75 wt%, 1.5 wt% or 3.0 wt% respectively. During the feed stage, the proportions of styrene were varied to achieve an overall proportion of 8 mol% styrene in the final product. The corresponding styrene proportions in the feed were 7.2 mol%, 6.1 mol% and 3.6 mol% for C1-3 respectively.

The MWD of the 1st stage latexes became much broader and of higher molecular weight as the solids content in the 1st stage was increased (Figure 6.7) because the chains were able to undergo multiple activation, propagation and deactivation cycles. There were also monomer droplets present in the experiment with a 1st stage solids content of 3.0 wt%

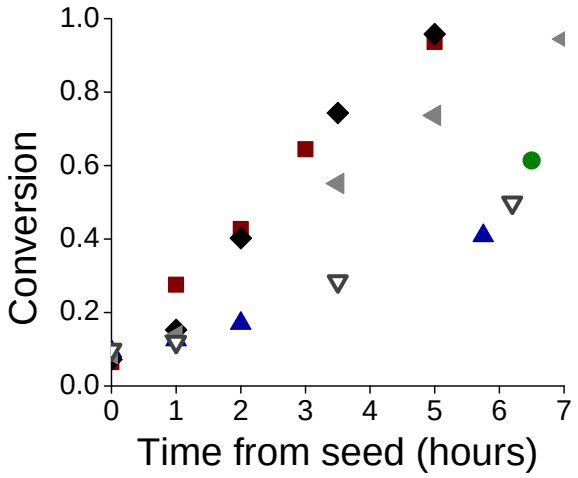

Figure 6.4: The conversion versus time (following the end of the 1st stage) profiles for experiments B1-6. The 1st stage latex had a solids content 1.5 wt% (92 mol% MMA, 8 mol% St for experiments B1-3 and 70 mol% MMA, 30 mol% St for experiments B4-6). The 1st stage latex was left for 20 minutes (■ 92 mol% MMA, 8 mol% St; ♦ 70 mol% MMA, 30 mol% St), 90 minutes (● 92 mol% MMA, 8 mol% St; ◀ 70 mol% MMA, 30 mol% St) or 300 minutes (▲ 92 mol% MMA, 8 mol% St; ▽ 70 mol% MMA, 30 mol% St) prior to the monomer feed (92 mol% MMA, 8 mol% St); M_n^{th} = 120,000 g·mol^{-1}, theoretical solids content = 17 wt%.

(C3) as the 1st stage was not transparent prior to the addition of the BlocBuilder MA® solution. The rates of polymerization (Figure 6.6) early in the 2nd (feed) stage were faster when there was a lower proportion of styrene in the system, with C3 being the fastest and C1 the slowest. However, as the polymerization continued, C3 slowed down considerably because of the irreversible termination since there was not enough styrene to effectively mediate the polymerization and the average K_{eq} in the 2nd stage was too small. The increased rate of termination from the outset in C3 was also demonstrated by a higher than theoretical M_n (indicating fewer chains) consistently observed throughout most of the polymerization (Figure 6.6b).

6.3.4 Effect of Initiator Concentration and Target Molecular Weight

Most of the experiments discussed here have a target theoretical M_n of 120,000 g·mol^{-1}, but two experiments (D1 and D2) were done targeting a lower M_n (65,000 g·mol^{-1}) with the same polymer content (17 wt%) and 8 mol% St in the 1st and 2nd stages as experiment B1, but contained higher concentrations of BlocBuilder MA® to investigated the influence of initiator concentration on the particle size and reaction rate. The 1st stage of D1 had a solids content of 1.8% (similar to previous experiments), resulting in a DP_n^{th} = 60 at the

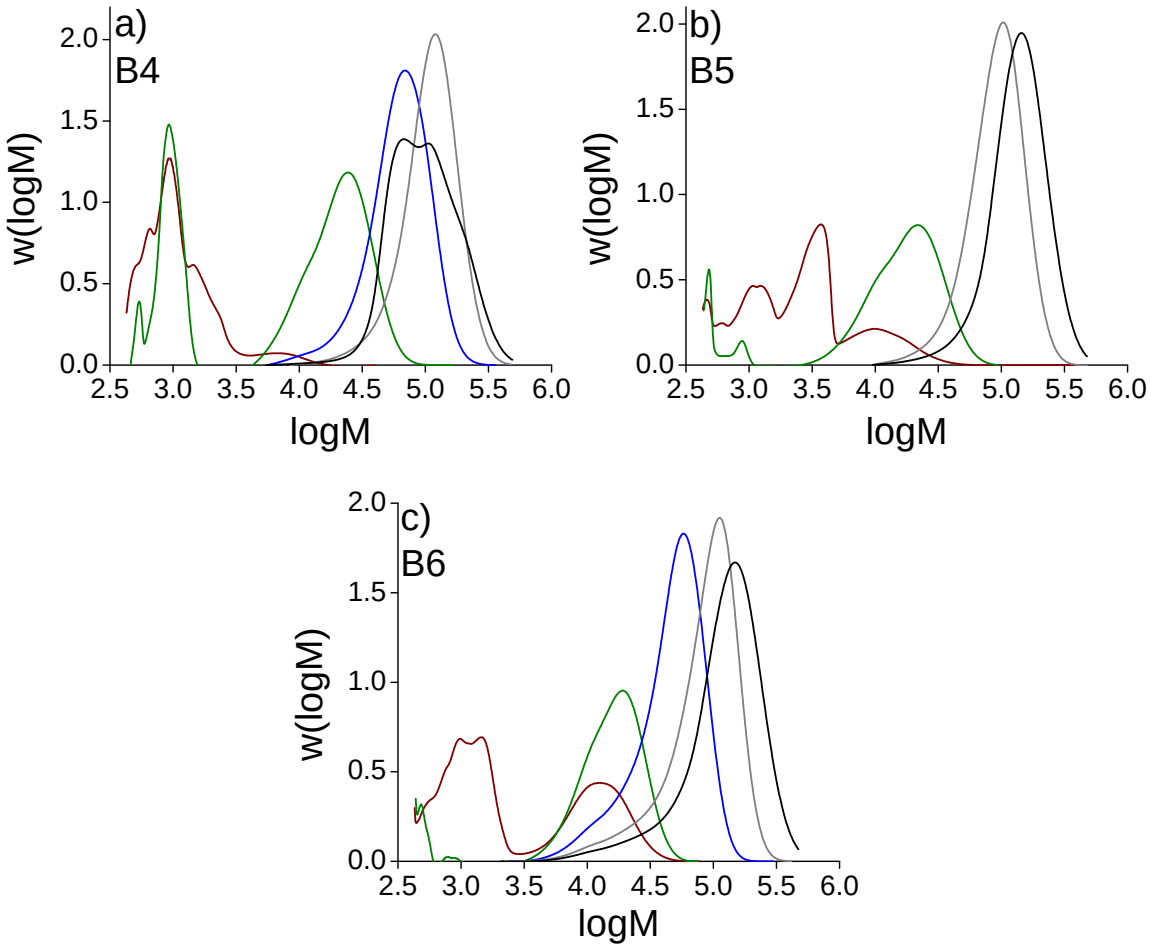

Figure 6.5: Molecular weight distributions for experiments B4-6. The 1st stage latex had a solids content 1.5 wt% (70 mol% MMA, 30 mol% St). The 1st stage latex remained for (a) 20 minutes (B4, MWD shown at 20 min (1st stage), 80 min, 140 min, 230 min, 320 min), (b) 90 minutes (B5, MWD shown at 90 min (1st stage), 150 min, 300 min, 510 min) and (c) 300 minutes (B6, MWD shown at 300 min (1st stage), 360 min, 510 min, 670 min, 1290 min) prior to the monomer feed (92 mol% MMA, 8 mol% St); M_n^{th} = 120,000 g·mol^{-1}, theoretical solids content = 17 wt%. The MWDs are normalized for area.

end of the 1st stage. The solids content of the 1st stage of D2 was 3.4%, to match the $DP_n{}^{th}$ = 120 of previous experiments. D2 showed significant tailing in the MWD (Figure 6.8b), indicating significant irreversible termination occurred during the polymerization. Also, this experiment had a slower rate of polymerization (final conversion of D2 = 80.5% in 9.5 hr) and did not reach the same high conversion as D1 (final conversion = 93.2% in 7.5 hr) (Figure 6.9a), suggesting there was a significant accumulation of SG1 in the system. However, both experiments produced a higher than theoretical M_n, indicating fewer chains than expected were initiated, a result of termination early in the polymerization (Figure 6.9b). In fact, the rate of polymerization for D1 was slower than that of B1 (final conversion = 93.7% in

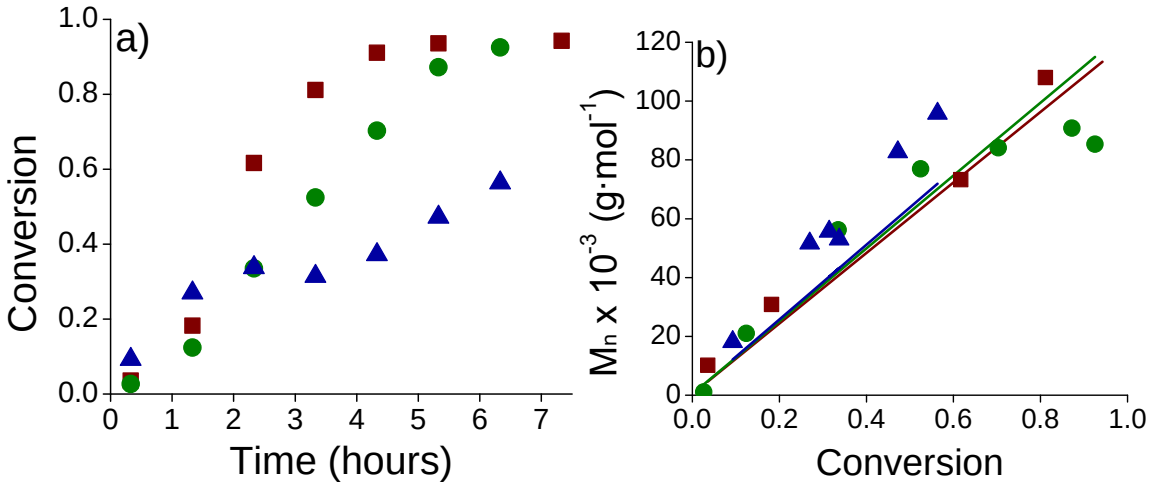

Figure 6.6: (a) The conversion versus time profiles and (b) the evolution of M_n and PDI with conversion for experiments C1-3. The 1st stage latexes had 0.75% (■), 1.5% (●) and 3.0% (▲) solids contents (70 mol% MMA, 30 mol% St). Following a 20 minute 1st stage, feed streams of 92.4 mol% MMA with 7.6 mol% St, 93.9 mol% with 6.1 mol% St and 96.4 mol% MMA with 3.6 mol% St respectively were added; M_n^{th} = 120,000 g·mol^{-1}, theoretical solids content = 17 wt%.

5.3 hr), even though D1 possessed double the number of chains, and would be expected to polymerize more quickly. This suggests that in both experiments with a target M_n of 60,500 g·mol^{-1} there were more instances of irreversible termination and higher concentrations of free SG1 present than in those experiments with a 120,000 g·mol^{-1} target.

The final particle sizes for the systems with a target M_w of 65,500 g·mol^{-1} were larger (37 nm for D1, Table 6.2) than those with a 120,000 g·mol^{-1} target (22 nm for B1, Table 6.2), although the experiments had identical monomer and surfactant concentrations. This is unexpected with respect to a traditional emulsion polymerization model where increases in surfactant concentration and ionic end groups aid in the stabilization of particles, leading to a higher number of particles in the system.[25] However, this is often observed experimentally in our laboratory with NMP and in other reports for different living chemistries in emulsion-based systems.[26, 27] This phenomenon has been referred to in the NMP literature as a possible side effect of superswelling.[6] The thermodynamic considerations of the superswelling theory was first presented by Luo et al.[28] for NMP miniemulsion polymerization. The large concentration of oligomers (the predominant initial product in living systems) present in the particles early in the polymerization lowers the chemical potential of the nucleated particles with respect to droplets or monomer-swollen micelles. This promotes enhanced monomer diffusion to the newly nucleated particles, and can lead to very broad

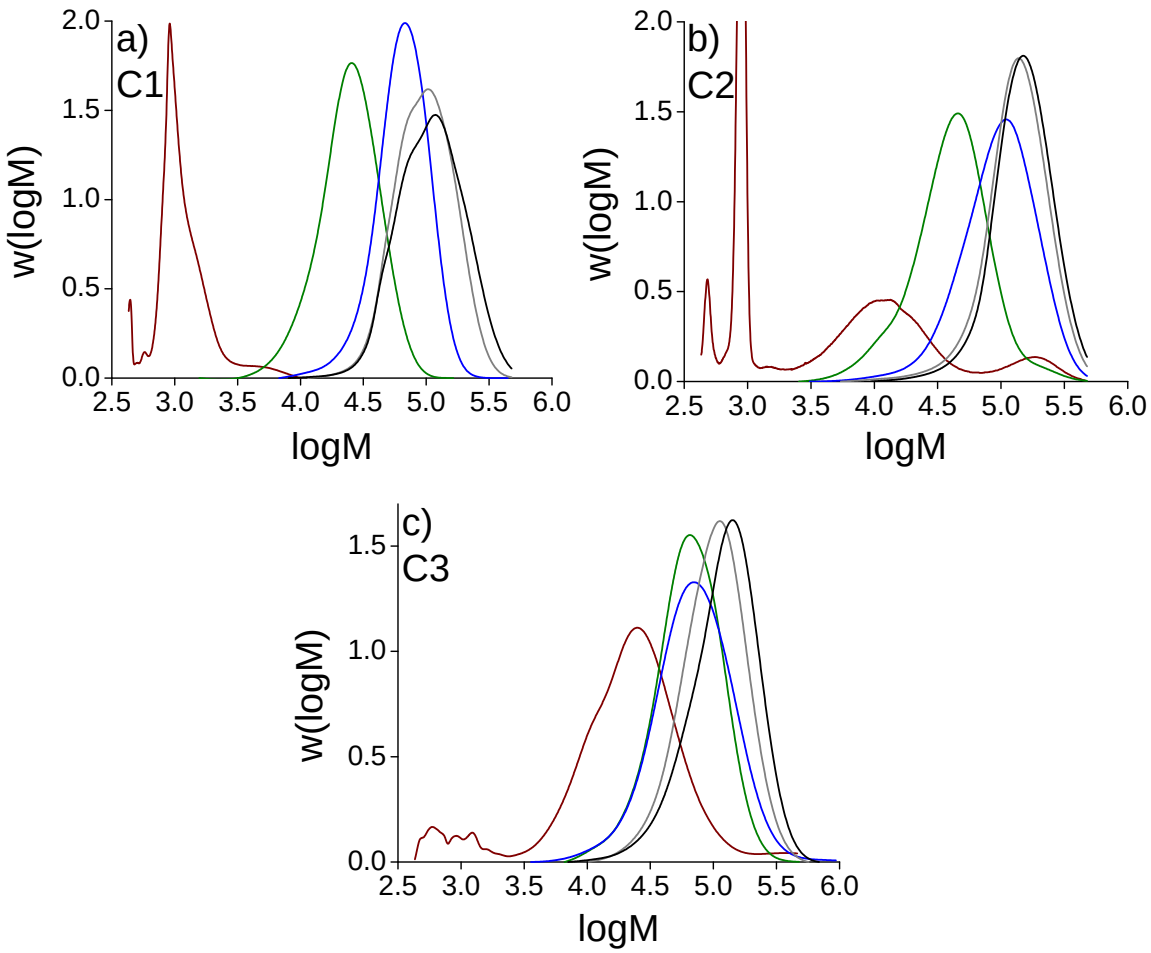

Figure 6.7: Molecular weight distributions for experiments C1-3. The 1st stage latex had (a) 0.8 wt%, (b) 1.5 wt% and (c) 3.2 wt% solid contents of (70 mol% MMA, 30 mol% St). Following a 20 minute 1st stage, feed streams of (a) 92.4 mol% MMA, 7.6 mol% St (C1, MWD shown at 20 min (1st stage), 140 min, 260 min, 320 min) (b) 93.9 mol% MMA, 6.1 mol% St (C2, MWD shown at 20 min (1st stage), 80 min, 140 min, 260 min, 320 min) and (c) 96.4 mol% MMA, 3.6 mol% (C3, MWD shown at 20 min (1st stage), 80 min, 200 min, 320 min, 380 min) were added; M_n^{th} = 120,000 g·mol^{-1}, theoretical solids content = 17 wt%, overall monomer compositions = 92 mol% MMA, 8 mol% St. The MWDs are normalized for area.

particle size distributions, or colloidal instability. Other theories for this correlation between size and initiator concentration have included differences in ionic strength effects and shell thickness when acrylic acid also present in the 1st stage.

At higher conversions, the M_n measured by GPC was often lower than that predicted theoretically for experiments conducted with a target M_n of 120,000 g·mol^{-1} (Figure 6.9b). This phenomenon has been studied in styrene TEMPO-mediated systems, where the high temperatures required lead to a significant population of thermally generated radicals, but chain transfer to monomer reactions have also been identified as a possible cause.[29, 30, 31]

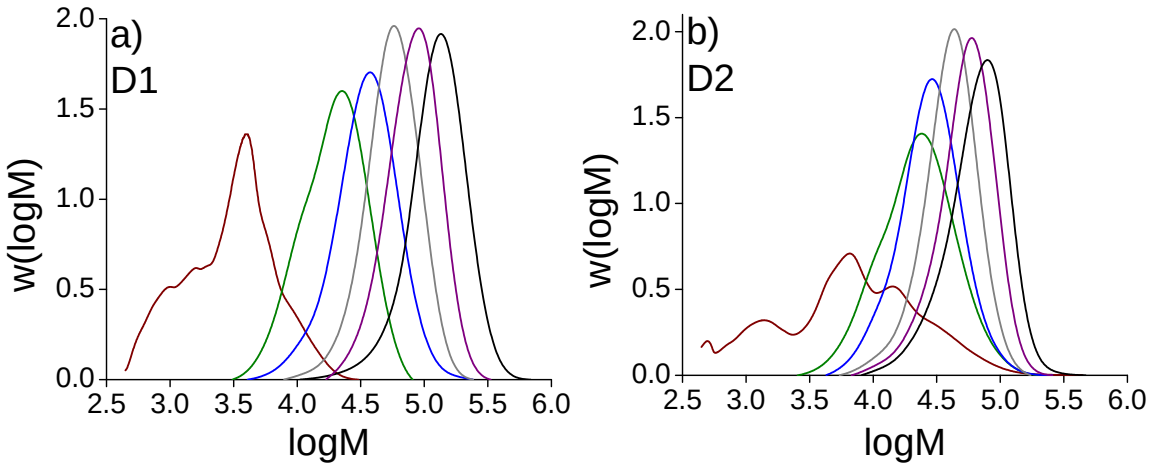

Figure 6.8: Molecular weight distributions for experiments D1 and D2. The 1st stage latex had a solids content of (a) 1.8 wt% (D1, MWD shown at 30 min (1st stage), 90 min, 150 min, 240 min, 330 min, 450 min) and (b) 3.4 wt% (D2, MWD shown at 30 min (1st stage), 90 min, 150 min, 240 min, 330 min, 450 min) of 92 mol% MMA and 8 mol% St. Following a 20 minute 1st stage, feed streams of 92 mol% MMA, 8 mol% were added; M_n^{th} = 65,500 g·mol^{-1}, theoretical solids content = 17 wt%. The MWDs are normalized for area.

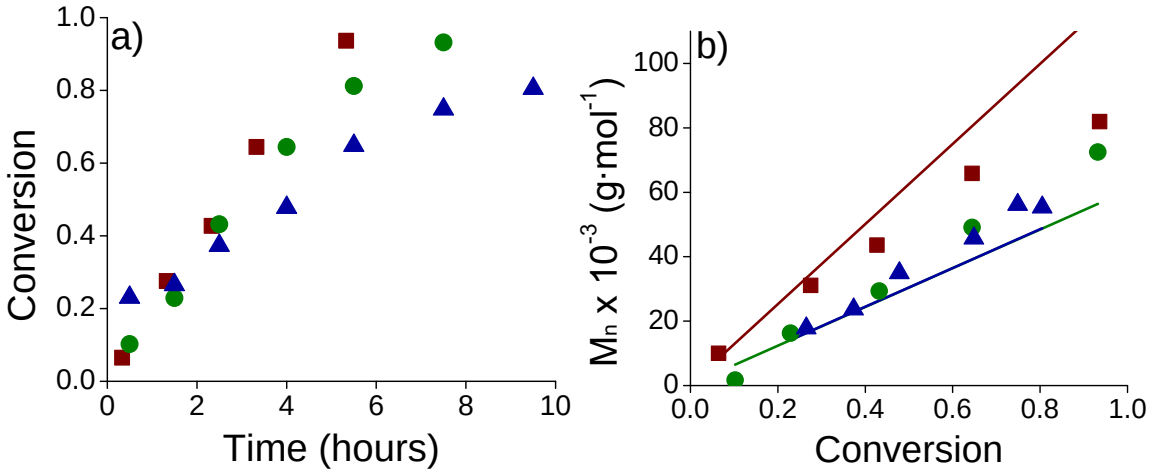

Figure 6.9: (a) The conversion versus time profiles and (b) the evolution of M_n with conversion for experiments B1, D1 and D2. The 1st stage latex had solids contents of 1.8 wt% (B1 ■, D1 ●) and 3.4 wt% (D2 ▲) (92 mol% MMA, 8 mol% St). Following a 20 minute 1st stage, feed streams of 92 mol% MMA, 8 mol% St were added; solids content = 17 wt%; M_n^{th} = 125,000 g·mol^{-1} (B1 ■), M_n^{th} = 65,500 g·mol^{-1} (D1 ●, D2 ▲)

This behavior has also been observed in butyl acrylate polymerizations where backbiting reactions can lead to similar observations.[32] However, in these MMA-co-St systems, backbiting and thermal initiation are not considered to be significant factors. Thus it is believed that lower than theoretical M_n observed when targeting high molecular weights may be due to chain transfer to monomer reactions, which do not lead to an accumulation of SG1, but

Table 6.4: Formulations and Polymerization Results for High Solids Microemulsion Latexes of MMA with a Small Proportion of Styrene.

	1st stage MMA: St:BB ratio	**1st stage time** (min)	**1st stage solids cont.**[a] (wt%)	**2nd stage feed** MMA: St:BB ratio	**surf/mon** (g/g)	**rxn. time** (hr)	**conv.** (%)	**final solids cont.**[a] (wt%)	M_n^{th} ($g \cdot mol^{-1}$)	M_n[b] ($g \cdot mol^{-1}$)	M_w[b] ($g \cdot mol^{-1}$)	**PDI**[b]	**size** (z_{avg}) nm	**Pdi** PSD	**#**[c] **chains /part.**
E1	81:31:1	30	1.7	2158:179:1	0.14	22.2	95.6	36.7	235,300	166,600	303,000	1.82	27.40	0.081	14.9
E2	110:10:1	30	1.7	2202:187:1	0.13	10.7	83.5	36.6	210,600	221,600	369,600	1.67	29.05	0.064	19.1
E3	41:18:1	22	1.8	117:102:1	0.13	13.3	93.9	39.3	126,200	152,400	241,900	1.59	33.01	0.041	54.4
E4	82:36:1	22	3.2	1132:99:1	0.19	13.3	89.0	37.2	121,000	152,500	217,000	1.42	40.44	0.050	97.7

[a] Solids content refers to the loading of the monomer in the system with respect to the other components.
[b] Measured on the Viscotek GPC.
[c] Calculated based on the volume average particle size.

do create shorter, but still growing, polymer chains. The chain transfer coefficient of MMA ($C_M = 2.3 \cdot 10^{-5}$ [33]) is sufficiently large to suggest this mechanism is likely to influence the molecular weight when such a low concentration of BlocBuilder MA® is added to the system.

6.3.5 High Solids Microemulsion Polymerization

Commonly, it is very difficult to achieve high solids contents with by microemulsion polymerization, because of the large quantity of surfactant required to stabilize the particles and the high viscosity associated with latexes of small particle sizes. The early success of our microemulsions at 17 wt% solids lead us to investigate the creation of a high solids, high molecular weight latexes using a similar method.

All of the microemulsion latexes with 40% polymer content (Table 6.4) were optically translucent with a bluish tinge and were free flowing. A monomodal particle size distribution evolution over the course of the polymerization was observed (Figure 6.10). The MWD shifted with conversion, indicative of a well-controlled and living system (Figure 6.11). Only a small bit of coagulum was observed for these polymerizations, with E1 possessing the most with less than 2% by weight.

When the M_n^{th} was reduced from 252,000 $g \cdot mol^{-1}$ (E2) to 134,000 $g \cdot mol^{-1}$ (E3), by the addition of more BlocBuilder MA® in the 1st stage (all other factors remaining constant), it was again observed that the particle size increased from 29 nm to 33 nm (Table 6.4), despite the addition of more stabilizing groups to the system. However, a greater increase in particle size was observed when the monomer content in the 1st stage was doubled, coupled with

a 1.5x increase in the surfactant concentration (E4), to target the same $DP_n{}^{th}$ of 120 in the 1st stage as E2. The increased particle size with increased monomer concentration and initiator concentration in the nucleation stage firmly suggest that superswelling is at work to enhance the diffusion of monomer towards the swollen nucleated particles.

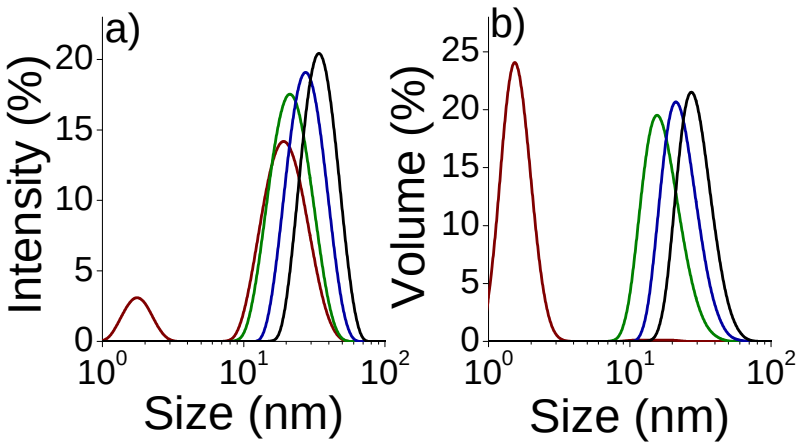

Figure 6.10: Particle size distribution for the high solids MMA-co-St microemulsion polymerization (E3). PSD was evaluated on a Malvern Nanosizer and both the (a) intensity PSD and (b) volume PSD are shown. Samples shown are obtained at 20 minutes (end of the 1st stage), 100 minutes, 170 minutes and 735 minutes. The PSDs are normalized for area.

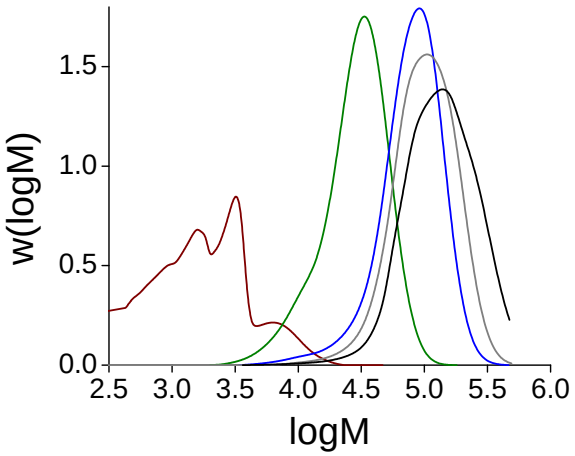

Figure 6.11: Molecular weight distributions for experiments E3. The 1st stage latex had a solids content of 1.8 wt% (70 mol% MMA; 30 mol% St). Following a 20 minute 1st stage, a feed stream of 92 mol% MMA with 8 mol% St was added; M_n^{th} = 134,000 g·mol^{-1}, theoretical solids content = 40 wt%. The MWD is shown at 20 min (1st stage), 100 min, 170 min, 285 min and 735 min. The MWDs are normalized for area.

Table 6.5: Microemulsion Formulation and Polymerization Results for the Creation of MMA-co-St-block-BMA-co and BMA-co-St-block-MMA-co-St Block Copolymers.

Experiment		**MMA-co-St-block-BMA-co-St (F1)**	**BMA-co-St-block-MMA-co-St (F2)**
First Stage	**1st stage** xMA:St:BB	79:31:1	45:19:1
	2nd stage (Feed 1) xMA:St:BB	485:31:1	300:29:1
	time (hr)	2.5	2.5
	conversion	86.8	81.3
	M_n[a] **(g·mol^{-1})**	50,340	40,950
	PDI[a]	1.55	1.45
Second Stage	**Final solids content**[a] (wt%)	18.2	17.6
	3rd stage (Feed 2) xMA:St:BB ratio	356:41:1	390:35:1
	time (hr)	11.5	7.5
	conversion	90.4	84.8
	M_n[b] **(g·mol^{-1})**	80,150	65,660
	PDI[b]	1.63	1.57
	PS intensity (nm)	26.3 (98%) + droplets	4.90 (52%), 64.5 (45%) + droplets
	PS volume (nm)	16.4	4.14 (99.9%), 48.3 (0.1%)
	PDI (PSD)	0.260	0.390

[a] Solids content refers to the loading of monomer in the system with respect to the other components.
[b] Reported on the Waters GPC

6.3.6 Synthesis of Block Copolymers in Microemulsion

The synthesis of (MMA-co-St)-block-(BMA-co-St) polymers was demonstrated in microemulsion with a 1st stage duration of 20 minutes and 30% St present in the 1st stage. (Table 6.5). Chain extension occurred in a controlled manner upon the addition of the BMA/St feed, and a clear shifting of the entire MWD was observed (Figure 6.12), indicating excellent livingness obtained following the first MMA stage. The particle sizes were quite small, around 26 nm at 90% conversion, and the particle size distribution remained monomodal through the polymerization.

Block copolymers were also made beginning with a BMA-co-St 1st stage, and BMA-co-St 2nd stage feed (both with 8 mol% St) and then chain extended by MMA (with 8 mol% St) to make latexes of 17% polymer solids (Table 6.5). Although this system was easily chain extended, as demonstrated by the shifting of the full MWD to higher molecular weights, the particle size distribution in the first BMA/St stage was bimodal, and remained

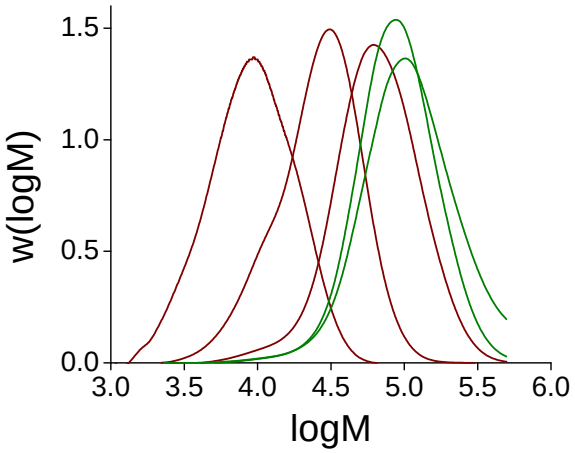

Figure 6.12: Molecular weight distributions for experiment F1, (MMA-co-St)-block-(BMA-co-St) copolymerization. The 1st stage latex had a solids content of 1.8 wt% (70 mol% MMA; 30 mol% St). Following a 20 minute 1st stage, the first monomer feed was added (92 mol% MMA; 8 mol% St); M_n^{th} = 63,000 g·mol^{-1}. 2.5 hours later, a second feed stream (92 mol% BMA; 8 mol% St) was added; M_n^{th} = 118,000 g·mol^{-1}, theoretical solids content = 18.2 wt%. The MWDs for the MMA-co-St block (–, shown at 30 min (1st stage), 90 min, 240 min) and the BMA-co-St block (–, shown at 330 min, 690 min) are included in the plot. The MWDs are normalized for area.

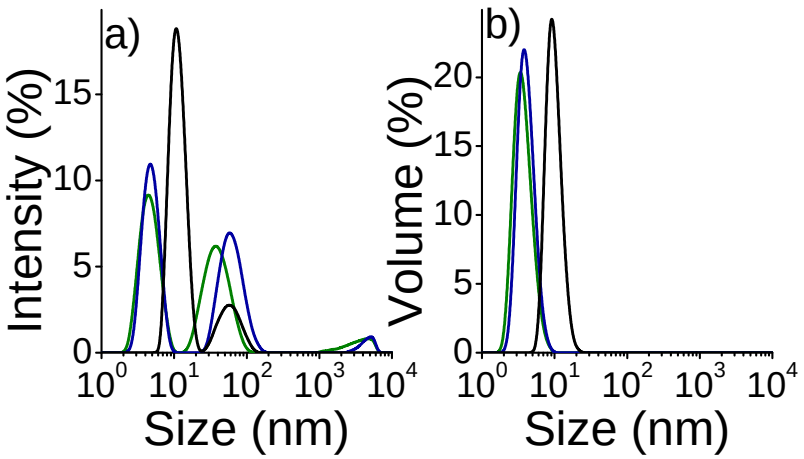

Figure 6.13: Particle size distribution for the (BMA-co-St)-block-(MMA-co-St) block copolymer microemulsion polymerization (F2). The PSD was evaluated on a Malvern Nanosizer and both the (a) intensity PSD and (b) volume PSD are shown. Particle sizes are shown at 30 minutes after the 1st stage (–), 120 minutes, following the BMA/St feed (–) and 660 minutes, following the MMA/St feed (–).The PSDs are normalized for area.

so following the addition of the MMA/St feed (Figure 6.11). Multiple nucleation mechanism (both aggregative and micellar) are believed to causes bimodal PSDs in a BMA-co-St 1st stage latex (explored in Chapter 7).

Figure 6.14: Selected microemulsion latexes: 17% solids both with 8 mol% and 30 mol% St in the 1st stage (B1, B4), (MMA-co-St)-block(BMA-co-St) latex (F1), (BMA-co-St)-block(MMA-co-St) latex (F2) and 40% solids latexes (E1, E3 and E4).

6.4 Conclusions

Well-controlled SG1-mediated microemulsion polymerizations yielded MMA-co-St latexes with very small particle sizes (<30 nm), monomodal PSDs, solids content up to 40% and high molecular weights (>100 g·mol^{-1}). Narrower MWDs were obtained when 30 mol% St was used in the 1st stage compared to 8 mol% because reactivation of the dormant chains following nucleation was minimized. A shorter 1st stage duration is preferred because complete nucleation is reached in less than 1 hour. Leaving the 1st stage longer resulted in irreversible termination and the accumulation of SG1, which slowed further polymerization. The breadth of the MWD of the final latex was broader when lower fractions of St were used in the 1st stage. This is not the result of enhanced irreversible termination, as the overall rate of polymerization did not depend on the fraction of styrene in the 1st stage, rather it is the result of the breadth of the MWD created during the 1st stage. When 8 mol% St was present in the 1st stage, multiple activation/deactivation cycles were observed, while only a single activation/deactivation was observed for the 1st stage with 30 mol% St. While the breadth of the MWD is broader with lower fractions of St in the 1st stage, it did not affect the livingness of the polymer chains.

Regardless of the concentration of styrene present in the 1st stage, 8 mol% St in the 2nd (monomer feed) stage provided excellent control over the MWD. Lower styrene concentrations in the feed resulted in faster polymerization rates initially, but the accumulation of SG1, the result of irreversible terminations, ultimately suppressed the polymerization rate.

Decreasing the target M_n by increasing the initiator concentration yields larger particles,

which is counterintuitive to what is expected in conventional emulsion when the concentration of stabilizing groups is increased. Increasing the monomer content during the 1st stage also leads to increased particle sizes, even in the presence of higher concentrations of surfactant micelles. Both of these phenomena are believed to be the result of superswelling during the nucleation stage, where monomer diffusion is enhanced to particles containing large concentrations of short oligomers.

Controlled microemulsion polymerizations with solids content close to 40% can be achieved with very small particle sizes (30–40 nm), low surfactant to monomer ratios (0.13–0.19 wt/wt), fast reaction rates and high molecular weights (100–200 g·mol^{-1}). These MMA-co-St microemulsion latexes can readily be chain extended with BMA-co-St to make block copolymers. Beginning with BMA-co-St in the 1st stage, rather than MMA-co-St, results in bimodal particle size distributions and is believed to be the result of multiple nucleation mechanisms (aggregative and micellar).

Acknowledgments

The authors wish to thank Michelle Edwards and Brian Ballios for their preliminary experiments in NMP microemulsion. We also thank Arkema, Inc for providing financial support and materials, and the Natural Sciences and Engineering Research Council of Canada (NSERC) for financial support.

References

[1] Georges, M. K., Veregin, R. P. N., Kazmaier, P. M., and Hamer, G. K. *Macromolecules* **26**(11), 2987–2988 (1993).

[2] Benoit, D., Harth, E., Fox, P., Waymouth, R. M., and Hawker, C. J. *Macromolecules* **33**(2), 363–370 (2000).

[3] Bon, S. A. F., Bosveld, M., Klumperman, B., and German, A. L. *Macromolecules* **30**(2), 324–326 (1997).

[4] Marestin, C., Noel, C., Guyot, A., and Claverie, J. *Macromolecules* **31**(12), 4041–4044 (1998).

[5] Nicolas, J., Charleux, B., and Magnet, S. *Journal of Polymer Science Part A: Polymer Chemistry* **44**(13), 4142–4153 (2006).

[6] Nicolas, J., Charleux, B., Guerret, O., and Magnet, S. *Angewandte Chemie International Edition* **43**(45), 6186–6189 (2004).

[7] Charleux, B. and Nicolas, J. *Polymer* **48**(20), 5813–5833 (2007).

[8] Charleux, B., Nicolas, J., and Guerret, O. *Macromolecules* **38**(13), 5485–5492 (2005).

[9] Nicolas, J., Dire, C., Mueller, L., Belleney, J., Charleux, B., Marque, S. R. A., Bertin, D., Magnet, S., and Couvreur, L. *Macromolecules* **39**(24), 8274–8282 (2006).

[10] Nicolas, J., Mueller, L., Dire, C., Matyjaszewski, K., and Charleux, B. *Macromolecules* **42**(13), 4470–4478 (2009).

[11] Wang, L. and Broadbelt, L. J. *Macromolecules* **43**(5), 2228–2235 (2010).

[12] Mchale, R., Aldabbagh, F., and Zetterlund, P. B. *Journal of Polymer Science Part A: Polymer Chemistry* **45**(11), 2194–2203 (2007).

[13] Dire, C., Belleney, J., Nicolas, J., Bertin, D., Magnet, S., and Charleux, B. *Journal of Polymer Science Part A: Polymer Chemistry* **46**(18), 6333–6345 (2008).

[14] Dire, C., Magnet, S., Couvreur, L., and Charleux, B. *Macromolecules* **42**(1), 95–103 (2009).

[15] Ming, W., Jones, F. N., and Fu, S. *Polymer Bulletin* **40**(6), 749–756 (1998).

[16] He, G., Pan, Q., and Rempel, G. L. *Macromolecular Rapid Communications* **24**(9), 585–588 (2003).

[17] Zetterlund, P. B., Wakamatsu, J., and Okubo, M. *Macromolecules* **42**, 6944–6952 (2009).

[18] Beuermann, S., Buback, M., Davis, T. P., Gilbert, R. G., Hutchinson, R. A., Kajiwara, A., Klumperman, B., and Russell, G. T. *Macromolecular Chemistry and Physics* **201**(12), 1355–1364 (2000).

[19] Chen, Y. J., Li, J., Hadjichristidis, N., and Mays, J. W. *Polymer Bulletin* **30**(5), 575–578 (1993).

[20] Thomson, M. E., Manley, A.-M., Ness, J., Schmidt, S., and Cunningham, M. F. *Macromolecules* **43**(19), 7958–7963 (2010).

[21] Maxwell, I. A., Morrison, B. R., Napper, D. H., and Gilbert, R. G. *Macromolecules* **24**(7), 1629–1640 (1991).

[22] Zetterlund, P. B. and Okubo, M. *Macromolecules* **39**(26), 8959–8967 (2006).

[23] Hiemenz, P. C. and Rajagopalan, R. *Principles of Colloid and Surface Chemistry*. Marcel Dekker, New York, (1997).

[24] Ben-Moshe, M. and Magdassi, S. *Colloids and Surfaces A: Physicochemical and Engineering Aspects* **250**(1-3), 403–408 (2004).

[25] Gilbert, R. G. *Emulsion Polymerization - a Mechanistic Approach*. Academic Press, San Diego, CA, (1995).

[26] Luo, Y. and Cui, X. *Journal of Polymer Science Part A: Polymer Chemistry* **44**(9), 2837–2847 (2006).

[27] Tonnar, J. and Lacroix-Desmazes, P. *Soft Matter* **4**(6), 1255–1260 (2008).

[28] Luo, Y., Tsavalas, J., and Schork, F. J. *Macromolecules* **34**(16), 5501–5507 (2001).

[29] Kruse, T. M., Souleimonova, R., Cho, A., Gray, M. K., Torkelson, J. M., and Broadbelt, L. J. *Macromolecules* **36**(20), 7812–7823 (2003).

[30] Gray, M. K., Zhou, H., Nguyen, S. T., and Torkelson, J. M. *Macromolecules* **36**(15), 5792–5797 (2003).

[31] Zetterlund, P. B., Saka, Y., McHale, R., Nakamura, T., Aldabbagh, F., and Okubo, M. *Polymer* **47**(23), 7900–7908 (2006).

[32] Ahmad, N. M., Charleux, B., Farcet, C., Ferguson, C. J., Gaynor, S. G., Hawkett, B. S., Heatley, F., Klumperman, B., Konkolewicz, D., Lovell, P. A., Matyjaszewski, K., and Venkatesh, R. *Macromolecular Rapid Communications* **30**(23), 2002–2021 (2009).

[33] van Berkel, K. Y., Russell, G. T., and Gilbert, R. G. *Macromolecules* **38**(8), 3214–3224 (2005).

Chapter 7

Nitroxide Mediated Surfactant-Free Emulsion Polymerization of n-Butyl Methacrylate with a Small Amount of Styrene

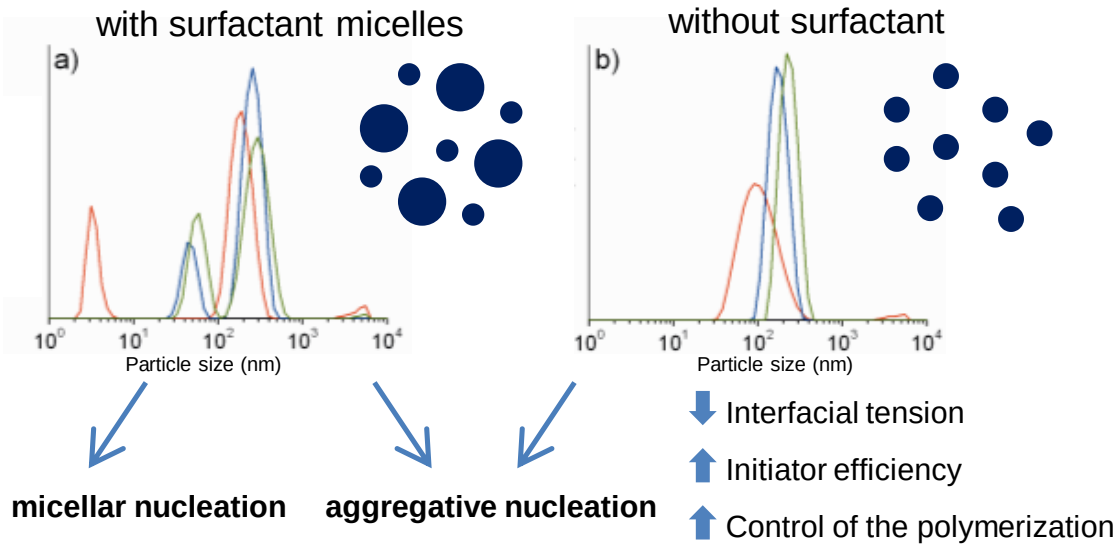

Preface

During the study on microemulsion polymerization (Chapter 6), bimodal latexes were created when a more hydrophobic monomer, n-BMA, rather than MMA, was present in the 1^{st} stage. This same phenomenon was also present in NMP emulsion polymerization with much lower surfactant concentrations than microemulsion. To eliminate micellar nucleation, the surfactant was removed from the system. While this produced monomodal particle size distributions, new problems in terms of poor initiator efficiency arose. Early experimental work for this was performed by Anna-Marie Manley, an undergraduate student.

Abstract

Nitroxide mediated emulsion polymerization of n-butyl methacrylate (BMA) can produce highly living and well controlled polymer chains when polymerized in the presence of 10 mol% styrene (St) using a one-pot, differential monomer addition technique. When n-BMA-co-St is polymerized in the presence of a surfactant above the critical micelle concentration, bimodal particle size distributions are obtained, likely as a result of combined micellar and aggregative nucleation mechanisms. This phenomenon is not observed for the more hydrophilic monomer system of methyl methacrylate and styrene. In the absence of surfactant, however, it is possible to prepare stable, monomodal latexes. Using *N*-*tert*-butyl-*N*-(1-diethylphosphono-2,2-dimethylpropyl) nitroxide (SG1), we report the first nitroxide mediated polymerization of n-butyl methacrylate with a small amount of styrene in a facile surfactant-free emulsion polymerization system. The surfactant-free system requires no separate macroinitiator synthesis step and produces highly living polymers with monomodal particle size distributions. The initiator efficiency can be increased by the addition of methyl acrylate, or by the addition of surfactant at concentrations below the critical micelle concentration in the absence of methyl acrylate.

7.1 Introduction

Controlled/living polymerization has emerged as a versatile and elegant method of creating polymers with tailored molecular architectures, including block copolymers and polymers with very narrow molecular weight distributions, under mild reaction conditions. Conducting these polymerizations in an emulsion polymerization system is highly desirable if these products are to be produced at an industrial scale.[1, 2] Early attempts to conduct nitroxide mediated *ab-initio* emulsion polymerization resulted in severe coagulation formation,[3, 4] but a two-step emulsion polymerization procedure[5, 6, 7] introduced by Charleux's group using the commercially available alkoxyamine initiator BlocBuilder MA® from Arkema, based on the nitroxide SG1 (*N*-*tert*-butyl-*N*-(1-diethylphosphono-2,2-dimethylpropyl) nitroxide), yields a coagulum-free latex. BlocBuilder MA® is water soluble in its carboxylated form when neutralized with a base. In the first step, a small amount of monomer is added to the aqueous phase along with surfactant and the alkoxyamine initiator in its ionized form to create 1st stage particles in the absence of monomer droplets. Following this, the remainder of the monomer can be added in a batch or semi-batch process.

While nitroxide mediated polymerization (NMP) has proved successful for styrenics and acrylates, polymerization of methacrylate monomers has, until recently, remained elusive due to their very high activation/deactivation equilibrium constant for reversible termination (K_{eq}). This causes a large quantity of irreversible termination to occur early on in the polymerization, leading to nitroxide accumulation, suppressing further polymerization. In systems with large excess of SG1 (>40 mol%), β-hydrogen transfer from the PMMA radical to the nitroxide can also become a significant chain ending event.[8, 9] It has been shown that methyl methacrylate (MMA) can be polymerized in a controlled manner, using SG1, through the addition of 4.4–8.8 mol% styrene (St), which decreases the equilibrium constant[10] and results in the majority of the dormant chains possessing the structure MMA-St-SG1.[11] The monomer n-butyl methacrylate (BMA) has also been demonstrated to polymerize in solution in a controlled manner in the presence of <10 mol% styrene and an additional 10 mol% SG1 with respect to BlocBuilder MA®. It was also noted that the lengthening of the alkyl tail of the monomer, BMA vs. MMA, leads to a lower degree of control as the rate constant of propagation increases.[12]

Surfactant-free SG1 mediated emulsion polymerization has been reported for styrene

using a bi-component initiation system (thermal decomposition of a water soluble initiator, potassium persulfate, in the presence of free SG1) in a two-step emulsion procedure.[13] The polymerization exhibited long induction periods prior to polymerization as a result of the reversible termination of SG1-capped styrene oligomers in the aqueous phase prior to nucleation coupled with broad particle size distributions, but did produce living polymer chains capable of being extended.

A surfactant-free emulsion polymerization of MMA with 4 mol% St was successfully conducted by first synthesizing an amphiphilic poly(methacrylic acid-co-styrene)-SG1 macroinitiator in a 1,4-dioxane solution.[14] Following purification, the macroinitiator was used as both a surfactant-like species and alkoxyamine initiator for the polymerization of MMA-co-St, which was added in a single shot. This procedure resulted in a well-controlled polymerization with high initiation efficiency, but produced bimodal particle distributions containing a small fraction of aggregates that were attributed to the presence of styrene at the outer surface of the particles. Monomodal PSDs are desirable if the latex is to be used for film forming applications, especially if specialized morphologies, such as core shell particles, are to be created. Herein we report the first nitroxide mediated polymerizations of n-butyl methacrylate with a small amount of styrene in a facile surfactant-free emulsion polymerization system, using the nitroxide SG1. Through the addition of the hydrophilic, fast propagating monomer methyl acrylate in the 1st stage, termination during the nucleation stage is suppressed. The surfactant-free system requires no separate macroinitiator synthesis step and produces highly living polymers with monomodal particle size distributions.

7.2 Experimental Section

Materials Styrene (St, Aldrich, >99%), n-butyl methacrylate (BMA, Aldrich, 99%) and methyl methacrylate (MMA, Aldrich, 99%) were purified by passing through columns packed with inhibitor remover (Aldrich). The compounds 2-((tert-butyl(1-(diethoxyphosphoryl)-2,2-dimethylpropyl)amino)oxy)-2-methylpropanoic acid (BlocBuilder MA®, supplied by Arkema, 99%), N-tert-butyl-N-(1-diethylphosphono-2,2-dimethylpropyl) nitroxide (SG1, supplied by Arkema, 89%), methyl acrylate (MA, Aldrich, 99%), Dowfax^{TM}8390 (Dow Chemicals, 35 wt.% solution in water), sodium dodecyl sulfate (SDS, Aldrich, >99%), sodium formaldehyde sulfoxylate (SFS, Aldrich, >98%) and sodium carbonate (Na_2CO_3, Aldrich,

>99%) were used as received.

Emulsion Polymerization BlocBuilder MA® (0.15 g, 0.392 mmol), Na_2CO_3 (0.037 g, 0.350 mmol) and DIW (4.0 g) were mixed and stored in a refrigerator overnight to form the ionized alkoxyamine initiator in solution. The 1st stage latex was prepared with a 35 wt.% Dowfax™8390 solution (2.0 g of solution, 1.1 mmol), butyl methacrylate (1.12 g, 7.89 mmol), styrene (0.35 g, 3.37 mmol, 30 mol% of monomer charge) and DIW (146 g). Following a 30 minute N_2 purge, the reaction mixture was immersed in a hot oil bath at 90°C and the similarly purged ionized BlocBuilder MA® solution was injected. Following the 1st stage (20 minutes), the monomer feed of butyl methacrylate (11.79 g, 83.03 mmol) and styrene (0.96 g, 9.23 mmol, 10 mol% of the second monomer charge) was added over 3 hours via a syringe pump. The reaction mixture, remaining under N_2, was stirred at a speed of 300 RPM and continued to react for up to 24 hours with samples withdrawn periodically. The average targeted molecular weight (M_n) of these experiments is 36,700 $g{\cdot}mol^{-1}$.

Surfactant-free emulsion polymerization BlocBuilder MA® (0.15 g, 0.392 mmol), Na_2CO_3 (0.037 g, 0.350 mmol) and DIW (4.0 g) were mixed and stored in a refrigerator overnight to form the ionized alkoxyamine initiator in solution. The 1st stage latex was prepared with methyl acrylate (0.101 g, 1.18 mmol), butyl methacrylate (1.12 g, 7.89 mmol), styrene (0.35 g, 3.37 mmol, 30 mol% of the monomer charge) and DIW (146 g). Following a 30 minute N_2 purge, the reaction mixture was immersed in a hot oil bath at 90°C, stirred at 600 RPM, and the similarly purged ionized BlocBuilder MA® solution was injected. Following the 1st stage (20 minutes) the stirring was slowed to 300 RPM and the monomer feed of butyl methacrylate (11.79 g, 83.03 mmol) and styrene (0.96 g, 9.23 mmol, 10 mol% of the second monomer charge) was added over 3 hours via a syringe pump. The reaction mixture remained under N_2 and continued to react for up to 24 hours with samples withdrawn periodically. When SG1 or SFS was also used, the SG1 (0.0083 g, 0.030 mmol) was added in combination with the 1st stage starting solution, while SFS (0.0036 g, 0.030 mmol) was dissolved in DIW and added at the end of the 1st stage prior to the beginning of the monomer feed. The average targeted molecular weight (M_n) of these experiments is 36,700 $g{\cdot}mol^{-1}$.

Emulsion Polymerization of MMA MMA-co-St emulsion polymerization both in the presence and absence of surfactant was conducted in a similar manner to the procedures listed above for BMA-co-St, but MMA was substituted for BMA on a mass basis. This substitution leads to 7 mol% St with respect to MMA, which is within the studied range of control of MMA by St for NMP.[10] The average targeted molecular weight (M_n) of these experiments is 36,700 g·mol^{-1}.

Characterization Monomer conversion was determined gravimetrically and reported based on the total amount of monomer added over the entire reaction. Gel Permeation Chromatography (GPC) was used to measure the molecular weight and polydispersity (PDI) of the polymer samples. The GPC was equipped with a Waters 2960 separation module containing four Styragel columns (HR 0.5, HR 1, HR 3, HR 4), coupled with a Waters 410 differential refractive index detector calibrated with standards ranging from 347 to 441,000 g·mol^{-1}. THF was used as the eluent with a flow rate of 1.0 mL·min^{-1}. A universal calibration was used to correct the molecular weights obtained for the ratio of PS and n-PBMA or PMMA. The Mark-Houwink parameters for PS are K = 1.14x10^{-5} L·g^{-1}, a = 0.716, for n-PBMA are K = 1.48x10^{-5} L·g^{-1}, a = 0.664[15] and for PMMA are K = 9.44x10^{-6} L·g^{-1}, a = 0.719.[16] Particle size measurements were done by dynamic light scattering on a Zetasizer Nano ZS from Malvern Instruments at a temperature of 25^{O}C and an angle of 173^{O}. Samples, other than the 1st stage, were diluted with DIW prior to measurement. Initiator efficiency is calculated from the deviation of the measured M_n from the theoretical M_n by initiator efficiency = M_n^{th}/M_n^{exp}.

7.3 Results and Discussion

In this work, nitroxide mediated emulsion polymerization of n-BMA incorporating a small amount of styrene was conducted both in the presence and absence of surfactant. As NMP of methacrylates with SG1 is complicated by the high K_{eq} of the tertiary carbon chain ends, Charleux found that MMA polymerization could be mediated by the addition of a low proportion of styrene (4.4–8.8 mol%).[10, 11] This same principle has been successfully applied in this study with another methacrylate, the more hydrophobic n-BMA, without the addition of excess SG1. β-hydrogen transfer from methacrylate-derived propagating

radicals to the nitroxide can be a major chain ending event when there is a large excess of SG1 present in the system (>40 mol% excess).[8, 9] The polymerizations described here are conducted in the absence of additional SG1 and styrene is used to lower the instances of bimolecular termination between the chains, which also minimizes the accumulation of SG1. As a result, these polymerizations operate in a range where β-hydrogen transfer is minimal. These n-BMA polymerizations were conducted in a two stage manner where a 1st stage latex was prepared by the addition of the ionized alkoxyamine initiator, BlocBuilder MA®, to an aqueous solution of surfactant (if used) and a small amount of monomer. Following the formation of the 1st stage latex, which remained optically transparent in the systems with surfactant and turned opaque white for the surfactant-free systems, an additional feed of BMA with 10 mol% styrene continued the polymerization. The emulsion polymerizations conducted with surfactant present above the CMC (critical micelle concentration) resulted in bimodal particle size distributions (PSD) while those conducted in the absence of surfactant micelles resulted in monomodal particle size distributions. As it will be shown, the surfactant-free system yields highly living polymers with monomodal particle size distributions. This surfactant-free nitroxide mediated emulsion polymerization is the first reported system for a methacrylate monomer that does not require prior synthesis of an amphiphilic alkoxyamine and can be conducted directly from commercially available materials. The formulations and polymerization results of this study are available in Tables 7.1 and 7.2, respectively.

7.3.1 Emulsion Polymerization in the Presence of Surfactant Above the CMC

Two stage emulsion polymerization of MMA with 7 mol% styrene (E1) produced well-controlled chains with a PDI below 1.33 and a monomodal particle size distribution (PSD). However, in a similar formulation with BMA and 10 mol% styrene (E2), while the polymerization was living as demonstrated by the growth of the entire molecular weight distribution (MWD) (please see Appendix E) over the course of the polymerization, the PSD was bimodal (Figure 7.1a).

It is suspected that the bimodality of the PSD for the BMA-co-St system is due to a combination of nucleation mechanisms, namely micellar nucleation and aggregative nu-

Table 7.1: Formulations for the Two Stage SG1-Mediated Emulsion and Surfactant-Free Emulsion Polymerizations of n-Butyl Methacrylate (BMA) and Methy Methacrylate (MMA) with 10 mol% Styrene (St).

Exp	**Surfactant concentration** [mmol·L^{-1}]	**1st stage formulation ratios (molar)** BMA:St:MA:BB:SG1:SFS	**2nd stage formulation ratios (molar)** BMA:St	**Total Solids** [%]
E1	7.78[a]	28.5[c]:8.8:0:1:0:0	299[c]:23.8	9.1
E2	7.78[a]	20.6:8.9:0:1:0:0	216:24.2	8.5
E3	0	20.1:8.8:0:1.0:0:0	106:12.0	5.0
E4	0	20.2:8.6:3.2:1:0:0	214:23.8	8.7
E5	0	20.4:8.8:3.2:1.0:0:0	212:23.6	8.6
E6	0	20.2:8.6:3.0:1.0:0.1:0	211:23.7	8.7
E7	0	20.4:2.4:3.0:1:0.2:0.2	229:24.0	8.9
E8	5.14[b]	20.2:8.8:0:1:0:0	211:26.7	9.3

The alkoxyamine initiator BlocBuilder MA® (BB) was added to the aqueous phase in its carboxylated form, neutralized with the weak base Na_2CO_3. Methyl acrylate (MA), excess SG1 nitroxide and the reducing agent sodium formaldehyde sulfoxylate (SFS) were also used in some of the experiments.

[a] Surfactant is Dowfax™8390, present in concentrations above the CMC

[b] Surfactant is SDS, present in concentrations below the CMC

[c] MMA is used rather than BMA

cleation, while the greater hydrophilicity of the MMA monomer may predominantly favor micellar nucleation. The large concentration of initiator present in the aqueous phase in the first few minutes of the 1st stage is extremely high by conventional emulsion polymerization standards, owing both to the low target molecular weights for the polymer (∼36,700 g·mol^{-1}) and the high rate of decomposition of BlocBuilder MA® at the reaction temperature ($k_{act,BB} = 3.4x10^{-2}$ L·mol·s^{-1} [17]). As a result, 95% of the initiator decomposes in the first 90 seconds of the polymerization. Therefore, both micellar and aggregative nucleation mechanisms, which occur in most emulsion polymerizations,[18] are important, although aggregative nucleation in the more hydrophobic BMA-co-St system occurs to a greater extent than in most conventional BMA emulsion polymerizations because of the conditions cited above.

Such a phenomenon has been observed in other two stage NMP emulsion systems. SG1 mediated emulsion polymerization of n-butyl acrylate (n-BA), a monomer with similar hydrophobicity to BMA (n-BA is slightly more hydrophilic), resulted in very broad PSDs[5, 7] with PDIs measured by dynamic light scattering which are similar to our own reported PDIs for the bimodal particles formed with BMA-co-St in the presence of surfactant. While bi-

Table 7.2: Polymerization Results for the Two Stage SG1-Mediated Emulsion and Surfactant-Free Emulsion Polymerizations of BMA and MMA with 10 mol% St.

Exp	**pH** (1^{st} stage)	**Conv.** [%]	**Time** [hr]	**pH** (end)	$\mathbf{M}_n^{th}$ [g·mol^{-1}]	$\mathbf{M}_n^{exp}$ [g·mol^{-1}]	**PDI**	**Initiator eff.**[%]	**PS** [nm] (intensity)	**PS** [nm] (volume)	**pdi** (PSD)
E1	7.91	64.5	11.4	5.35	23,000	30,200	1.33	78.0	469	49	0.116
E2	8.40	38.3	23.1	5.18	14,500	20,800	1.35	69.8	432(61%), 77 (39%)	451 (39%), 71 (61%)	0.542
E3	-	30.0	22.0	-	6,000	11,000	1.55	54.5	233	246	0.094
E4	8.39	67.5	23.1	6.22	25,100	38,400	1.48	65.2	237	246	0.036
E5	-	49.1	22.0	-	18,400	26,500	1.52	69.5	236	246	0.066
E6	-	36.4	22.0	-	13,683	16,184	1.53	84.5	595 (59%), 217 (41%)	576 (76%), 212 (24%)	0.274
E7	8.28	57.0	23.0	6.29	22,256	34,713	1.92	64.1	487	501	0.081
E8	8.09	50.0	11.2	7.14	18,464	30,179	1.61	61.2	408 (74%), 120 (26%)	439 (73%), 107 (27%)	0.325

modal PSDs have not been observed by our group for an MMA-co-St emulsion system (E1) with the surfactant Dowfax^{TM}8390, a bimodal PSD observed by light scattering was reported by Dire *et al.*[14] for the surfactant-free polymerization of MMA-co-St with an amphiphilic alkoxyamine initiator/surfactant combination. The bimodal PSD was attributed to the formation of aggregates due to the presence of styrene in the amphiphilic outer layer of the particles. However, no large particles could be identified by transmission electron microscopy.[14]

In the emulsion polymerization literature,[18] it is common to discuss nucleation mechanisms in terms of the z-meric length and the j_{crit} length. The z-meric length is the minimum length aqueous phase oligomers reach prior to becoming sufficiently surface active to enter a micelle or particle. These water soluble oligomers may grow longer than the z-meric length if they do not encounter a micelle. The critical length at which an oligomer becomes insoluble in the aqueous phase and forms a precursor particle is known as the j_{crit} value.

One important difference in the MMA and BMA emulsion systems is the difference in hydrophobicity of the two monomers. The z-meric lengths for St and BMA have been reported as 2, while the z-meric length is closer to 4-5 for the more hydrophilic MMA with a persulfate terminal group.[19] Tsai and Fitch[20] have measured the j_{crit} length of MMA to be approximately 65 with a persulfate end group, although Maxwell *et al.*[19] have observed

the minimum chain length of insolubility to be 10-11 under similar experimental conditions but using different analytical techniques. The j_{crit} values of the more hydrophobic monomers, BMA and St, are reported as 4.[19] The j_{crit} and z-meric lengths can be estimated for the copolymer systems of MMA-co-St and BMA-co-St based on a weighted average of the homopolymer j_{crit} and z-meric lengths with respect to the concentration of each of the monomers present in the aqueous phase. When the monomers were added to the aqueous phase in concentrations greater than their saturation, the saturation concentration was used.[19] Following the activation of the alkoxyamine initiator in the aqueous phase and propagation of the MMA-co-St aqueous oligomer, this oligomer is able to enter into a micelle or particle (z-meric length ∼4–5) prior to reaching its j_{crit} value (∼10), where aggregative nucleation occurs. However, BMA is much more hydrophobic and is a faster propagating monomer (possessing a higher k_p) than MMA, so the BMA-co-St water soluble oligomers add units more quickly and possess a lower j_{crit} value (∼4) than the MMA-co-St oligomers Therefore, it is probable that some BMA-co-St oligomers will begin aggregating and precipitating prior to entering a micelle or existing particle (z-meric length ∼2), especially in a system with very high initiator fluxes. While this discussion is based on chains with a persulfate end group, the behaviour is likely similar for oligomers with a BlocBuilder MA® end group (COO^-).

7.3.2 Surfactant-Free Emulsion Polymerization

In surfactant-free emulsion polymerization of BMA-co-St, oligomers can only undergo aggregative nucleation due to the absence of surfactant micelles. Early experiments (E3) suffered from poor initiator efficiency and slow polymerization rates because of termination during nucleation, which occurs in the 1st stage of the polymerization. In aggregative nucleation, several water soluble oligomers precipitate to form a precursor particle. However, when using BlocBuilder MA®, which has a very high rate of decomposition at the reaction temperature, about 95% of the water soluble oligomers are present in their active, propagating form in the first 90 seconds of the polymerization. The aggregation of these radicals in small particles results in irreversible termination. This leads to an accumulation of SG1 in the system which suppresses further polymerization due to the persistent radical effect. While the initiator efficiencies of these initial experiments were low, they did produce

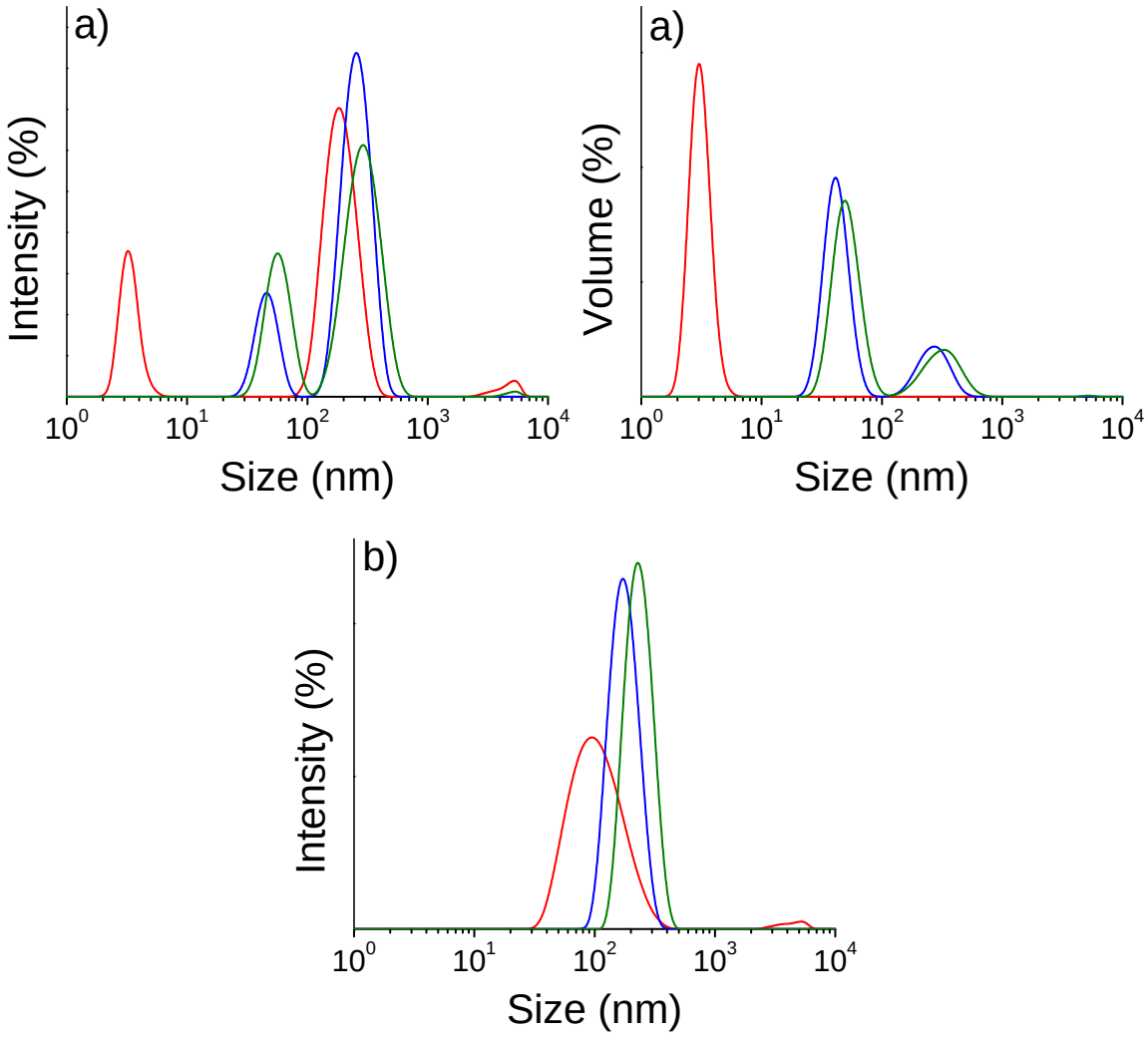

Figure 7.1: Particle size distributions by dynamic light scattering for (a) emulsion polymerization of BMA-co-St with 7.78 mmol·L^{-1} of surfactant Dowfax^{TM}8390 (E2), both the intensity and volume PSDs are shown for samples taken after the 1st stage (25 minutes), 5.5 hours and 23.1 hours and (b) surfactant-free emulsion polymerization of BMA-co-St with methyl acrylate in the 1st stage (E4), only the intensity PSD is shown for samples taken after the 1st stage (20 minutes) (-), 6.5 hours (-) and 23.1 hours (-).The PSD curves are normalized for area.

monomodal PSDs, the goal of this series of experiments.

Increasing the Initiator Efficiency by the Addition of Methyl Acrylate

Low BlocBuilder MA® initiator efficiencies in styrene miniemulsions were found to be caused by extensive termination of the oligomers in the aqueous phase, and the accumulation of excess SG1, leading to extremely slow growth of the oligomeric radicals in the aqueous phase prior to entry into the monomer droplets.[21] The initiator efficiency was shown to be

greatly increased by the addition of a small amount of the hydrophilic, fast propagating monomer methyl acrylate (MA), leading to much more efficient oligomer entry into the miniemulsion droplets.[21] We believe that in our system, methyl acrylate adds preferentially to the oligomeric chain over BMA and St as it is propagating in the aqueous phase and lowers the overall interfacial tension during aggregative nucleation. Lower interfacial tension then minimizes the number of oligomers (and their charged end groups) required to stabilize the precipitating particles, thus lowering the instances of termination between these species. The addition of MA monomer during the 1st stage (at an equivalent of 3 MA units per chain), greatly improved the initiator efficiencies of the resulting latexes (E4 and E5), while creating highly living polymers as demonstrated by the growth of the full MWD over the course of the reaction (Figure 7.2 and Appendix E) and narrow, monomodal PSDs (Figure 7.1b). A similar phenomenon of increased initiator efficiency is demonstrated when surfactant is present but in concentrations below the CMC and in the absence of MA (E8). The surfactant lowers the interfacial tension of the particles formed by aggregative nucleation and with fewer oligomers present per particle and an increased initiator efficiency is observed.

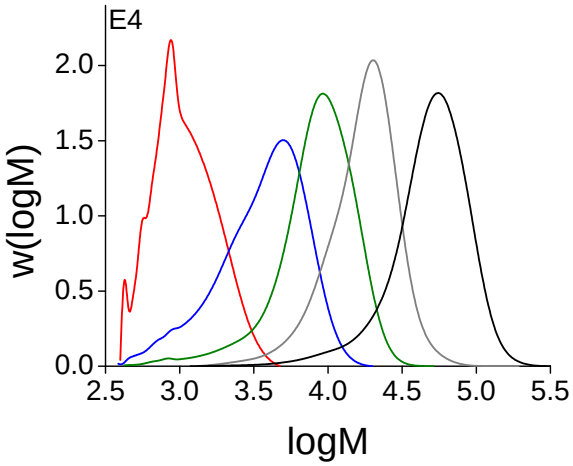

Figure 7.2: Molecular weight distributions for the two stage, surfactant-free emulsion polymerization of BMA with 10 mol% styrene (E4). Samples shown for 1st stage (20 minutes) (-), 2.3 hours (-), 4.4 hours (-), 6.5 hours (-) and 23.1 hours (-). The MWD curves are normalized for area.

E4 shows a linear trend of $\ln(1 \cdot (1\text{-conversion})^{-1})$ vs. time (Figure 7.3a) for the latter part of the polymerization, indicating that there is little loss of chains in the system. However, the first two samples, after the 1st stage and one hour after the monomer feed

commenced, indicate that there were fewer radicals present in the system at the start of the polymerization; this is the opposite of the tends previously observed by Nicolas et al.[11] for an MMA-co-St system. They observed that there is was higher concentration of propagating radicals very early on in the reaction and the system only reached a linear trend of ln(1·(1-conversion)$^{-1}$) vs. time later when the MMA-St-SG1 termination sequence was established. Those polymerizations were conducted in batch with 4.4–8.8 mol% St concentrations. The system presented here is quite different, as there is 30 mol% St in the 1st stage but only 10 mol% St in the feed. The additional styrene in the 1st stage inhibits the polymerization through the formation of St-St-SG1 chains ends which are slower to reactivate; therefore, this system is expected to have a lower concentration of propagating chains present in the system during the feed stage and for the first hour or so of the polymerization until the excess St added is consumed and the regular formation of MMA-St-SG1 end groups commences. Further evidence of the living nature of this system is exemplified through the full shifting of the MWD (Figure 6.2), a linear relationship between ln(1·(1-conversion)$^{-1}$) vs. time (Figure 7.3a) and a continually increasing M_n over the course of the polymerization (Figure 7.3b).

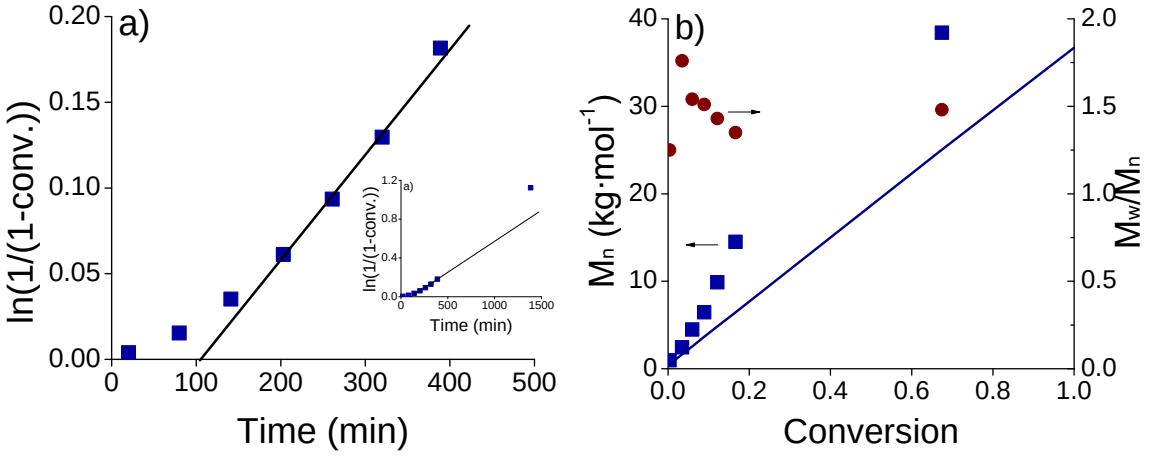

Figure 7.3: Kinetic plots for the surfactant-free, two stage emulsion polymerization of BMA with 10 mol% styrene (E4). The system was only semi batch for the 1st hour of the polymerization. (a) The ln(1·(1-conversion)$^{-1}$) vs. time plot for samples taken during the first 7.5 hours with an inlay of the same plot including all the samples up to 22 hours. (b) The number average molar mass (M_n) and polydispersity (M_w/M_n) vs. conversion plot (the full line represents the theoretical M_n).

Addition of SG1 and Reducing Agents

The initiation efficiency was increased with addition of 10% excess SG1 (with respect to BlocBuilder MA®) in the nucleation stage, which should shift the equilibrium to favor dormant chains. When SG1 was added alone (E6), the polymerization was much slower and exhibited an induction period at the start of the polymerization; however the initiation efficiencies showed a dramatic improvement, up to 85% from 54% without SG1 (E6 and E3 respectively). It appears that many of the oligomers were reversibly terminated either prior to or during nucleation, protecting them from being irreversible terminated upon aggregative nucleation with other oligomers. However, the extra SG1 appears to have had a detrimental effect on the PSD, resulting in a very broad and possibly bimodal PSD throughout the polymerization. One possible explanation for this is that the presence of the excess SG1, along with 30% St in the 1st stage, produced water soluble oligomers that were capped with SG1 prior to reaching the j_{crit} value and precipitating. In environments high in free SG1, the dormant state is favored; therefore, these water soluble oligomers may have remained dormant for an extended period of time, continuing past the time when the monomer feed was started. These water soluble oligomers, with an ionized COO^- group, could act as amphiphilic chains and stabilize monomer droplets or form micelles which are nucleated later, leading to a bimodal PSD. However, further characterization is required to fully understand this phenomenon.

Experiments with 20% excess SG1 in the 1st stage and subsequent addition of the reducing agent SFS (also 20% with respect to the initial concentration of BlocBuilder MA®) prior to the monomer feed were conducted (E7). SFS is a reducing agent which scavenges free SG1 and can restore the activation/deactivation equilibrium towards the active form. While these systems were living, as demonstrated by the growth of the entire MWD (please see the Appendix E for the full MWDs of all the experiments discussed here), they did not show any improvement in the initiator efficiency compared to the case with no SG1 (E4), and the MWD was more polydisperse. While the PSD was monomodal, the size of the particles was very large (∼500 nm). Interestingly, the experiment with excess SG1 but no SFS addition (E6) had two particle size domains: a large diameter domain (500-600 nm) which matches the particle size obtained in the experiment with addition of SG1 and SFS (E7), and a smaller domain (∼200 nm) which matches closely the particle sizes

obtained in the experiments without excess SG1 (E4). The very large particle size domain created in the experiments where SG1 is present may be due to the superswelling effect, where the oligomers (which are shorter and present for a longer time when excess SG1 is present) may be shifting the chemical potential so that the earliest nucleated particles become superswollen with monomer with respect to the later formed particles. A discussion of this has been presented for an *ab-initio* RAFT system.[22] The colloidal stability and particle size is known to be very sensitive to ionic strength in NMP emulsion; however the concentration of SFS added to the system is extremely small and these effects can likely be discounted. The 1st stage of the E6 was monomodal, which suggests that the bimodality of the PSD occurred during the monomer feed. It is possible that water soluble oligomers may have still been present which could have formed micelle-like species to encourage a secondary micellar nucleation. These micelle-like species would have disappeared following the addition of SFS in experiment E7.

7.4 Conclusion

SG1 mediated emulsion polymerization of n-BMA with 10 mol% styrene, both in the presence and absence of surfactant, yielded well-controlled polymerizations with highly living polymer chains. In the presence of surfactant above the CMC, bimodal particle size distributions are observed, which can be attributed to the presence of two different nucleation mechanisms: micellar and aggregative nucleation. SG1 mediated polymerization of MMA-co-St in the presence of surfactant above the CMC, however, results in monomodal PSDs. Surfactant-free emulsion polymerization of BMA-co-St gives monomodal particle size distributions, but suffers from poor initiator efficiencies and slow rates of polymerization as irreversible termination occurs during nucleation. The initiator efficiency can be greatly improved by the addition of a very small amount of the hydrophilic monomer methyl acrylate in the 1st stage, or alternatively when surfactant is added in concentrations below the CMC in the absence of MA. We propose that the increase in initiator efficiency is the result of lower interfacial tension in presence of both MA and surfactant below the CMC. The addition of excess SG1 greatly increases the initiation efficiency, but at the cost of slower polymerization and very broad PSDs. The addition of the reducing agent SDS to consume the excess SG1 does not impart greater control than simply through the addition of the MA

during the 1st stage. This study represents the first instance of well controlled nitroxide mediated polymerization of n-butyl methacrylate with a small proportion of styrene in a simple, one-pot surfactant-free emulsion polymerization system. The elimination of surfactant from the system not only allows for better control over the particle size distribution but it is also an important advance for further applications, where the presence of a large quantity of surfactant can be deleterious to both product properties and performance.

Acknowledgments

We wish to thank Arkema for providing financial support, materials and fruitful discussions and the Natural Sciences and Engineering Research Council of Canada (NSERC) for financial support.

References

[1] Cunningham, M. F. *Progress in Polymer Science* **33**(4), 365–398 (2008).

[2] Zetterlund, P. B., Kagawa, Y., and Okubo, M. *Chemical Reviews* **108**(9), 3747–3794 (2008).

[3] Bon, S. A. F., Bosveld, M., Klumperman, B., and German, A. L. *Macromolecules* **30**(2), 324–326 (1997).

[4] Marestin, C., Noel, C., Guyot, A., and Claverie, J. *Macromolecules* **31**(12), 4041–4044 (1998).

[5] Nicolas, J., Charleux, B., and Magnet, S. *Journal of Polymer Science Part A: Polymer Chemistry* **44**(13), 4142–4153 (2006).

[6] Nicolas, J., Charleux, B., Guerret, O., and Magnet, S. *Angewandte Chemie International Edition* **43**(45), 6186–6189 (2004).

[7] Charleux, B. and Nicolas, J. *Polymer* **48**(20), 5813–5833 (2007).

[8] Mchale, R., Aldabbagh, F., and Zetterlund, P. B. *Journal of Polymer Science Part A: Polymer Chemistry* **45**(11), 2194–2203 (2007).

[9] Dire, C., Belleney, J., Nicolas, J., Bertin, D., Magnet, S., and Charleux, B. *Journal of Polymer Science Part A: Polymer Chemistry* **46**(18), 6333–6345 (2008).

[10] Charleux, B., Nicolas, J., and Guerret, O. *Macromolecules* **38**(13), 5485–5492 (2005).

[11] Nicolas, J., Dire, C., Mueller, L., Belleney, J., Charleux, B., Marque, S. R. A., Bertin, D., Magnet, S., and Couvreur, L. *Macromolecules* **39**(24), 8274–8282 (2006).

[12] Lessard, B. and Maric, M. *Journal of Polymer Science Part A: Polymer Chemistry* **47**(10), 2574–2588 (2009).

[13] Nicolas, J., Charleux, B., Guerret, O., and Magnet, S. *Macromolecules* **38**(24), 9963–9973 (2005).

[14] Dire, C., Magnet, S., Couvreur, L., and Charleux, B. *Macromolecules* **42**(1), 95–103 (2009).

[15] Beuermann, S., Buback, M., Davis, T. P., Gilbert, R. G., Hutchinson, R. A., Kajiwara, A., Klumperman, B., and Russell, G. T. *Macromolecular Chemistry and Physics* **201**(12), 1355–1364 (2000).

[16] Hutchinson, R. A., McMinn, J. H., Paquet, D. A., Beuermann, S., and Jackson, C. *Industrial and Engineering Chemistry Research* **36**(4), 1103–1113 (1997).

[17] Nicolas, J., Mueller, L., Dire, C., Matyjaszewski, K., and Charleux, B. *Macromolecules* **42**(13), 4470–4478 (2009).

[18] Gilbert, R. G. *Emulsion Polymerization - a Mechanistic Approach.* Academic Press, San Diego, CA, (1995).

[19] Maxwell, I. A., Morrison, B. R., Napper, D. H., and Gilbert, R. G. *Macromolecules* **24**(7), 1629–1640 (1991).

[20] Fitch, R. M. and Tsai, C. H. *Polym. Colloids, Proc. Symp.* , 103–116 1970 (1971).

[21] Nicolas, J., Charleux, B., Guerret, O., and Magnet, S. *Macromolecules* **37**(12), 4453–4463 (2004).

[22] Luo, Y. and Cui, X. *Journal of Polymer Science Part A: Polymer Chemistry* **44**(9), 2837–2847 (2006).

Chapter 8

Conclusions and Recommendations

8.1 Conclusions

Changing the reaction medium of controlled radical polymerization from the more traditional bulk or solution systems to the more industrially preferable aqueous dispersed phase presents very interesting challenges as the main locus of polymerization is now inside nanometer scale particles. Two of the most poorly understood phenomena of this were investigated here, both experimentally and theoretically: compartmentalization of the mediating species and radicals inside the particles, and the nucleation process that creates these particles. Because many of the principles of CRP in the dispersed phase can be relevant to different types of controlled chemistries, where a mediating species is used to control the chain growth, investigations into atom transfer radical polymerization (ATRP), catalytic chain transfer (CCT) and nitroxide mediated polymerization (NMP) were undertaken. From this research, the main conclusions are as follows.

Compartmentalization effects were investigated through mathematic simulations for ATRP and CCT. The effects of compartmentalization on the individual reactions occurring inside the particles by discrete numbers of mediating agents are similar for the two chemistries: 1) increases in the rate of combination of the radicals and mediating agents as they are compartmentalized into smaller and smaller particles and 2) the creation of vastly different polymer products than would be predicted using the global concentration of mediating agents, as is done for bulk systems.

In aqueous dispersed phase ATRP polymerizations, compartmentalization effects can influence the rate of polymerization, the control of the PDI and the livingness of the polymer

formed. Segregation of the deactivating species, $CuBr_2$, into the particles is the result of using the highly hydrophobic ligand EHA_6TREN, which minimizes transfer to the aqueous phase. For the highly active catalyst system $CuBr/EHA_6TREN$, it was found that for small particle sizes, both the rate of polymerization and the number of units added per activation decreased proportionally to the volume of the particles. It was also found that there exists a window of particle sizes where the rate of polymerization is higher than that of an equivalent bulk system but where the PDI and the degree of termination remain below that of bulk, indicating an optimal region of particle sizes in which to operate. Whereas in bulk ATRP systems, the rate of polymerization is directly controlled by an equilibrium ratio of Cu(I)/Cu(II), this is not true for the compartmentalized system, where the rate is instead controlled by enhanced deactivation and also the relative concentrations of Cu(I) and Cu(II), which are dependent on the size of the particles. In addressing the industrial relevance of ATRP, decreasing the concentration of transition metal catalyst required is very important; however, as this study shows, this may not be easily done in the dispersed phase. Lower catalyst concentrations lead to slower rates of polymerization as well as higher PDIs. However, polymerizations conducted under these conditions do possess a greater livingness.

In CCT seeded emulsion systems, compartmentalization of the mediating agents between the particles results in multimodal MWDs (molecular weight distributions), and the cause of this compartmentalization is the increased diffusional resistance to transfer of the catalytic chain transfer agent (CCTA) between the particles, which is a function of viscosity. This work resulted in the first simulations which demonstrate the effect of segregation of both the propagating radical and a mediating species on the chain length distribution for any CRP emulsion system. The multimodal MWD observed experimentally in seeded CCT emulsion polymerization can be reproduced by our simulations and confirm that the diffusional resistance against CCTA transfer between particles limits the ability of the CCTA to effectively mediate numerous polymer particles. In instances of fast CCTA diffusion, for example in a miniemulsion system, the expected degree of polymerization can be predicted by the Mayo equation using the average concentration of CCTA per particle in the system. However, when the diffusional resistances are significant, for example in a seeded emulsion polymerization system, the individual contributions to the CLD can be attributed to the compartmentalization of CCTA in the particles, whereby the peaks at different degrees of

polymerization are due to polymerization in the presence of zero or more CCTA molecules inside each particle over the course of the polymerization.

A dependence of the particle size on the concentration of initiator (or target molecular weight) has been observed in a wide variety of *ab-initio* CRP emulsion and two stage emulsion systems. To make the production of these specialty polymers economically viable at the industrial scale, high solids content formulations are necessary and control over the particle size is important to create colloidally stable latexes at these conditions. Although we have studied particle nucleation only in nitroxide mediated emulsion polymerization, many of the conclusions and systems could be applicable to other similar chemistries – most especially for *ab-initio* RAFT (Reversible Addition Fragmentation Transfer) emulsion polymerization, where commercially available, water soluble RAFT agent initiators are available.

To this end, we studied how the characteristics of the 1st stage latex will influence the colloidal stability of high solids latexes targeting a variety of molecular weights in SG1 mediated NMP. Minimizing the size of the 1st stage latex particles appears to be the best way to maintain colloidal stability at high solids; however these 1st stage latex particles are very sensitive to changes in ionic strength, buffering, the type of base used to ionize the Di-BlocBuilder and the concentration of initiator. We have found that using Na_2CO_3 in excess, rather than NaOH, to ionize the DiBB results in smaller 1st stage latex particle sizes while also providing sufficient buffering capability to maintain the DiBB surface charges. The drastic changes in the 1st stage latex particle size with changes in initiator concentration are the result of superswelling during nucleation, where large concentrations of short oligomers enhance the diffusion of monomer to the particles. We have demonstrated that colloidally stable latexes can be created at 45 wt.% solids for n-BA mediated by Di-BlocBuilder with final molecular weight targets >70 kg·mol^{-1}. There is a very clear trend of increasing particle size with increasing initiator concentration, making the creation of low target M_n difficult. All of the high solids polymerizations were controlled, but the breadth of the MWD increased with increasing conversion.

The connection between particle size and target molecular weight can also be used in a positive manner to create well-controlled, SG1-mediated, MMA-co-St microemulsion latexes. These microemulsons have small, monomodal particle size distributions, low sur-

factant to monomer ratios, fast reaction rates and solids content up to 40 wt.% and high molecular weights. Narrower molecular weight distributions were obtained when 30 mol% St was used in the 1st stage compared to 8 mol% because reactivation of the dormant chains following nucleation was minimized. Leaving the 1st stage latex for periods longer than 1 hour resulted in irreversible termination and the accumulation of SG1, which slowed further polymerization. 1st stage latexes with more styrene present were more robust, experiencing lower amounts of termination and narrower molecular weight distributions when left for long periods of time prior to feeding the rest of the monomer. These MMA-co-St microemulsions can easily be chain extended with BMA-co-St in one step, but the presence of BMA-co-St in the seed stage leads to bimodal particle size distributions when (BMA-co-St)-block-(MMA-co-St) polymers are made.

To understand the influence of monomer choice on the nucleation process, an n-BMA emulsion system was explored further. SG1 mediated polymerization of MMA-co-St, in the presence of surfactant above the CMC, results in monomodal PSDs; however when the more hydrophobic monomer n-BMA is used, bimodal particle size distributions are observed. The bimodality is the result of two different nucleation mechanisms: micellar and aggregative nucleation. Eliminating micellar nucleation by conducting surfactant-free emulsion polymerization of BMA-co-St gives monomodal particle size distributions, but suffers from poor initiator efficiencies and slow rates of polymerization as irreversible termination occurs during nucleation. The initiator efficiency was improved by the addition of a very small amount of the hydrophilic monomer methyl acrylate in the 1st stage to lower the interfacial tension of the system during aggregative nucleation. The elimination of surfactant from the system not only allows for better control over the particle size distribution but it is also an important advance for further applications, where the presence of a large quantity of surfactant can be detrimental to both product properties and performance.

8.2 Recommendations for Future Work

Because of the interdisciplinary nature of the work done in this thesis, it is very easy to suggest investigations of different factors across a wide range of controlled radical chemistries and monomer types. In particular, we would like to make the following recommendations for future work based on research conducted in this thesis.

In Chapter 4 we demonstrated modeling of the full molecular weight distribution of CCT, but application of similar techniques to other CRP systems, most specifically those which undergo reversible termination (e.g. ATRP and NMP) or regenerative transfer (e.g. RAFT) would be particularly powerful. Unfortunately, simulations can only be conducted in regimes where "memory" effect on the dormant polymer chain population will not be a problem. In highly compartmentalized systems, the population of dormant polymer chains will be different within particles containing different concentrations of mediating agents. Unfortunately, the population balance approach assumes that the MWD of all the polymer populations are similar throughout all the particles. As a result, the effects of mediating agent compartmentalization cannot be accurately seen in the MWD with the current population balance approach. However, modeling by monte carlo simulations can avoid this problem.

More simplistic modeling, like that used by the method of moments to estimate the rate, livingness and PDI for ATRP systems (Chapter 3) is an excellent way of capturing these compartmentalization effects for a wide variety of controlled chemistries. However, in truly low catalyst concentration ATRP systems, it would be interesting to see if compartmentalization effects also manifest themselves on the activating agent, CuBr, in addition to the deactivation agent, $CuBr_2$. All simulations to date assume that CuBr is present in such high concentrations that it need not be considered as a compartmentalization species; however, this assumption will become invalid as lower catalyst concentration systems, with extremely high activity ligands, are sought.

The challenges of nucleation in NMP dispersed phase systems are not yet solved, and while the impact of the coupling of particle size with initiator concentration can be minimized (Chapter 5), it is not yet fully eliminated. Experimenting with mixed *ab-initio* nucleation in the presence of pre-fabricated amphiphilic, surfactant-like initiators may off set this coupling tendency, as increasing the initiator concentration in *ab-initio* systems increases the particle size whereas increases in the concentration of amphiphilic initiators tends to decrease it. This, or the use of a dead polymer seed latex, could be the solution to achieving high solids, low target molecular weight latexes by NMP.

Novel, core-shell, block copolymer particles could be created beginning with either the microemulsion (Chapter 6) or the surfactant-free (Chapter 7) formulations presented in

this work. In particular, inverse core-shell, block copolymer particles (where the more hydrophobic monomer resides at the polymer-water interface of the particles) could be created by anchoring the more hydrophobic polymer to the surface through the COO^- groups present on BlocBuilder MA® initiator groups.

Appendix A

Compartmentalization in Dispersed Phase ATRP

A.1 Equation Derivation

The rate of change of the singly distinguished particle distribution, $dS_{i,j,k}/dt$, can be checked against the modified Smith Ewart equations, $dN_{i,j}/dt$, by

$$\sum_{k} \frac{dS_{i,j,k}}{dt} = (i)\frac{dN_{i,j}}{dt} \tag{A.1}$$

A.2 Implementation of the Computer Simulation

The model was implemented in fortran, using the OED solver DLSODI, as a fully integrated set of differential equations using a backwards Euler method. The maximum number of radicals (i) and maximum number of Cu(II) molecules (j) are flexible, provided the simulations are recompiled before using. Other input parameters (including the rate constants of the polymerization reactions and the particle size) are stored in a separate input file and can be modified without recompiling the executable file.

At each time step (1 second), all of the ODEs are integrated. The integration loop is setup such that the following equations are solved simultaneously.

$$N_{0,0} = 1 - \sum_{i=1}^{I_{max}} \sum_{j=0}^{J_{max}} N_{i,j} - \sum_{j=1}^{J_{max}} N_{0,j} \tag{A.2}$$

$$\sum_{i=i}^{I_{max}} \sum_{j=0}^{J_{max}} \frac{dN_{i,j}}{dt} \tag{A.3}$$

$$\sum_{j=1}^{J_{max}} \frac{dN_{0,j}}{dt} \tag{A.4}$$

$$\sum_{i=0}^{I_{max}} \sum_{j=0}^{J_{max}} \frac{d\lambda_{i,j}^{(1)}}{dt} \tag{A.5}$$

$$\sum_{i=0}^{I_{max}} \sum_{j=0}^{J_{max}} \frac{d\lambda_{i,j}^{(2)}}{dt} \tag{A.6}$$

$$\frac{d\mu^{(0)}}{dt} \tag{A.7}$$

$$\frac{d\mu^{(1)}}{dt} \tag{A.8}$$

$$\frac{d\mu^{(2)}}{dt} \tag{A.9}$$

$$\frac{d\xi^{(0)}}{dt} \tag{A.10}$$

$$\frac{d[M]}{dt} \tag{A.11}$$

$$\frac{d[Cu(I)]}{dt} \tag{A.12}$$

$N_{0,0}$ is the only equation which is not integrated and is calculated as the remainder of the other Smith-Ewart Equations to maintain a closed set of equations and minimize drift occurring from truncation errors. Before this was made the permanent modification to the model, the equations were all tested by keeping an integrated form of $dN_{0,0}/dt$ and the output was checked to ensure that $\sum_{i=0}^{I_{max}} \sum_{j=0}^{J_{max}} N_{i,j} = 1$.

After equations A.2 - A.12 were solved simultaneously, $\bar{n}$, $\bar{n}_{chain}$, $\bar{n}_{Cu(II)}$, $\bar{n}_{Cu(II)chain}$,

PDI, etc were calculated at the end of each time step and the results written to an output file.

At each time step, many checks are made to ensure that the boundary conditions of the model are not being approached and that the equations are closed. These include

$$[Cu(I)]_0 = [Cu(I)] + [Cu(II)] = [Cu(I)] + \frac{\bar{n}_{Cu(II)}}{N_A V_p} \tag{A.13}$$

$$\mu_0^{(0)} = \frac{\bar{n}}{N_A V_p} + \mu^{(0)} + 2\xi^{(0)} \tag{A.14}$$

If one or both of these balances do not hold from the beginning of the simulations, it is likely that the equations are not closed and there is a problem with the code. If these balances hold for the first portion of the simulation but begin to drift at larger time steps, it is likely that one or both of the boundary conditions (maximum number of radicals, equation A.14, or Cu(II) molecules equation A.13, per particle) are being approached. This can happen when the initial concentration of chains, $\mu_0^{(0)}$, is too high or the particle size is too large. It is the accumulation of Cu(II) in such particles that limits the conversion to which the simulations can be run.

Appendix B

Compartmentalization in Catalytic Chain Transfer

B.1 Kinetic Scheme for Free Radical Polymerization

Fundamental steps occurring within the polymer particles include propagation, bimolecular termination by disproportionation, which is the dominant termination mechanism for MMA polymerization,[1] and chain transfer to monomer. These reactions are summarized below, along with their corresponding reaction frequencies, expressed in s^{-1}.

Propagation

$$R^{\bullet}_{short} + M \xrightarrow{k_p} R^{\bullet}_1 \qquad f_p = k_p M \tag{B.1}$$

$$R^{\bullet}_j + M \xrightarrow{k_p} R^{\bullet}_{j+1} \qquad f_p = k_p M \tag{B.2}$$

Termination

$$R^{\bullet}_{short} + R^{\bullet}_{short} \xrightarrow{k_t} P_{short} \qquad f_t = k_t / 2 N_A V_p \tag{B.3}$$

$$R^{\bullet}_{short} + R^{\bullet}_{j} \xrightarrow{k_t} P_j \qquad f_t = k_t/2N_AV_p \tag{B.4}$$

$$R^{\bullet}_{j} + R^{\bullet}_{k} \xrightarrow{k_t} P_j + P^{=}_{k} \qquad f_t = k_t/2N_AV_p \tag{B.5}$$

Transfer to monomer

$$R^{\bullet}_{j} + M \xrightarrow{k_{fm}} P_j + R^{\bullet}_{short} \qquad f_{fm} = k_{fm}M \tag{B.6}$$

B.2 Generalized Form of the Distinguished Particle Distributions

$$\begin{aligned}\frac{dS_{0,1,j,c}}{dt} =& -[\rho + f_p + f_{cin} + (c)f_{cdes} + f_{fm} + (c)f_{trans}]S_{0,1,j,c} \\ &+ f_pS_{0,1,j-1,c} + f_{cin}S_{0,1,j,c-1} + (c+1)f_{cout}S_{0,1,j,c+1} + \frac{1}{2}\rho S_{0,2,j,c} \\ &+ \left[f_{des} + \frac{1}{2}\rho\right] S_{1,2,j,c} + \sum_{j=1}^{\sigma} f_pN_{1,1,c}\end{aligned} \tag{B.7}$$

$$\begin{aligned}\frac{dS_{0,2,j,c}}{dt} =& -[\rho + f_p + f_{cin} + (c)f_{cout} + 2f_{fm} + 2(c)f_{trans} + 2f_t]S_{0,2,j,c} \\ &+ f_pS_{0,2,j-1,c} + f_{cin}S_{0,2,j,c-1} + (c+1)f_{cout}S_{0,2,j,c+1} \\ &+ f_pS_{1,2,j,c} + \sum_{j=1}^{\sigma} f_pN_{1,2,c}\end{aligned} \tag{B.8}$$

$$\begin{aligned}\frac{dS_{1,2,j,c}}{dt} = &- [\rho + f_{des} + f_p + f_{cin} + (c)f_{cout} + f_p + f_{fm} + (c)f_{trans} + 2f_t]S_{s,i,j,c} \\ &+ \rho S_{0,1,j,c} + [f_{fm} + (c)f_{trans}]S_{0,2,j,c} + f_p S_{1,2,j-1,c} + f_{cin} S_{1,2,j,c-1} \\ &+ (c+1)f_{c,out} S_{1,2,j,c+1} + \underset{j=1}{\sigma} 2f_p N_{2,2,c}\end{aligned} \tag{B.9}$$

$$\frac{dP_j}{dt} = \frac{1}{N_A V_p}\left[\begin{array}{l}(f_{fm} + (c)f_{trans})\,(S_{0,1,j,c} + S_{0,2,j,c} + S_{1,2,j,c}) \\ +\frac{1}{2}\rho\,(S_{0,2,j,c} + S_{1,2,j,c}) + 2f_t S_{1,2,j,c} + 2f_t S_{0,2,j,c}\end{array}\right] \tag{B.10}$$

B.3 Derivation of f_{des}

Radical exit is a very important mechanism, especially when there is a significant amount of chain transfer. Monomeric radical exit is often considered to be a diffusion process where the radicals are considered to have the same characteristics as the monomer.[2] Often it is the diffusion of the monomeric radical away from the particle in the aqueous phase that is rate determining, but at very high conversions and internal viscosity, the diffusion of the radical through the particle is also limiting. Because these experiments are conducted at very high internal viscosity, diffusion will be considered limiting in both the particle and aqueous phase by[2]

$$f_{des} = \frac{3D_{part}D_{aq}}{\left(\frac{C_p}{C_W}D_{part} + D_{aq}\right)r^2} \tag{B.11}$$

where D_{part} diffusion coefficient of in the particle phase, D_{aq} is the diffusion coefficient in the aqueous phase, C_p is the concentration of monomer in the particle phase, C_w is the concentration of monomer in the aqueous phase and r is particle radius. The D_{part} ($4.58{\cdot}10^{-12}$ $m^2{\cdot}s^{-1}$) is estimated by the diffusion of monomer in the particle at a high conversion (p = 80%) by the correlation given by Gilbert[2] for MMA at 50^{o}C. The diffusion of monomeric radicals in the aqueous phase, D_{aq} ($1.9{\cdot}10^{-9}$ $m^2{\cdot}s^{-1}$),[3] is calculated by the

Wilke-Chang correlation for dilute systems.[4] All simulations were conducted with f_{des} = $1.35{\cdot}10^4$ s^{-1}, $8.48{\cdot}10^3$ s^{-1}, and $5.38{\cdot}10^3$ s^{-1} for the 65 nm, 82 nm and 103 nm particle respectively. We also show that the conclusions drawn from the CLD with respect to particle size cannot be attributed to difference in f_{des} alone. Figure B.1 shows that, all other conditions being equal, a higher f_{des} leads to a lower concentration of transfer-dominated chains (because of enhanced exit), but has no effect on the formation of two populations.

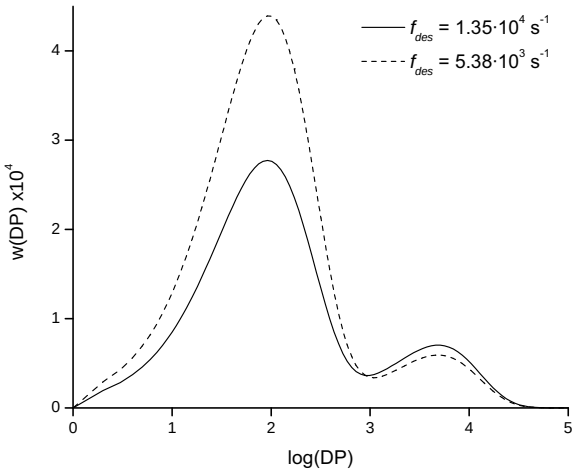

Figure B.1: w(DP) plot for the simulated CLD of 103 nm particles at 30% conversion, assuming k_{trans}^{app}= $1.5{\cdot}10^7$ L·mol^{-1}·s^{-1}, k_t= $2.0{\cdot}10^{12}$ L·mol^{-1}·s^{-1}, f_{cout} = 10^{-3} s^{-1} and $\bar{n}_{\mathrm{CCTA}}$ = 1.0. The frequency of radical entry into the particles remained at ρ = 1 s^{-1} for all simulations but the frequency of radical exit was varied.

B.4 Effect of k_t on the Chain Length Distribution

In the simulations for the seeded emulsion system, the instantaneous conversion is over 0.8, which can lead to diffusional resistances to the movement of the radical chains and lower the rate constant of termination[5] (k_t) below the value listed in Table 4.2. In addition, the rate constant of termination was increased far above any realistic value (to $2.0{\cdot}10^{12}$ L·mol^{-1}·s^{-1}) in the majority of the seeded simulations to mimic a zero-one system where termination occurs instantaneously upon the entry of a new radical into a particle already containing a propagating radical. These conditions were chosen because, as termination occurs primarily by termination by disproportionation, the creation of a small disproportionation product (at moderate to low k_ts) following a bimolecular termination in particles containing no

CCTA can obscure the true contribution to the CLD by transfer-derived polymer, which is the predominant product in particles containing a CCTA. We have run simulations at varying k_ts (Figures B.2–B.4) here to demonstrate that, although the assumption of a very high k_t may not have been physically correct, it is still appropriate as it does not change the conclusions presented in this work: that there are contributions to the CLD from bimolecular termination and catalyzed chain transfer. Lower values of k_t lead to a DP of the termination-dominated polymer population and can also lead to some broadening in the CLD of the transfer-dominated population if the disproportionation product and the transfer-derived product overlap.

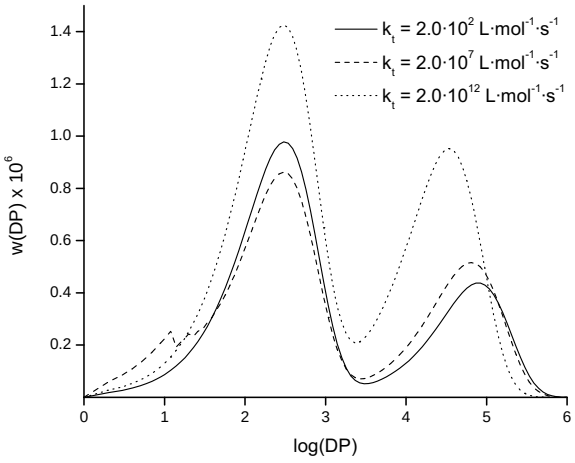

Figure B.2: w(DP) plot for the simulated CLD of 65 nm particles at 30% conversion, assuming k_{trans}^{app}= 1.5·10^6 L·mol^{-1}·s^{-1}, $\bar{n}_{\mathrm{CCTA}}$= 0.5, ρ = 0.1 s^{-1} and f_{cout} = 10^{-4} s^{-1}. The rate coefficient of termination was varied to simulate conditions with very different diffusional resistances.

The simulations at different k_t values show that two distinct polymer populations can be seen when k_t is 2.0·10^{12} L·mol^{-1}·s^{-1}. When k_t is 2.0·10^7 L·mol^{-1}·s^{-1}, a smaller, tertiary population of chains can be distinguished on the CLD: the disproportionation product from the bimolecular termination reactions. Thus, when k_t is 2.0·10^7 L·mol^{-1}·s^{-1}, this peak overlaps with the transfer-dominated peak both when k_{trans}^{app} is 1.5·10^7 L·mol^{-1}·s^{-1} and 1.5·10^6 L·mol^{-1}·s^{-1}. This illustrates the rationale behind using k_t = 2.0·10^{12} L·mol^{-1}·s^{-1} to mimic a zero-one system. Simulations were also conducted with k_t = 2.0·10^2 L·mol^{-1}·s^{-1} to simulate systems with severe diffusional resistance.[5] Again, two populations can be seen, and the disproportionation product (which is large) overlaps with the bimolecular-termination

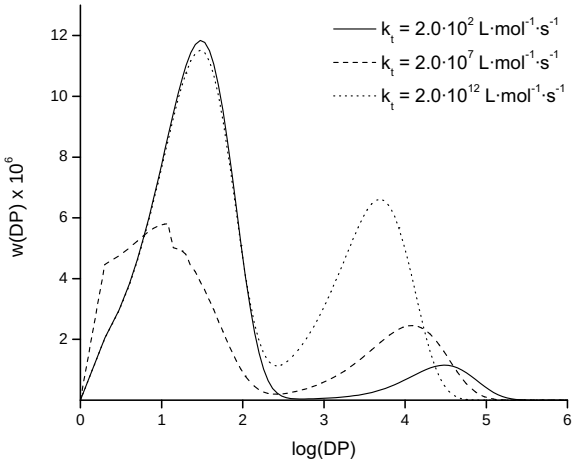

Figure B.3: w(DP) plot for the simulated CLD of 65 nm particles at 30% conversion, assuming k_{trans}^{app}= 1.5·10^7 L·mol^{-1}·s^{-1}, $\bar{n}_{\mathrm{CCTA}}$= 0.5, ρ = 1.0 s^{-1} and f_{cout} = 10^{-4} s^{-1}. The rate coefficient of termination was varied to simulate conditions with very different diffusional resistances.

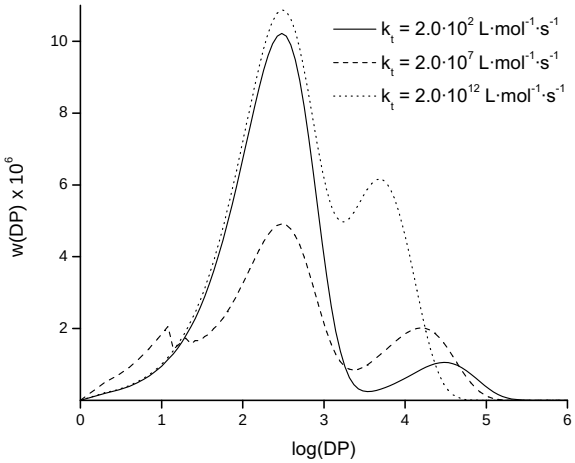

Figure B.4: w(DP) plot for the simulated CLD of 65 nm particles at 30% conversion, assuming k_{trans}^{app}= 1.5·10^6 L·mol^{-1}·s^{-1}, $\bar{n}_{\mathrm{CCTA}}$= 0.5, ρ = 1.0 s^{-1} and f_{cout} = 10^{-4} s^{-1}. The rate coefficient of termination was varied to simulate conditions with very different diffusional resistances.

population, which is broader.

B.5 Effect of k$_p$ on the Chain Length Distribution

Similarly to k$_t$, the values of k$_p$ also decrease when the viscosity inside the particles becomes high. However this effect is only observed for very high conversions (>75%),[6] as the propagation reaction occurs between a small molecule and a long chain (rather than two long chains as is the case for the termination reaction). Again, similar to the discussion for

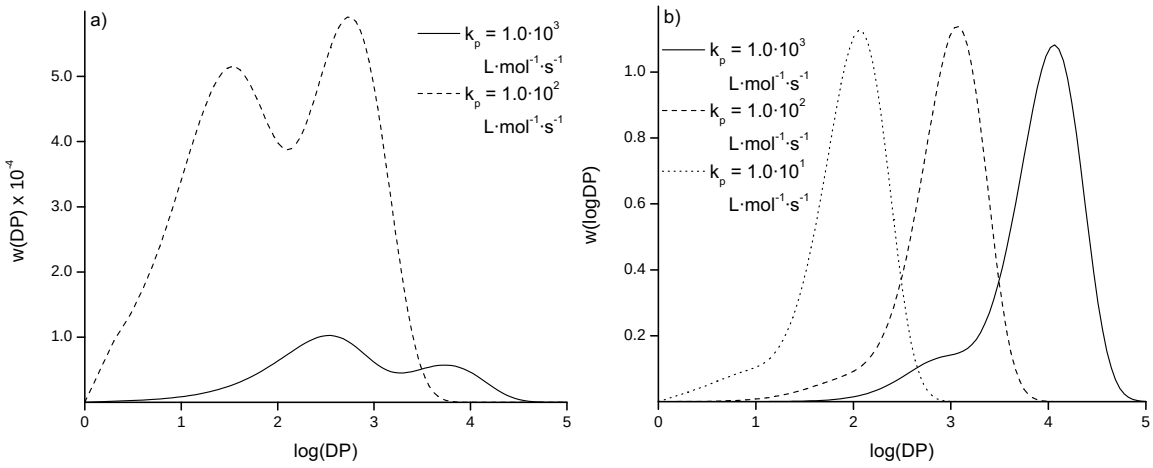

Figure B.5: (a) w(DP) and (b) w(logDP) plots for the simulated CLD of 65 nm particles at 10% conversion, assuming k_{trans}^{app}= 1.5·10^6 L·mol^{-1}·s^{-1}, $\bar{n}_{\mathrm{CCTA}}$= 0.5, ρ = 1.0 s^{-1}, k_t= 2.0·10^{12} L·mol^{-1}·s^{-1}, andf_{cout} = 10^{-3} s^{-1}. The rate coefficient of propagation was varied to simulate conditions with very different diffusional resistances.

k$_t$, while the chosen k$_p$ may not be physically correct (although estimating an appropriate k$_p$ is extremely challenging as it can change dramatically in this region), it does not change the main conclusions of the paper. Figure B.5 shows that two polymer populations can still be observed, although the DP of these is dependent upon the propagation rate coefficient.

References

[1] Odian, G. *Principles of Polymerization.* John Wiley & Sons, Inc, (2004).

[2] Gilbert, R. G. *Emulsion Polymerization - a Mechanistic Approach.* Academic Press, San Diego, CA, (1995).

[3] Kemmere, M., Cleven, M., van Schilt, M., and Keurentjes, J. *Chemical Engineering Science* **57**(18), 3929–3937 (2002).

[4] Hines, A. L. and Maddox, R. N. *Mass Transfer Fundamentals and Applications.* Prentice Hall, Upper Saddle River, New Jersey, (1985).

[5] Beuermann, S. and Buback, M. *Progress in Polymer Science* **27**(2), 191–254 (2002).

[6] Le, T. T. and Hill, D. J. *Polymer International* **52**(11), 1694–1700 (2003).

Appendix C

High Solids NMP Emulsion with Di-BlocBuilder

C.1 Titration Curves to Determine the pKa of BlocBuilder MA® and Di-BlocBuilder

The pKa of BlocBuilder MA® and Di-BlocBuilder was determined by titration of an 0.1M NaOH solution into a solution of BlocBuilder MA® (or Di-BlocBuilder) dissolved in a mixture of anhydrous ethanol and water. This is the same method used previously to determine the pKa of another di-alkoxyamine (DIAMA).[1] The pH probe was calibrated with aqueous standards (pH 4, 7 and 10) and the observed aqueous pH was corrected for the water/alchohol mixture by applying the method described in Bates.[2] The corrected pH ($\mathrm{p}a_H*$) is calculated by:

$$\mathrm{p}a_H^* = \mathrm{p}H - \alpha \tag{C.1}$$

When the ethanol content in the alcohol/water mixture is below 0.5, the term α varies in a nearly linear fashion with ethanol content (Figure C.1)

The acid dissociation constant (pKa) is the midpoint of a titration curve. The simplest way to determined this is that the midpoint is the maximum of a $d\mathrm{Vol}/d\mathrm{pH}$ versus pH plot. The base formulations for these titrations are listed in Table C.1 and the titration curves for BlocBuilder MA® and Di-BlocBuilder are shown in Figures C.2 and C.3 respectively.

Therefore, the pKas of BlocBuilder MA® and Di-BlocBuilder are estimated as 5.90 and 6.66 respectively.

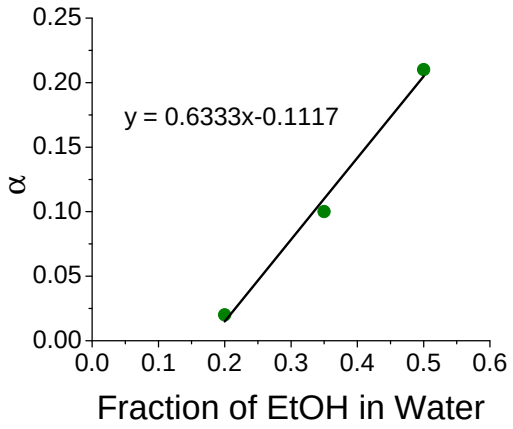

Figure C.1: Variation of α with ethanol content.

Table C.1: Formulations for the Titrations of BlocBuilder MA® and Di-BlocBuilder with NaOH in a Water/Ethanol Mixture

Exp.	**Alkoxyamine**	**Acidic End Groups** (mmol)	**Ethanol** (g)	**Water** (g)	**pKa**
A	BB	0.556	10.60	13.33	5.96
B	BB	1.21	19.32	21.84	6.00
C	BB	0.366	17.73	24.40	5.75
D	DiBB	1.13	20.26	25.13	6.59
E	DiBB	1.08	12.18	15.92	6.78
F	DiBB	0.457	8.72	10.12	6.69
G	DiBB	0.399	17.64	22.25	6.56

The titrations were done with a 0.106 M NaOH solution.

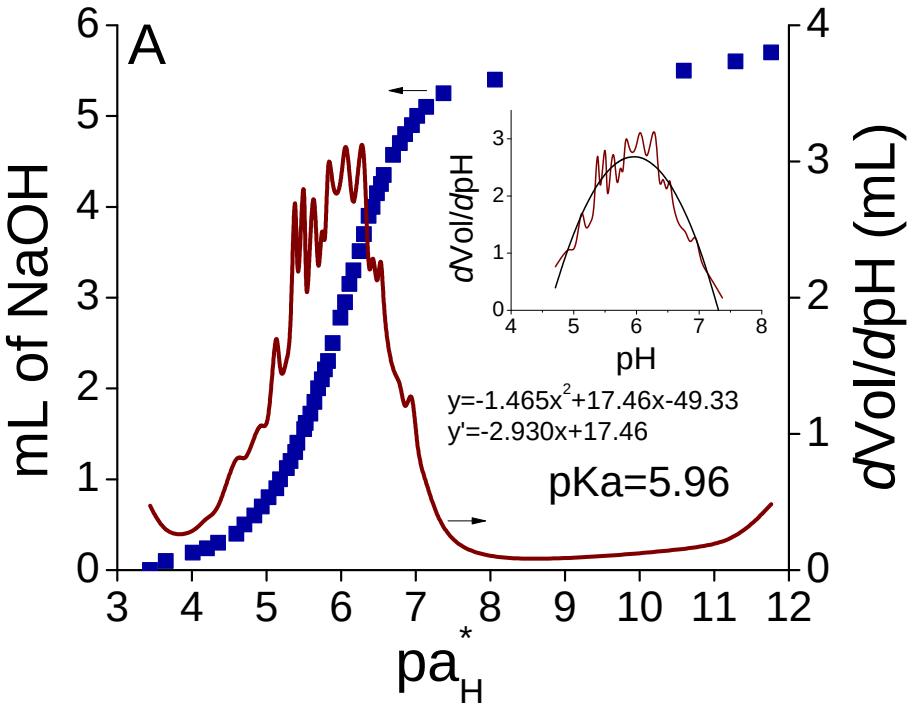

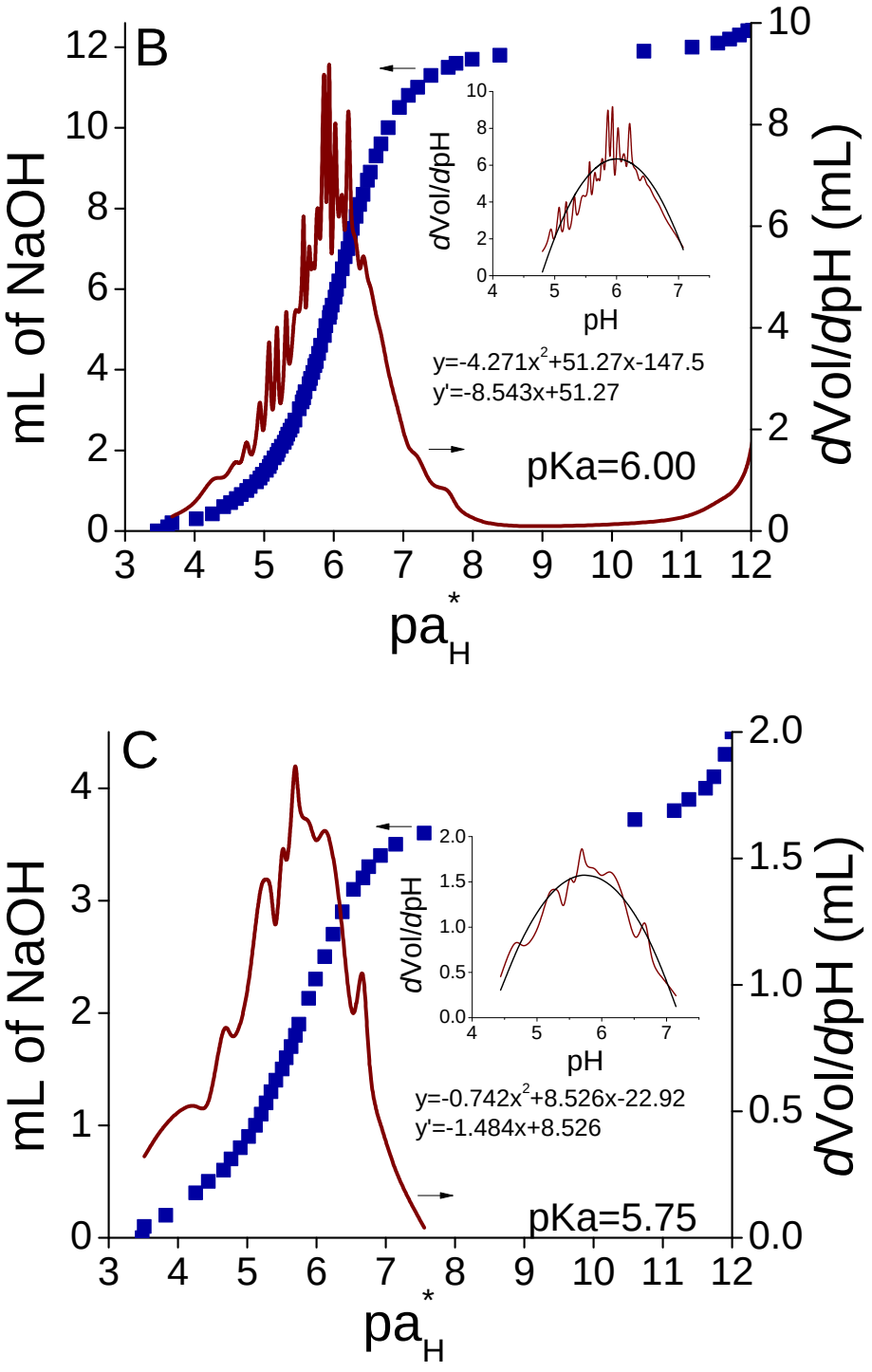

Figure C.2: Titration curves for BlocBuilder MA®

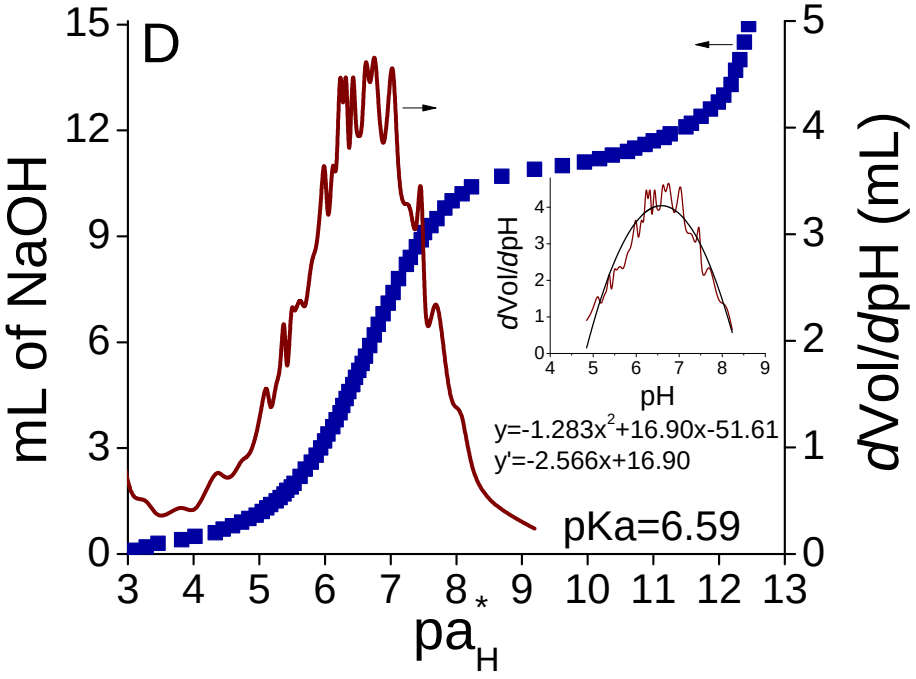
D
mL of NaOH
dVol/dpH (mL)
pa*H
dVol/dpH
pH
y=-1.283x²+16.90x-51.61
y'=-2.566x+16.90
pKa=6.59

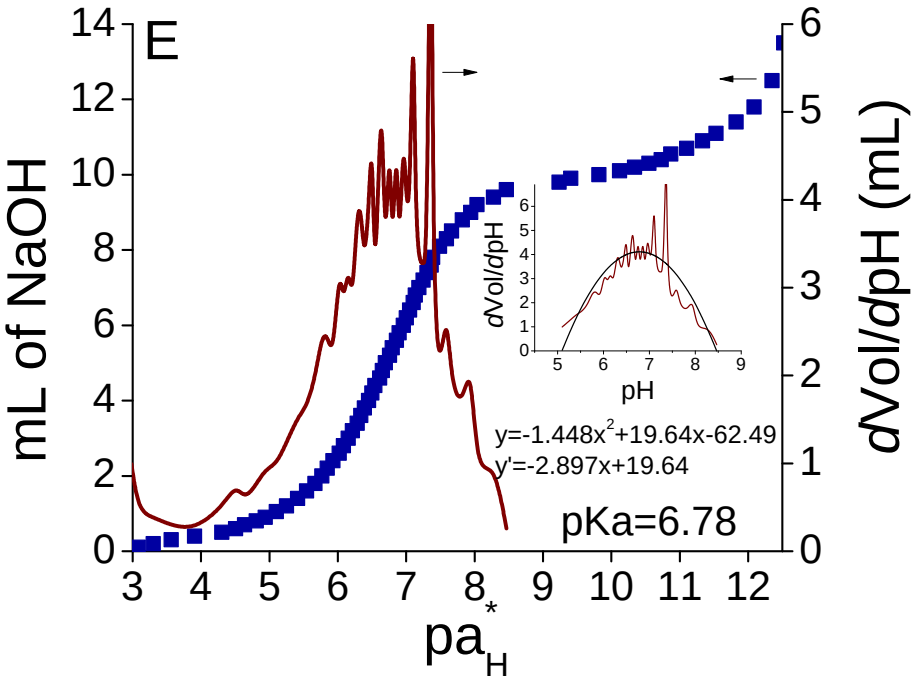
E
mL of NaOH
dVol/dpH (mL)
pa*H
dVol/dpH
pH
y=-1.448x²+19.64x-62.49
y'=-2.897x+19.64
pKa=6.78

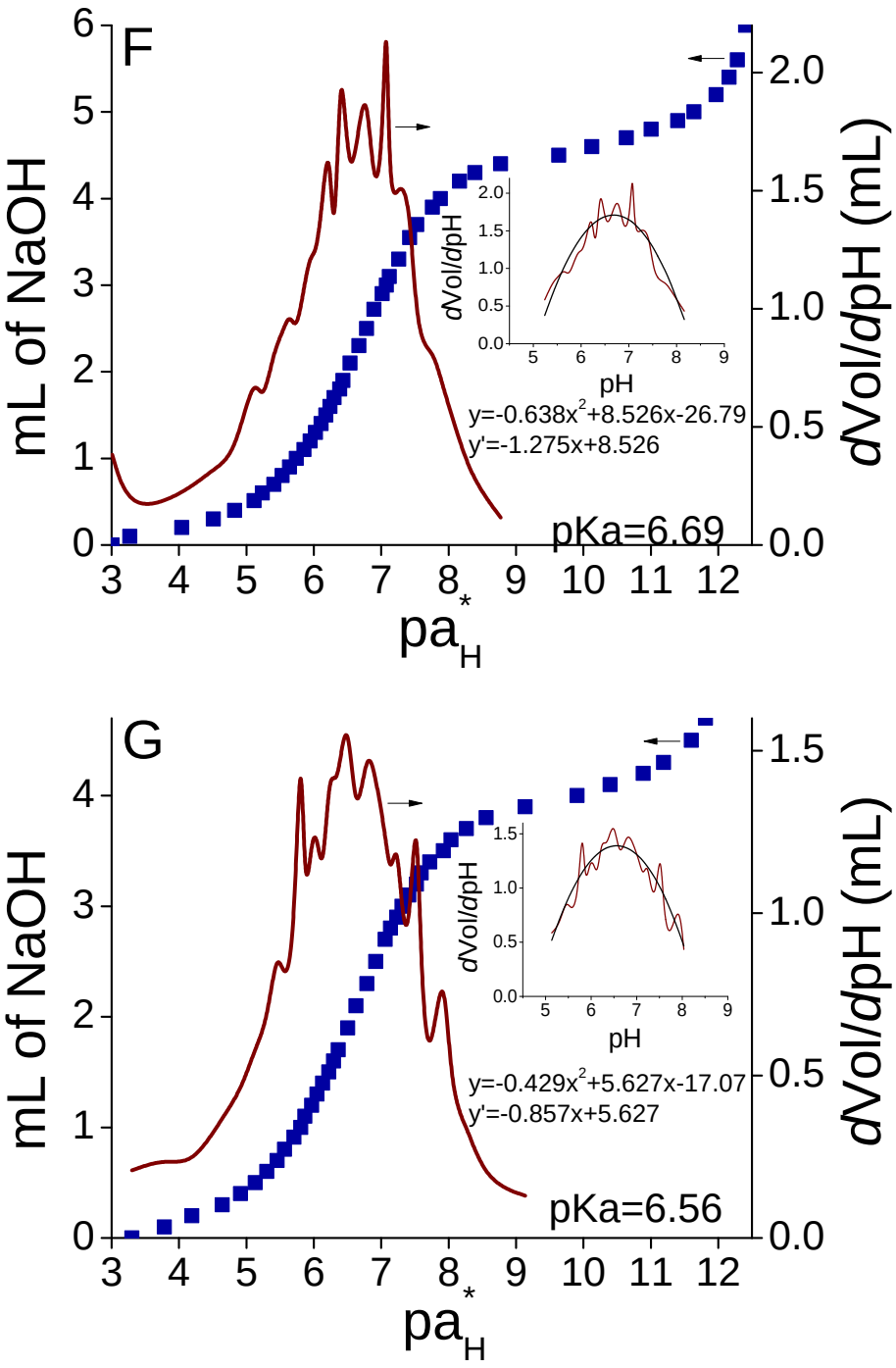

Figure C.3: Titration curves for Di-BlocBuilder

C.2 pKa of BlocBuilder MA® and Di-BlocBuilder

The experimental pKas for BlocBuilder MA® and Di-BlocBuilder are higher than the predicted pKas for the methacrylic acid groups (4.65 for a single unit and as high as 5.45 for oligomers of methacrylic acid[3]). Therefore, it is possible that BlocBuilder MA® and Di-BlocBuilder exist in a zwitterionic form in water, where the the acidic site on alkoxyamine is deprotonated. A potential ionization mechanism is shown in Figure C.4. The presence of this zwitterionic form can account for the higher pKas for both BlocBuilder MA® and Di-BlocBuilder compared to that estimated solely by the carboxylic form.

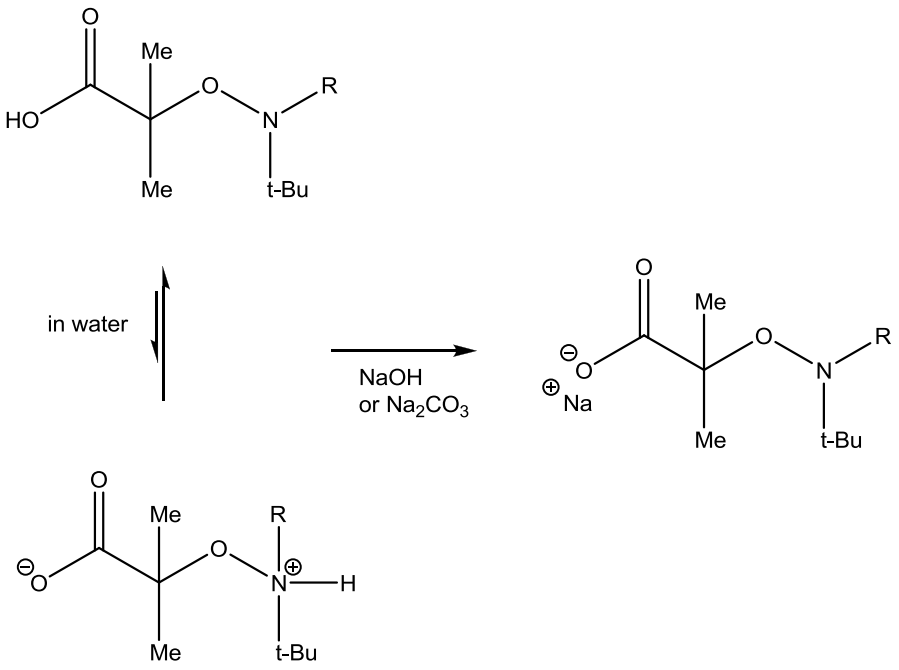

Figure C.4: Proposed zwitterionic form of BlocBuilder MA® in water and its ionization to its water soluble form with base.

C.3 pH drop in the system prior to nucleation

Throughout all of the nucleation experiments, a significant drop in pH over the entire reaction was observed. After nucleation, the drop in pH was always associated with an increase in the particle size and can be, in part, attributed to the burying of charged surface groups inside the particles. However, the drop in pH prior to nucleation (nucleation always

occurs around pH ∼7.5) is less understood. When the system was ionized with Na_2CO_3 or only a stoichiometric amount of NaOH, nucleation occurred within minutes of reaching 120^{O}C. However, when the initial pH was much higher (closer to pH 11 when excess NaOH is used) there was a significant induction period prior to nucleation (which again occurred at pH ∼7.5).

The most likely cause of this drop in pH prior to nucleation is the hydrolysis of butyl acrylate into the water soluble acrylic acid. At room temperature butyl acrylate is known to have a 243 minute (4.05 hour) half life at pH 11, a 1100 day half life at pH 7 and a 2800 day half life at pH 2.[4] The hydrolysis of BA into acrylic acid will be accelerated at 120^{O}C.

Several experiments were conducted, the most notable using BA, water and NaOH. The starting pH (prior to purging and heating the reactor) was 11.5, but the pH dropped to 4.88 after heating to 120^{O}C over the course of an hour. While this is a radical drop in pH, only 2.6x10^{-3}% of the BA was converted to acrylic acid. After a further hour at 120^{O}C the pH was 4.33 and 8.2x10^{-3}% of the BA was hydrolyzed. When the buffer Na_2CO_3 was added with BA and water, the pH drop was not as significant (starting pH 10.33, pH after one hour of heating was 9.52 and after a further hour at 120^{O}C the pH was 7.36).

Experiments were also conducted with ethyl benzene (the saturated analogue of styrene, styrene was not chosen because of an interaction between the inhibitor 4-tert-butylcathechol and NaOH), NaOH and water. The initial pH was 11.14 and after 3 hours at 120^{O}C, the pH dropped to 9.32 (1.11x10^{-7}% of acid created with respect to the ethyl benzene in the system). Since ethyl benzene is unlikely to undergo a hydrolysis reaction, this drop in pH may be attributed to the deprotonation of the Si-OH groups on the surface of the glass reactor.

A very small amount of BA hydrolyzing into acrylic acid leads to a dramatic decrease in the pH at the start of the reaction. To minimize hydrolysis, beginning with a lower pH (by using only stoichiometric amounts of NaOH or Na_2CO_3) is preferable. However, the hydrolysis of BA is self-regulating – the hydrolysis of BA leads to the creation of acrylic acid, which lowers the pH of the system and, in turn, slows the rate of hydrolysis.

References

[1] Nicolas, J., Charleux, B., Guerret, O., and Magnet, S. *Macromolecules* **38**(24), 9963–9973 (2005).

[2] Bates, R. G. *Medium effects and pH in nonaqueous solvents.* Determination of pH: Theory and Practice. John Wiley & Sons, New York, 2nd edition (1973).

[3] Ness, J. S. and Schmidt, S. C. (2008).

[4] United Nations Environmental Programme Chemicals. Technical Report Screening Information Data Set (SIDS) for n-Butyl Acrylate 141-32-2, (2004).

Appendix D

High Solids Microemulsion Polymerization

D.1 Estimation of the Concentration of Free SG1 Early in the Polymerization

Assuming limited termination, the rate of change of free radicals in the system can be estimated by

$$\frac{d[R\bullet]}{dt} = k_{act}[BB] - k_{deact}[SG1][R\bullet] \tag{D.1}$$

Applying the quasi-steady-state assumption, and assuming that BlocBuilder MA® activates to form a free radical and a free SG1 in pairs, the concentration of free SG1 in the system can be estimated as

$$[SG1] = \left(\frac{k_{act}[BB]}{k_{deact}}\right)^{0.5} \tag{D.2}$$

Using the initial concentration of BlocBuilder MA® in the system, [BB] = 1.45 mmol·L^{-1}, the rate coefficient of activation of BlocBuilder MA® initiator at 90^{o}C, k_{act} = 3.4·10^{-2} s^{-1},[1] and the rate coefficient of deactivation for a chain possessing an St• end group, k_{deact} = 4.6·10^{6} L·mol^{-1}·s^{-1} [1] (the choice of the St• end group rather than MMA• is appropriate because the re-activation of a dormant chain with MMA as the terminal group will be extremely fast[1] such that the period of time which that chain was dormant is insignificant), the concentration of free SG1 is calculated as [SG1] = 3.3·10^{-6} mol·L^{-1} or 2.0·10^{18} molecules·L^{-1}.

D.2 Estimation of the Expected Degree of Polymerization for the First Activation Step.

The average degree of polymerization for the first activation step can be estimated by

$$DP = \frac{R_p}{R_{deact}} = \frac{\bar{k}_p[M]}{k_{deact}[SG1]} \tag{D.3}$$

Where $\bar{k}_p$ is the average rate coefficient of propagation for the copolymer system (see below), k_{deact} is the deactivation rate coefficient for the addition of an SG1 to an St• chain end (k_{deact} = $4.6{\cdot}10^6$ L·mol^{-1}·s^{-1} [1]), as described earlier, and [M] and [SG1] are the concentrations of monomer and SG1 respectively in the system. The average DP can be estimated in two ways – firstly assuming all the monomer and SG1 are present in the aqueous phase and monomer swollen micelles play no significant role, or, alternatively, that the majority of the monomer is present inside the micelles and the first deactivation step will occur between a propagating chain and an SG1 molecule within the monomer swollen micelle.

Because this is a copolymerization system, the reactivity ratios, r_1 and r_2, and the monomer feed concentrations, f_1 and f_2, need to be taken into account in determining $\bar{k}_p$ by[2]

$$\bar{k}_p = \frac{r_1 f_1^2 + 2 f_1 f_2 + r_2 f_2}{\left(r_1 f_1 / \bar{k}_{p11}\right) + \left(r_2 f_2 / \bar{k}_{p22}\right)} \tag{D.4}$$

$$\bar{k}_{p11} = \frac{k_{p111}[r_1 f_1 + f_2]}{r_1 f_1 + [f_2 / s_1]} \tag{D.5}$$

$$s_1 = \frac{k_{p211}}{k_{p111}} \tag{D.6}$$

where r_{MMA} = 0.4929, r_{St} = 0.4829, s_{MMA} = 0.6014, s_{St} = 0.3615, $k_{p,MMA}$ = 1640 L·mol^{-1}·s^{-1} and $k_{p,St}$ = 900 L·mol^{-1}·s^{-1}.6 Thus when 8 mol% and 30 mol% styrene is added to the 1st stage, $\bar{k}_p$ = 1491 L·mol^{-1}·s^{-1} and $\bar{k}_p$ = 1200 L·mol^{-1}·s^{-1} respectively.

1) Theoretical DP for all reactions occurring in the aqueous phase Earlier we calculated the average concentration of SG1 in the system in the absence of partitioning between the aqueous phase and the monomer swollen micelles as [SG1] = $3.3{\cdot}10^{-6}$ mol·L^{-1}.

Because both MMA and St have similar molecular weights, $[M]_{aq}$ is 1.7 mol·L^{-1} in both the 8 mol% and 30 mol% St 1st stage experiments, A1 and A2 respectively (Section 6.3.1). Thus, with equation D.3, the average DP each chain would reach in the aqueous phase, in the absence of entry into the monomer swollen micelles, is DP^{th}_{aq} = 768 and 618 for the 8 mol% and 30 mol% St systems respectively.

2) Theoretical DP upon entry into a monomer swollen micelle Because deactivation of the propagating oligomers by SG1 is unlikely to occur in the aqueous phase prior to these chains reaching their z-meric lengths (∼4) and entering into a micelle, it is more practical to calculate the average length of each chain prior to deactivation as DP^{th}_{mic} = 4 +$DP_{in\ micelle}$. DP^{th}_{mic} can be determined assuming there is an SG1 molecule present inside that micelle with which the chain can undergo a deactivation reaction

$$DP^{th}_{mic} = 4 + \frac{\bar{k}_p[M]}{k_{deact}\frac{1}{N_A V_p}} \tag{D.7}$$

where [M] is the concentration of monomer inside the micelles, [M] = 9.2 mol·L^{-1} for both the 8 mol% St and 30 mol% St because of their similar molecular weight and densities, and N_A is Avogadro's number and Vp is the volume of the monomer swollen micelle. Based on dynamic light scattering measurements of Dowfax^{TM}8390 micelles in solution (see below), we will assume a diameter of 2 nm for our monomer swollen micelles, resulting in $N_A V_p$ = 2.5 L·mol^{-1}. Using Equation D.7, this results in DP^{th}_{mic} ∼4 for both the 8 mol% and 30 mol% systems as deactivation occurs almost instantaneously upon entry of a chain into a particle containing an SG1 molecule ($DP_{in\ micelle}$ = 0.075 and 0.060 for the 8 mol% and 30 mol% styrene systems respectively).

D.3 Estimation of the Aggregation Number of Dowfax^{TM}8390

The aggregation number, N, of the surfactant Dowfax^{TM}8390 was estimated in two different manners and an appropriate order-of-magnitude estimate for N was made. For spherical micelles, the aggregation number can be determined by geometric considerations,[3] assuming each micelle occupies a cone shaped volume within the sphere. If information about the radius of the micelle, R_{mic}, and the surface area of the head group, a_0, are known, N can

be determined by

$$N = \frac{4\pi {R_{mic}}^2}{a_0} \tag{D.8}$$

1) Estimation of the radius of the micelle by empirical correlation The radius of the micelle can be estimated assuming that it is equivalent to the elongated length of the surfactants hydrophobic tail, $\ell_{\max}$. Dowfax^{TM}8390 possesses a monoalkylated tail of 16 carbons (number of C molecules, $n_c = 16$) so $\ell_{\max}$can be estimated as 2.178 nm from[3]

$$\ell_{\max} = (0.154 + 0.1265 n_c)\ nm \tag{D.9}$$

The surface occupied by a Dowfax^{TM}8390 type surfactant has been previously estimated as a_0 = 1.66–2.49 nm (depending on the Gibbs pre-factor used in the estimation, the value is assumed be to be 2 or 3).[4]

This estimates N for our surfactant between 24–36. The use of $\ell_{\max}$ as R_{mic} could contain a great deal of error, as the correlation is normally applied for surfactants with a single headgroup (not double like Dowfax^{TM}8390) and assumes that there is full extension of the C16 tail towards the center of the micelle. Stronger repulsing head groups tend lead to lower aggregation numbers, and in these cases the assumption that the hydrophobic tail would be fully extended may not hold. Thus it is believed that the N estimated here may be high.

2) Estimation of the radius of the micelle by light scattering Surfactant dissolved in DIW (at 10x its CMC) was analyzed by dynamic light scattering. The intensity and volume average particle sizes were estimated at 3.48 nm and 1.82 nm respectively. Using the same a_0 above and R_{mic} estimated from the intensity particle size, N is calculated between 15–23.

Because our experimental system also contains a small concentration of electrolyte (which tends to increase N), we have chosen to use N $\sim$25 in our calculations of the concentration of micelles present at the start of the polymerization.

D.4 Estimation of the Concentration of Micelles Early in the Polymerization

Dowfax^{TM}8390 is known to have a very low CMC,[4] and an order of magnitude estimate of the concentration of micelles present at the start of the polymerization can be made by: [micelles] = [surfactant]$_0 \cdot N^{-1} \cdot N^A$, which yields $1.86 \cdot 10^{21}$ micelles$\cdot L^{-1}$ for our polymerization. As a conservative estimate, we will assume our microemulsion systems have an initial micelle concentration of 10^{21} micelles$\cdot L^{-1}$, which is two orders of magnitude higher than the number normally cited for traditional emulsion polymerization of 10^{19} micelles$\cdot L^{-1}$.[5]

References

[1] Nicolas, J., Mueller, L., Dire, C., Matyjaszewski, K., and Charleux, B. *Macromolecules* **42**(13), 4470–4478 (2009).

[2] Charleux, B., Nicolas, J., and Guerret, O. *Macromolecules* **38**(13), 5485–5492 (2005).

[3] Hiemenz, P. C. and Rajagopalan, R. *Principles of Colloid and Surface Chemistry.* Marcel Dekker, New York, (1997).

[4] Ben-Moshe, M. and Magdassi, S. *Colloids and Surfaces A: Physicochemical and Engineering Aspects* **250**(1-3), 403–408 (2004).

[5] Gilbert, R. G. *Emulsion Polymerization - a Mechanistic Approach.* Academic Press, San Diego, CA, (1995).

Appendix E

SG1 Mediated Surfactant-Free Emulsion Polymerization

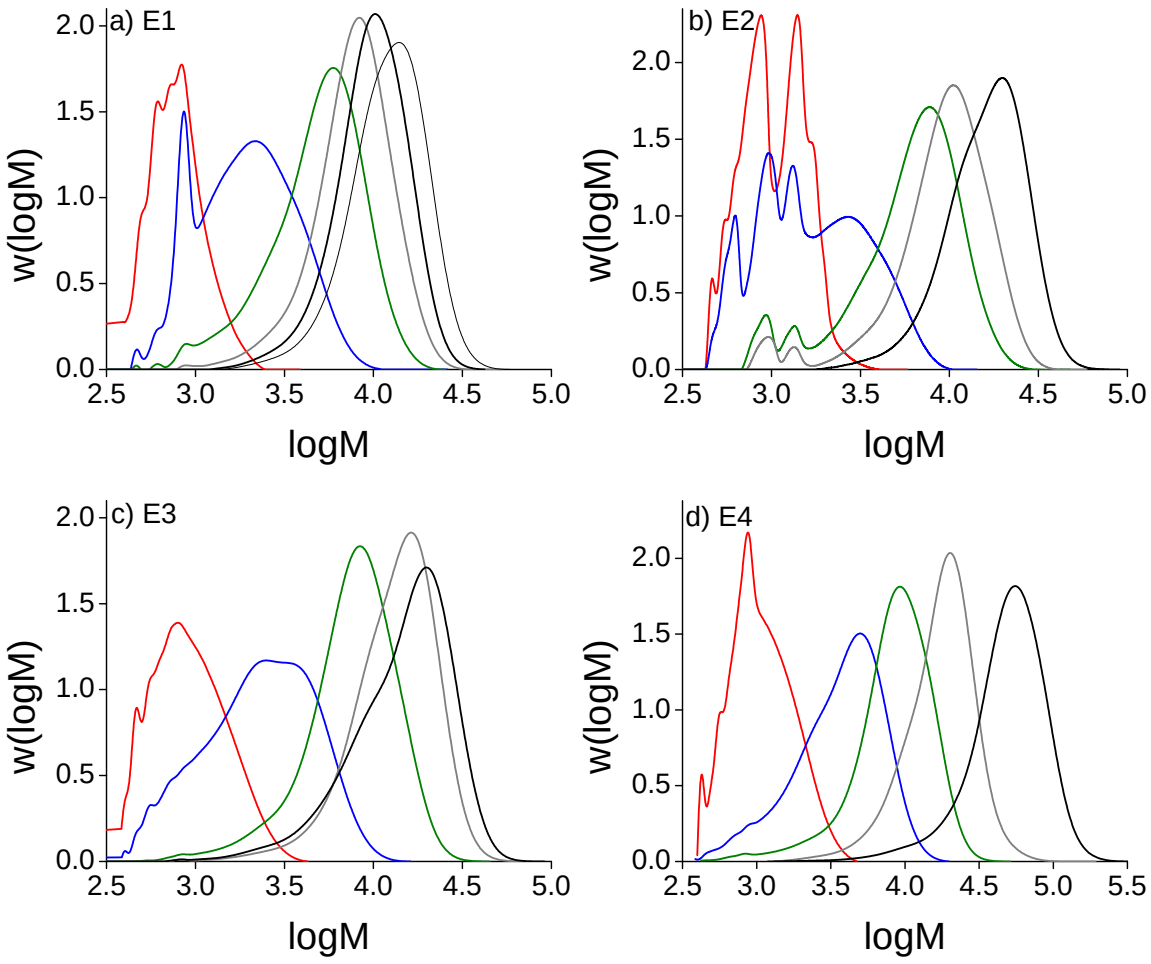

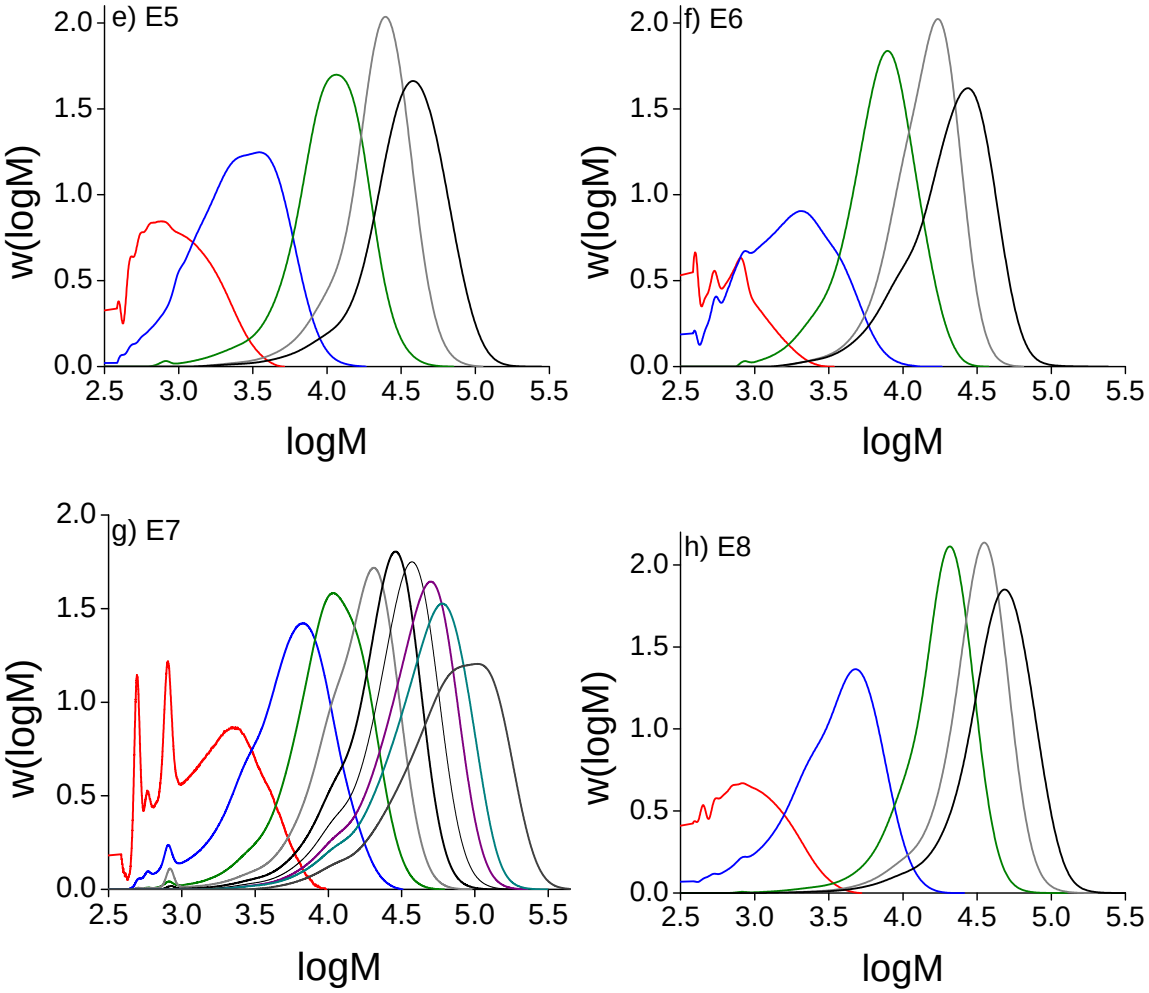

Figure E.1: Full molecular weight distributions of all experiments listed in Table 7.2. The contribution of the 1st stage latex is included in all MWDs (-). (a) Two stage emulsion polymerization of MMA-co-St with Dowfax^{TM}8390 above the CMC (E1). (b) Two stage emulsion polymerization of BMA-co-St with Dowfax^{TM}8390 above the CMC (E2). (c) Surfactant-free, two stage emulsion polymerization of BMA-co-St with no methyl acrylate present in the 1st stage (E3). (d) Surfactant-free, two stage emulsion polymerization of BMA-co-St with 3 units of methyl acrylate per chain present in the 1st stage (E4). (e) Surfactant-free, two stage emulsion polymerization of BMA-co-St with 3 units of methyl acrylate per chain present in the 1st stage (E5). (f) Surfactant-free, two stage emulsion polymerization of BMA-co-St with 3 units of methyl acrylate per chain and 10 mol% excess SG1 present in the 1st stage (E6). (g) Surfactant-free, two stage emulsion polymerization of BMA-co-St with 3 units of methyl acrylate per chain and 20 mol% excess SG1 present in the 1st stage, 20 mol% of the reducing agent SFS was added prior to the monomer feed (E7). (h) Two stage emulsion polymerization of BMA-co-St with SDS below the CMC and no methyl acrylate present in the 1st stage (E8).